Titre: Title:	Critical heat flux in non-uniform heated tubes
Auteur: Author:	Jingyang Sun
Date:	2005
Type:	Mémoire ou thèse / Dissertation or Thesis
Référence: Citation:	Sun, J. (2005). Critical heat flux in non-uniform heated tubes [Master's thesis, École Polytechnique de Montréal]. PolyPublie. https://publications.polymtl.ca/7683/

Document en libre accès dans PolyPublie
Open Access document in PolyPublie

URL de PolyPublie: PolyPublie URL:	https://publications.polymtl.ca/7683/
Directeurs de recherche: Advisors:	Alberto Teyssedou
Programme: Program:	Unspecified

UNIVERSITÉ DE MONTRÉAL

CRITICAL HEAT FLUX IN

NON-UNIFORM HEATED TUBES

JINGYANG SUN

DÉPARTEMENT DE GÉNIE PHYSIQUE

ÉCOLE POLYTECHNIQUE DE MONTRÉAL

MÉMOIRE PRÉSENTÉ EN VUE DE L'OBTENTION

DU DIPLÔME DE MAÎTRISE ÈS SCIENCES APPLIQUÉES

(GÉNIE ENERGÉTIQUE)

DECEMEMBER 2005

Canada

UNIVERSITÉ DE MONTRÉAL

ÉCOLE POLYTECHNIQUE DE MONTRÉAL

Ce mémoire intitulé:

CRITICAL HEAT FLUX IN

NON-UNIFORM HEATED TUBES

présenté par: SUN Jingyang

en vue de l'obtention du diplôme de : Maîtrise ès sciences appliquées

a été dûment accepté par le jury d'examen constitué de :

M. MUREITHI Njuki-William, Ph.D., président

M. TEYSSEDOU Alberto, PhD., membre et directeur de recherche

M. TAPUCU Altan, D.Sc.A., membre

To my parents, my wife Jing, my daughter Jiaxin and my son Jeffrey.

ACKNOWLEDGMENTS

I am deeply indebted to my research director, Professor Alberto Teyssedou for the support and encouragement he provided during the course of this investigation.

This study was carried out at the Heat Transfer Loop facility of Thermohydraulic Laboratory of École Polytechnique de Montréal. The completion of this work was made possible by the invaluable encouragement and assistance given by Dr. Andrei Olekhnovitch to whom I am very grateful.

Many thanks go to Serguei, Nihan, Noreddine, Jean, Armando, Maxime, Karthikan and Benoit for giving valuable suggestions and for providing generous aids during my research.

Thanks to my sister and my brothers and all my friends who gave me encouragenment all the times.

Above all, I want to thank my wife Jing and my daughter Jiaxin for their support and patience during the past years.

RÉSUMÉ

《 Le Flux de Chaleur Critique 》 (FCC) est un critère important dans la conception de beaucoup d'équipements thermiques employés par l'industrie énergétique et sa compréhension est cruciale pour l'operation securitaire des réacteurs nucléaires refroidis à l'eau et les chaudièrer à tubes d'eau.

L'objectif de ce projet consiste à l'étude des conditions de FCC semblables à celles rencontrés dans des chaudières industrielles à tubes d'eau, qui sont soumies au chauffage angulaire nonuniforme. Les données de FCC obtenues dans une telle condition de chauffage sont très rares. La complexité des expériences a obligé les chercheurs à employer des sections d'essais courtes couvrant une gamme limitée de conditions thermohydrauliques. D'autre part, ce type de recherche est aussi très utile pour les réacteures CANDU de nouvelle génération.

Les expériences preséntées dans ce document ont été effectuées dans la boucle thermique vapeur-eau de l'École Polytechnique en changeant le sous-refroidissement à l'entrée, la vitesse massique de l'écoulement ainsi que la pression de sortie. Des sections d'essais d'épaisseur de paroi uniforme et nonuniforme ont été fabriqueés et installées dans la boucle. La nonuniformité de chauffage a été obtenue en utilisant différentes épaisseurs de paroi de la conduite. La puissance appliquée a été augmentée graduellement jusqu'à ce que des conditions de FCC soient atteintes.

Les données collectées sont traitées pour établir différentes relations entre le FCC et les conditions thermohydrauliques (le sous-refroidissement à l'entrée, la vitesse massique, pression) ou des paramètres géométriques (longueur de chauffage, rapport de flux de chaleur). En employant de nouvelles méthodes semi-analytiques, le FCC peut être prédit avec une bonne précision. Nouvelles connaissances au sujet du FCC dans des conditions de chauffage nonuniforme ont été obtenues à partir de ce travail de recherches.

ABSTRACT

The "Critical Heat Flux" (CHF) is an important design parameter for many thermal equipments used by the power industry and its understanding is crucial for the safety operation of pressurized water-cooled nuclear reactors and industrial boilers.

The objective of this project consists in studying CHF conditions similar to those encountered in industrial boiler water-wall tubes, which are subjected to non-uniform circumferential heating. CHF data obtained under such a heating condition are very scarce. The complexity of the experiments has limited the investigators to use short test sections covering very limited range of thermal hydraulic parameters. Also, this research topic is also useful for the next generation CANDU reactor.

The experiments were carried out in the École Polytechnique steam-water thermal loop by changing the inlet subcooling, flow rate and outlet pressure. Test sections having uniform and non-uniform wall thickness were manufactured and installed in the loop. The nonuniformity of heating over the perimeter was established by varying the wall thickness over the perimeter. The power applied was increased step by step until CHF conditions were reached.

The collected data was treated to represent different relationships between CHF and thermal hydraulic conditions (inlet subcooling, flow rate, pressure) or geometry parameters (heated length, non-uniform heat flux ratio). By using new semi-analytical methods, CHF can be predicted with good accuracy. Moreover, new insights about CHF under non-uniform heating condition were obtained from this research work.

CONDENSÉ EN FRANÇAIS

Dans ce projet nous avons étudié le Flux de Chaleur Critique (FCC) dans des tubes chauffés circonférentiellement de façon non-uniforme. Ces tubes sont semblables à ceux rencontrés dans des chaudière industrielles de type tubes à eau, qui sont soumis au chauffage circulaire nonuniforme. D'autre part, le FCC pour des conditions de chauffage nonuniforme peut aussi avoir lieu dans les réacteurs CANDU de nouvelle génération; ainsi cette titre de recherche est aussi très utile. Comme nous savons que les conditions de FCC doivent être évités dans le fonctionnement normal des réacteurs nucléaires et d'autres machines opérant à de flux de chaleur élevés, nous devons développer des corrélations empiriques fiables afin de prévoir le FCC pour différents géométries et conditions thermohydrauliques.

Pratiquement, les FCC dans des conditions de chauffage nonuniforme sont plus fréquents que les FCC dans des conditions de chauffage uniforme. L'examen de la littérature de l'effet du chauffage nonuniforme sur le FCC a démontré qu'il n'y a aucun accord entre les résultats obtenus par différents chercheurs. Ainsi, l'objectif de ce projet consiste à étudier l'effet du chauffage nonuniforme sur le FCC dans un large éventail de conditions d'écoulement.

Le présent mémoire de maîtrise se compose d'une introduction et de six chapitres.

En introduction, l'origine et la signification du problème de FCC ont été présentées. A la fin de cette partie, la portée de l'étude courante a été esquissée et l'objectif de la recherche a été défini. Les objectifs de cette recherche sont :

1. L'étude de l'effet du chauffage non-uniforme sur le FCC dans un large éventail de conditions d'écoulement afin d'obtenir plus d'informations sur les caractéristiques du CHF dans un écoulement en ébullition.

2. L'utilisation des méthodes semi-analytiques pour améliorer l'exactitude de la prévision du FCC.

Le chapitre 1 présente la terminologie et les définitions de l'écoulement ascendant en ébullition par convection forcée dans des tubes. La terminologie et les définitions associées, telles que les variables, les configurations des écoulements et les modes de transfert de chaleur, aideront les lecteurs à mieux comprendre les figures et les discussions.

Le chapitre 2 présente une revue de la littérature sur la FCC dans des tubes chauffés pour les écoulements verticaux ascendants. Au début, les mécanismes qui peuvent provoques le FCC ont été discutés. Étant donnée que le mécanisme utilisé pour expliquer le départ de l'ébullition nucléée (DNB) est différent des mécanismes utilisés pour expliquer le phénomène de l'assèchement, le régime d'ébullition saturé a été séparé du régime d'ébullition sous-refroidi, i.e., titre faible. La discussion sur le régime d'ébullition sous-refroidi (titre faible) a été brièvement passée en revue pour la raison que le liquid entrant est sous-refroidi et que le flux de chaleur n'est pas assez élevé pour provoquer la caléfaction. Les travaux sont principalement focalisés sur le régime d'ébullition saturé ou on a discuté trois concepts différents : le concept du titre limite proposé par Doroshchuk (1966), le concept d'écoulement secondaire circulaire proposé par Butterworth (1972) et le concept de longueur d'écoulement annulaire dispersé proposé par Olekhnovitch *et al.* (1999b). Dans le concept de Doroshchuk (1966), on a suggéré que quand l'assèchement se produit, il existe un titre limite et le FCC perd sa signification. Butterworth (1972) a essayé d'expliquer le phénomène de FCC par la création et l'existence d'un écoulement circulaire secondaire de liquide sur la surface interieure du tube. Il a proposé un modèle de propagation de film circulaire pour le régime d'écoulement annulaire en considérant la longueur de chauffage, le diamètre interne de tube, le coefficient de propagation de film et la nonuniformité du flux de chaleur augulaire. Dans le concept de longueur d'écoulement annulaire dispersé, l'utilisation de la représentation du FCC en fonction de la longueur d'écoulement annulaire dispersé peut réduire considérablement la dispersion des données, par rapport à celles observées quand on utilise la représentation du FCC en fonction du titre thermodynamique. Olekhnovitch *et al.* (1999b) ont déduit que les mécanismes qui contrôlent le FCC sont le débit massique d'écoulement dans le film liquide au

début de l'écoulement annulaire dispersé et le flux de chaleur appliqué. À la fin du chapitre 2, un examen des expériences de FCC effectuées à l'aide des tubes chauffés nonuniformerent est présenté. On a trouvé qu'il n'y a aucun accord entre les résultats obtenus par différents chercheurs.

Le montage exérimental ainsi que les procédures expérimentales utilisées dans ce travail sont détaillés dans le chapitre 3. Les expériences dans cette étude ont été effectuées en utilisant une boucle thermique. Les principales caractéristiques de fonctionnement de cette boucle sont :

Puissance thermique	10 - 400 kW;
Pression d'opération	3 - 40 $bars$;
Débit massique	0.05 - 1.7 kg/s;
Sous-refroidissement à l'entrée	0 - 100 ^oC.

La boucle thermique est constituée d'un ballon de vapeur, d'un condenseur, de pompes de circulation, d'un échangeur de chaleur, de deux pré-chauffeurs, d'une section d'essais et d'un système de contrôle.

Trois sections d'essais ayant une longueur chauffée de 3.55 m et de diamètre interne de 22.2 mm ont été employées pendant les essais. Deux de ces sections d'essais sont fabriqués à l'aide de tubes SS316 Extra-forts avec une géométrie de paroi externe excentrique. La troisième section d'essais ayant une épaisseur de paroi uniforme est employée pour obtenir des données de FCC de référence. La différence dans l'épaisseur de paroi nous permet de changer le rapport de flux de chaleur, $\frac{q"_{max}}{q"_{min}}$, de 1:1, 4.7:1 et 8.3:1. La chaleur est produite par effet Joule en appliquant un courant continu à la paroi de la section d'essais. La puissance électrique contrôlée est appliquée au moyen de deux plaques en cuivre; le déplacement de ces plaques permet d'obtenir des longueurs chauffées différentes. La section d'essais est équipée avec des thermocouples pour la détection du commencement du FCC et pour déclencher le contrôleur de puissance. Quatorze thermocouples chromel-alumel sans mise à la terre (type K, 0.5 millimètre de diamètre extérieur) sont soudés sur la surface externe du tube. Pour protéger la

section d'essais, deux groupes de six thermocouples reliés en parallèle sont utilisés pour déclencher le contrôleur de puissance. Les expériences sont effectuées en changeant le débit et le sous-refroidissement à l'entrée, et la pression de sortie. Puisque l'objectif principal des expériences est de collecter des données sur un large éventail de conditions d'écoulement, le sous-refroidissement à l'entrée est variée de 5 à 40 °C, le débit est varié de 300 à 1600 kg/m^2s, et la pression de sortie est variée de 10 à 40 $bars$. Lors chaque expérience, la température à l'entrée de la section d'essais est contrôlée avec une précision de ±0.3 °C, le débit est maintenu constant avec une plage de variation de ±0.002 l/s et la pression de sortie a été maintenue constante avec une plage de variation maximale de ±0.05 bar. La conception de la boucle permettent de mener les expériences sans fluctuation appréciable de basse fréquence de débit et de pression. Une fois que les paramètres d'écoulement sont établis et contrôlés, la puissance appliquée à la section d'essais est graduellement augmentée jusqu'à l'apparition des premières fluctuations de température à la paroi. Après que la première fluctuation de température est détectée, le système d'acquisition de données est déclenché. La puissance appliquée est gardée à cet état au moins pendant 10 secondes afin de finir l'acquisition de données pour le FCC; l'intervalle de l'acquisition de données est de 0.25 s. Après cette période de 10 secondes, la puissance continue d'augmenter et le contrôleur de puissance est déclenché dès qu'un grand saut de la température à la paroi (plus de 40 °C) est détecté et l'acquisition de données est arrêtée.

Le chapitre 4 et le chapitre 5 sont les parties principales du mémoire. Les résultats détaillés des essais et l'analyse de données sont présentés dans ces deux chapitres. Une étude approfondie du FCC pour les écoulements verticaux à faible pression est présentée avec un total d'environ 1000 points de FCC obtenus, avec trois différentes longueurs de chauffage et trois distributions angulaire de flux de chaleur pour des tubes ayant un diamètre interne de 22.2 mm.

Au chapitre 4, trois concepts différents du problème d'assèchement dans des conditions d'ébullition saturé sont discutés. Trois différentes représentations des données sont employées, à savoir: la représentation du FCC en fonction du titre thermodynamique, la représentation du FCC en fonction de la longueur de l'écoule-

ment annulaire dispersé, et la représentation des Flux de Chaleur Critique moyen et local en fonction du titre thermodynamique.

En fixant le flux massique et la pression, nous pouvons obtenir des figures reprèsentant le FCC vs. le titre thermodynamique à la sortie de la section d'essais pour trois différentes longueurs de chauffage et trois distributions angulaire de flux de chaleur. Par la régression des données expérimentales, nous avons calculé une série de lignes droites ayant des coefficients de régression qui sont fonction des conditions d'écoulement; ceci est utilisé pour construire une table des coefficients de régression.

Une fois que la table de coefficients de régression est établie, le FCC peut être prédit pour différentes titres thermodynamiques. Les résultats des essais prouvent que le FCC calculé par cette méthode dite de remplacement directe a une précision limité, i.e., les erreurs relatives et absolues (RMS de CHF_{DSM}) sont respectivement de 11.2% et 144.76 kW/m^2. La raison d'une telle imprécision pourrait être simplement due au fait que le titre thermodynamique n'est pas un paramètre mesuré. En effet il est affecté par plusieurs facteurs, tels que la pression de sortie, le sous-refroidissement à l'entrée, l'isolation thermique, etc.

La précision de la méthode de prédiction des FCC proposée a été par la suite améliorée considérablement en introduisant le critère basé sur le bilan thermique. Dans la méthode dite directe, le FCC varie inversement au titre thermodynamique, c'est-à-dire, plus élevé est le titre thermodynamique, plus bas est le FCC. D'autre part, du bilan thermique, le titre thermodynamique augmente avec l'augmentation du flux de chaleur. Si nous plaçons la courbe représentant la corrélation de FCC versus le titre et la courbe représentant le bilan thermique, sur le même graphique, ces deux courbes se croisent dans un point. La valeur du FCC correspondant à ce point de croisement correspond à la valeur de FCC prédite par l'approche de la méthode du bilan thermique, (CHF_{HBM}). En général la prédiction du FCC par la méthode de bilan thermique est obtenue par itération, dans cette étude cependant, nous constatons que cette valeur pourrait être obtenue analytiquement en résolvant un système d'équations couplées. Les résultats d'essais montrent que

le FCC prédit par cette méthode, i.e., le bilan thermique, a une précision plus élevée; les erreurs relatives et absolues (RMS de CHF_{HBM}) sont respectivement de 2.3% et 33.4 kW/m^2. La bonne précision de cette méthode est due à l'évaluation simultanée du flux de chaleur et du titre, avec le flux de chaleur considéré de façon implicite. Par conséquent, cette méthode constitue une approche implicite.

Afin de représenter le FCC en fonction de la longueur de la région d'écoulement annulaire dispersé (L_{dan}), la corrélation de Levitan et de Borevskiy (1989) pour calculer cette longueur est utilisée. Selon Levitan et Borevskiy, la détermination de la longueur L_{dan} exige la connaissance du titre thermodynamique, x_{dan}, correspondant au début de l'écoulement annulaire dispersé. Le titre x_{dan} est relié au nombre de Weber du film de liquide de l'écoulement annulaire, $We_f = G^2 d/\rho_g \sigma$, et à la densité du liquide et de la vapeur. Une étude entreprise sur la relation entre L_{dan} et FCC prouve que cette relation a la forme d'une fonction hyperbolique. Cette relation nous a permis de représenter L_{dan} et 1/FCC par deux coefficients de régression. L'application de cette règle sur toutes les données expérimentales est utilisée pour compléter le tableau des coefficients de régression.

Une fois que le tableau des coefficients de régression est établi, le FCC peut être prédit pour différentes longueurs d'écoulement annulaire dispersé. Semblable à l'approche bassée sur titre thermodynamiques, nous pouvons aussi utiliser les calculs directs ou la méthode de bilan thermique. Les résultats prouvent que le FCC prédit par la méthode de substitution directe est moins précise que la méthode du bilan thermique, cependant la différence entre les deux méthodes reste plus faible. Les erreurs relatives et absolues pour la méthode directe (RMS de CHF_{DSM}) sont respectivement de 2.6% et 37.25 kW/m^2, tandis que les erreurs relatives et absolues pour la méthode de bilan thermique (RMS de CHF_{HBM}) sont respectivement de 2.2% et 30.44 kW/m^2.

La dernière partie du chapitre 4 est la représentation du FCC comme une fonction du Flux de Chaleur Critique moyen et local versus le titre thermodynamique. L'idée provient d'une étude analytique effectuée par Butterworth (1972), et Kitto et al. (1982) qui ont certifié cette théorie. Les représentations des données de

la présente étude prouve que certains accords qualitatifs existent, comme l'a démontré Kitto *et al.* (1982). Mais une comparaison avec les recherches ultérieures n'ont pas été conduites à cause du manque de lieu entre différentes sources de données (pression différente, diamètre différent, etc.).

En chapitre 5, une étude de l'effet de flux de masse et de pression sur le FCC a été entreprise par l'approche du titre thermodynamique et l'approche de longueur d'écoulement annulaire dispersé. Nous avons observé que le flux de masse a un effet linéaire, de manièreque le FCC décroît de façon linéaire avec l'accroissement des flux massiques. Tandis que l'effet de la pression sur le FCC est beaucoup plus complexe, la variation du FCC avec la pression est non linéaire et non monotone.

En utilisant le tableau de régression, une série de relations pour la prédiction du FCC est établie. L'utilisation de ces relations de régression, nous a permis d'effectuer une analyse de tendances paramétriques du FCC comme fonction des différentes variables thermohydrauliques. L'analyse paramétrique basée sur ces relations de régression indique des caractéristiques du FCC que nous n'avons pas observées dans le passé. L'étude du FCC avec le chauffage non-uniforme nous a aidés à obtenir plus d'informations sur les phénomènes ébullition et du FCC.

Quelques conclusions et recommandations sont adressées dans le chapitre 6, elle sont résumées comme suit :

- Pour des pressions faibles, les résultats expérimentaux prouvent que la longueur de chauffage a une influence importante sur le FCC. Cette caractéristiques du FCC est tout à fait différente de celles observées à des pressions moyennes et élevées (Groeneveld *et al.*, 1996), dans lesquelles l'influence de la longueur de chauffage est faible ou inexistante.

- Nous avons constaté qu'une augmentation de la longueur de chauffage provoque une diminution de l'effet de la distribution augulaire sur le FCC moyen.

- Les comparaisons des résultats démontrent que le FCC augmente avec

l'augmentation du flux de masse ou de la pression, cependant à mesure que le débit augmente la dépendance avec le flux de masse ou la pression diminue.

- Le FCC est inversement proportionnel à l'enthalpie de l'eau, l'enthalpie de l'eau à l'entrée a une influence croissante avec l'augmentation de débit de masse et de la pression.

- L'influence du chauffage nonuniforme sur le FCC montre que l'augmentaion de l'irregularit, $\frac{q''_{max}}{q''_{min}}$, provoque une diminution du FCC. Cependant, avec l'augmentation de débit de masse et de la pression l'effet de la distribution augulaire du flux de chaleur devient moins marqué.

- Dans la région des titres élevés, le flux maximal de chaleur nonuniforme s'approche du flux de chaleur moyen (i.e., uniforme).

- Dans la région des titres moyens ($x = 0.3 - 0.6$), le flux de chaleur moyen non-uniforme semble s'approcher du flux de chaleur moyen uniforme.

- Il a été établi que l'utilisation de la représentation du FCC en fonction de la longueur d'écoulement annulaire dispersé plutôt que en fonction du titre thermodynamique peut réduire considérablement l'éparpillement de données.

- Avec un nombre limité de constantes empiriques, la méthode présentée dans ce mémoire permet de prédire le FCC avec une précision acceptable, autant dans des conditions de chauffage uniforme que non-uniforme.

- Dans l'approche du titre thermodynamique, l'utilisation de la méthode de bilan thermique est meilleur que la méthode "directe" pour prédire FCC. Les erreurs relatives et absolues obtenues avec la méthode "directe" sont respectivement de 11.2% et 144.76 kW/m^2. Les erreurs relatives et absolues obtenues en utilisant la méthode de bilan thermique sont respectivement de 2.3% et 33.4 kW/m^2.

- Quand on utilise l'approche bassée sur la longueur de la région d'écoulement annulaire dispersé pour prédire le FCC, la différence entre la méthode "directe" et la méthode de bilan thermique reste plus faible. Les erreurs relatives et absolues obtenues avec la méthode "directe" sont respectivement de 2.6% et 37.25 kW/m^2. Et les erreurs relatives et absolues obtenues en utilisant la méthode de bilan thermique sont respectivement de 2.2% et 30.44 kW/m^2.

- Une liaison entre différentes sources de données obtenues dans des conditions de pression, diamètre et sous-refroidissement différentes a besoin d'être établie. Actuellement, l'utilisation de la présente étude pour la prédiction de FCC pour les écoulements à pression élevée n'est pas suggérée.

TABLE OF CONTENTS

LIST OF FIGURES

LIST OF TABLES

LIST OF APPENDIX

NOMENCLATURE

CHF Critical Heat Flux

DNB Departure from Nucleate Boiling

DSM Direct Substitution Method approach

HBM Heat Balance Method approach

ONB Onset of Nucleate Boiling

OSV Onset of Significant Vaporization

A	Cross-section area of the tube	$[m^2]$
A_k	Flow area of phase k	$[m^2]$
$B0$	Co-efficient in the regression formula	
$B1$	Co-efficient in the regression formula	
$C0$	Co-efficient in the regression formula	
$C1$	Co-efficient in the regression formula	
D	Inside diameter of the tube	$[m]$
$D0$	Co-efficient in the regression formula	
$D1$	Co-efficient in the regression formula	
G	Mass flux	$[kg/m^2s]$
g	Acceleration due to gravity	$[m/s^2]$
h_f	The enthalpy of the liquid	$[kJ/kg]$
h_g	The enthalpy of the vapor	$[kJ/kg]$
h_{fg}	The latent heat of evaporation	$[kJ/kg]$
h_{in}	Liquid subcooling enthalpy at inlet of the tube	$[kJ/kg]$
J	Superficial velocity	$[m/s]$
K	The spreading coefficient for the secondary circumferential flow	$[1/m]$
L	Heated length	$[m]$
L_B	Vapor blanket length	$[m]$
LD	Ratio of heated length over the inside diameter of the tube	$[m]$
L_{dan}	Dispersed annular flow length	$[m]$

NF	Nonuniform factor	
P	Pressure	$[N/m^2]$
Pe	Peclet Number	
Pr	Prandtl Number	
Q	Thermal power applied on the tube	$[kW]$
$q"$	Heat flux	$[kW/m^2]$
$q"_{max}$	Local maximum heat flux	$[kW/m^2]$
$q"_{mean}$	Equivalent mean heat flux	$[kW/m^2]$
$q"_{min}$	Local minimum heat flux	$[kW/m^2]$
$\overline{q}_{cr}$	The average critical heat flux	
	under nonuniform heating condition	$[kW/m^2]$
q_{cr}^0 or $q_{c,unif}$	The average critical heat flux	
	under uniform heating condition	$[kW/m^2]$
q_{cr}^{max} or $q_{c,H}$	The peak heat flux at CHF	
	under nonuniform heating condition	$[kW/m^2]$
Re	Reynolds Number	
T_{in}	Inlet water temperature	$[^0C]$
T_{sat}	Saturated water temperature	$[^0C]$
t	Temperature	$[^0C]$
U_B	Vapor blanket velocity	$[m/s]$
W	Mass flowrate	$[kg/s]$
We_f	Weber number of the film	
W_{f0}	The initial liquid film mass flow rate	$[kg/s]$
x	Thermodynamic quality	
x_{cr}	Thermodynamic quality at critical heat flux condition	
x_{dan}	Thermodynamic quality corresponding to	
	the onset of the dispersed annular flow	
x_{exit}	Thermodynamic quality at the exit of the tube	
x_{fr}	Limiting quality	
x_w	Working steam quality of the medium	
Z	Heated length of the tube (variable)	$[m]$
α	Void fraction	

δ	Liquid sublayer thickness	$[m]$
ΔW_f	The total change in the film flow rate over the length L_{dan}	$[kg/s]$
ρ_f	Density of the liquid	$[kg/m^3]$
ρ_g	Density of the steam	$[kg/m^3]$
σ	Surface tension	$[N/m]$
μ_f	Dynamic viscosity of the liquid	$[kg/(m.s)]$

INTRODUCTION

Two-phase flow systems are used as means of heat transfer in many engineering fields, such as thermal power plants, nuclear power plants, jet and rocket engines, etc. However, this efficient means of heat transfer is not boundless. Under some flow boiling conditions, it is observed that the cooling fluid cannot completely wet the heated surface, resulting in a considerable decrease of the heat transfer coefficient. This situation is referred to as the "Critical Heat Flux" (CHF).

Because of the complexity of the mechanism and apparently different conditions that can bring about of CHF in flow boiling, there is still disagreement on the terminology that should be used to designate the phenomena. The terms most widely used for identifying CHF are: burnout, dryout, boiling crisis, departure from nucleate boiling (DNB), boiling crisis of the first kind and second kind. The term "burnout" implies physical destruction of the heated surface. Most measurements on the "burnout heat flux" are, in fact, measurements of the heat flux at which a sharp rise in surface temperature takes place. The terms "departure from nucleate boiling" and "dryout" imply specific mechanisms, therefore, are not sufficient for a general description of the phenomenon. The term "CHF condition" has been chosen in this study, as recommended by Collier (1972), to denote the state of the system when the sudden deterioration in heat transfer coefficient has just occurred, and the term "CHF" has been chosen to describe the value of heat flux at which this state of the system first occurs.

Since the CHF conditions must be avoided in the normal operation of nuclear reactors and other thermal engines, reliable theoretical or empirical correlations are needed to predict them for various geometries and thermal hydraulic conditions. With improved theoretical methods, the system can thus be confidently designed to operate as close as possible to but not exceeding CHF.

For the past half-century, nearly all experimental work and theoretical effort relating to CHF has been aimed at producing design information for high flux facilities, of which the majority of experimental data were for vertical up flow

of water in uniformly heated tubes. The study of vertical upward flow in uniformly heated tubes is used as the basis for the study of CHF in other geometries and flow conditions. With some adjustments the results obtained from uniformly heated vertical tubes were extended to more complicated geometries and thermal hydraulic conditions.

There exist numerous compilations of CHF data for water in uniformly heated tubes established by different scientists. Among them the Thompson and Macbeth (1964) compilation was the first of its kind with the widest range of flow conditions and geometry. The Becker (1971) compilation had the widest range in the parameter of pressure for a tubular geometry. The new 1995 CHF look-up table is so far the most complete compilation (Groeneveld et al., 1996). Most existing empirical correlations are based on the above data sets and/or separate experiments for specific conditions.

Analytical models for predicting CHF conditions based on different theories and concepts were also proposed. But due to the complexity of CHF phenomena, until now, there have been no successful models that are able to handle all flow conditions and geometries.

Compared with the study of CHF under uniform heat flux distribution condition, few works have been carried out in the study of CHF in circumferentially nonuniform heated tubes. The complexity of the experiments has limited the investigators to use short test sections covering very limited thermal hydraulic conditions. A review of the effect of nonuniform heating on CHF has shown that there is no agreement between results obtained by different researchers. Thus, the objective of this project consists in studying the effect of angularly nonuniform heating on CHF by covering a wide range of flow conditions.

This study consists of two parts:

1. Study CHF for boiling water flows in circumferentially uniform round heated tubes

   The CHF in the saturated boiling regime with positive exit qualities have

been studied. The test section having a uniform wall thickness is used to obtain reference data. The influence of pressure on CHF has been investigated in the pressure range of 10 to 40 *bars*. The effects of heated length on the CHF have been studied for heated lengths of 1.8 m, 2.5 m and 3.55 m. The effects of inlet flow conditions (inlet subcooling) and the flow velocities on CHF have also been investigated. The results are presented as relationships between CHF and thermal hydraulics and/or geometry parameters.

2. Study CHF for boiling water flows in circumferentially nonuniform heated tubes

    The test procedure of this part of the research is similar to that of the first part, but the emphasis is focused on the study of the influence of nonuniform heating on CHF. Two test sections, having the same heated length and IDs as the test section used in the first part of the research work, are manufactured. Both of them are manufactured from X-strong SS316 tubes with an outer eccentric geometry. The difference in wall thickness permits us to achieve the heat flux ratio ($\frac{q''_{max}}{q''_{min}}$) of 4.7 and 8.3. The study of CHF under nonuniform heat flux distribution condition helped us to gain more information about the characteristics of CHF in flow boiling. Some of the characteristics of the CHF phenomena become apparent only under nonuniform heat flux distribution conditions.

Therefore, the objectives of this research are:

1. To study the effect of nonuniform heating on CHF by covering a wide range of flow conditions in order to gain more information on the behaviour of CHF in boiling fluids.

2. To use a semi-analytical method to develop correlations for predicting CHF conditions in water cooled channels.

CHAPTER 1

FORCED CONVECTION BOILING
IN UP FLOW TUBES

Forced convection boiling in up flow tubes and channels is perhaps the most complex phase-change process. In the following section some of the fundamental concepts are presented before proceeding to the discussion on flow boiling phenomenon.

1.1 Definition of variables

Mass flux, G

Mass flux is defined as the total mass flow rate divided by the cross-sectional flow area, thus:

$$G = \frac{\rho_l Q_l + \rho_g Q_g}{A_l + A_g}, \tag{1.1}$$

where A_l and A_g are the coss-sectional area occupied by liquid and gas respectively; Q_l and Q_g are the volumetric flow rate of the liquid and the gas phase respectively and ρ_l and ρ_g are the density of the liquid and the steam respectively.

Subcooling , ΔT_{sub} , Δh_{sub}

A fluid at a temperature below its saturation temperature is said to be subcooled. The degree of subcooling is defined as the difference between the saturation temperature and the temperature of the fluid,

$$\Delta T_{sub} = T_{sat} - T. \tag{1.2}$$

It can also be written as $T - T_{sat}$, then $\Delta T_{sub} < 0$.

In some cases, the degree of subcooling is defined in terms of enthalpy, thus:

$$\Delta h_{sub} = h_{sat} - h. \tag{1.3}$$

Average void fraction, $\langle \alpha \rangle$

At any instant, a given point within the tube may be occupied by the liquid phase or by the vapour phase. The void fraction is commonly defined as a time-averaged area occupied by the gas phase g (A_g) with respect to the total area occupied by the mixture (A), then:

$$\langle \alpha_g \rangle = \frac{A_g}{A}. \tag{1.4}$$

The void fraction depends on the flow pressure, channel geometry, vapor and liquid flow rates and the orientation of flow with respect to gravity.

Thermodynamic quality, x

One of the parameters that was used to analyse CHF is the thermodynamic quality at the end of the heated length. The thermodynamic quality can be written as:

$$x = \frac{h_{mix}(P_{out}) - h_f(P_{out})}{h_{fg}(P_{out})} = \frac{h_{in}(P_{in}) + Q/W - h_f(P_{out})}{h_{fg}(P_{out})}, \tag{1.5}$$

where:

h_{mix} and h_f : are the enthalpies of the mixture and the saturated liquid respectively, kJ/kg;

h_{fg}: latent heat of evaporation, kJ/kg;

Q: thermal power applied on the tube, kW;

W: mass flow rate, kg/s;

For a flow under thermal equilibrium conditions (no temperature difference between the phases), the thermodynamic quality is equal to the real quality of the flow, which means that it reflects the ratio of mass flow rate of the steam phase over the total mass flow rate.

1.2 Thermodynamics of a liquid and steam mixture

The Figure 1.1 shows a process of phase change for a pure substance in a pressure-volume-temperature coordinate system. Liquid only exists along the line AB and vapor only exists along the line CD. Liquid and vapor co-exist along the line BC. The saturation curve is the locus of points such as B and C. Along the line BC the pressure remains constant and the volume of the unit mass mixture (specific volume, v) is determined by its heat content (enthalpy, h). The values of the pressure and temperature corresponding to saturation state are known as the saturation pressure (P_{sat}) and saturation temperature (T_{sat}) respectively.

AB-BC-CD or DC-CB-BA are considered as stable equilibrium phase states. However, other metastable or unstable states can occur where the process does not follow the trace of AB-BC-CD or DC-CB-BA. For example, it is possible with care to reduce the pressure imposed on a liquid at constant temperature along a line AB without the formation of vapor at point B. Likewise it is possible to increase the pressure imposed on a vapor along a line DC without the formation of liquid at C. The PVT co-ordinates of these metastable states lie along an extrapolation of AB to B' or DC to C'. Point B' may also be reached by carefully increasing the liquid temperature above the saturation temperature corresponding to the imposed static pressure; this process is referred to as superheating and the metastable liquid state is referred to as superheated liquid. Similar statement can be made about the vapor state at C' where the equivalent cooling process is termed supersaturation and the metastable vapor state is referred to as a supersaturated vapor.

1.3 The boiling process

Vapor may form either from evaporation or nucleation. The formation of vapor at a planar interface occurs when the liquid temperature is increased partially
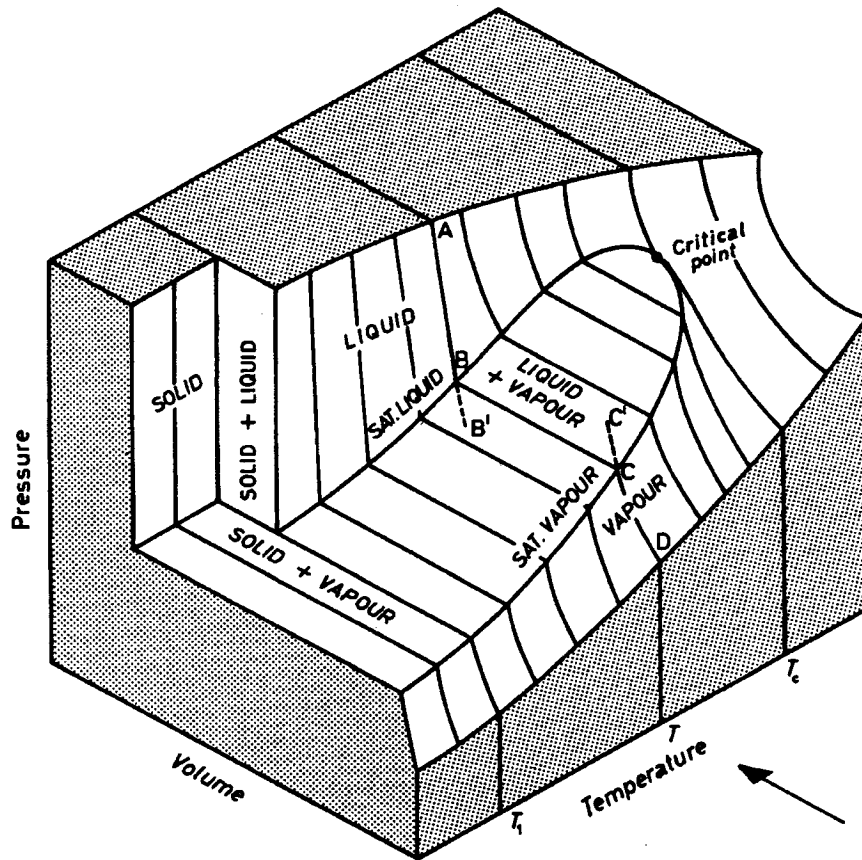
Figure 1.1: Pressure-volume-temperature surface for a pure substance.
(Collier, 1972)

above the corresponding saturation temperature. The term "evaporation" denotes vapor formation at a continuous liquid surface such as the interface between the liquid film and vapor core in annular flow. Evaporation and condensation at a planar interface can be described in terms of the imbalance of molecular fluxes passing through the interface from the vapor and liquid phases respectively.

For vapor nucleation, however, it is more complicated, in fact it is always related to metastable or unstable equilibrium state. Initial considerations relating to the formation of vapor from a metastable liquid or an unstable equilibrium state invariably start from the equation defining the mechanical equilibrium of a spherical vapor nucleus (radius r^*) in a liquid at constant temperature (T_g) and

pressure (P_f). Thus;

$$P_g - P_f = \frac{2\sigma}{r^*}. \tag{1.6}$$

Where P_g is the vapor pressure inside the bubbles and P_f is the imposed liquid pressure corresponding to a saturation temperature T_{sat}. The curvature of the interface lowers the vapor pressure (P_g) inside the nucleus compared with that above a planar interface (P_∞) for the same liquid temperature. It may be shown that

$$P_g = P_\infty exp(-2\sigma v_f M/r^* RT) \approx P_\infty \left(1 - \frac{2\sigma v_f}{P_\infty r^* v_g}\right). \tag{1.7}$$

Alternatively from (1.6) and (1.7),

$$P_\infty - P_f = \frac{2\sigma}{r^*}\left(1 + \frac{v_f}{v_g}\right). \tag{1.8}$$

To calculate the liquid superheat ($T_g - T_{SAT}$) corresponding to the pressure difference ($P_\infty - P_f$), here we first introduce the Clausius-Clapeyron equation, as

$$\frac{dp}{dT} = \frac{h_{fg}}{T(v_g - v_f)}. \tag{1.9}$$

If the specific volume of the liquid is small ($v_g \gg v_f$) and $Pv_g = MRT$ then,

$$\frac{1}{p}dp = \frac{h_{fg}M}{RT^2}dT. \tag{1.10}$$

Integrated Equation (1.10) from P_f to P_∞ and from T_{SAT} to T_g:

$$ln\left(\frac{P_\infty}{P_f}\right) = -\frac{h_{fg}M}{R}\left(\frac{1}{T_g} - \frac{1}{T_{sat}}\right) = \frac{h_{fg}M}{RT_gT_{sat}}(T_g - T_{sat}). \tag{1.11}$$

Substituting Equation (1.8) and rearranging,

$$(T_g - T_{sat}) = \frac{RT_{sat}T_g}{h_{fg}M} ln \left[1 + \frac{2\sigma}{P_f r^*} \left(1 + \frac{v_f}{v_g} \right) \right]. \qquad (1.12)$$

If $v_g \gg v_f$ and $(2\sigma/P_f r^*) \ll 1$ then Equation (1.12) simplifies to

$$(T_g - T_{sat}) = \Delta T_{sat} = \frac{RT_{sat}^2}{h_{fg}M} \frac{2\sigma}{P_f r^*}. \qquad (1.13)$$

Equation (1.13) implies that liquid superheat is a must for vapor nucleation.

It will be observed from Equation (1.13) that the size of the equilibrium vapor nucleus (r^*) becomes smaller as the superheat (ΔT_{sat}) is increased, i.e., as a result of a decrease in system pressure (P_f) along a line BB' (figure 1.1). Close to B' the size of the equilibrium nucleus approaches molecular dimensions. Thermal fluctuation occur in the metastable liquid and there is a small but finite probability of a cluster of molecules with vapor-like energies coming together to form a vapor embryo of the size of the equilibrium nucleus. This process of vapor formation in a metastable liquid is referred to as "homogeneous nucleation". From equation (1.13), on the other hand, we can image that to form vapor nucleus under homogeneous nucleation condition, big superheat of the liquid is required. For example, for water at atmospheric pressure the liquid temperature corresponding to a nucleation rate of 107 $cm^{-3}s^{-1}$ is 320.7 ^0C, i.e., a superheat of 220.7 ^0C. This value of superheat is much greater than any experimental value which has been measured for water (Knapp, 1958) even under very carefully controlled conditions. It is possible to state that, for water at least, homogenous nucleation from a metastable liquid state can be discounted as a mechanism for vapor formation. However, homogenous nucleation can and does occur in organic liquids.

Foreign bodies and container surface furnish normally provide ample nuclei to act as centres of vapor formation. This method of vapor generation from pre-existing nuclei is termed "heterogeneous nucleation." Examples of pre-existing nuclei are non-condensable gas bubbles held in suspension in the liquid and gas- or

vapor-filled cracks or cavities in container surfaces (known as nucleation "sites") or in suspended foreign bodies in the bulk liquid. The presence of a dissolved gas, say air, in the liquid necessitates the gas partial pressure being taking into account when considering the mechanical equilibrium of the vapor nucleus. Thus Equation (1.6) is modified as:

$$P_g + P_a - P_f = \frac{2\sigma}{r_c}, \tag{1.14}$$

where r_c represented the critical radius of active cavity on the heated wall to form a bubble (figure 1.2).
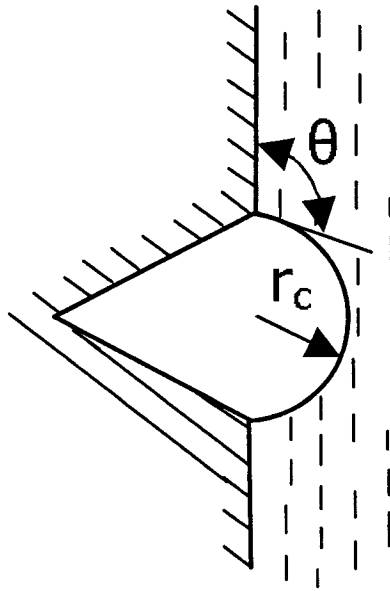
Figure 1.2: Nucleation from cavities.

With Equation (1.14), Equation (1.12) becomes:

$$T_g - T_{sat} = \frac{RT_{sat}T_g}{h_{fg}M} ln\left[1 + \left(\frac{2\sigma}{P_f r_c} - \frac{P_a}{P_f}\right)\left(1 + \frac{v_f}{v_g}\right)\right]. \tag{1.15}$$

The presence of dissolved gas reduces the superheat required to maintain a bubble of radius r_c in unstable equilibrium on the heated surface.

We have discussed the three forms of vapor formation: evaporation, homogeneous nucleation and heterogeneous nucleation. Now we will discuss the bubble detachment diameter and frequency.

The size and shape of vapor bubbles departing from a heated surface strongly depend on the way with which they are formed. The prime forces acting on a vapor bubble during the later stages of its growth are buoyancy and hydrodynamic drag forces attempting to detach it from the surface and surface tension and liquid inertial forces acting to prevent detachment. The liquid inertial force is a dynamic force resulting from the displacement of liquid during bubble growth. The growth velocity of a bubble and hence the inertial force is a strong function of the liquid superheat which, in turn, is inversely proportional to the size of the active cavity. A small cavity forms a bubble with a faster growth rate than that from a large cavity. Hatton and Hall (1966) have considered all the forces acting on a growing bubble and have conducted that for small cavity size ($r_c < 0.01$ mm for water at atmospheric pressure) the bubble size at departure is dictated mainly by a balance between buoyancy and liquid inertial forces. For large cavity sizes, the growth rate decreases, the dynamic forces become small, and the bubble size at departure is set by a balance between buoyancy and surface tension forces. Fritz (1935) considered this latter case and proposed the equation:

$$D_d = 0.0208\theta \left[\frac{\sigma}{g(\rho_f - \rho_g)} \right]^{\frac{1}{2}}, \qquad (1.16)$$

where D_d is the bubble departure diameter and θ is the contact angle (Figure 1.2) between the subcooled liquid and the bubble.

Individual nucleation sites emit bubbles with a constant frequency, the value of which varies from site to site. Jacob (1958) observed that the product of bubble frequency and departure diameter was a constant which Zuber (1963) has evaluated in the following form:

$$fD_d = 0.59 \left[\frac{\sigma g(\rho_f - \rho_g)}{\rho_f^2} \right]^{\frac{1}{4}}, \tag{1.17}$$

where f is the bubble departure frequency.

Under the conditions where the bubble departure process is governed by dynamic forces the relationship becomes $fD_d^2 = constant$. For water at atmospheric pressure, the bubble departure diameters are in the range of $1 - 2.5\ mm$ and bubble frequencies in the range $20 - 40\ s^{-1}$.

1.4 Pool boiling

Pool boiling is defined as boiling from a heated surface submerged in a large volume of stagnant liquid. This liquid may be at its boiling point in which case the term saturated boiling is employed or below its boiling point when the term subcooled pool boiling is used. The results of investigations concerning the heat transfer rates in pool boiling are usually plotted on a graph of surface heat flux (ϕ) against the heated wall surface temperature (T_w) - the "boiling curve". Such a curve for the boiling of water at atmospheric pressure is shown diagrammatically in the Figure 1.3.

Different regions of the boiling curve are well identified - In the Figure 1.4 these regions are:

(a) The natural convection region AB where temperature gradients are set up in the pool and heat is removed by natural convection from the free surface and hence by evaporation to the vapor space.

(b) The onset of nucleate boiling (ONB) where the wall superheat becomes sufficient to cause vapor nucleation at the heated surface. This may occur close to the point where the curves AB and B'C meet as is usually the case for water at atmosphere pressure and above. Alternatively it may occur at much larger superheats than those required to support fully developed nucleate boiling, resulting in a sharp drop in surface temperature from B
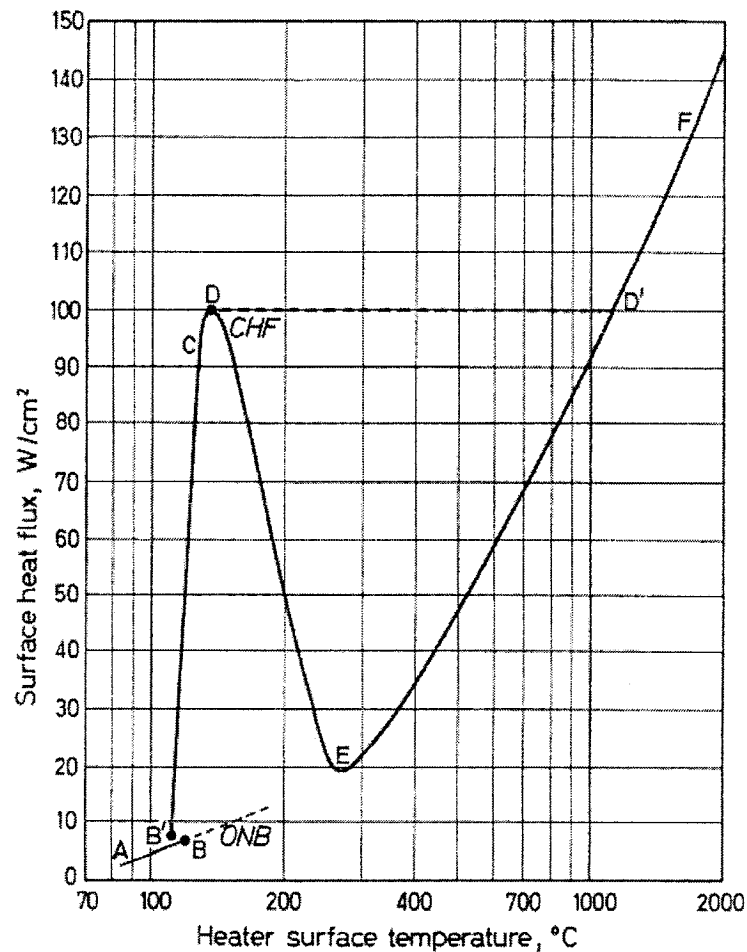
Figure 1.3: Pool boiling curve for water at atmospheric pressure.
(Collier, 1972)

to B' for the case of a constant surface heat flux. This latter behavior is associated with fluids at very low pressures, e.g., water at below atmospheric pressure and liquid metals in particular.

(c) The nucleate boiling region (B'C) where vapor nucleation occurs at the heating surface. Starting with a few individual sites at low heat fluxes the vapor structure changes, as the heat flux is increased, as a result of bubble coalescence and finally, at high heat fluxes, vapor patches and columns are formed close to the surface.
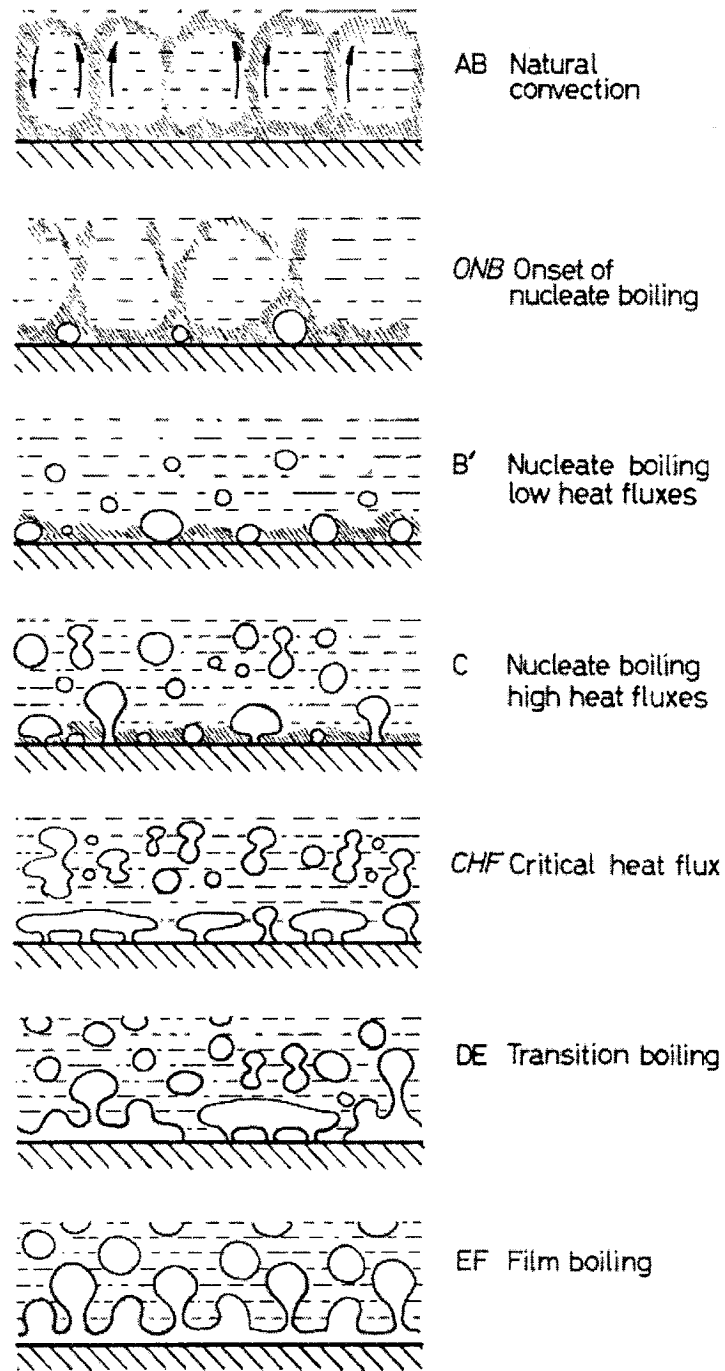
Figure 1.4: The various stages in the pool boiling curve
(Collier, 1972).

(d) The critical heat flux (CHF or point D) marks the upper limit of nucle-

ate boiling where the interaction of the liquid and vapor streams causes a restriction of the liquid supply to the heating surface.

(e) The transition boiling region (DE) is characterized by the existence of an unstable vapor blanket over the heating surface that releases large pockets of vapor at more or less regular intervals. Intermittent wetting of the surface is believed to occur. This region can only be studied under conditions of constant surface temperature.

(f) The film boiling region EF where a stable vapor film covers the entire heating surface and vapor is released from the film periodically in the form of regularly-spaced bubbles. Heat transfer is accomplished principally by radiation as the surface temperature is increased.

1.5 Forced convective boiling

We have discussed thermodynamics of liquid and steam mixture, the boiling process and boiling from a heated surface submerged in a large volume of stagnant liquid - pool boiling. When a liquid is circulated to a heated channel, the boiling process can be quite different from that of pool boiling. In the succeeding sections the forced convection boiling will be discussed in details. Due to the fact that the heat transfer modes in forced convection boiling fluids are related to the two-phase flow patterns, this subject will be discussed in the next section.

1.5.1 Flow Patterns

In order to better understand the flow boiling phenomenon, the characterization of the configuration of the liquid and vapor phase is essential. Suppose that subcooled water is fed at the bottom of a heated vertical tube, the liquid and vapor generated along the tube form a variety of configurations known as flow patterns. These flow patterns evolve from one to another along the heated length of the tube. These changes occur due to the following two reasons: firstly, the departure from thermodynamic equilibrium coupled with the presence of radial temperature gradients in the channel; secondly, the departure from local hydrodynamic equilibrium throughout the channel. The occurence of a particular flow

pattern depends on the flow conditions such as pressure, flow velocity, heat flux, and channel geometry. Figure 1.5 shows the evolution of the various flow patterns in vertical heated tubes.

Bubbly flow

The bubbly flow pattern is characterized by a continuous liquid phase, and a dispersed gas under the form of small bubbles. The upper limit of bubbly flow in tubes is between 20% and 30% void fraction.

Slug or plug flow

With increasing the content of steam, the coalescence of bubbles occurs. Eventually the bubble diameter approaches that of the tube, these big bullet-shaped bubbles are seperated by slug of liquid which contains dispersed small bubbles.

Annular flow and dispersed annular flow

Under sufficiently high vapor flow rates conditions, the liquid is pushed aside and flows along the walls of the tube forming an annulus while the vapor flows in the centre of the tube. With high velocity and large turbulence, droplets may be entrained from the liquid film towards the vapor core.

Drop flow

When the vapor velocity is very high relative to the liquid, the liquid can be sheared from the wall, and broken into droplets. The lower limit for drop flow in tubes is about 95% void fraction.

1.5.2 Heat transfer Regimes (or Boiling Regimes)

Flow boiling is generally very complicated. In addition to flow pattern changes, different vaporization mechanisms may be encountered at different locations along the tube. Nucleate boiling is usually the dominant heat transfer mechanism near the onset of boiling. As more vapor is generated in the fluid and the void fraction
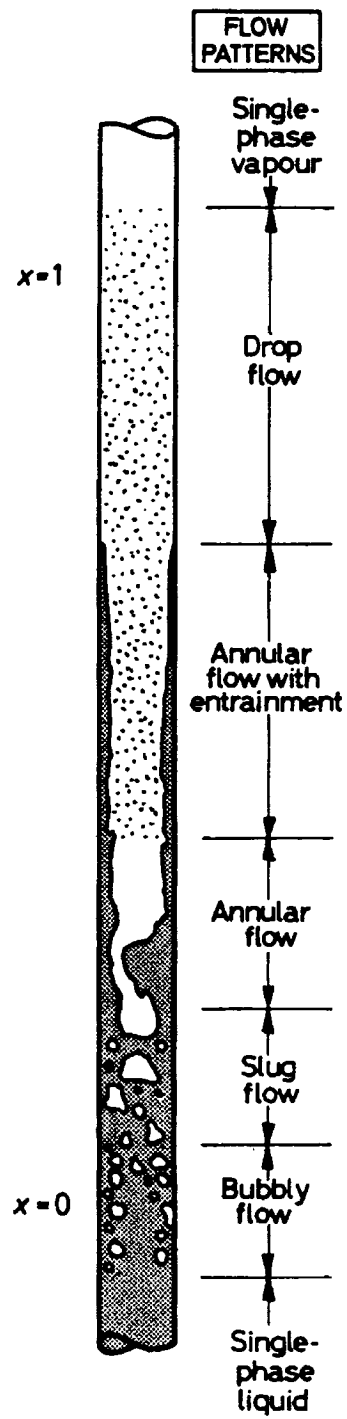
Figure 1.5: Flow patterns in a vertical evaporator tube
(Collier, 1972).

increases, the flow undergoes a transition to an annular configuration and evaporation from the liquid-vapor interface becomes increasingly important. In some cases, as the liquid film on the wall gets thinner, nucleate boiling is completely suppressed and film evaporation becomes the only active mechanism. Therefore, underneath different flow patterns, the boiling mechanism may differ. The occurrence of one or the other form of boiling depends on the heat flux at the heated surface, the flow rate, the inlet temperature of the liquid and the system pressure. Similarly to the pool boiling curve given in the Figure 1.3 for water at atmospheric pressure, the heat transfer regimes in forced convective boiling can be adequately described using the boiling curve shown in Figure 1.6.
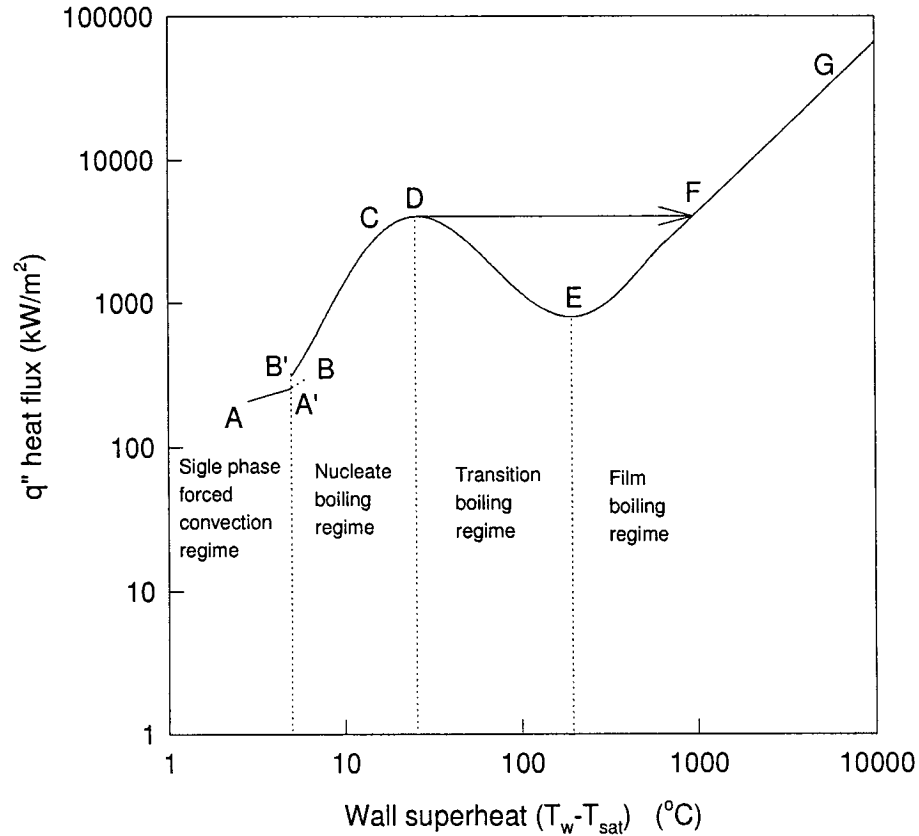
Figure 1.6: Boiling curve of a heat flux controlled surface in forced convection flow boiling of water (Deng, 1998).

The single phase forced convection regime - AA'

When a subcooled liquid is fed into a uniformly heated tube, and the tube wall temperature (Tw) is below the temperature necessary for nucleation, the process of heat transfer is single phase forced convection.

Subcooled nucleate boiling regime - A'B

Downstream of a certain point, the wall superheat becomes sufficient to cause vapor bubbles to form at the heating surface while the bulk liquid is still subcooled. This point is called the onset of nucleate boiling (ONB) - point A'. Because most of the liquid is still subcooled, the bubbles do not detach from the wall but grow and collapse while they are attached to the wall. As the bulk of liquid heats up, the bubbles start to detach and condense slowly as they move through the liquid. The point at which bubbles can depart from the wall before condensation is called the onset of significant vaporization (OSV) - point B'. The boiling and turbulence enhance heat transfer and the wall temperature ceases to rise as fast as in the single phase convection region. Since the bulk temperature is still below the saturation temperature, this regime is called the subcooled nucleate boiling regime.

The saturated nucleate boiling regime - BC

The saturated nucleate boiling regime starts when the bulk liquid temperature reaches the saturation temperature. The liquid temperature stops rising in this region because the bulk fluid has reached thermal equilibrium. Bubbly flow, slug flow and annular flow patterns can exist in the saturated nucleate boiling regime. When the bubbles become numerous, they may start to agglomerate into larger bubbles thus changing the flow pattern into slug or churn flow. As boiling continues, the bubbles merge into a vapor core in the tube while the liquid remains partially in a film on the walls and partially as entrained droplets in the vapor core. Thus, the flow becomes annular flow.

Forced convection vaporization regime - CD

The annular flow regime leads to a transition of heat transfer mechanism from boiling to evaporation. When the liquid film on the tube wall becomes too thin to maintain wall superheat to form bubbles, heat is carried away from the wall by forced convection through the liquid film to the liquid-vapor interface. The liquid film evaporates at the liquid-vapor interface. This heat transfer mode is called the forced convection vaporization regime.

The Critical Heat Flux (CHF) - point D

CHF is reached at the point where the liquid film on the wall becomes depleted owing to liquid entrainment and evaporation. The wall temperature rises abruptly since vapor heat transfer is much less efficient than liquid heat transfer. A theoretical model has been developed to predict CHF in the annular flow regime by Walley (1987). It should be noted that CHF could occur before the film "dryout" takes place. If the imposed heat flux is too high, it is possible that the vapor generation rate in the nucleate boiling regime becomes so high as to establish a vapor film that separates the liquid from the wall. This situation leads also to CHF. Due to the blanketing of the heated wall by vapor and high wall heat fluxes, this tpye of CHF provoques a very rapid increase of the wall temperature which usually destroy the heated element. Therefore, this type of CHF is called "departure from nucleate boiling".

The transition boiling regime - DE

The transition boiling regime is characterized by the existence of an unstable vapor blanket over the heating surface that releases large patches of vapor at regular intervals. However, in real systems, the transition boiling regime cannot be observed when the wall heat flux increases over CHF; a temperature jump leads the system to film boiling regime.

The film boiling regime - FG

The film boiling regime starts when a stable layer of vapor film is formed over the entire heating surface and prevents liquid from wetting the surface. Heat transfer is accomplished mainly by radiation as the surface temperature increases.

CHAPTER 2

LITERATURE REVIEW ON CHF IN VERTICAL UP FLOW HEATED TUBES

The forced convection boiling heat transfer is one of the principal and most efficient methods for cooling heated surfaces. The increase of heat transfer coefficient during the course of boiling is due to the process of evaporation and the additional agitation to the thermal boundary layer caused by the detaching bubbles generated on the heated surface. The fundamental questions posed are: what is the maximum heat flux that can be applied without damaging the heated surface and how can this limit condition be predicted?

2.1 Mechanistic models for predicting CHF

Presently, the mechanisms that bring about the CHF in forced convection boiling flows are not completely understood. One common agreement, however, is that CHF has a strong relationship with flow patterns. In subcooled nucleate boiling, the pattern is mostly bubbly flow. A variety of mechanisms have been proposed to describe the CHF phenomenon. For saturated boiling, the flow pattern is mostly annular flow; the mechanism could be quite different compared to that of subcooled boiling flow, and several concepts have been proposed. In order to discuss the research work carried out by previous investigators, it is convenient to divide the domain into two categories:

- Subcooled boiling or low quality boiling flow conditions and

- Saturated boiling flow conditions

2.1.1 CHF under subcooled or low quality boiling flow conditions

There are at least three different models that describe the CHF conditions in this region. These mechanisms are:

a) Boundary layer separation models

In this theory, it is postulated that in the subcooled liquid flow, discrete vapor bubble generating sites exist on the heating surface; CHF occurs when the liquid between the nucleation sites is forced out by the growing vapor bubbles. As a result, a continuous vapor boundary layer appears which separates the liquid from the heating surface. The correlations of Kutateladze and Leont'ev (1966) and Tong and Hewitt (1972) have been proposed to determine the occurrence of the CHF conditions based on this approach.

b) Limit of vapor removal and bubble crowding models

In this model, it is assumed that the limitation to the vapor removal rate by the axial transport of bubbles lead to the shortage of liquid flowing to the wall. Weisman et al. (1983) considered a critical value of void fraction on the bubble layer adjacent to the wall, which was brought about through the balance between the outward flow of vapor bubbles and the inward flow of liquid at the bubble-layer/bulk-flow interface.

c) Dryout of the liquid sublayer under vapor clots models

Lee and Mudawar (1988) proposed a model by assuming that the onset of CHF is a result of the dryout of a thin liquid sublayer under vapor clots flowing over the wall. Based on a similar idea, Kato (1990) assumed a vapor blanket length L_B which is equal to the critical wavelength and determined by Helmholtz instability of the liquid and vapor interface. He correlated the vapor blanket velocity U_B, with the Von Karman (1939) velocity distribution near the tube wall. CHF was assumed to occur when the liquid sublayer having an initial thickness δ is exhausted by evaporation during the passage of the vapor blanket.

2.1.2 CHF under the saturated boiling flow conditions.

Compared with the models for predicting CHF conditions for subcooled boiling or low quality boiling flow conditions, the mechanistic models for predicting CHF conditions for saturated boiling flows are far from be established. But there

are several concepts on CHF for saturated boiling flows that have been proposed: the limiting quality concept proposed by Doroshchuk (1966), the secondary circumferential flow concept proposed by Butterworth (1972) and the dispersed annular flow length concept proposed by Olekhnovitch *et al.* (1999b).

a) The limiting quality concept

Between the 1960s and 70s, the former USSR laboratories and several USA and Japanese research groups observed that in the region of dispersed annular flow, the deterioration of the heat transfer can occur at a given quality. Therefore, CHF becomes undetermined in the coordinate system (CHF, x_{cr}). Doroshchuk (1966) identified this phenomenon as "boiling crisis of the second kind". The notion of CHF losses its meaning in the boiling crisis of the second kind; that is why the terms "boiling crisis" is introduced.

The relationship between the heat flux and the critical quality, according to Doroshchuk, is represented schematically in the Figure 2.1. The curve AA'B corresponds to the boiling crisis of the first kind. Point A' represents both onset of the dispersed-annular flow and the inversion point of the influence of mass flux on the $CHF(x_{inv})$: when $x < x_{inv}$, an increase in mass flux G increases CHF, but when $x > x_{inv}$, CHF decrease with increasing the mass flux, as shown in the Figure 2.2.

According to Doroshchuk, for high heat fluxes and for pressures $P \leq 115$ bars, the dispersed annular flow appears in the subcooled flow region. For high subcoolings, the boiling crisis is introduced by the transition from nucleate boiling to film boiling. While in the case of dispersed annular flow, the disappearance of the liquid film near the heated wall is the origin of the boiling crisis. Therefore, the relation between the CHF and the quality are different for segments the AA' and A'B. In the first case, it is represented by an inclined straight line, while in the second case it is represented by a concave curve. Generally, the difference between segments AA' and A'B is quite small, that is why the experimental data in this region are treated together by a continous line AB. This line, according to
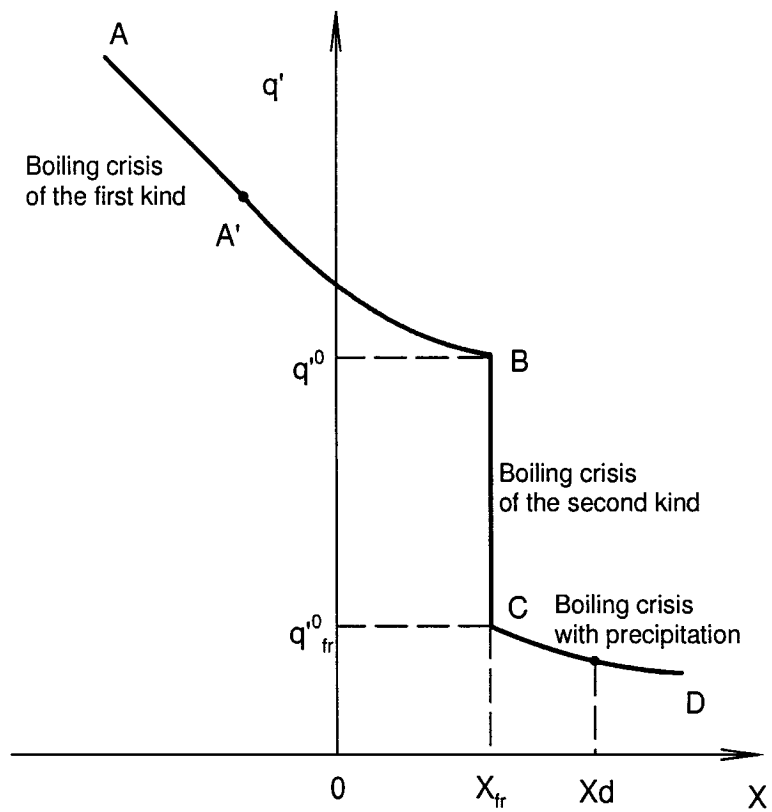
Figure 2.1: Relationship between CHF and quality (Doroshchuk, 1980);
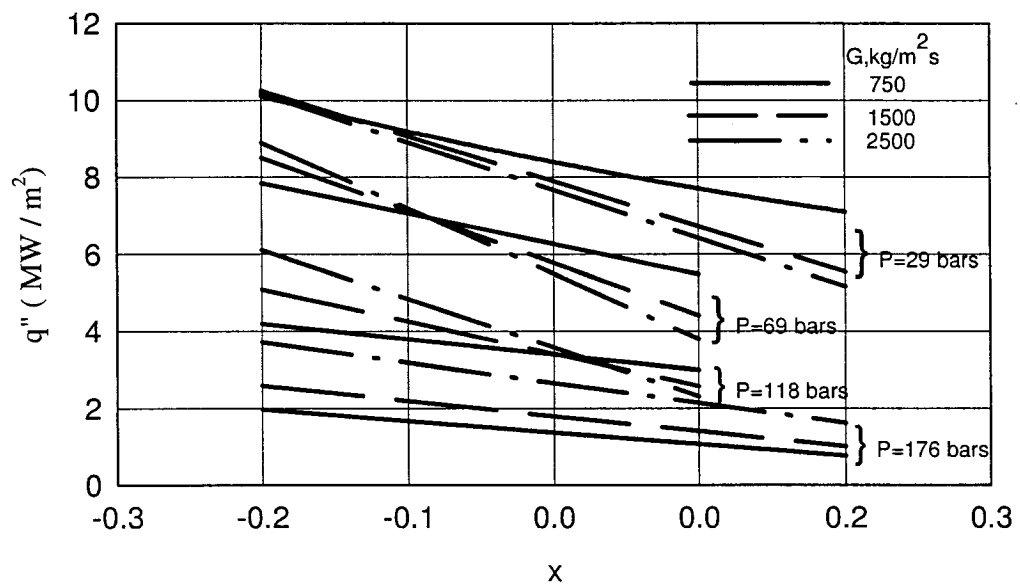
Figure 2.2: Effects of flow rate on CHF (Doroshchuk, 1980).

Doroshchuk, corresponds to the boiling crisis of the first kind.

Let's analyze the influence of mass flux on CHF. For high subcooled flow conditions, CHF increases considerably with increasing the mass flux. As the sub-cooling decreases, the influence of mass flux on CHF also decreases and at the inversion point x_{inv}, the influence of mass flux on CHF totally disappears. It is interesting to note that the inversion point x_{inv} shifts towards the higher quality region with increasing pressures and becomes positive after $P = 115$ $bars$. In order to better understanding the influence of mass flux on CHF, it is important to take into account the tube wall-wise liquid mass flux that replaces the liquid carried away by bubbles detaching from the heated surface. According to Doroshchuk, the tube wall-wise liquid mass flux depends on the transversal component of the turbulent velocity of the liquid and the hydraulic resistance of the boiling layer. The hydraulic resistance of the boiling layer depends on its thickness and the con-centration of vapor bubbles in this layer. In other words, when the temperature of the liquid increases, there is a decrease in subcooling and an increase in the thick-ness of the boiling layer which results in an increase in the hydraulic resistance. This is why the boiling crisis takes place at lower values of heat flux.

An increase in the mass flux causes an increase of the transversal component of the turbulent velocity of the liquid and hence the CHF. The maximum influence of the mass velocity on CHF takes place at the greatest subcooling when the boiling layer is not thick enough. If the subcooling decreases, the thickness of this boiling layer increases and the effect of G on CHF diminishes. This influence disappears completely when the vapor bubbles at the center of the tube coalescence to form a continuous vapor core. Therefore, a non-equilibrium thermodynamic annular flow is established. This configuration is characterized by saturated vapor in the center of the tube and a thermodynamic non-uniform liquid film (partially saturated water and partially subcooling water) near wall of the tube. The peripheral region of the vapor core condenses when it comes in contact with the subcooled liquid. On the other hand, the core is maintained by vapor bubbles that detach from the heated wall. As the mixture enthalpy increases, the degree of thermodynamic non-equilibrium of the flow decreases and the normal annular regime is gradually

established.

When thermodynamic non-equilibrium annular flow is achieved, liquid droplets are entrained in the vapor core. Some of the droplets are produced by the rupture of the liquid film by the bubbles when they detach from the heated wall, while some of the droplets are ruptured from the crest of the waves at the liquid-vapor interface by the vapor flow. For certain value of the heat flux, the combination of these two factors and the generation of vapor on the heated surface could cause, according to Doroshchuk, a loss of contact between liquid and the heated surface. If the liquid film becomes very thin, before its disappearance, boiling no longer exists in the liquid film and the heat transfer occurs directly by evaporating the liquid film at the interface. Under these two cases, it is important to note that after the formation of an annular flow structure, CHF depends on the thickness of the liquid film near the heated wall.

In summary, when $x < x_{inv}$, the increase in mass flux promotes the liquid flow to the heated surface and postpones the boiling crisis to higher heat fluxes. When $x > x_{inv}$, an increase in G causes a decrease in the thickness of the liquid film near the wall; thus, causing an increase of the tear off of the wavy liquid film surface, that decreases CHF.

Following the hypothesis of Doroshchuk (1966), let's now analyze the influence of the pressure on CHF. As the pressure increases, the latent heat of evaporation decreases. According to the author, in this case, the vapor bubbles condense very quickly and as a consequence, x_{inv} shifts to higher values. Moreover, as the pressure increases, the difference between the water density and the vapor density diminishes. For high pressures and for high qualities, the liquid film on the tube wall becomes enough thick that the boiling can occur inside the film. This signifies that nucleate boiling can take place not only in subcooled flow but also in annular liquid film as long as the quality does not surpass x_{inv}.

For certain combination of P, G and x, when the liquid film becomes very thin, waves are no longer formed on its surface. The quality at this point is called $x_{\Delta P}$ (Doroshchuk, 1980) because this quality corresponds to a decrease of the axial
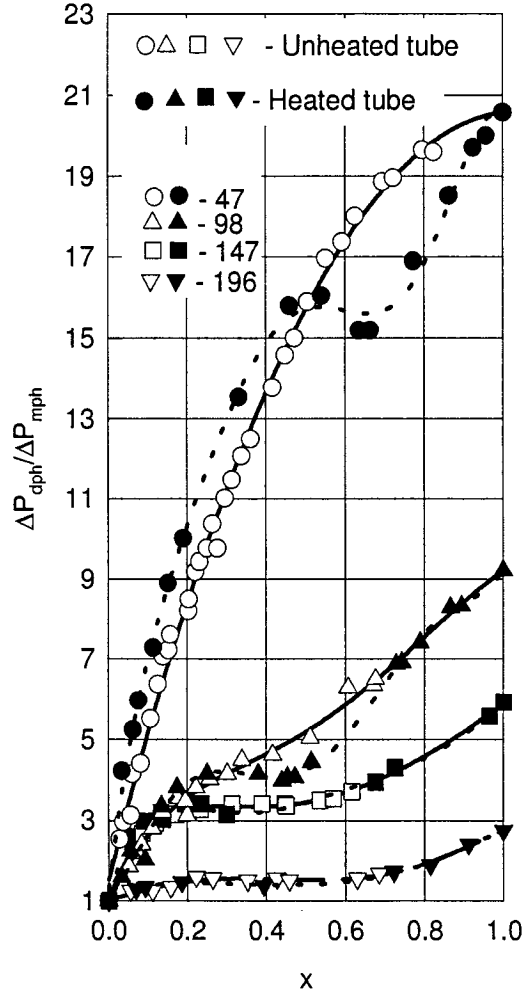
Figure 2.3: Pressure loss of two-phase flow as a function of
the thermodynamic quality (Tarasova and Leont'ev, 1965)
$(D = 8.5mm; \; L = 1.2m; \; G = 2000kg/m^2s; \; q' = 300 - 500kW/m^2)$.

pressure loss along the tube (Figure 2.3).

According to Doroshchuk (1980), this decrease can be explained by the change on the structure of liquid film surface. For $x < x_{\Delta P}$, the interface of the liquid film is very wavy, causing a higher hydraulic resistance. The disappearance of the wave on the interface, for $x > x_{\Delta P}$, diminishes this kind of resistance. It is important to emphasize that no influence of heat flux on $x_{\Delta P}$ has been found.

For $q" > q"^0_{fr}$ (where $q"^0_{fr}$ is the heat flux at point C in Figure 2.1), the water droplets present in the vapor core do not deposit on the liquid film due to the resistance from the vapor flux originated from the interface. The liquid film subsequently becomes thinner and thinner due to evaporation until a complete dryout occurs. Let's consider two sections of the channel. The first one, where the dispersed microfilm annular flow starts, and the second one, where the CHF takes place. Without the deposition of liquid droplets from the vapor core on the liquid film, the vapor flow rate between these two sections increases proportionally with the liquid flow rate inside the microfilm in the first section and the ratio of the densities of the two phases. According to Doroshchuk, the liquid flow rate inside the microfilm only depends on the mass velocity of the flow. The ratio of the densities of the two phases is determined by the pressure of the system. In consequence, we can conclude that during the evaporation of the liquid microfilm, the increase in quality, Δx, depends mainly on the pressure and the mass velocity. Considering that $x_{\Delta P}$ and Δx do not depend on the heat flux applied on the heated tube, the limiting quality: $x_{fr} = x_{\Delta P} + \Delta x$, at which the heat transfer crisis of the second kind occurs, is also independent of heat flux. In the coordinate system $(x, q")$, the region of the heat transfer crisis of the second kind is represented by the vertical line BC in the Figure 2.1.

When the water droplets present in the vapor core deposit on the microfilm (according to Doroshchuk, this takes place at very low or very high mass flux, high pressure and relatively low heat flux), the dry out of the liquid film is delayed and the heat transfer crisis occurs at x_d which is higher than x_{fr} (Figure 2.1). In this case, x_d not only depends on G and P but also on $q"$, since heat flux influences the precipitation of the droplets on the film. This kind of crisis is called "heat transfer crisis of the second kind with droplets precipitation on the film" or "precipitation crisis." The function $q"_d = f(x_d)$ is illustrated in Figure 2.1 by the curve CD. The experiments confirm that $q"_d$ increases with increasing both pressure and mass flux.

As $q"_d$ decreases, the precipitation of the droplets on the microfilm increases and as a consequence, x_d increases. For a given heat flux, an equilibrium is estab-

lished between the heat flux applied on the wall and the heat required to evaporate the droplets deposited on the film. Thus the graphical representation of the function $q"_d = f(x_d)$, tends to an asymptotic value. Note that the precipitation crisis occurs at low heat flux and causes less damage than the boiling crisis of the first kind and the second kind without droplets precipitation.

In analyzing the results and the observations of Doroshchuk, Hewitt (1978) had made the following remarks:

- The form of the curves presented in Figure 2.1 is not always observed in the experiments when subcooled water was used at the entry of the test sections;

- In most experiments of the former USSR, in the domain of limiting quality, the two-phase mixture had been used as inlet flow to the test tube. The inlet flow conditions (subcooled liquid or steam water mixture), and the L/d ratio, have certain influence on the CHF. Hence the generality of this curve is doubtful.

- For given inlet flow conditions, it is observed that the critical quality is practically independent of the tube length. Experiments where the liquid flow rate in the film was measured as a function of local quality, have demonstrated that the entrainment of droplets in the first part of the tube is approximately counterbalanced by the precipitation in the second part of the tube (Figure 2.4). Therefore, the fact that the critical quality is constant can be explained without the hypothesis that there are no droplets precipitation on the liquid film.

"The recommendations about the critical heat flux" of the Academy of Science of USSR (1980) are based on the concept of the boiling crisis of the first kind and the boiling crisis of the second kind. They are presented in two tables: the first one gives the values of critical heat flux as a function of pressure, mass flux and quality, and the second one gives the value of the limiting quality. The values of CHF and limiting qualities have been obtained experimentally, for a given pressure and mass
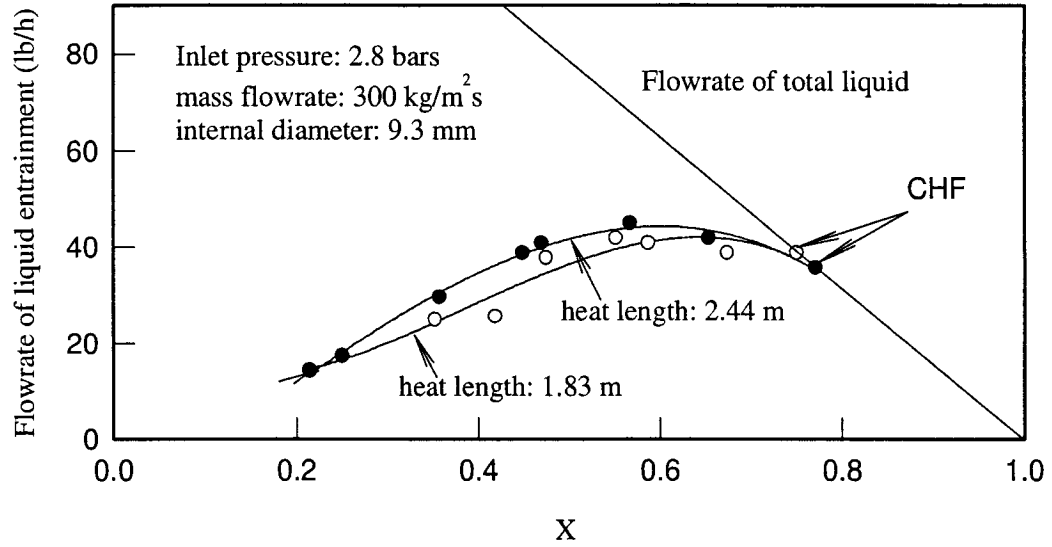
Figure 2.4: Liquid entrainment (Bennett *et al.*, 1966)

flux. Levitan and Borevskiy (1989) had proposed the following formula to calculate the thermodynamic quality that corresponds to the onset of the dispersed annular flow:

$$x_{dan} = (2.7 \pm 0.3) We_f^{-0.25} \left(\frac{\rho_f}{\rho_g}\right)^{-0.33}, \tag{2.1}$$

where:

$We_f = G^2 D/\rho_g \sigma$ is the Weber Number of the liquid film;

ρ_f and ρ_g are the density of the liquid and the steam respectively;

σ is the surface tension.

The relationship for calculating the limited quality, x_{fr}, has been determined (Levitan and Orlova, 1990) from the entrainment diagram for adiabatic two-phase flow. This is obtained by tracing the horizontal tangential line until it intersects the line $(1 - x)$ representing total liquid flow rate which yields:

$$x_{fr} = 6.57 \times 10^{-3} \left(\frac{\sigma}{\mu_f}\right) \left(\frac{\rho_g}{\rho_f}\right)^{0.125} \left(\frac{\rho_f \rho_g}{G^2 gD}\right)^{0.25}, \qquad (2.2)$$

where μ_f is the dynamic viscosity of the liquid.

The values obtained by this relation have been compared with the values presented by the Academy of Science of the USSR (1980). The agreement between predicted values given by this relation and those obtained experimentally (Figure 2.5) is satisfactory.
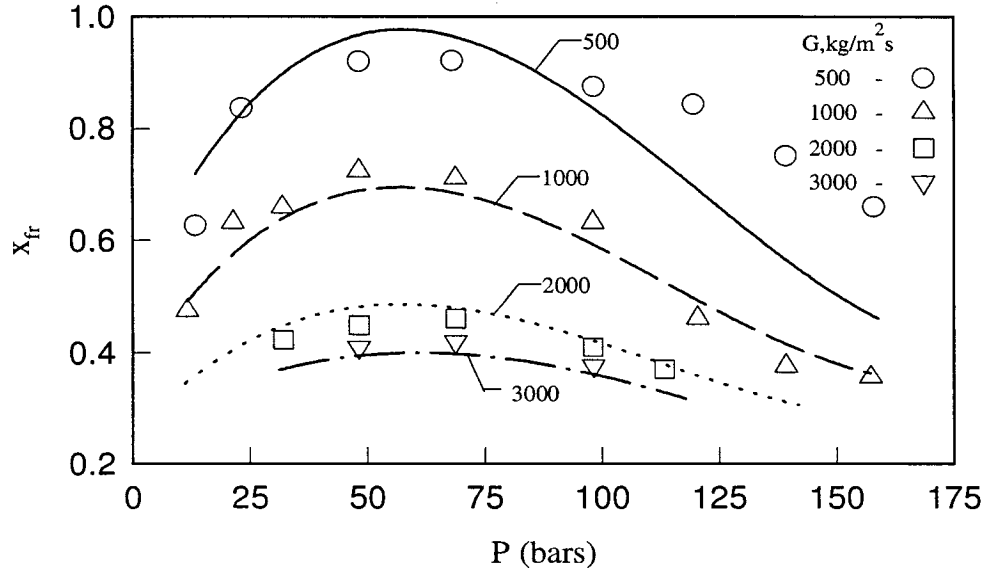
Figure 2.5: The limited quality vs. flow pressure (Levitan and Boreveskiy, 1989)

b) Secondary circumferential flow concept

Butterworth (1972) made an analytical study on vertical up flow tubes and developed the secondary circumferential flow concept approach for non-uniform heating conditions. The mechanism proposed by Butterworth to explain the CHF phenomena is based upon the existence of a secondary circumferential flow of the liquid around the tube inside surface. As the local peak heat flux location approaches the operating conditions associated with CHF in a uniformly-heated

tube, a circumferential flow of liquid from the lower heat flux regions to the peak heat flux region occurs. This circumferential flow, which is imposed upon the existing axial flow, makes it more difficult for a stable vapor film to develop on the inside wall of the tube. Therefore, a higher local heat flux is required at the peak heat flux location before the CHF can occur.

At high qualities, the distinct annular film and low (if any) void fraction near the tube wall would enhance a secondary circumferential flow; thus, tending to cause the CHF mechanism to rely on the average heat flux instead of the local value.

At the other extreme (subcooled boiling), the lack of a distinctive annular film and high void fraction near the tube wall would tend to retard or prevent the secondary circumferential flow from taking place; thus, making the CHF highly localized.

Butterworth analyzed a circumferential film spreading model for the annular flow regime, that permited him to write:

$$\frac{\overline{q}_{cr}}{q_{cr}} = \frac{1}{1 + (D_i^2/Kz)\alpha},$$ (2.3)

$$\alpha = \frac{q_{cr}^{max}}{\overline{q}_{cr}} - 1,$$ (2.4)

where:

$\overline{q}_{cr}$ is the average critical heat flux for nonuniform heating conditions;

q_{cr}^{max} is the local peak heat flux for nonuniform heating conditions;

q_{cr} is the critical heat flux for uniform heating conditions;

D_i and z are the internal diameter and heated length of the tube, respectively;

K represents a spreading coefficient for the secondary circumferential flow, assumed to be 0.9.

c)The dispersed annular flow length concept

Olekhnovitch *et al.* (1998) conducted a study on the critical heat flux under low-pressure vertical flow conditions. A total of 476 CHF points were obtained using a uniformly heated tube having an internal diameter of 8 mm. The experimental conditions used for these tests were:

Heat length	0.75 - 3.5 m;
Tube wall thickness	1.0 and 2.0 mm;
Mass flux	1000 - 6000 kg/m^2s;
Pressure	5 - 40 $bars$;
Flow quality	5 - 75%.
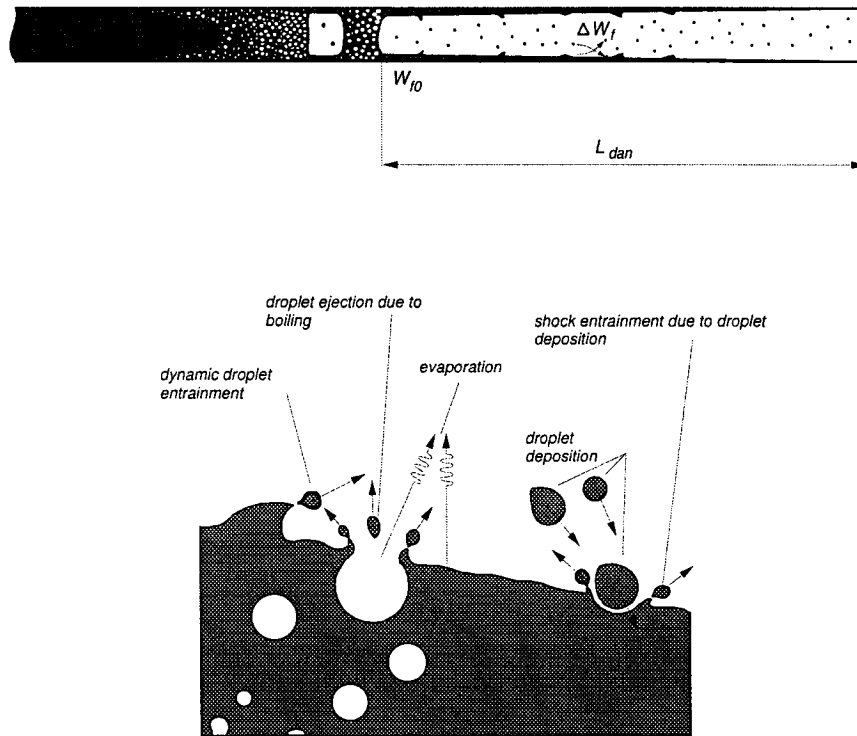
Figure 2.6: Principal parameters and basic mass transfer mechanism of diabatic dispersed-annular flow(Olekhnovitch*et al.*, 1999b).

The results of the experiments have shown that for heated length $L \geq 0.75m$ and mass flow rate $G \leq 6000\ kg/m^2s$, the critical quality was always positive and its value was never lower than 5%. At low pressures, the density of the liquid phase is considerably greater than that of the vapor phase, the void fraction corresponding to these qualities are therefore very high ($\alpha \sim 0.9$). Under these conditions, it may be assumed that the CHF takes place when the flow structure is the dispersed annular flow. It is further assumed that the critical phenomena come about as a result of the dryout of the liquid film due to evaporation. Thus, neglecting the pressure loss along the heated length, the condition of disappearance of the liquid film at the end of the heated length is written as (Figure 2.6):

$$\pi \cdot D \cdot L_{dan} \cdot CHF = h_{fg}(P_{out}) \cdot (W_{f0} + \Delta W), \qquad (2.5)$$

where L_{dan} is the length over which the dispersed annular flow takes place; W_{f0}, the mass flow rate in the liquid film at the point where the dispersed annular flow is formed; ΔW_f is the total change in the film flow rate over the length L_{dan} caused by various mechanisms such as:

- Entrainment of droplets from the surface of the liquid film by the vapor core;

- Deposition of droplets entrained in the vapor core back to the liquid film;

- Ejection of droplets from the liquid film into the vapor core due to the droplet impact on the interface;

- Ejection of droplets from the liquid film into the vapor core due to boiling (for diabatic flow only).

Under adiabatic flow conditions the formation of dispersed annular flow takes place at a given void fraction or at a certain quality which is dependent on the pressure and the mass flow rate. The mass flow rate in the liquid film at the point of onset of this flow pattern is equally determined by the same parameters, that is P and G. In the case of diabatic flows, the development of the dispersed annular

flow region can be affected by the vapour generation on the heated surface. This can cause an entrainment of the liquid from the wall towards the centre of the tube by the vapour bubbles upstream of the point where dispersed annular flow occurs. The rate of vapour generation is directly related to the heat flux. It can thus be postulated that for diabatic flows the film mass flow rate, W_{f0}, depends on the pressure, the mass flow rate and the heat flux:

$$W_{f0} = f_1(P, G, CHF). \tag{2.6}$$

The intensity of the mechanical mass transfer (i.e., not due to evaporation) between the liquid film and the vapor core is influenced by a number of factors. It is quite likely that the intensity of each of the aforementioned mechanisms can be represented as a function of the local flow parameters. However, it is clear that, for a given pressure, mass flow rate and length L_{dan}, it is the heat flux and the liquid film mass flow rate, W_{f0}, which will have the greatest influence on this mass transfer. For example, the intensity of the droplet deposition, and thus the intensity of the ejection of droplets from the liquid film into the vapor core due to this deposition are determined by the forces of the vapor phase acting on the droplets. However, beyond the onset of the dispersed annular flow, it is only the heat flux that influences the hydrodynamic conditions in the vapor core, specifically, the local vapor velocity and the normal vapor mass flux which can prevent droplets from being deposited on the liquid film. The mechanical entrainment of droplets from the liquid film also depends on the velocity of the vapor as well as the mass flow rate in the liquid film. The latter being dependent on the initial film flow rate, W_{f0}, and on the intensity of the evaporation of the liquid film and consequently on the heat flux. Finally, the intensity of ejection of droplets due to boiling, if it takes place in the liquid film, depends only on the heat flux. Generalizing the above arguments, the total change in the liquid film flow rate over the length L_{dan} can be defined by the following relationship:

$$\Delta W_f = f_2(P, G, L_{dan}, CHF). \tag{2.7}$$

The Equation (2.5) may therefore be expressed in the following functional form:

$$\pi \cdot D \cdot L_{dan} \cdot CHF = h_{fg}(P_{out}) \cdot [f_1(P, G, CHF) + f_2(P, G, L_{dan}, CHF)] , \quad (2.8)$$

or

$$CHF = f(P, G, D, L_{dan}). \quad (2.9)$$

The length L_{dan} can be determined by using the critical quality. Based on a heat balance, this length can be expressed by the following relationship:

$$L_{dan} = \frac{G h_{fg}(x_{cr} - x_{dan})D}{4CHF} \quad (2.10)$$

and the critical quality is calculated by a heat balance as:

$$x_{cr} = \frac{1}{h_{fg}} \left(\frac{4\pi L \cdot CHF}{GD} - \Delta h_{sub} \right) . \quad (2.11)$$

The determination of the length L_{dan} requires the knowledge of the thermodynamic quality x_{dan} corresponding to the onset of the dispersed annular flow. Equation(2.1) proposed by Levitan and Borevskiy (1989) can be used for this purpose. This correlation is based on the use of a large data bank obtained from holographic studies of adiabatic two-phase flows. Levitan and Orlova (1990) also recommended this correlation for diabatic flow conditions.

Up to now, it has been assumed that the pressure does not change along the heated length and is equal to the outlet pressure. The pressure loss which are normally quite high under low pressure two-phase flow conditions can be taken into account if the quality x_{dan} is calculated in terms of the inlet pressure (for simplicity it will be assumed that the pressure drop upstream of the onset of

dispersed annular flow is negligible). Carrying out a heat balance for the region upstream of x_{dan} one obtains:

$$x_{dan} \cdot h_{fg}(P_{in}) = h_{in} + 4CHF \cdot [L - L_{dan}(P_{in})] / (GD) - h_f(P_{in}). \qquad (2.12)$$

Arranging the Equation(2.12), one obtains a new correlation for calculating L_{dan} given by:

$$L_{dan} = L - \frac{G \cdot D \cdot [x_{dan} \cdot h_{fg}(P_{in}) - h_{in} + h_f(P_{in})]}{4 \cdot CHF}. \qquad (2.13)$$

The experimental results show that the representation of the CHF as a function of dispersed annular flow length can reduce the scatter of the data considerably, compared with the representation of the CHF as a function of the thermodynamic quality (Olekhnovitch et al., 1999a). The Figure 2.7 and the Figure 2.8 show the comparisions between two CHF representations. According to Olekhnovitch et al. (1999b) this is due to the mass flow rate in the liquid film at the point of inception of dispersed annular flow and applied heat flux which seems to be the variable that controls the CHF phenomena.
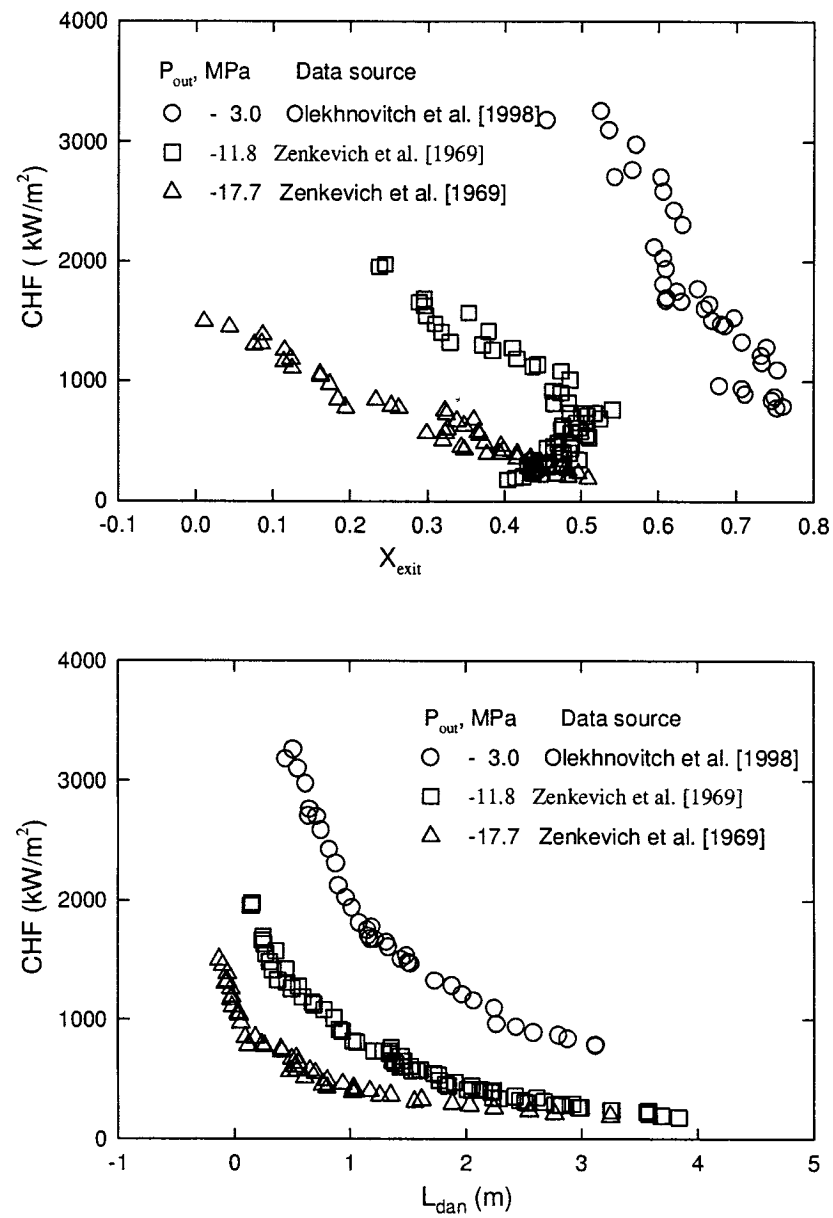
Figure 2.7: A comparison between two CHF representations under different outlet pressure conditions (Olekhnovitch *et al.*, 2000a).
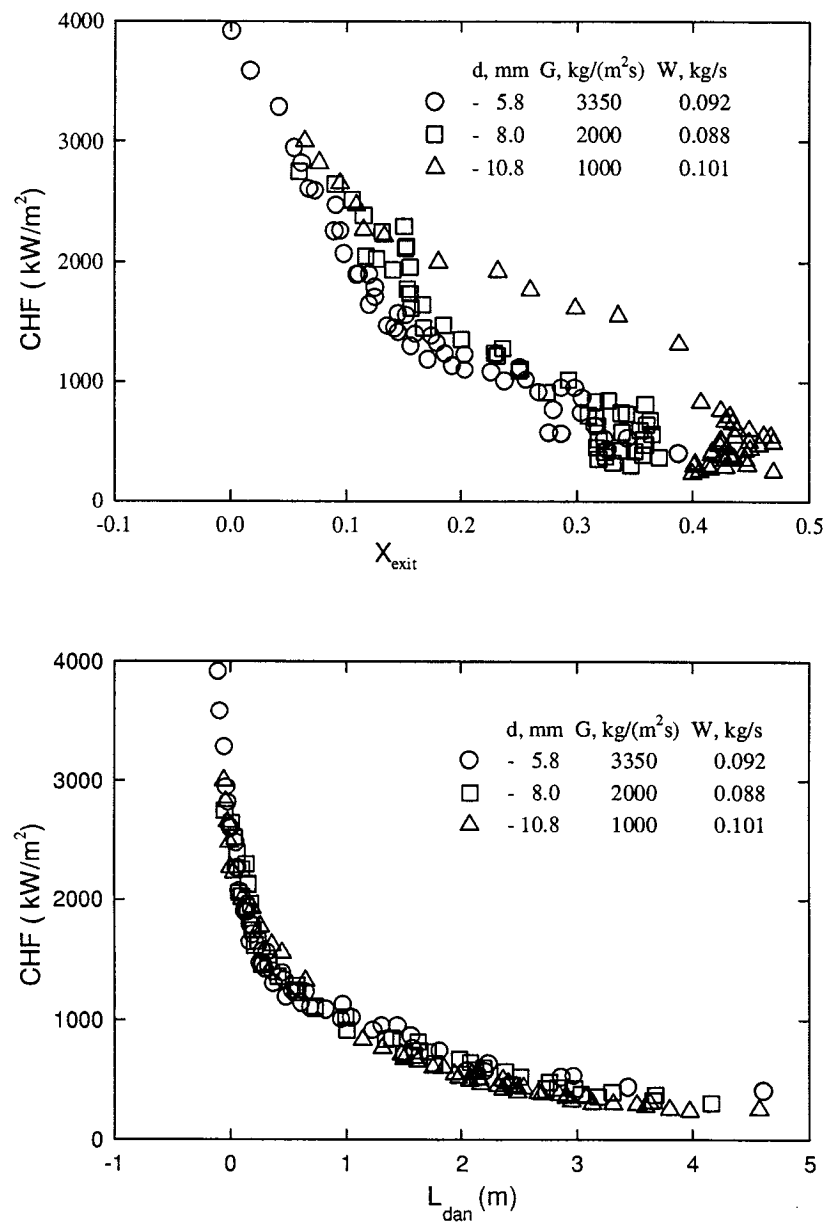
Figure 2.8: A comparison between two CHF representations
for different diameters(Olekhnovitch *et al.*, 2000a).

2.2 Review of CHF experiments carried out

using non-uniform heated tubes

As compared with the research work carried out on CHF under uniform heating conditions, fewer are the investigations that have been conducted experiments on CHF under nonuniform heating conditions. However, in industrial application, CHF under nonuniform heating conditions are more common than CHF under uniform heating conditions. Moreover, to some extent, CHF under uniform heating conditions can be considered as a special case of CHF under nonuniform heating conditions, where the nonuniformity becomes to one.

The former USSR scientists (Alekseev *et al.*, 1965; Glusker *et al.*, 1985; Gendelev *et al.*, 1988) conducted CHF research under nonuniform heating conditions similar to those encourtered in high capacity boilers. The result is very practical for guiding boiler operation, but due to the limitation of test conditions the analyses are more qualitative than quantitative. Glusker *et al.* (1985) conducted CHF experiment on water-wall tubes of supercritical boilers during the boiler unloading at variable pressure in the steam-water circuit. The results of these tests have shown that deteriorated temperature conditions could arise in tubes subjected to stratification even when the mean vapor content on the heated surface is less than the limiting quality value. In one of the cases, the deteriorated temperature condition developed in the peripheral tubes of the central panels of the boiler, where, due to nonuniform distribution of steam-water mixture, the inlet steam quality could locally exceed the limiting quality.

The Doroshchuk (1966) limiting quality is used to determine boiling crisis of the second kind in Glusker *et al.* (1985) research. The data showed that the boiling crisis of the second kind develops in the water walls of boilers operated at variable pressure, when working steam quality of the medium (x_w) reaches or exceeds the limiting quality (x_b). However, test results showed that the Doroshchuk's calculation of the limiting quality for one-sided heating tubes results in an overestimation which can lead to incorrect evaluation of temperature conditions on the heated surface.

The results of the tests also have shown that the deterioration in temperature conditions of water wall tubes occurred at flow pressures of 13 to 17 MPa. Within this range of flow pressures it is difficult to ensure a high convection heat transfer because in this case x_b between 0.3 and 0.5, that corresponds to the steam quality of the mixture in the water walls tubes under a variable pressure.

Alekseev *et al.* (1965) carried out circumferential nonuniform heating CHF tests in tubes. The experimental conditions were as follows:

Heated length	400 mm;
I.D.	10 mm;
Mass flux	500 - 5000 kg/m^2s;
Pressure	58.8 - 176.6 $bars$;
$q^{"}{}_{max}/q^{"}{}_{mean}$	1.0,1.2,1.28,1.5.

The results of the tests have shown that CHF is inversely related to the pressure and when the mass flux increases the dependence of CHF on the pressure decreases. Also, CHF is inversely related to the inlet enthalpy of the water, which has an influence that increases with the mass flux. As per the effects of nonuniformity on CHF, the results show that the mean CHF drops as $\frac{q^{"}{}_{max}}{q^{"}{}_{mean}}$ increases. The influence of nonuniformity on CHF falls with increasing pressure and mass flux.

Becker *et al.* (1988) performed heat transfer tests for a water flow in a high-pressure test loop using a tube of 7 m in length and 24.69 mm I.D. that was heated on one side. For the simulation of one-side heating, the tube was silver-plated over one-half of its circumference. The measurements were carried out for pressures between 50 and 200 $bars$, mass fluxes between 500 and 2500 kg/m^2s and hot side heat fluxes of up to 1157 kW/m^2. For the circumferentially nonuniform heated tube, the results showed that the occurrence of the boiling crisis is controled by local variables, similarly to the observations of Doroshchuk, i.e., local hypothesis for uniformly heated tubes. Therefore the measured CHF can be predicted fairly well by means of the model developed by Doroshchuk for uniformly heated tubes.

The combined effects of nonuniform circumferential heating and tube inclination on CHF have been investigated by Kitto and Wiener (1982). In order to produce the nonuniform heat flux, they welded Inconel bars longitudinally to one side of stainless steel tubes. The nonuniform electrical resistance of the tube allowed them to attain nominal peak-to-average heat flux ratios ($q"_{max}/q"_{mean}$) of up to 2.05. Steam/water flows at 186 $bars$ were studied for 15°, 30° and 90° inclinations from the horizontal. The parameters chosen for carrying out this study are as follows:

Heat length	5385 mm/ (5334 mm, ribbed);
Inside diameter /equivalent volumetric average diameter	38.6 mm/(37.9 mm, ribbed);
Mass flux	271 - 1760 kg/m^2s;
Pressure	18.6 MPa;
$q"_{max}/q"_{min}$	3.96;
$q"_{max}/q"_{mean}$	2.05/(1.91, ribbed);
Outlet thermodynamic quality	-60% to 100% SBW.

Based on the results obtained from these experiments, the following effects were observed:

- The CHF corresponding to nonuniform peak heat flux was always greater than the uniform average heat flux.

- At low thermodynamic qualities or high inlet subcoolings, the CHF for nonuniform peak heat flux seems to approach to that the uniform average heat flux, indicating that CHF is a function of the local flow variables.

- As the thermodynamic quality is increased, (from nucleate boiling to annular/convective boiling), the CHF for nonuniform average heat flux appears to approach to that of uniform average heat flux, indicating that CHF is a function of averaged flow variables.

- For inclined smooth tube, the CHF for nonuniform peak heat flux coincides

with that of uniform mean heat flux.

The results obtained with a vertical tube agreed with the theoretical study of Butterworth (1972). Comparing this method to their data, Kitto and Wiener (1982) found a very good qualitative agreement, however they have noted that the spreading coefficient for the secondary circumferential flow, K, should be made a function of vapor quality instead of having a constant value of 0.9.

Narial et al. (1993) investigated CHF of subcooled boiling of water flowing in tubes under peripherally nonuniform heating conditions. The thickness of the tube wall was partly reduced in order to simulate the nonuniform heat flux condition. Experiments were conducted, both with and without internal twisted tape (straight tube), for tubes exposed to extremely high heat flux conditions (5 - 25 MW/m^2), similar to those that would be used in the future fusion reactors. The parameters chosen to carry out this study were:

Mass flux of (water):	4000, 7000 kg/m^2s;
Inlet temperature:	about 40^oC;
Outlet pressure:	0.1, 0.6, 1.1, 1.5 MPa;
Heated length:	100 mm;
Inside diameter:	6 mm;
Tube wall thickness:	0.35 mm for thicker part
	and 0.15 mm for thinner part;
Thinned part angle:	$180, 90, 0^0$.

In straight tube, the local peak heat flux (the maximum heat flux) for CHF under nonuniform heating condition was slightly higher than the CHF under uniform heating condition. According to Narial et al. (1993) this is due to the relative lower thermodynamic qualities at the outlet under nonuniform heating condition compared with the uniform heating condition.

In tubes with an internal twisted tape, the local peak heat flux (the maximum heat flux) at the CHF under nonuniform heating condition was higher than the CHF under uniform heating condition by 20 to 60%, even though the average

qualities were almost the same as those under uniform heating condition. The effect of nonuniform heating on CHF was explained by the alternate development and disruption of bubble boundary layer.

To some extent, Narial's research work (1993) confirmed the existence of Butterworth's (1972) secondary circumferential flow mechanism, both in nonuniform heating with and without internal twisted tape (straight tube). In general, stronger secondary circumferential flow could be produced with the existence of internal twisted tape.

Remizov and Sapankevich (1975) studied the dependence of burnout on the nonuniformity of the heat flux over the tube perimeter for pressures of 255, 981, and 1765.8 N/cm^2, thermodynamic quality in the burnout zone varied from -0.2 to 0.8 and mass flux from 200 - 2000 kg/m^2s. The inside diameter of the test section was varied from 8.8 to 10.2 mm and the heated length from 0.2 to 0.6 m. The results have shown that burnout always occurred at a point of the perimeter of the tube where the heat flux was a maximum.

Remizov and Sapankevich (1975) observed that in the subcooled water region the curve for q_{cr}^{max} has a tendency to converge to the curve for q_{cr} in a uniformly heated tube with the same thermodynamic quality. In the region of high thermodynamic quality these curves diverge, the critical heat flux in a uniformly heated tube been lower.

The influence of nonuniform heating on CHF shows that the higher the heat flux nonuniformity $\frac{q''_{max}}{q''_{mean}}$, the lower the average values of CHF, for the same thermodynamic quality in the burnout zone. However, with increasing the pressure the effect of nonuniformity on the average values of CHF diminishes.

The combined effects of nonuniform circumferential heating and tube internal diameter on the critical heat flux show that for small inside diameter (I.D.= 6 mm), the nonuniform heating affects only the maximum CHF, while the average value of CHF is independent of the heat distribution. The effect of nonuniform heating on the maximum CHF decreases considerably with increasing I.D.

Miropol'skii (1958) compared CHF results obtained with uniform and nonuniform heated tubes having $I.D. = 6.0$ mm, heat length $L = 150$ mm $(L/D = 25)$ and $I.D. = 18.65$ mm, $L = 500$ mm $(L/D > 25)$ for pressures ranging from 2.5, 9.8 and 17.6 MPa and mass fluxes of $200 - 2000kg/m^2s$. In both uniform and non-uniform heated, the nature of the limiting quality was preserved but the values of q_{cr} with nonuniform heating were 1.6 - 1.8 times higher than those for uniform heating. He observed that CHF increases with increasing the $(q"_{max}/q"_{mean})$ from 1.5 to 3.7 and the $\frac{q"_{max}}{q"_{min}}$ from 3 to 18. However the effect of nonuniform heating decreased with increasing the pressure from 9.8 to 17.6 MPa. A formula has been proposed for calculating a critical heat flux ratio given by:

$$\frac{q"^{max}_{cr}}{q"^{0}_{cr}} = 1 + 12\frac{1 - 0.4x}{Pe_f^{0.5}Pr_f^0}\left(\frac{q"_{max}}{q"_{mean}} - 1\right), \qquad (2.14)$$

where q^0_{cr} and q^{max}_{cr} are critical heat flux under uniform and nonuniform heating respectively; Pe_f and Pr_f are Peclet and Prandtl Numbers for the liquid phase.

Gendelev *et al.* (1988) investigated the combined effects of nonuniform circumferential and axial heating on the CHF. The test section was 10 m long with a I.D. of 20 mm, that consisted of nine pairs of half-meter segments welded together. The cross section of the tube wall thickness of each pair was calculated in conformity with the curves of distribution of heat fluxes over the height and perimeters. The nonuniformity of heating over the height was adopted in correspondence with the nonuniform heating typically observed in the furnaces of high-capacity boilers. This axial heat flux distribution was obtained by increasing the cross section area of the tube wall thickness of each segment. Nonuniformity of heating over the perimeter was obtained by fabricating tubes with nonuniform wall thickness over the perimeter. The principal parameters used to carry out this study are:

Heat length	10 m;
Internal diameter /equivalent volumetric average diameter	20 mm;
Mass flux	500 - 1500 kg/m^2s;

Outlet pressure	11.8,14.7,17.6,19.6 MPa;
Heat flux	150 - 700 kW/m^2;
Outlet thermodynamic quality	10% to 90% SBW.

The results were presented in a x_{cr}, $q"_{cr}$ coordinate system; thus, the existence of various characteristic regions can be clearly observed: in the region of subcooling or low void fraction, a linear relationship between CHF and $x_{cr}(q)$ existed (CHF decreases with increasing of x_{cr}), In the region of dispersed flow regime an almost independent or very slight dependence on x_{cr} (x_{cr} in this region is called as x_{fr},limiting quality, by Doroshchuk) on q" was observed and, finally, in the region of low heat fluxes an increase in x_{cr}, with decreasing the heat flux was observed. This condition corresponds to the crisis of the second kind with precipitation. The region where x_{fr} exists decreases with increasing both the mass flux and the pressure.

The effect of nonuniform heating increases with increasing the flow pressure: the relative difference between the critical quality with nonuniform and uniform heating $\delta x = (x_{cr,nonunif} - x_{cr,unif})/x_{cr,unif}$ increases from -(40 -50)% at $P =$ 11.8 MPa to (40 -50)% at $P = 19.6$ MPa. For $P = 14.7$ MPa, there is practically no difference in the critical quality, i.e., in this case the effect of nonuniform heating seems to be insignificant.

Humphries et $al.$ (1984) carried out CHF experiments for both uniform and side-heated vertical tubes of 32 mm and 53 mm bore up to 10 m long for pressures ranging from 110 to 205 $bars$ and mass flux from 400 to 3300 kg/m^2s. Test results showed that for dryout at low steam qualities, the peak heat fluxes for the side-heated tubes are comparable to the CHF for uniformly heated tubes. At high dryout steam qualities the circumferential average heat fluxes of the side-heated tubes are comparable to the CHF for uniformly heated tubes. However the dryout behavior at intermediate steam qualities is more complex, some times involving sequencial areas of rewetting and dryout. The effect of nonuniform heating on CHF shows that the values of CHF increases with increasing the degree of nonuniformity.

CHAPTER 3

EXPERIMENTAL FACILITY AND PROCEDURES

3.1 The heat transfer loop

The experiments presented in this document have been carried out by using the École Polytechnique steam-water thermal loop. The principal operating characteristics of the heat transfer loop are:

Thermal power	10 - 400 kW;
Operating pressure	3 - 40 $bars$;
Water flow rate	0.05 - 1.7 kg/s;
Test section inlet sub-cooling	0 - 100 $^{\circ}C$.

The Figure 3.1 shows a diagram of the test facility. It consists of a steam drum, a condenser, a circulating pump, a heat exchanger, two pre-heaters and a test section. Heat is produced directly in the test section by the Joule effect using a direct current (DC). The DC power is controlled from the primary side of a power transformer with silicon controlled rectifiers (SCRs). To provide the test section with the required DC voltage (up to 100 V) the output from the power transformer is rectified by a three phase bridge. Depending on the electrical resistance of the test section, the maximum current through the test section may be up to 5000 A. In order to reduce any current fluctuations which could induce electrical noise in the instrumentation, a high power low pass filter is connected between the rectifiers and the test section. It provides a 40 dB reduction in noise.

The steam drum - condenser system allows the pressure at the exit of the test section to be accurately controlled. The degree of subcooling at the inlet of the test section is controlled by means of two preheaters connected in series which can deliver up to 75 plus 15 kW of additional heating power. To ensure a minimum of dispersed solid particles and dissolved oxygen, the water is chemically treated

and its quality is periodically verified. Since high temperature and pressure runs tend to deteriorate the quality of the water, the inventory of the loop is regularly replaced.
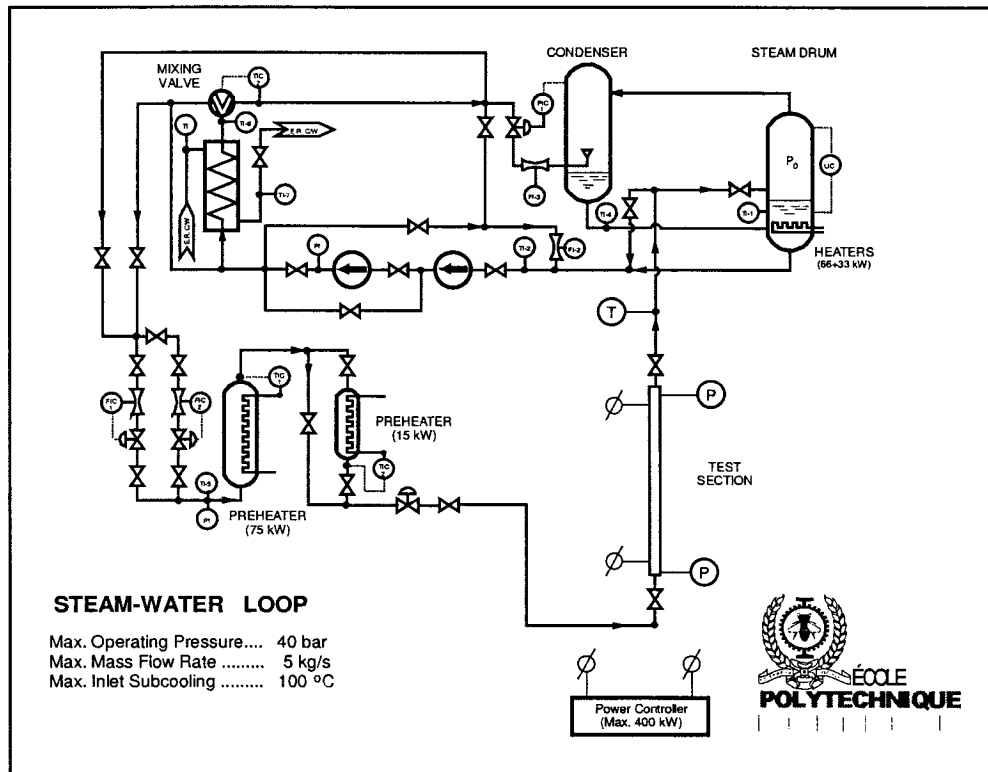
Figure 3.1: The heat transfer loop.

3.2 The test section

The experimental data presented in this thesis has been obtained on three 3.55 m long vertical test sections having an inside diameter of 22.2±0.1 mm. Two of them are manufactured from X-strong SS316 tubes with eccentric geometry. The third test section with a uniform wall thickness is used to obtain reference CHF data. The difference in wall thickness allows us to obtain heat flux ratios, $\frac{q''_{max}}{q''_{min}}$, of 4.7 and 8.3. The Figure 3.2 shows a cross-sectional view of the nonuniformly heated test sections. In order to easily change the test section a "Swagelok" design in conjunction with standard stainless steel flanges has been used to connect it to

the rest of the loop. The electric potential from the power controlled is applied to the test section by means of two copper clamps; by moving the upstream clamp different heated lengths can be obtained. In order to assure an appropriate electric contact, the copper clamps are silver braced on the test section. The thermal expansion of the test section is absorbed by a special constant tension device which avoids the deformation of the tube.

$q''max/q''min=4.7$ $q''max/q''min=8.3$
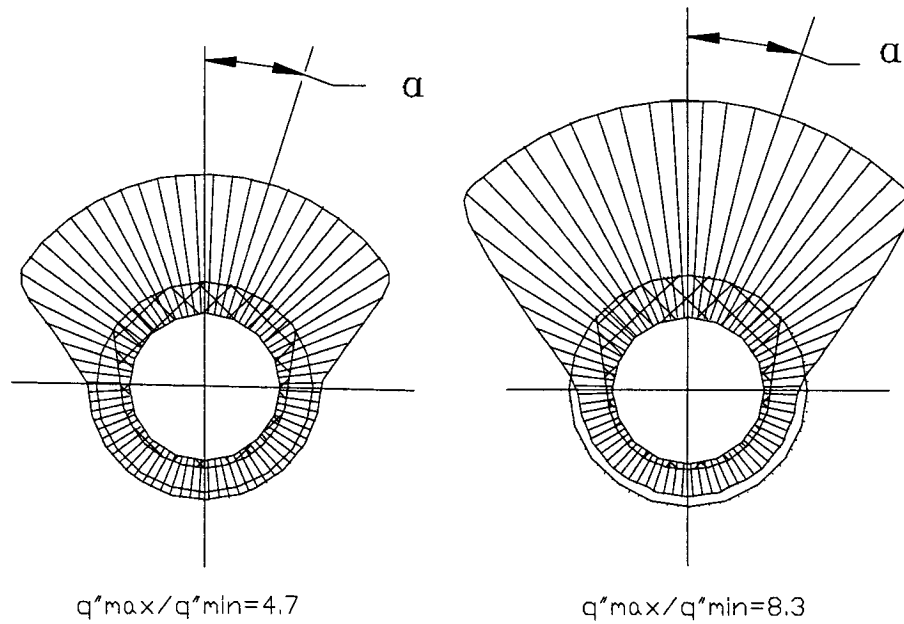
Figure 3.2: Cross-sectional view and heat flux distribution of the non-uniform heated test sections.

To ensure that the test section is not affected by successive CHF experiments, its external surface has been frequently checked by visual inspection; if any deformation of the test section is observed, it is replaced by a new one.

3.3 The instrumentation

The test sections are instrumented with thermocouples to detect the incipient dryout and to trip the power controller. The Figure 3.3 shows the arrangement as used for experiments carried out with a nonuniform heated tube. Fourteen chromel-alumel (K type, 0.5 mm O.D.) ungrounded thermocouples are spot welded

on the external surface of the tube. To protect the test section, two groups of six thermocouples connected in parallel are used to trip the power controller. Tests were carried out to determine the response time of this configuration; in all cases the response time was less than 150 ms, only the amplitude of the signals was affected by the parallel connection. The signals produced by the thermocouples are recorded in real time, and some of them are also collected by a data acquisition system for later analysis.
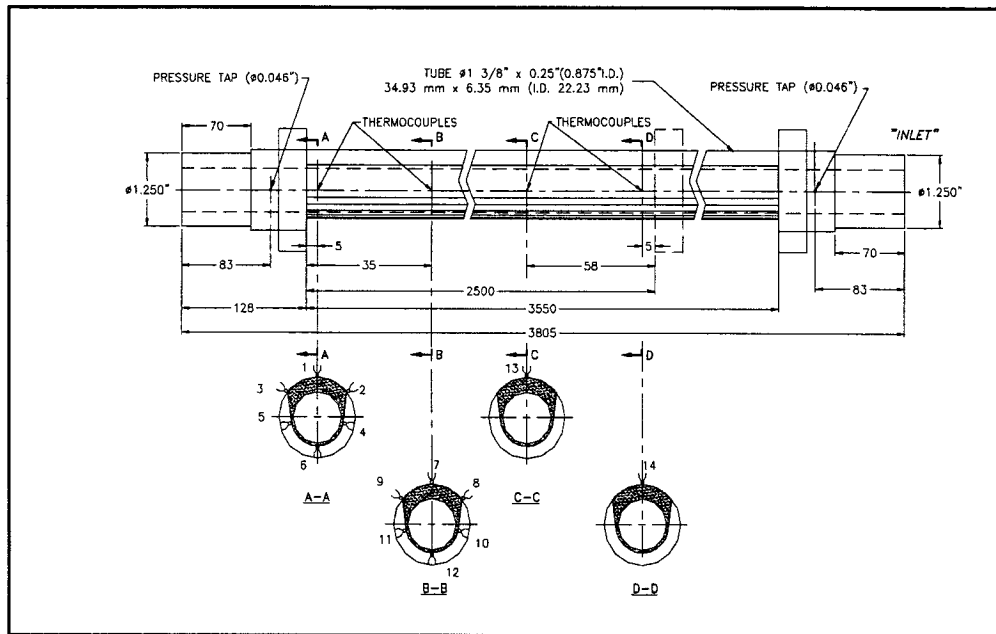
Figure 3.3: Instrumented test section (Location of the thermocouples).

The power applied to the test section is simultaneously measured by two different methods. The first one consists of an analog multiplier that gives the power as a product of the voltage drop multiplied by the electric current obtained from a 50 mV - 5000 A, 1% calibrated shunt. The output from the analog multiplier is also used in the feed-back loop of the power controller. The second method consists of a numerical sampling and multiplication of the aforementioned parameters carried out by the computer through the data acquisition system. In this case the electric current passing through the test section is measured with a high accuracy

LEM unit. Along with the surface temperature, other flow parameters are also recorded and collected. The inlet and outlet temperatures of the flow are measured with RTDs calibrated to ± 1 $^{\circ}C$ of the readings in the range of interest. The absolute pressures at the inlet flange and at a pressure tap located 80 mm downstream of the lower face of the upper copper clamp are measured with 750 $psia$ "Sensotec" pressure transducers with an accuracy of $\pm 0.1\%$ full scale (FS); the pressure difference between this pressure tap and the outlet flange is measured with a 100 $psia$ "Sensotec" pressure transducer with an accuracy of 0.25% FS. The inlet flow rate is measured with "Flow Technology" turbine flow meters with an accuracy of $\pm 1\%$ of the readings. In order to avoid the fluctuations caused by electrical induction from the exterior high current cable, the turbine flow meter is shielded with a steel box. The flow rate is corrected by the temperature readings obtained from an RTD located at the exit of the flow meter flow line.

Displacement devices and miniature video cameras are used to monitor the upstream electric copper plate and the deformation of the tube caused by the nonuniform heating.

3.4 Experimental procedures

The data presented in this thesis have been obtained for vertical up flows, using three different geometries (uniform, nonuniform with $\frac{q''_{max}}{q''_{min}}$ ratios of 4.7 and 8.3) and three different heated lengths (1.8, 2.5 and 3.55 m). The experiments were carried out by changing the inlet sub-cooling, the flow rate and outlet pressure. Since the main objective of the experiments was to collect data over a wide range of flow conditions, the inlet subcooling was varied from 5 $^{\circ}C$ to 40 $^{\circ}C$, the flow rate was varied from 300 kg/m^2s to 1600 kg/m^2s, and the outlet pressure was varied from 10 $bars$ to 40 $bars$. During each run, the temperature at the inlet of the test section was controlled with an accuracy of ± 0.3 $^{\circ}C$, the flow rate was kept constant with a maximum variation range of ± 0.002 l/s and the outlet pressure was kept constant with a maximum variation range of ± 0.05 bar. The inherent characteristics of the loop make it possible to run the experiments without any appreciable low frequency flow rate and pressure fluctuations. Once the flow

parameters were established and controlled, the power applied to the test section was gradually increased until the first wall temperature spike was detected. The Figure 3.4 shows typical CHF detection criterion used during the tests. After the first wall temperature spike was detected, the data acquisition system was triggered on. Under this condition, the power is kept constant for a period of at least for 10 seconds (this power is then used to calculate the corresponding value of CHF). After this 10 sec period, the power continued to be increased and the power controller is tripped as soon as a large wall temperature jump, usually higher than 40 ^oC, occurs; at the same time the data acquisition system is also triggered off.
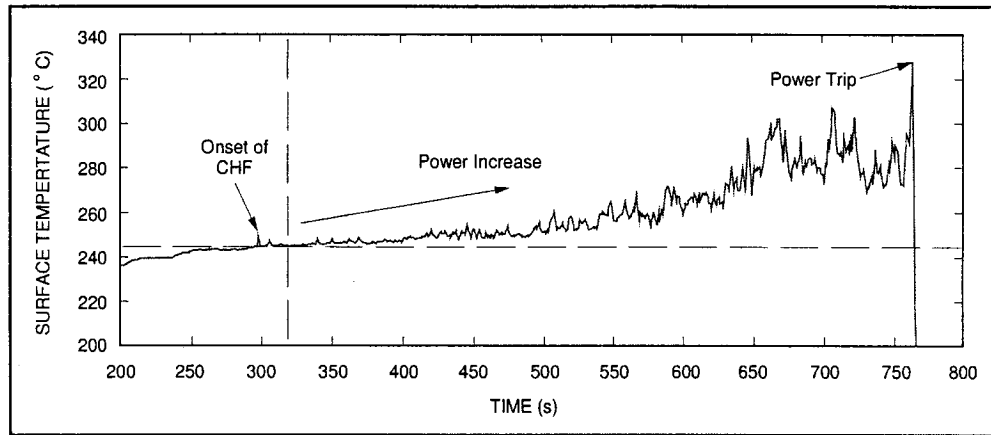
Figure 3.4: CHF detection criterion.

CHAPTER 4

CHF DATA IN UNIFORM AND NON-UNIFORM HEATED TUBES

It was postulated that CHF (Collier, 1972) for water flows in vertical uniformly heated tube is a function of five independent variables; thus:

$$CHF = f\left(G, (\Delta T_{sub})_i, P, D, z\right). \tag{4.1}$$

Since dry-out almost invariably occurs at the exit of the heated section, it can be also expressed in terms of the exit conditions as:

$$CHF = f\left(G, x(z), P, D, z\right). \tag{4.2}$$

Based on the above equation, the parameters involved in the present CHF research include the inlet subcooling, the mass flux, the outlet pressure, the heated length and the heat flux ratio. By changing one of the parameters, different combinations of CHF test can be organized. Over 1000 CHF test points were obtained by using a uniform and two non-uniform heated tubes having an internal diameter of 22.2 mm. The experimental conditions used for these tests were:

Inlet subcooling	5 - 40 ^0C;
Mass flux	300 - 1600 kg/m^2s;
Pressure	10 - 40 $bars$;
Heated length	1.8, 2.5, 3.55 m;
Heat flux ratio, $\frac{q''_{max}}{q''_{min}}$	1.0, 4.7, 8.3;
Flow quality	20 - 70%.

The results are presented in the following section.

4.1 CHF representation as a function of the thermodynamic quality

One of the parameters that was used to analyze CHF is the relative enthalpy of the flow or, in other words, the thermodynamic quality evaluated at the end of the heated length:

$$x = \frac{h_{mix}(P_{out}) - h_f(P_{out})}{h_{fg}(P_{out})} = \frac{h_{in}(P_{in}) + Q/W - h_f(P_{out})}{h_{fg}(P_{out})}, \qquad (4.3)$$

where:

h_{mix} and h_f : enthalpy of the mixture and saturated liquid respectively, (kJ/kg);

h_{fg}: latent heat of evaporation, (kJ/kg);

Q: thermal power applied on the tube, (kW);

W: mass flow rate, (kg/s).

Under thermal equilibrium condition, the thermodynamic quality becomes equal to the real quality of the flow, which means that it reflects the ratio between the mass flow rates of steam phase to the total mass flow rate of the mixture. Apart from the thermodynamic quality, some variables and definations are needed to be introduced before presenting CHF data.

Measured critical heat flux value, (CHF_{MEAS})

CHF_{MEAS} is the measured heat power for a CHF condition, divided by the internal surface of the test section.

Direct Substitution CHF value, (CHF_{DSM})

The direct substitution is the method used to predict CHF and CHF margins by using CHF regression correlations (i.e., CHF= $f(x)$ or $CHF = f(L_{dan})$),

obtained under constant flow pressure, mass flux and tube diameter conditions. The CHF value obtained by using this method is called "direct substitution CHF value", (CHF_{DSM}).

Heat balance CHF value, (CHF_{HBM})

The heat balance is a method used to predict CHF and CHF margins by using CHF regression correlations (i.e., CHF= $f(x)$ or $CHF = f(L_{dan})$) and an equation that takes into account the heat balance, i.e., taking into account the fact that quality changes with the heat flux. The CHF value obtained by using this approach is called the "heat balance CHF value" , (CHF_{HBM}) (Figure 4.1).
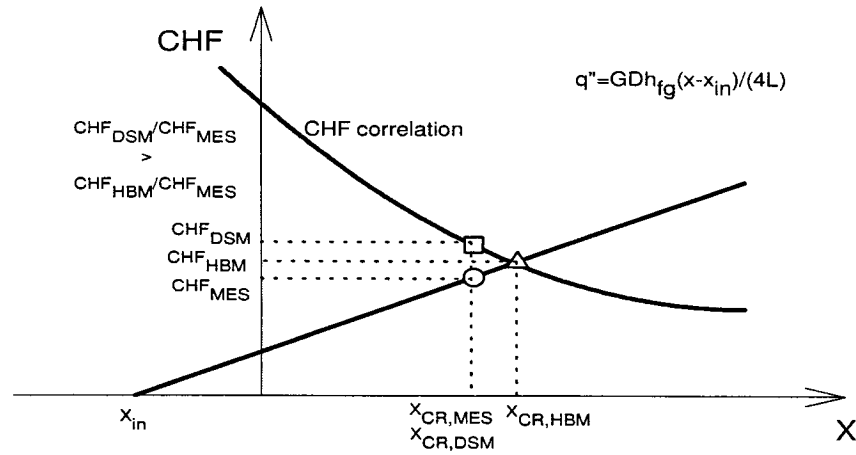
Figure 4.1: Heat balance and CHF curves
(Olekhnovitch *et al.*, 2000b).

4.1.1 Overall trends of the CHF data
(Thermodynamic quality representation)

For given mass fluxes and pressures, the CHF data obtained for different heated lengths and nonuniform heating conditions are shown in Figures 4.2 through 4.5.

From Figures 4.2 to 4.5, it can be observed that for given mass fluxes and pressures, the CHF curves shift toward the lower quality and lower CHF direction with increasing the heat flux nonuniformity $\frac{q''_{max}}{q''_{min}}$, indicating that the higher is the heat flux nonuniformity $\frac{q''_{max}}{q''_{min}}$, the lower is the values of CHF. However, at high pressure, i.e., 40 *bars*, CHF curves of different heat flux ratios tend to approach to each other with increasing mass flux, indicating that the effect of nonuniformity on the CHF decreases with increasing both the pressure and the mass flux.

From Figures 4.2 to 4.5, it can be observed that for a given exit flow pressure, the CHF curves group shifts toward the lower quality and higher CHF direction with increasing the mass flux, indicating that CHF increases with increasing the mass flux at a given exit flow pressure.

For a given exit flow pressure (Figures 4.2 through 4.5), each small bar that consists of the CHF data of the same heated length under different inlet subcooling tends to turn around a certain point and becoming increasingly steeper with increasing mass flux, indicating that the effect of the inlet subcooling on the CHF increases with increasing mass flux at a given exit flow pressure.

The comparisons between Figures 4.2 to 4.4 shows that for a given mass flux the CHF curves shift toward the higher quality and higher CHF direction with increasing the flow pressure, indicating that CHF increases with increasing the pressure at a given mass flux. However, the comparison between Figure 4.4 and Figure 4.5 showed that after 30 *bars* the CHF curves shift toward the lower quality and lower CHF direction with increasing the flow pressure, indicating that CHF dereases with increasing the pressure at a given mass flux. The effect of pressure on CHF is quite complex, there exist an inversion point between 30 and 40 *bars*, before this point CHF increases with pressure. After this point, CHF decreases with increasing pressure.

A summary of the effect that the different flow variables have on CHF is presented in the Figure 4.6.
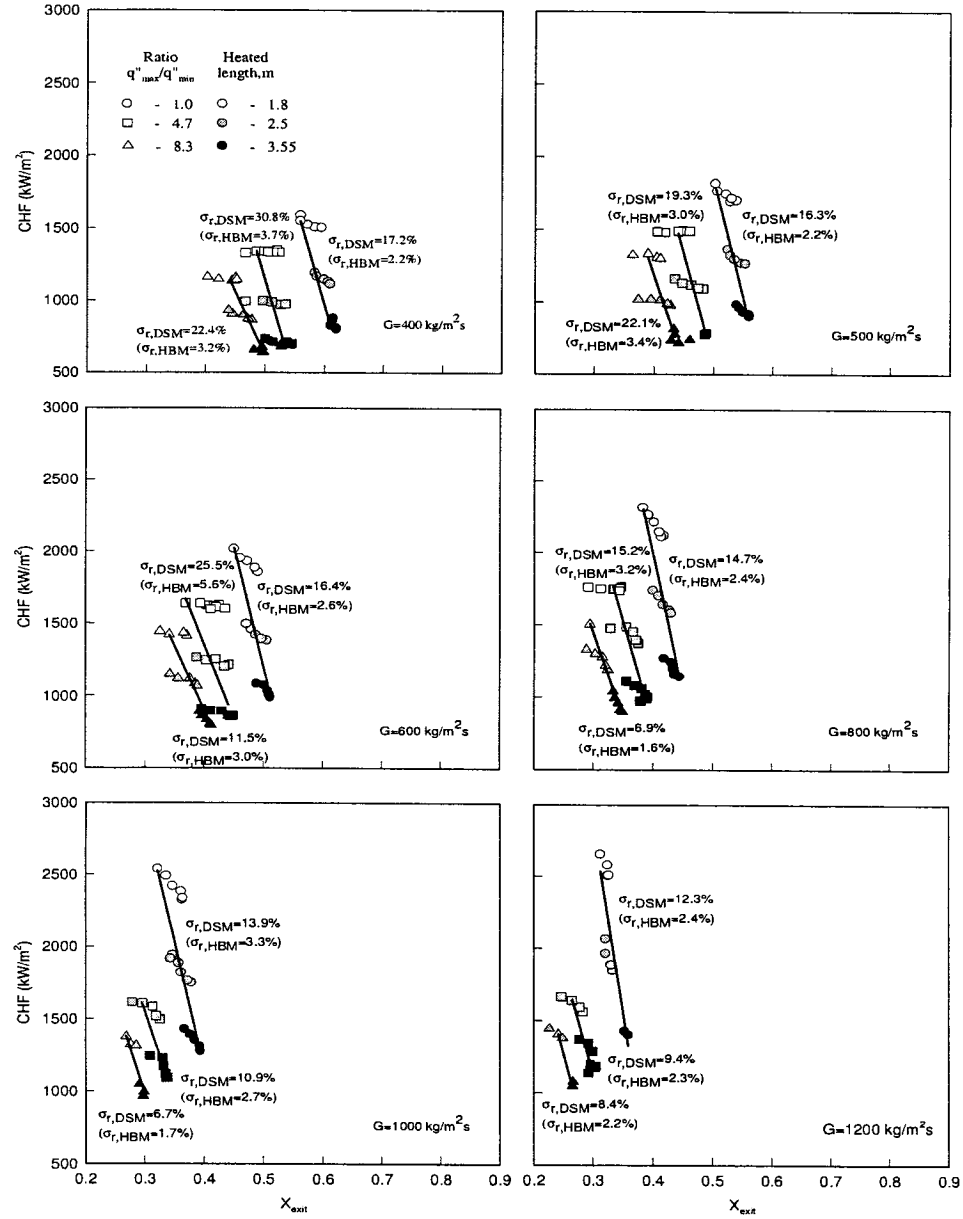
Figure 4.2: CHF as a function of the thermodynamic quality at the exit of the test section ($P_{out} = 10$ $bars$; $G = 400, 500, 600, 800, 1000, 1200$ kg/m^2s).
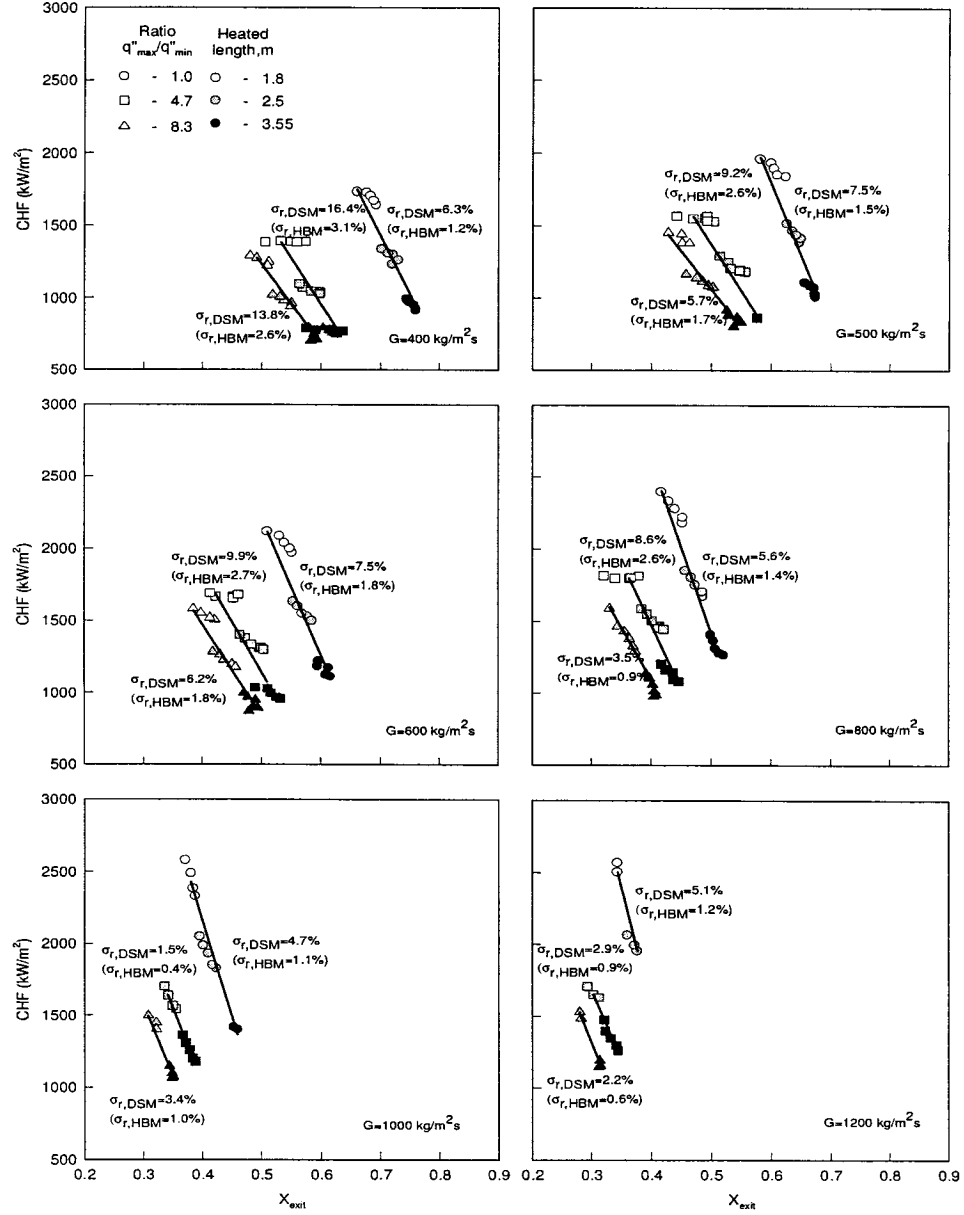
Figure 4.3: CHF as a function of the thermodynamic quality at the exit of the test section ($P_{out} = 20$ $bars$; $G = 400, 500, 600, 800, 1000, 1200$ $kg/m^2 s$).
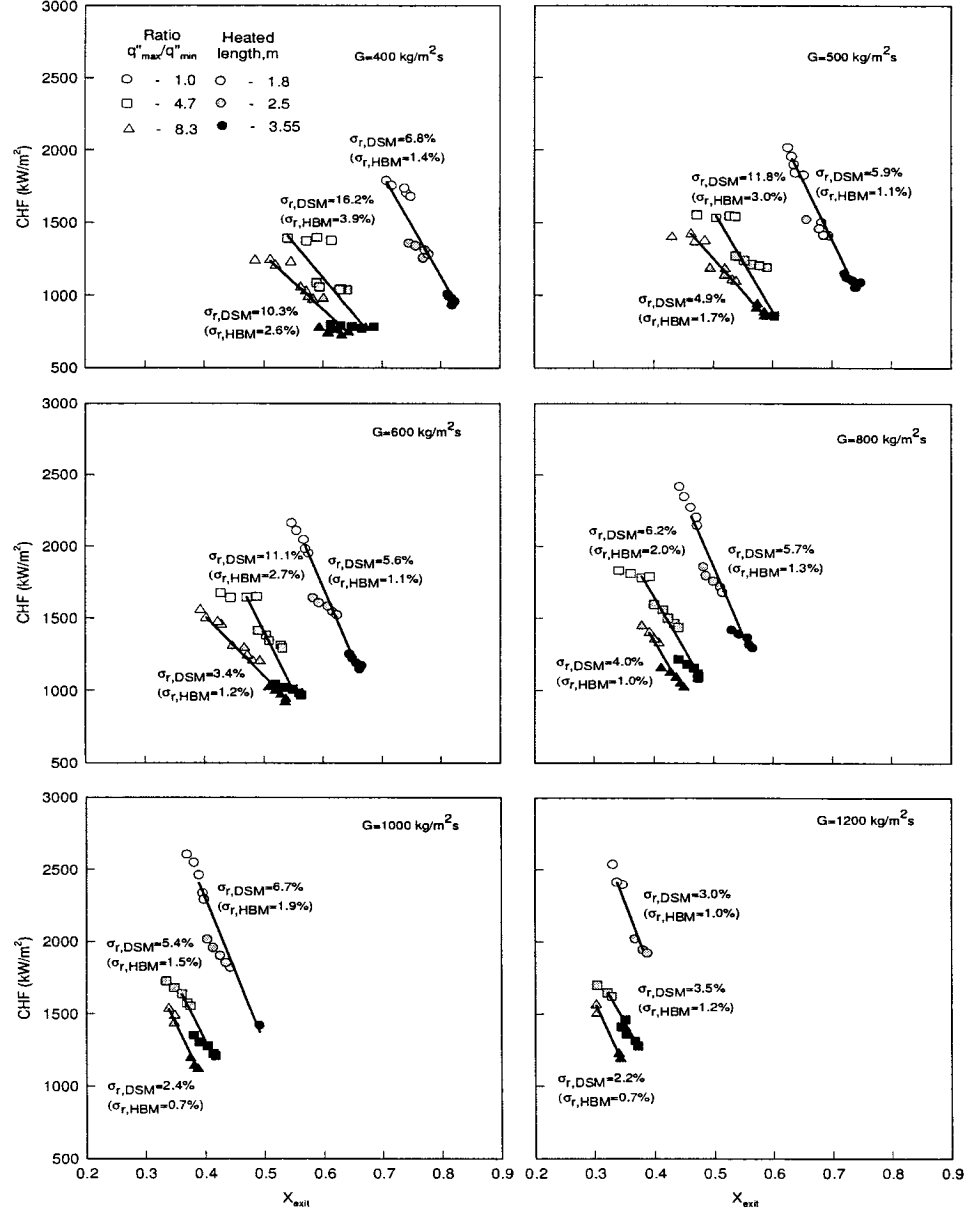
Figure 4.4: CHF as a function of the thermodynamic quality at the exit of the test section ($P_{out} = 30\ bars; G = 400, 500, 600, 800, 1000, 1200\ kg/m^2 s$).
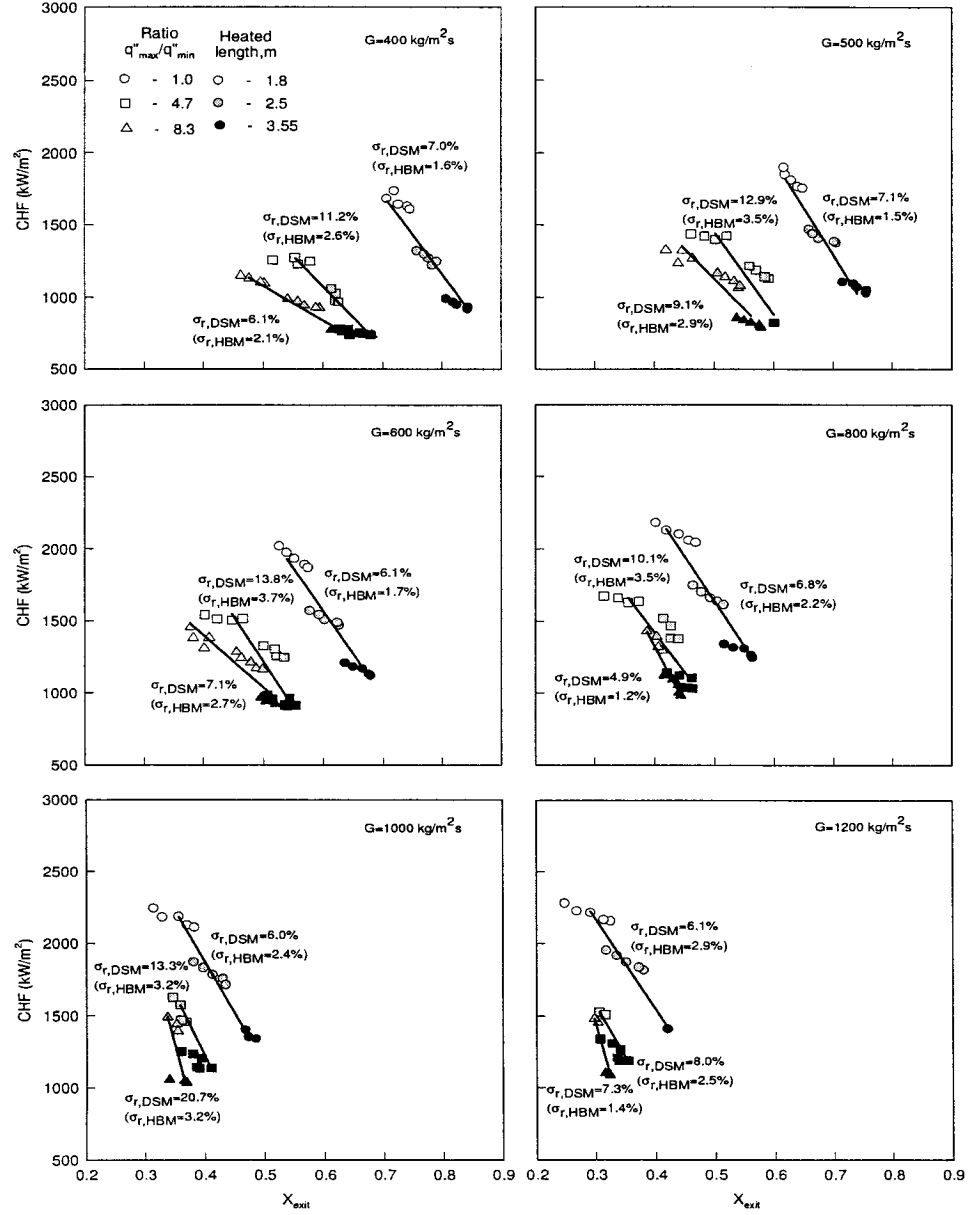
Figure 4.5: CHF as a function of the thermodynamic quality at the exit of the test section ($P_{out} = 40$ $bars$; $G = 400, 500, 600, 800, 1000, 1200$ kg/m^2s).
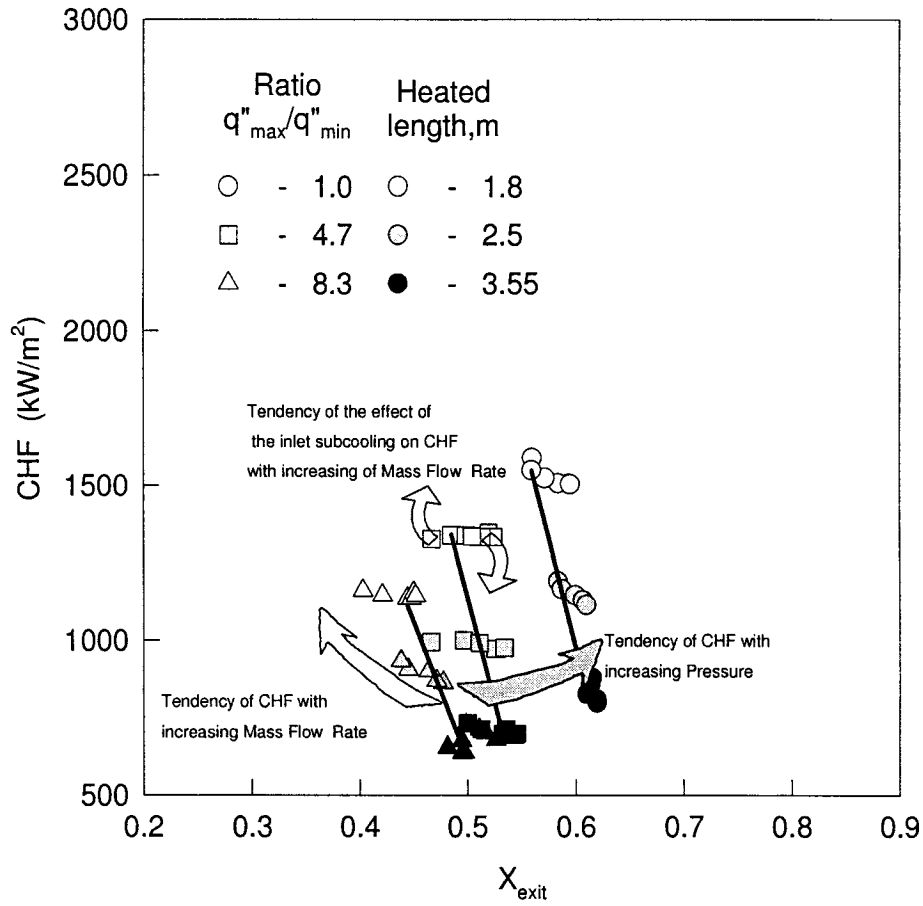
Figure 4.6: CHF as a function of different flow parameters
$(G = 300 - 1600 \ kg/m^2 s; \ P_{out} = 10 - 40 \ bars; \ \Delta T_{SAT} = 5 - 40 \ ^\circ C)$.

4.1.2 Regression of the CHF data

The Figure 4.7 shows the values of CHF as a function of the thermodynamic quality, x, for a given mass flux and pressure. Note that the results shown in this figure were obtained for three different heated lengths and three different angular heat flux distribution. Ignoring the effect of the inlet subcooling on CHF, a linear regression is then applied to each group of data (i.e., data for the same circumferential heat flux distribution and for a given mass flux and pressure). The regression coefficients B0 and B1 for each group are given in Table 4.1. Then, CHF_{DSM} can be calculated by the following equation:

$$CHF_{DSM} = B0 + B1 \cdot x. \qquad (4.4)$$
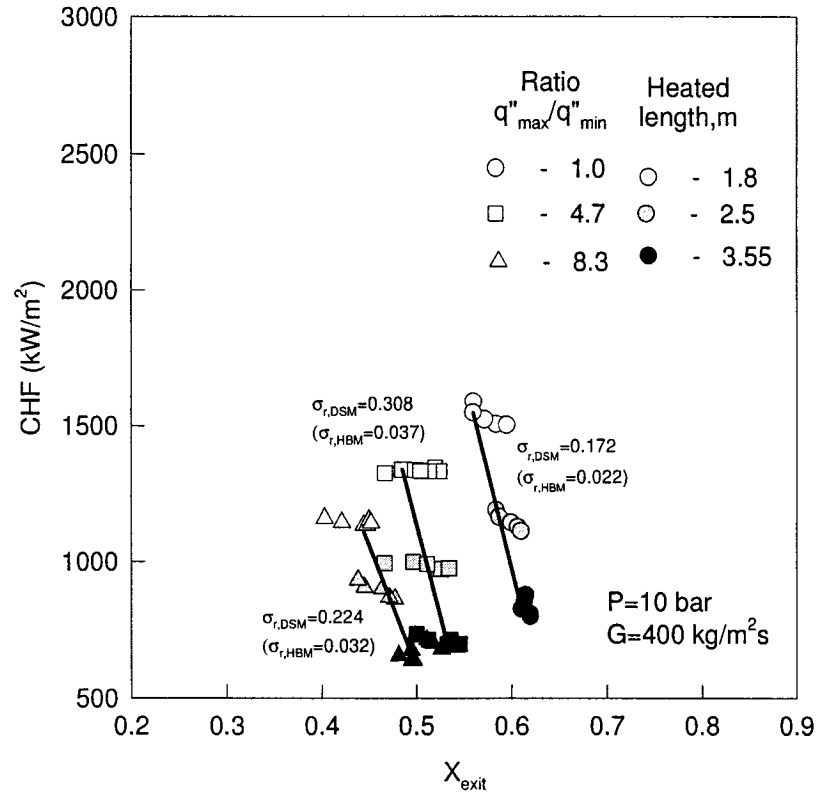
Figure 4.7: CHF as a function of the thermodynamic quality
at the end of the heated length.

Figure 4.8 shows how the CHF, (CHF_{HBM}) can be obtained from a heat balance. By expressing the quality as a function of the heat flux, i.e., $x = f(q")$, then CHF will take place at at point "A" in the Figure 4.8.

From the CHF regression line, at point A, we have:

$$CHF_{HBM} = B0 + B1 \cdot x_{HBM}, \qquad (4.5)$$

and from a heat balance carried out at point A, we have:

Table 4.1: Regression coefficients based on the thermodynamic quality method $(CHF = B0 + B1 * x)$.

| | | | | P, bars | | | | | | | |
| | | | | 10 | | 20 | | 30 | | 40 | |
$q"_{max}/q"_{min}$		G, kg/m²s		B0	B1	B0	B1	B0	B1	B0	B1
	1.0		400	9506	-14223	7044	-8022	6838	-7140	5538	-5474
			500	9836	-16008	7708	-9871	7205	-8327	5897	-6584
			600	9544	-16708	6955	-9500	7443	-9557	5162	-5989
			800	9597	-19056	7320	-11801	6611	-9525	4757	-6236
			1000	8157	-17473	7541	-13439	6372	-10171	4725	-7129
			1200	10604	-25837	8211	-16614	6089	-10883	4053	-6267
	4.7		400	7938	-13604	4718	-6273	3990	-4786	3598	-4213
			500	7927	-14670	4551	-6366	4995	-6845	4278	-5663
			600	5430	-10198	4640	-6992	5503	-8194	4385	-6341
			800	6455	-14120	5058	-8958	4459	-7039	3596	-5448
			1000	5252	-12322	5269	-10599	4678	-8417	4593	-8426
			1200	5382	-14171	4519	-9477	4016	-7360	3666	-6998
	8.3		400	5072	-8918	3948	-5446	3139	-3733	2270	-2391
			500	6083	-12260	3669	-5212	3519	-4531	3200	-4145
			600	4410	-8771	3993	-6302	3171	-4140	2850	-3629
			800	4910	-11585	3957	-7157	4071	-6826	4479	-7892
			1000	4893	-13065	4578	-9991	4466	-8648	6808	-15787
			1200	5024	-15036	4475	-10548	4258	-8937	5878	-14811

$$x_{HBM} = \left(h_{in} + \frac{CHF_{HBM} \cdot \pi \cdot D \cdot L}{w} - h_f \right) / h_{fg}, \tag{4.6}$$

or

$$x_{HBM} = \left(h_{in} + \frac{4CHF_{HBM} \cdot LD}{G} - h_f \right) / h_{fg}, \tag{4.7}$$

where:

LD : ratio of heated length to tube internal diameter (L/D).
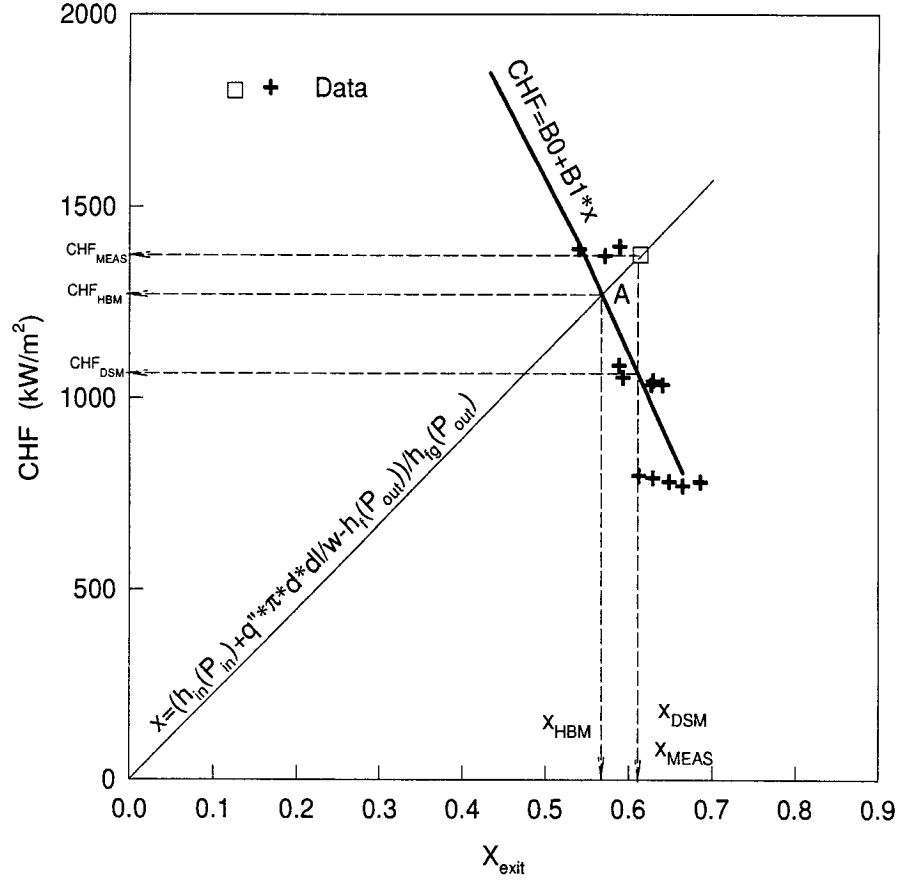
Figure 4.8: Regression line of the CHF under the form: $CHF = f(x_{exit})$.

Substituting Equation (4.6) or (4.7) into Equation (4.5) and arranging terms, we have:

$$CHF_{HBM} = (B0 \cdot h_{fg} + B1 \cdot h_{in} - B1 \cdot h_f) / \left(h_{fg} - \frac{B1 \cdot \pi \cdot D \cdot L}{w} \right), \quad (4.8)$$

thus, we can write:

$$CHF_{HBM} = (B0 \cdot h_{fg} + B1 \cdot h_{in} - B1 \cdot h_f) / \left(h_{fg} - \frac{4B1 \cdot LD}{G} \right). \quad (4.9)$$

This equation represents the CHF value obtained by using the heat balance method.

The performance of the prediction tools we developped (Equations (4.4) to (4.9)) is determined by calculating the relative and absolute RMS values. In terms of the direct substitution approach and the heat balance approach, we have $\sigma_{r,DSM}$, σ_{DSM} and $\sigma_{r,HBM}$, σ_{HBM} respectively. They are calculated by using the following equations:

$$\sigma_{r,DSM} = \sqrt{\sum_{k=1}^{n} \left(\frac{CHF_{DSM}^k - CHF_{MES}^k}{CHF_{MES}^k} \right)^2 /(n-m)}, \qquad (4.10)$$

$$\sigma_{DSM} = \sqrt{\sum_{k=1}^{n} \left(CHF_{DSM}^k - CHF_{MES}^k \right)^2 /(n-m)} \qquad kW/m^2, \qquad (4.11)$$

$$\sigma_{r,HBM} = \sqrt{\sum_{k=1}^{n} \left(\frac{CHF_{HBM}^k - CHF_{MES}^k}{CHF_{MES}^k} \right)^2 /(n-m)}, \qquad (4.12)$$

$$\sigma_{HBM} = \sqrt{\sum_{k=1}^{n} \left(CHF_{HBM}^k - CHF_{MES}^k \right)^2 /(n-m)} \qquad kW/m^2, \qquad (4.13)$$

where:

$\sigma_{r,DSM}$: relative RMS errors of the direct substitution approach;

σ_{DSM}: absolute RMS errors of the direct substitution approach;

$\sigma_{r,HBM}$: relative RMS errors of the heat balance approach;

σ_{HBM}: absolute RMS errors of the heat balance approach.

4.1.3 Comparison between CHF_{MEAS} and CHF_{DSM}

Based on the regression coefficient given in Table 4.1 and using the Equations (4.4) and (4.9), we can apply the direct substitution approach (CHF_{DSM}) and the heat balance approach (CHF_{HBM}) to estimate the CHF under different flow and heating conditions. The comparisons between the predicted and measured values, i.e., CHF_{DSM} and CHF_{MEAS} , CHF_{HBM} and CHF_{MEAS} are shown in Figure 4.9 and Figure 4.10. From these figures, we can observe that heat balance approach seems to be more accurate than direct substitution approach. The relative and absolute RMS errors of CHF_{HBM} are 2.3% and 33.4 kW/m^2 respectively, while the relative and absolute RMS errors of CHF_{DSM} are 11.2% and 144.76 kW/m^2 respectively.
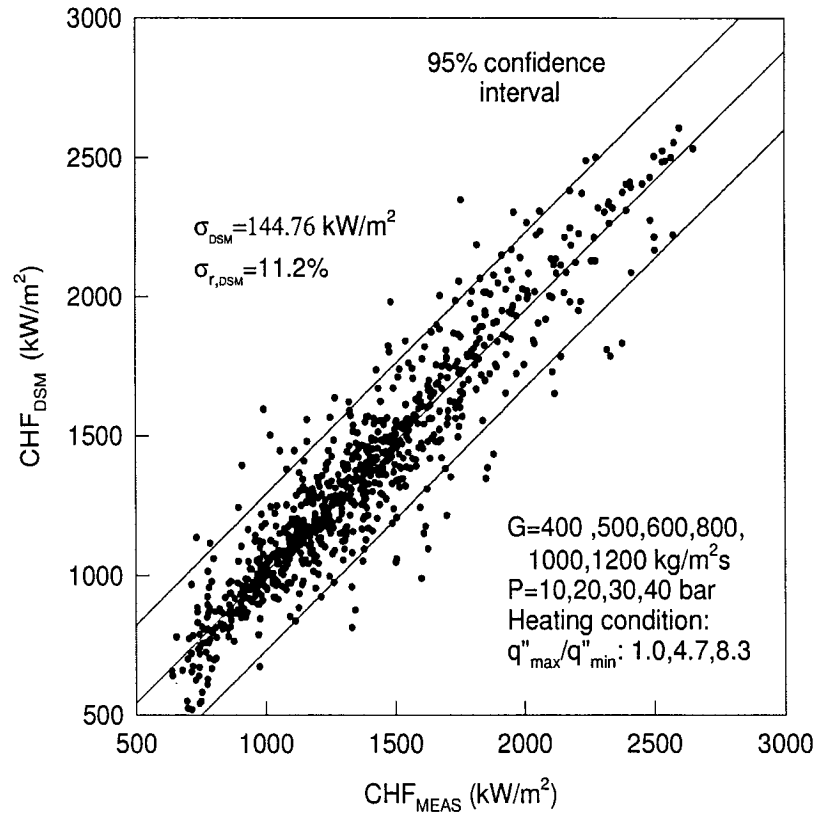
Figure 4.9: A comparison between CHF_{MEAS} and CHF_{DSM}
(CHF_{DSM} is calculated by using the coefficients
given in the Table 4.1 and the Equation (4.4)).
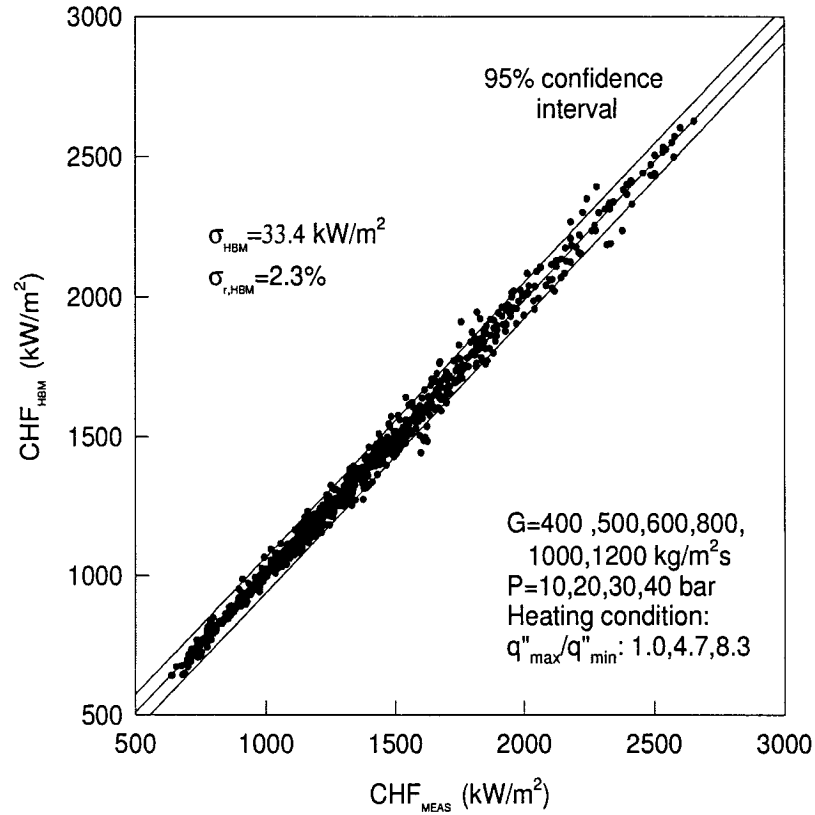
Figure 4.10: A comparison between CHF_{MEAS} and CHF_{HBM}
(CHF_{HBM} is calculated by using the coefficients
given in the Table 4.1 and the Equation (4.8)).

The better accuracy of the HBM is due to the fact that it takes into consideration both the heat flux and the quality at the same time. Note that in the HBM the heat flux is considered in an implicit manner, therefore, this method is an implicit approach. On the other hand, the DSM is obtained by an explicit approach based on the thermodynamic quality. As we know, the thermodynamic quality is affected by a number of factors, such as pressure, inlet subcooling, flow rate; thus, it is very difficult to precisely calculate the thermodynamic quality. Since for low mass flux conditions there is a large dispersion in the values of quality caused by the inlet subcooling, the explicit DSM approach of calculating the CHF (Equation 4.4) is subjected to large errors, (i.e., a relative RMS error of 11.2%).

The advantage of the HBM approach is that as soon as we know the inlet

flow conditions we can estimate the CHF with a good accuracy by using a reduced number of coefficients (24 coefficients for each heat flux ratio, $\frac{q"_{max}}{q"_{min}}$) and Equation (4.9), without the necessity of using the exit thermodynamic quality, which is undetermined.

4.2 CHF representation as a function of the length of the dispersed annular flow region

It is a common practice to represent the CHF data as a function of the thermodynamic quality. In the 1995 CHF look-up table (Groeneveld et al., 1996), which is so far one of the most complete worldwide compilation of CHF data, CHF is presented as a function of flow pressure, P, mass flux, G, and the thermodynamic quality, x. But according to Doroshchuk (1966), in a large region of the dispersed annular flow, the deterioration of the heat transfer always occurs at a certain constant, limiting quality value; thus, the notion of CHF losses its meaning. It is still not clear whether the limiting quality phenomenon really exists or not. If it exists, the use of the critical heat flux as a function of the thermoldynamic quality to predict CHF could introduce huge errors. In the present study, big data scatter occured when presenting CHF data in a CHF, x_{exit} coordinate system for low mass flux conditions (Figures 4.2 to 4.5). For this reason, other researchers have recently proposed a different CHF data representation by using more appropriate coordinate systems. Olekhnovitch (1998) and Olekhnovitch et al. (1999a,b; 2000a) conducted CHF studies under low and medium flow pressure conditions by using vertical round test sections heated uniformly. The authors were able to show that the use of the length over which the dispersed annular flow, L_{dan}, occurs as a coordinate, permits the scatter in the CHF data to be considerable reduced. In particular, this new representation of the CHF data eliminates the drawback related to the existence of the limiting quality boundary. According to the authors, this reduction of the scattering is due to mechanisms that control the CHF phenomena, for instance, the mass flow rate in the liquid film at the point of inception of the dispersed annular flow and the applied heat flux.

Following the same idea presented by Olekhnovitch et al., in the following

section, we will represent CHF as a function of the length over which the dispersed annular flow occurs.

By carrying out a heat balance in a two-phase flow similar to that shown in the Figure 4.11, the length over which the dispersed annular flow occurs can be written as:

$$L_{dan} = L - \frac{G \cdot D \cdot [x_{dan} \cdot h_{fg}(P_{in}) - h_{in} + h_f(P_{in})]}{4 \cdot CHF}, \qquad (4.14)$$

where x_{dan} is the thermodynamic quality corresponding to the onset of the dispersed annular flow.

According to Levitan and Borevskiy (1989) and Levitan and Orlova (1990) x_{dan} is calculated by:

$$x_{dan} = (2.7 \pm 0.3)We_f^{-0.25} \left(\frac{\rho_f}{\rho_g}\right)^{-0.33}, \qquad (4.15)$$

where

$We_f = G^2 d/\rho_g \sigma$ is the Weber Number of the liquid film;

ρ_f and ρ_g are the density of the liquid and the steam respectively;

σ is the surface tension.
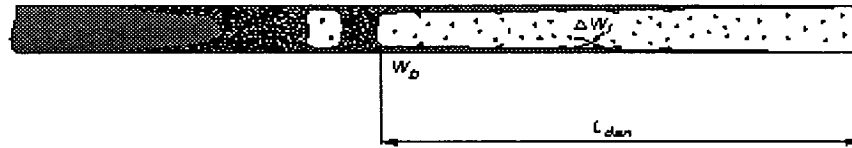
Figure 4.11: Two-phase dispersed annular flow in a straight tube.

It is apparent that Equation (4.14) can now be used for estimating the CHF by applying both the DSM and HBM methods. The next section will present this

new CHF representation for both methods.

4.2.1 Regression of the CHF data

From Equation (4.14), one can say that L_{dan} is proportional to $1/CHF$. Based on the experimental results obtained during this work, we can plot the data as a function of $1/CHF$ as is shown in the Figure 4.12. This figure shows that there is a linear relationship between L_{dan} and $1/CHF$. Therefore, for the DSM method, the complet data set was fitted by using regression lines having the form given by the following equation:

$$L_{dan} = B0 + B1/CHF_{DSM}. \qquad (4.16)$$

Then, Equation (4.16) can be used to calculate the CHF_{DSM} as a function of L_{dan}; thus:

$$CHF_{DSM} = B1/(L_{dan} - B0). \qquad (4.17)$$

The values of the coefficients B0 and B1 for each group are given in Table 4.2.

Figure 4.13 shows both Equation (4.14) and Equation (4.16). From this figure, it is apparent that the equality between these equations that corresponds to the intersection between the two lines, represents the inverse of the CHF determined by using the HBM method. Therefore we can write:

$$L_{dan} = B0 + \frac{B1}{CHF_{HBM}}. \qquad (4.18)$$

From a heat balance, we have:

$$L_{dan} = L - \frac{G \cdot D \cdot (x_{dan} \cdot h_{fgi} - h_{fin} + h_{li})}{4 \cdot CHF_{HBM}}. \qquad (4.19)$$

Substituting Equation (4.18) into Equation (4.19) and arranging terms, yields:
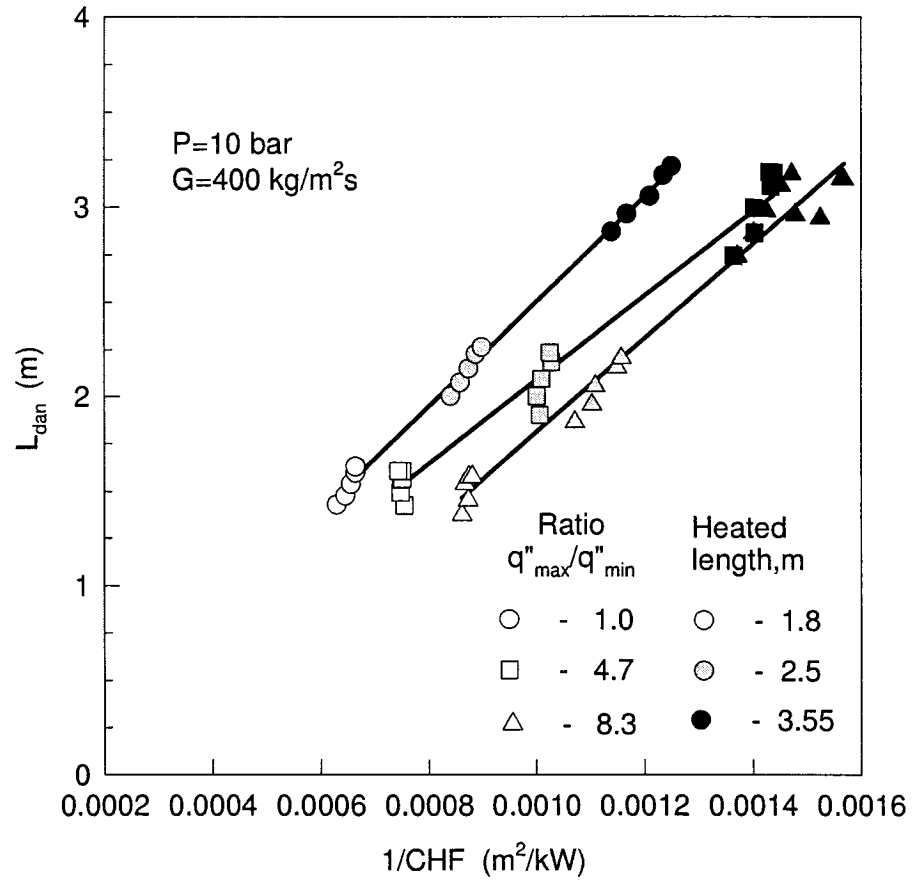
Figure 4.12: A representation of L_{dan} vs. $1/CHF$

$(P = 10\ bars, G = 400\ kg/m^2s)$.

$$CHF_{HBM} = [G \cdot D \cdot (x_{dan} \cdot h_{fgi} - h_{fin} + h_{li})/4.0 + B1]/(L - B0), \qquad (4.20)$$

where the quality at the point where the disperse annular flow occurs is calculated by:

$$x_{dan} = 2.7We_f^{-0.25}\left(\frac{\rho_f}{\rho_g}\right)^{-0.33}, \qquad (4.21)$$

with the Weber number calculated as:

Table 4.2: Regression coefficients based on
the length of the dispersed annular flow method
($L_{dan} = B0 + B1/CHF$ or $CHF = B1/(L_{dan} - B0)$).

				P, bars						
				10		20		30		40	
q''_{max}/q''_{min}	G, kg/m²s			B0	B1	B0	B1	B0	B1	B0	B1
	1.0		400	-0.2718	2772	-0.4431	3314	-0.4622	3373	-0.5606	3336
			500	-0.2295	3054	-0.4364	3669	-0.6242	3974	-0.7379	3925
			600	-0.2483	3354	-0.5262	4078	-0.6926	4366	-0.8678	4375
			800	-0.2950	3864	-0.6403	4712	-0.8336	5053	-1.0555	5027
			1000	-0.4039	4386	-0.7956	5410	-0.9696	5650	-1.4992	6034
			1200	-0.4051	4747	-0.6369	5402	-1.0318	5994	-1.9849	7099
	4.7		400	-0.1371	2225	-0.3599	2556	-0.4732	2636	-0.7501	2711
			500	-0.2783	2662	-0.6085	3237	-0.6536	3233	-0.8633	3246
			600	-0.1890	2761	-0.6602	3564	-0.7973	3693	-0.7996	3990
			800	-0.6074	3663	-0.9604	4341	-1.1321	4552	-1.1509	4192
			1000	-0.7196	4096	-0.9571	4698	-1.3184	5175	-0.9138	4211
			1200	-0.9416	4598	-1.2538	5348	-1.6107	5868	-1.2639	4784
	8.3		400	-0.6869	2496	-0.8842	2898	-0.8911	2859	-1.6561	3367
			500	-0.5228	2583	-0.8997	3270	-1.2063	3618	-1.0241	3143
			600	-0.6453	2945	-0.8270	3447	-1.2660	3981	-1.4345	3909
			800	-0.8568	3514	-1.0083	4009	-1.123	4225	-0.8254	3676
			1000	-0.6391	3523	-0.8686	4124	-1.0536	4483	-0.3093	3180
			1200	-0.9730	4092	-1.1205	4706	-1.3625	5124	-0.5793	3660

$$We_f = G^2 D/\rho_g \sigma, \tag{4.22}$$

where:

G: is the mass flux $(kg/m^2 s)$;

D: is the tube internal diameter (m);

ρ_f and ρ_g : are the densities of the liquid and the steam respectively (kg/m^3);

σ : is surface tension (N/m).

Even though the Figure 4.12 does not correspond to a conventional CHF presentation, i.e., $(L_{dan}$, CHF$)$, by knowing the regression coefficients B0 and B1, it can be transformed into $(L_{dan}$, CHF$)$. The results of this transformation are shown in the Figure 4.14.
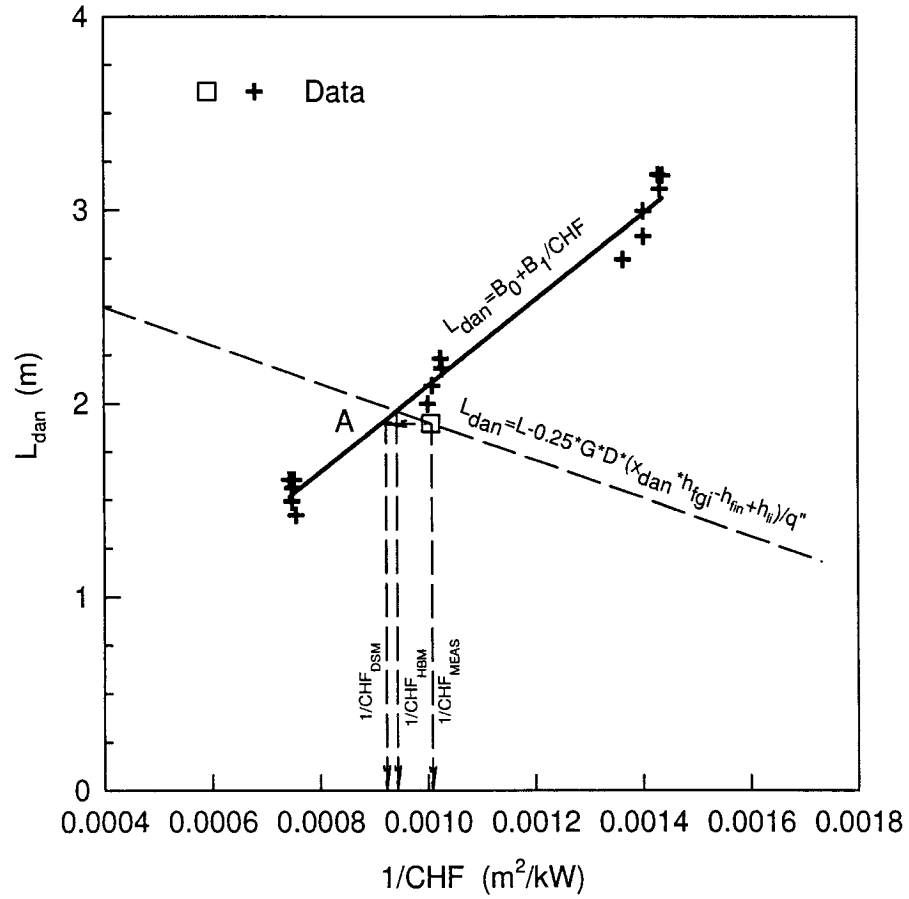
Figure 4.13: Regression line of the CHF under the form: $CHF = f(L_{dan})$.
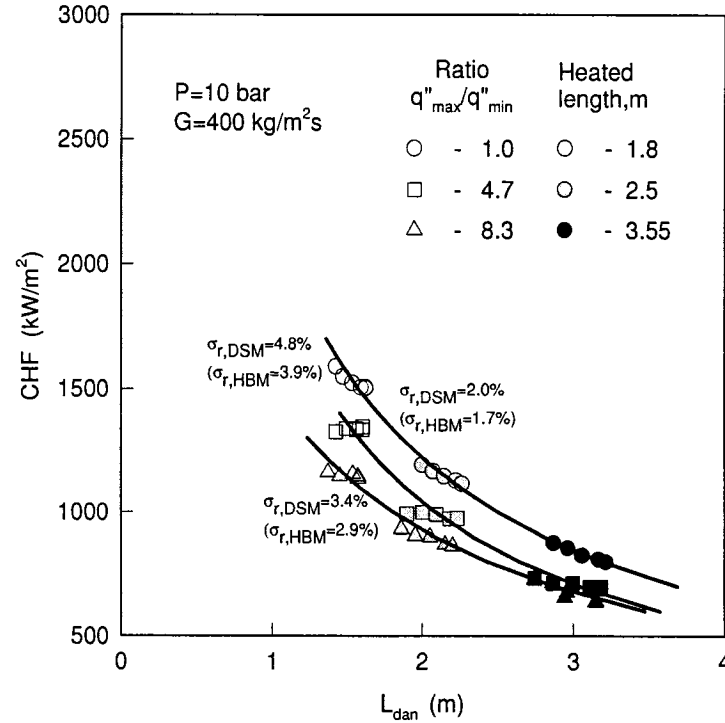
Figure 4.14: CHF as a function of L_{dan}.

4.2.2 Overall trends of the CHF data
(Dispersed annular flow length representation)

The Figures 4.15 to 4.18 show the results obtained by using the aforementioned technique for the ensemble of the experimental data. Note that in these figures the values of $\sigma_{r,DSM}$, $\sigma_{r,HBM}$ are also given. Even though the RMS errors obtained by using the HBM are smaller than those obtained by using the DSM, the difference is not very significant.

From Figures 4.15 to 4.18, it is seen that the huge scatter observed in the data when they are represented as a function of the thermodynamic quality is substantially reduced by using the length of the dispersed annular flow region. The procedure proposed to determine this length in the present research is appropriate. Based on the experimental results the following effects were observed:

- For a fixed outlet pressure, CHF increases with increasing mass flux;

- The effect of pressure on CHF is quite complex, there exist an inversion point between 30 and 40 *bars*, before this point CHF increases with pressure (see Figures 4.15, 4.16 and 4.17). After this point, CHF decreases with increasing the pressure (compare Figures 4.17 and 4.18);

- The comparison between the data obtained under uniform heating conditions with those obtained under nonuniform heating conditions shows that for a given heated length the CHF is lower for nonuniform heating. It is interesting to note (see Figures 4.15 to 4.18 at mass flux 400, 500 and 600 kg/m^2s)that the effect of the heat distribution decreases with increasing the heated length. Moreover, this effect also decreases with increasing the flow pressure (compare Figures 4.15 and 4.18).
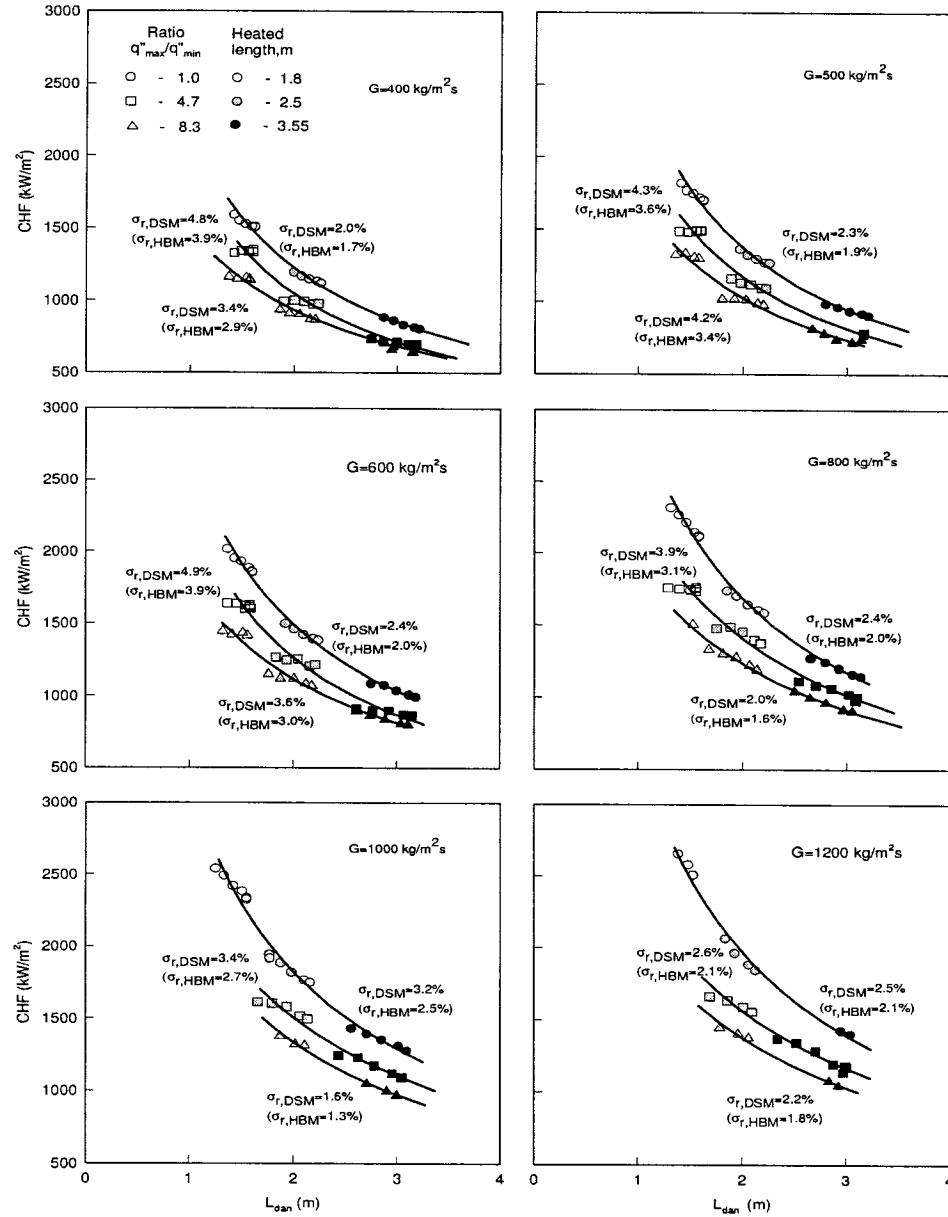
Figure 4.15: CHF as a function of the dispersed annular flow length, L_{dan} $(P_{out} = 10\ bars; G = 400, 500, 600, 800, 1000, 1200\ kg/m^2 s)$.
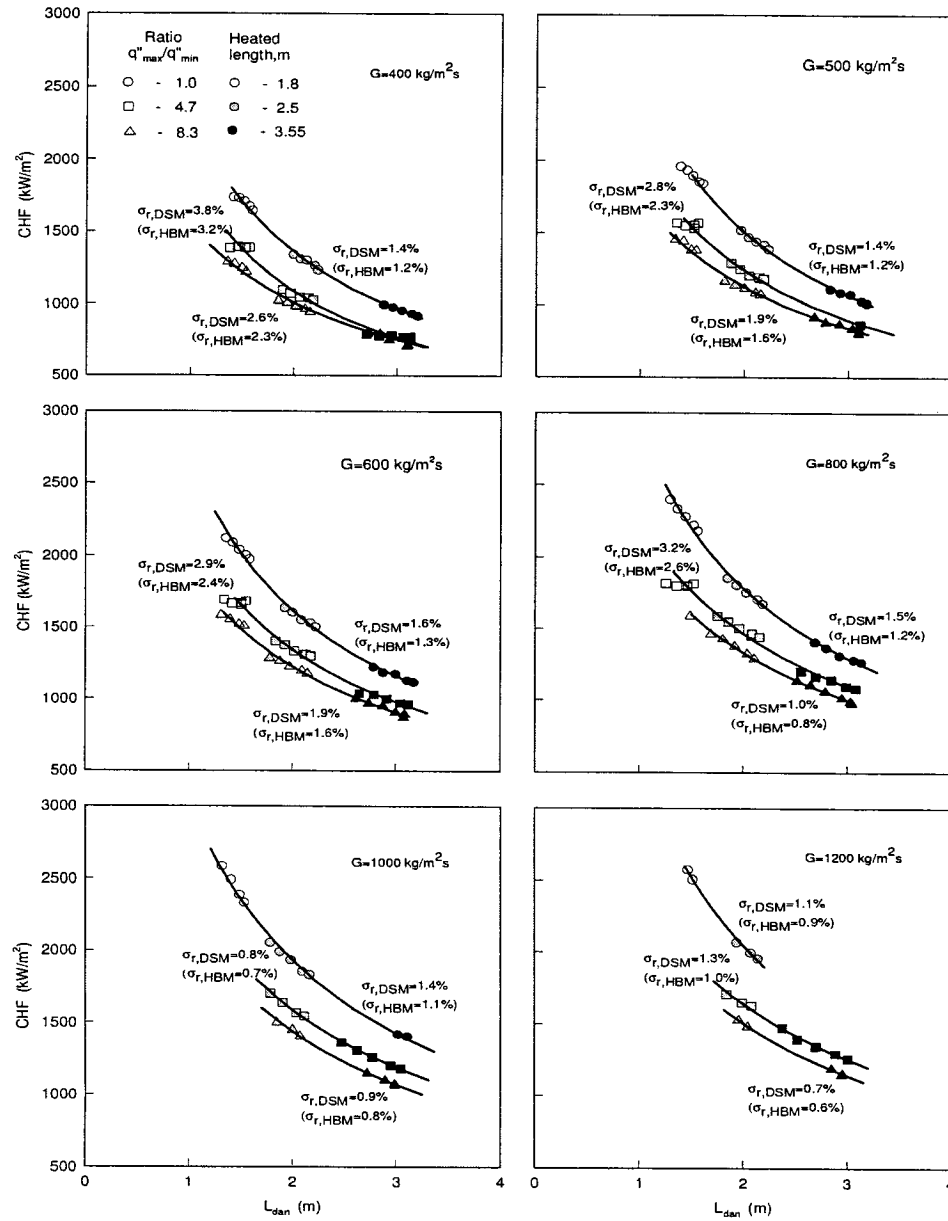
Figure 4.16: CHF as a function of the dispersed annular flow length, L_{dan} ($P_{out} = 20$ $bars; G = 400, 500, 600, 800, 1000, 1200$ kg/m^2s).
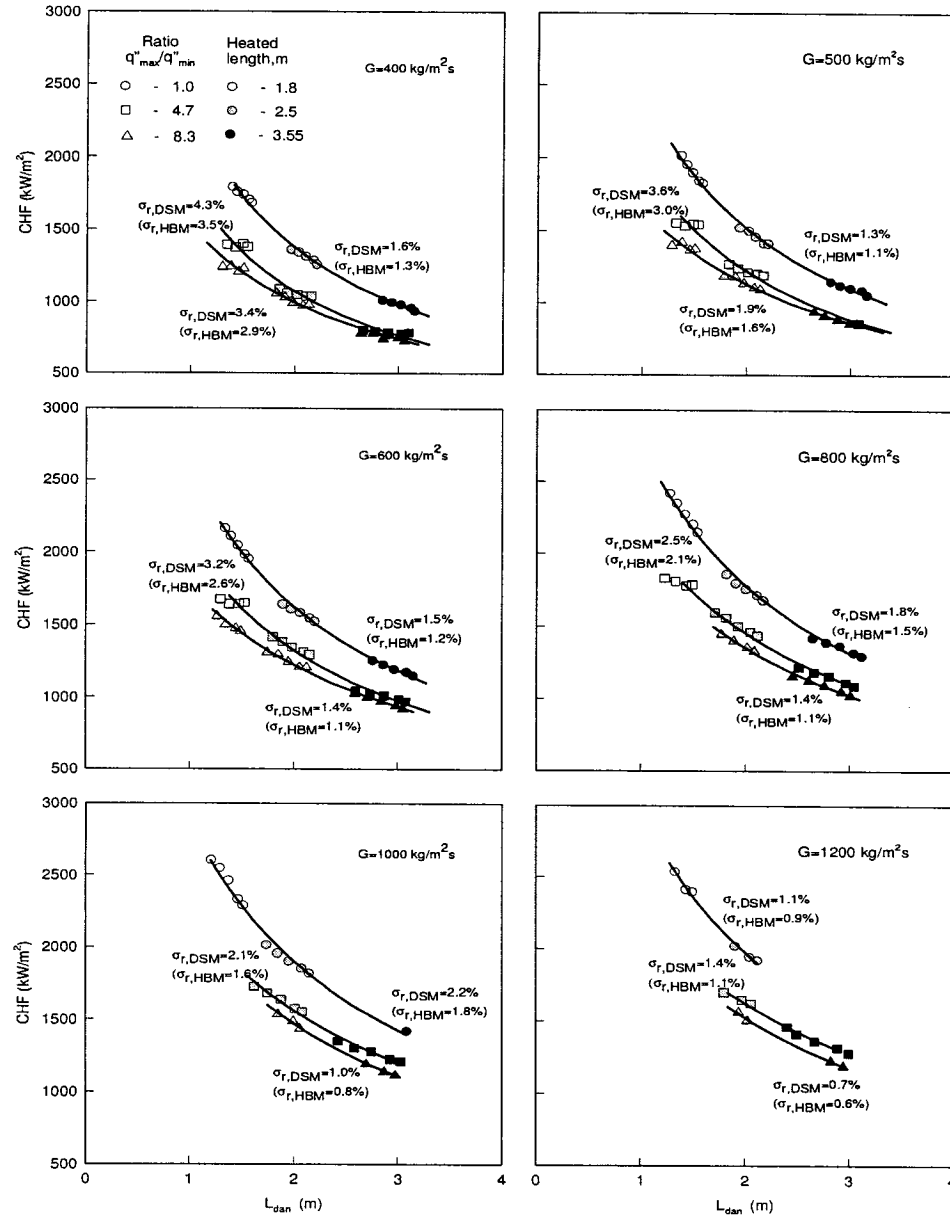
Figure 4.17: CHF as a function of the dispersed annular flow length, L_{dan} ($P_{out} = 30$ bars; $G = 400, 500, 600, 800, 1000, 1200$ kg/m^2s).
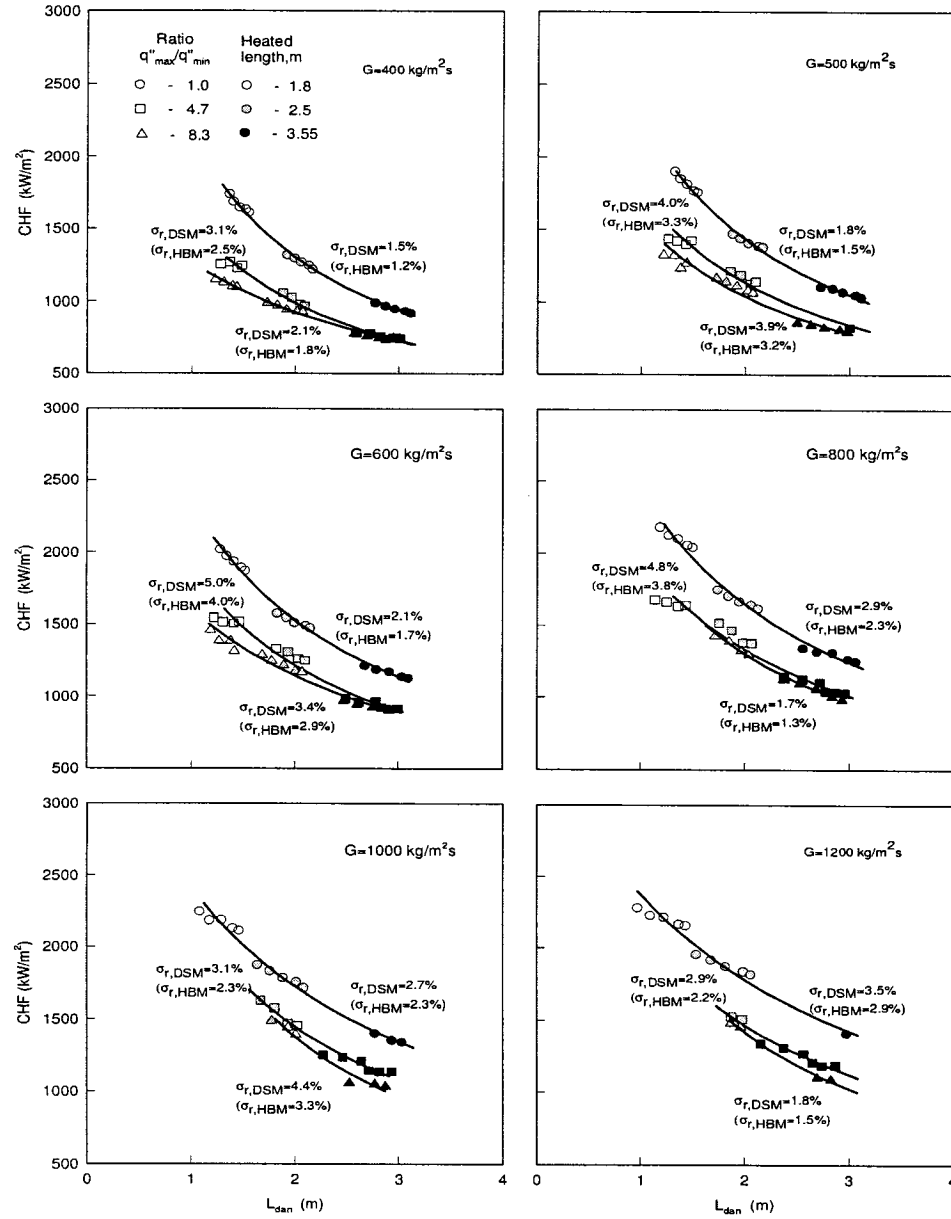
Figure 4.18: CHF as a function of the dispersed annular flow length, L_{dan} ($P_{out} = 40$ $bars$; $G = 400, 500, 600, 800, 1000, 1200$ kg/m^2s).

4.2.3 Comparison between CHF_{MEAS} and CHF_{DSM}

The Equation (4.17) and (4.20) are used to fit the CHF data by using both the DSM and HBM methods. Note that the values of the regression coefficients B0 and B1, are given in the Table 4.2. The results of these regrssions are shown in the Figure 4.19 and 4.20. A comparision between these figures and the Figures 4.9 and 4.10 (i.e., figures obtained by using the thermodynamic quality) shows that the use of the dispersed annular flow length yields a much better result.
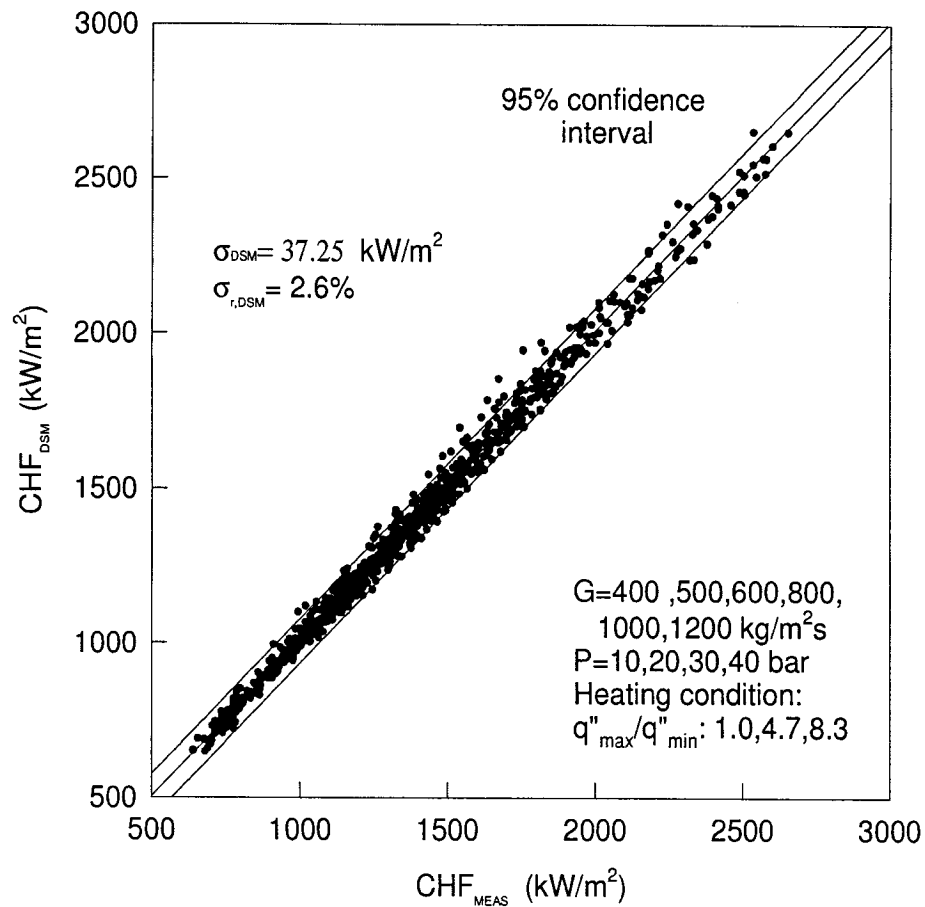
Figure 4.19: A comparison between CHF_{MEAS} and CHF_{DSM}
(CHF_{DSM} is calculated by using the coefficients
given in the Table 4.2 and the Equation (4.17)).
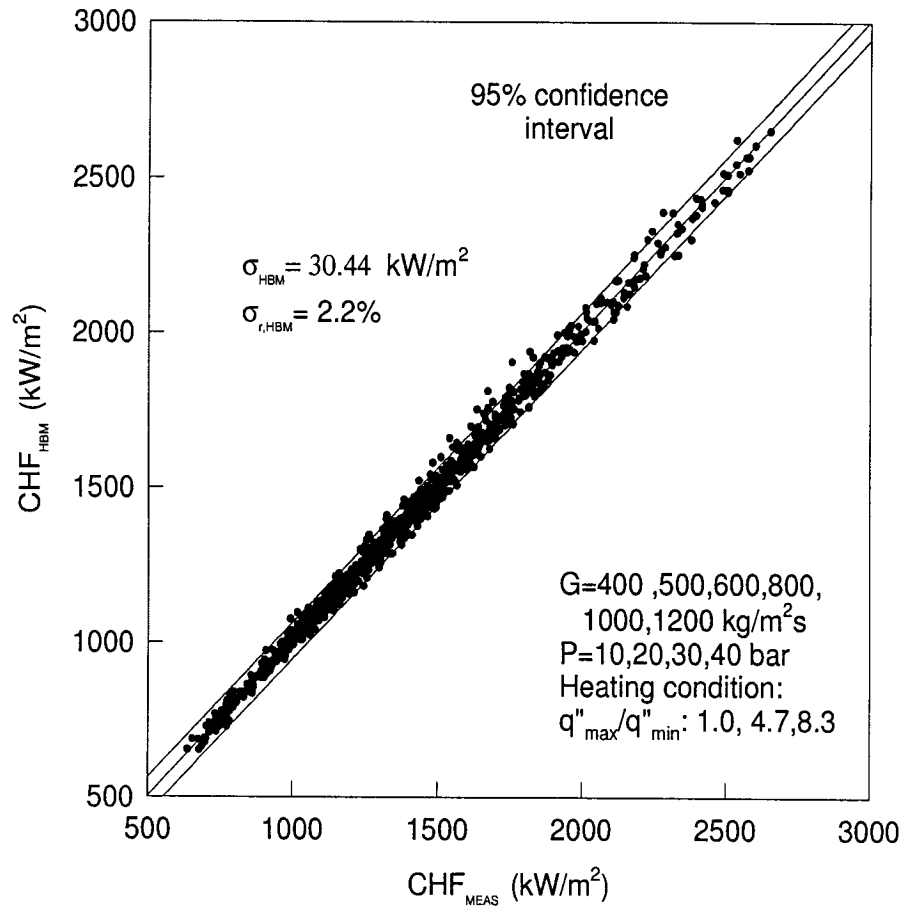
Figure 4.20: A comparison between CHF_{MEAS} and CHF_{HBM}
(CHF_{HBM} is calculated by using the coefficients
given in the Table 4.2 and the Equation (4.20)).

4.3 Average and local critical heat flux versus the thermodynamic quality

Kitto and Weiner (1982) investigated the combined effects of nonuniform circumferential heating and tube inclination on CHF. In order to obtain non-uniform heat flux distributions, they welded Inconel bars longitudinally to one side of stainless steel tubes. Since the tubes were heated by Joule effect, the nonuniform electrical resistance of the tube allowed them to attain nominal peak-to-average heat flux ratios ($q"_{max}/q"_{mean}$) of up to 2.05. Steam/water flows at 186 *bars*

were studied for 15°, 30° and 90° inclinations from the horizontal plane. The flow parameters chosen for this study are the followings:

Heated lengths	5385 $mm/$ (5334 mm, ribbed);
Tube internal diameter/equivalent volumetric average diameter	38.6 $mm/(37.9$ mm,ribbed);
Mass fluxes	271 - 1760 kg/m^2s;
Pressure	18.6MPa;
$q_{cr}^{max}/q_{cr}^{min}$	3.96;
q_{cr}^{max}/q_{cr}^{m}	2.05/(1.91,ribbed);
Outlet thermodynamics quality	-60% to 100% SBW(steam by weight).
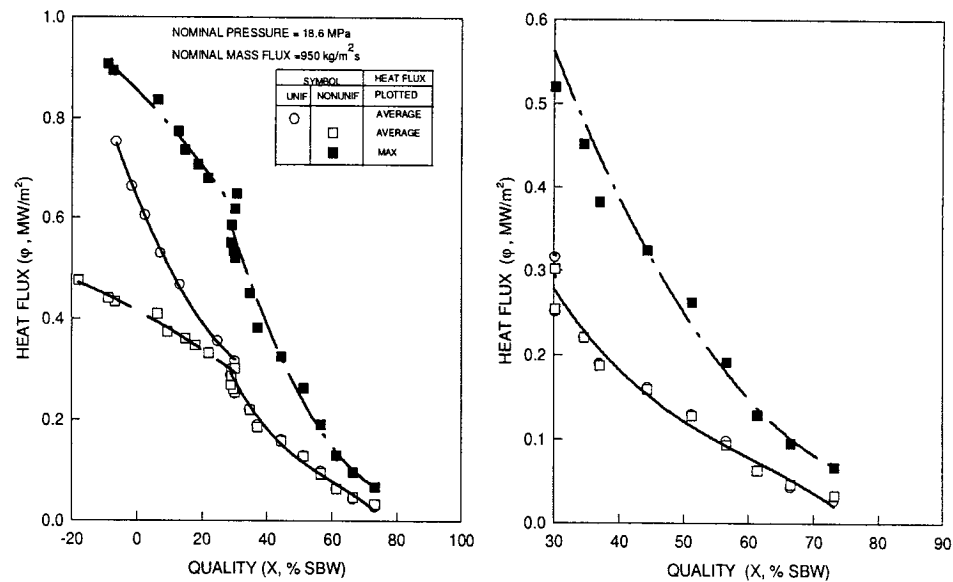
Figure 4.21 Vertical smooth tube CHF data from Kitto and Weiner (1982)
$(P = 18.6$ MPa; $G = 950$ kg/m^2s; $L = 5385$ mm;
$I.D. = 38.6$ mm; $\frac{q"_{max}}{q"_{min}}$: 3.96; x_{exit}: -20% to 73% SBW).

The Figure 4.21 shows the CHF data obtained by Kitto and Weiner (1982); based on these test results, the following effects are observed:

• At CHF conditions, the nonuniform peak heat flux was always greater than

uniform average heat flux.

- At low quality or high inlet subcooled condition, the nonuniform peak heat flux seems to approach the uniform average heat flux, indicating that for low quality the CHF depends on the local variables.

- As the quality increases and the flow pattern passes from nucleate boiling to annular/convective boiling, the nonuniform average heat flux appears to approach the uniform average heat flux, which indicats that for high quality the CHF depends on the average flow variables (i.e., cross-sectional average value).

The experimental conditions of the present CHF study (see Chapter 3) are:

Heated length	1800 - 3550 mm;
Tube internal diameter	22 mm;
Mass flux	400 - 1600 kg/m^2s;
Pressure	10 - 40 $bars$;
q''_{max}/q''_{mean}	1.0, 2.01, 2.37;
q''_{max}/q''_{min}	1.0, 4.7, 8.3.

Due to the pressure range of the present study is quite different to that of Kitto and Weiner (1982)'s, the comparisons between the CHF data of the present study and that of Kitto and Weiner (1982)'s can not be carried out. However, some qualitative trends can be observed by representing CHF as functions of the average and local Critical Heat Flux versus the thermodynamic quality (see Figures 4.22 to 4.24). These results permit the following conclusions to be carried out:

- Using the nonuniform peak heat flux to correlate CHF data seems to collapse the CHF data of different nonuniform heating along a same line, therefore reducing the dispersion of the CHF data.

- The influence of nonuniform heating on CHF shows that the higher is the nonuniformity q''_{max}/q''_{mean}, the lower is the mean values of CHF. How-

ever, the effect of nonuniform heating on CHF decreases with increasing the pressure.

- Moreover, our results also show that the effect of nonuniform heating decreases with increasing the heating length.
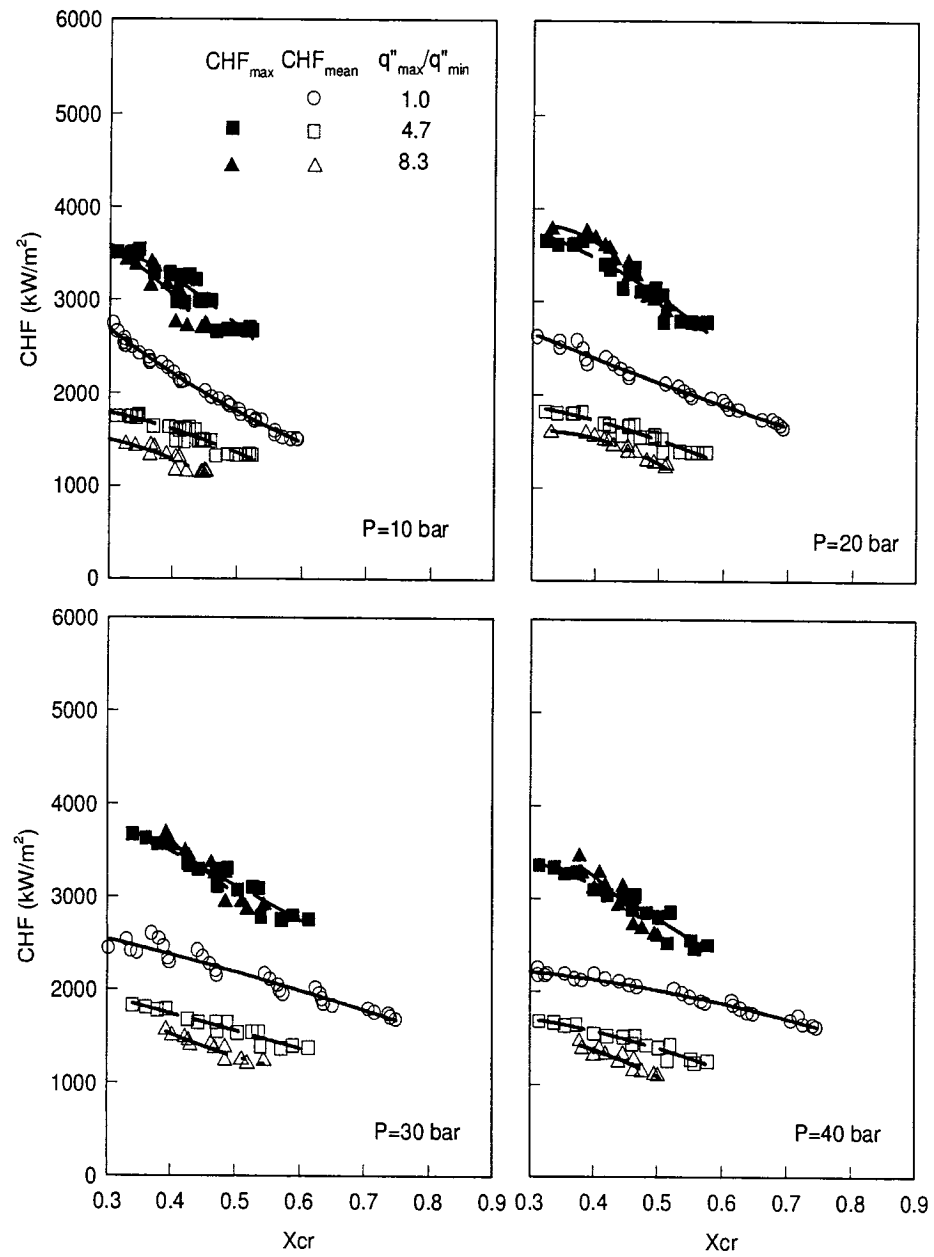
Figure 4.22: CHF data for vertical nonuniform heated flows
$(L = 1.8 \ m; \ I.D. = 22 \ mm; \ \frac{q"_{max}}{q"_{min}} = 1.0, 4.7, 8.3)$.
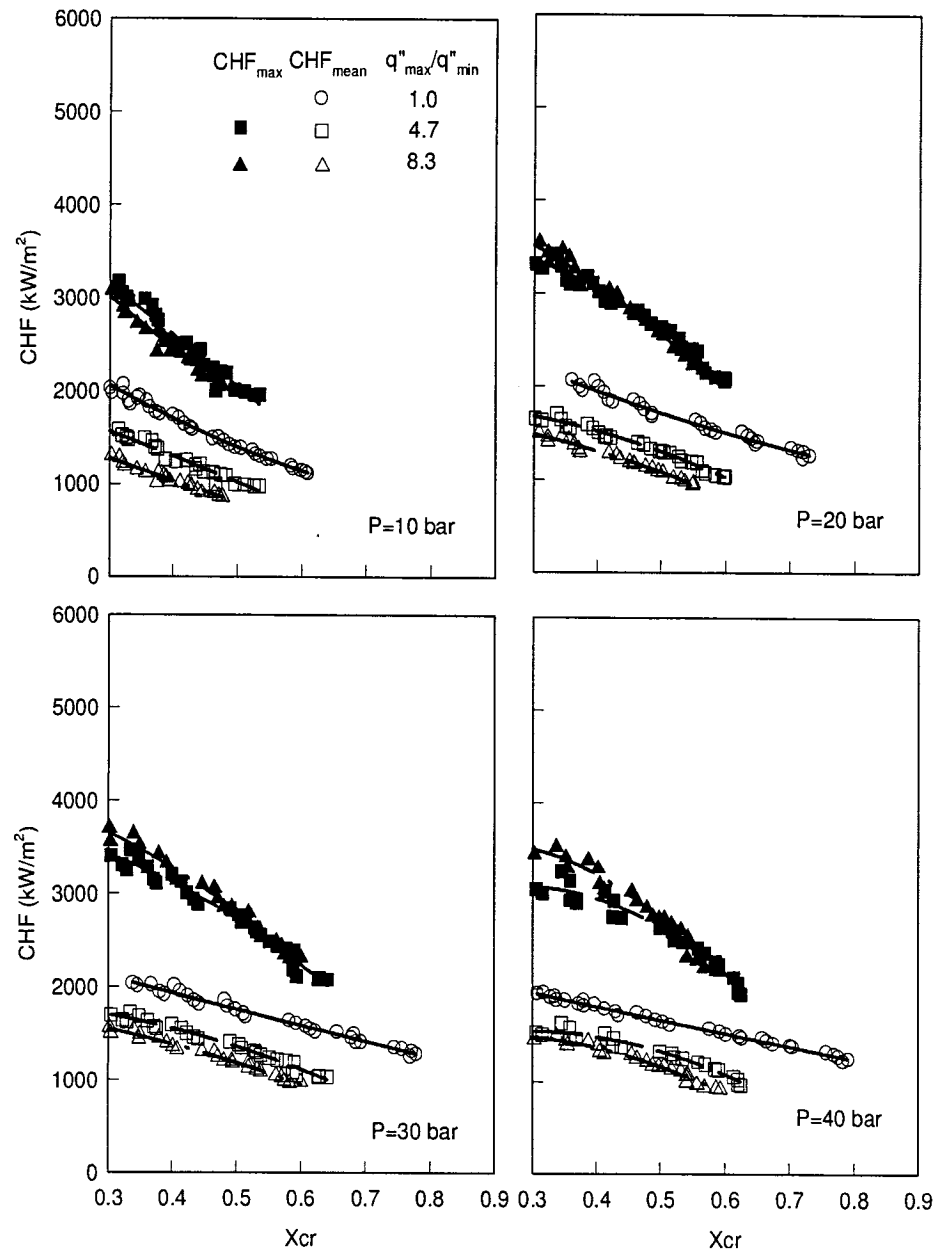
Figure 4.23: CHF data for vertical nonuniform heated flows $(L = 2.5\ m;\ I.D. = 22\ mm;\ \frac{q''_{max}}{q''_{min}} = 1.0, 4.7, 8.3)$.
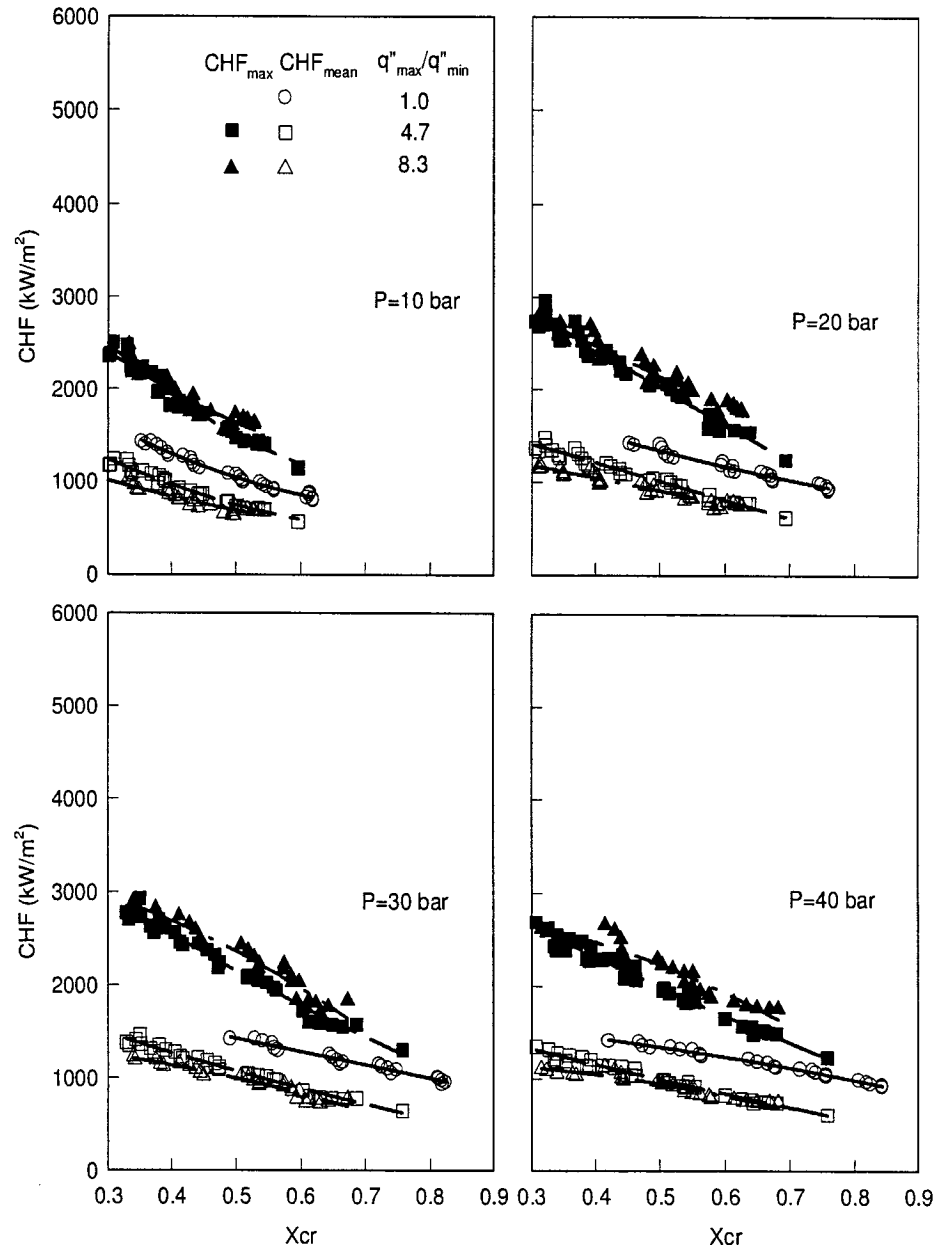
Figure 4.24: CHF data for vertical nonuniform heated flows
$(L = 3.55\ m;\ I.D. = 22\ mm;\ \frac{q"_{max}}{q"_{min}} = 1.0, 4.7, 8.3)$.

CHAPTER 5

DEVELOPMENT OF CHF CORRELATION METHOD

Even though we have shown that CHF can be correlated by using linear regressions having the general form given by Equation (4.4), (4.8), (4.17) and (4.20), before starting to develop a correlation, it is necessary to study how the flow parameters affect the coefficients B0 and B1.

In the following section we will present the effect of mass flux and pressure on these coefficients for the two CHF representations discussed in Chapter 4 (i.e., thermodynamic quality and disperse annular flow length).

5.1 Thermodynamic quality CHF representation

As discussed in Chapter 4 the thermodynamic quality is the most commonly used flow variable for representing the CHF data (Doroshchuk 1966; Groeneveld *et al.*1996). However, we have noticed that this flow variable is not able to reduce the scattering observed in the experimental data. Due to its broad utilization, in the next sections the effect of different flow variables will be discussed.

5.1.1 The effect of the mass flux on CHF

The regression coefficients B0 and B1 given in the Table 4.1 are plotted as a function of the mass flux for a given pressure and geometric configuration in Figures 5.1 through 5.3.

From these figures, it is apparent that the effect of the mass flux can be introduced by a linear regression of the coefficients having the following form:

$$B0 = C0 + C1 \cdot G, \tag{5.1}$$

$$B1 = D0 + D1 \cdot G, \tag{5.2}$$

where the coefficients C0, C1, D0 and D1 are function of the pressure.

5.1.2 The effect of the pressure on CHF

As pointed out, the coefficients C0, C1, D0 and D1 are function of the flow pressure. The values of these coefficients are plotted as a function of pressure in the Figure 5.4 through 5.7. These points can be fitted by using appropriate polynomial expressions. The following generalized equation for calculating C0, D0, C1, and D1 is proposed:

$$C_n \ or \ D_n = E(0) + E(1) \times P + E(2) \times P^2 + E(3) \times P^3, \qquad (5.3)$$

with $n = 0 \ or \ 1$.

The values obtained for the coefficients E(0), E(1), E(2) and E(3) are given in the Table 5.1. Then, the use of this table in conjunction with the Equation (5.1) through (5.3), Equations (4.4) and (4.8) provide a convenient tool for predicting CHF. It is important to remark that the use of high order polynomial limits the applicability of the proposed correlation to flow conditions similar to those presented in this document.
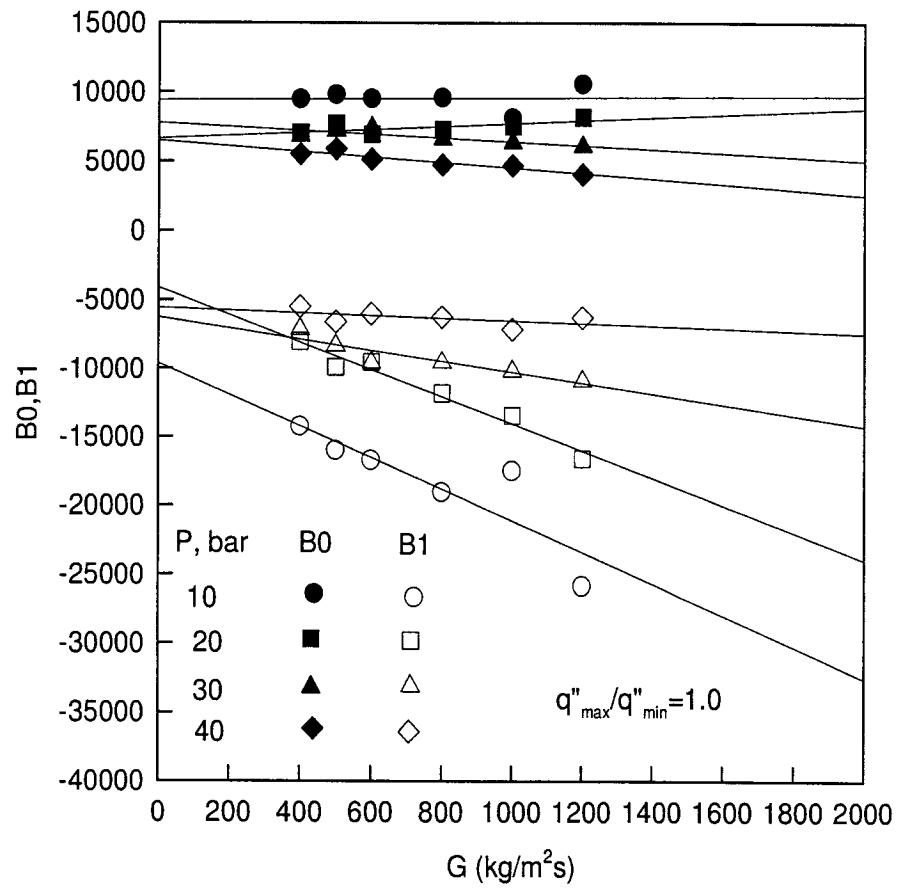
Figure 5.1: The effect of the mass flux on the regression coefficients B0 and B1 for $\frac{q''_{max}}{q''_{min}} = 1.0$.
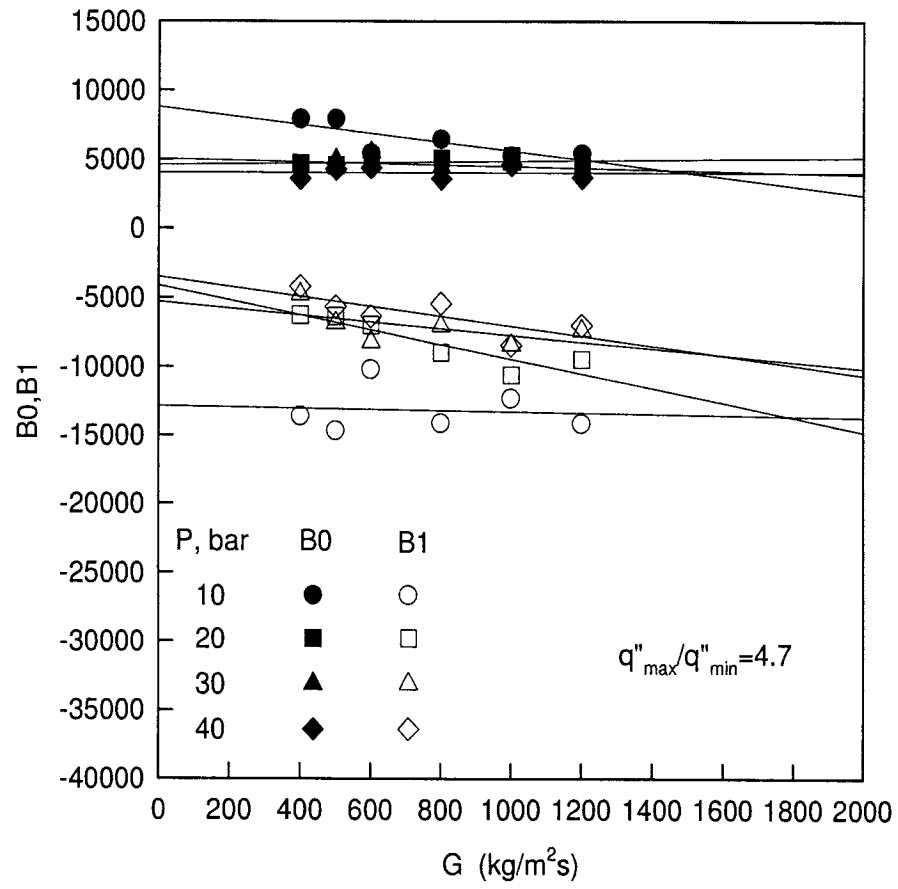
Figure 5.2: The effect of the mass flux on the regression
coefficients B0 and B1 for $\frac{q''_{max}}{q''_{min}} = 4.7$.
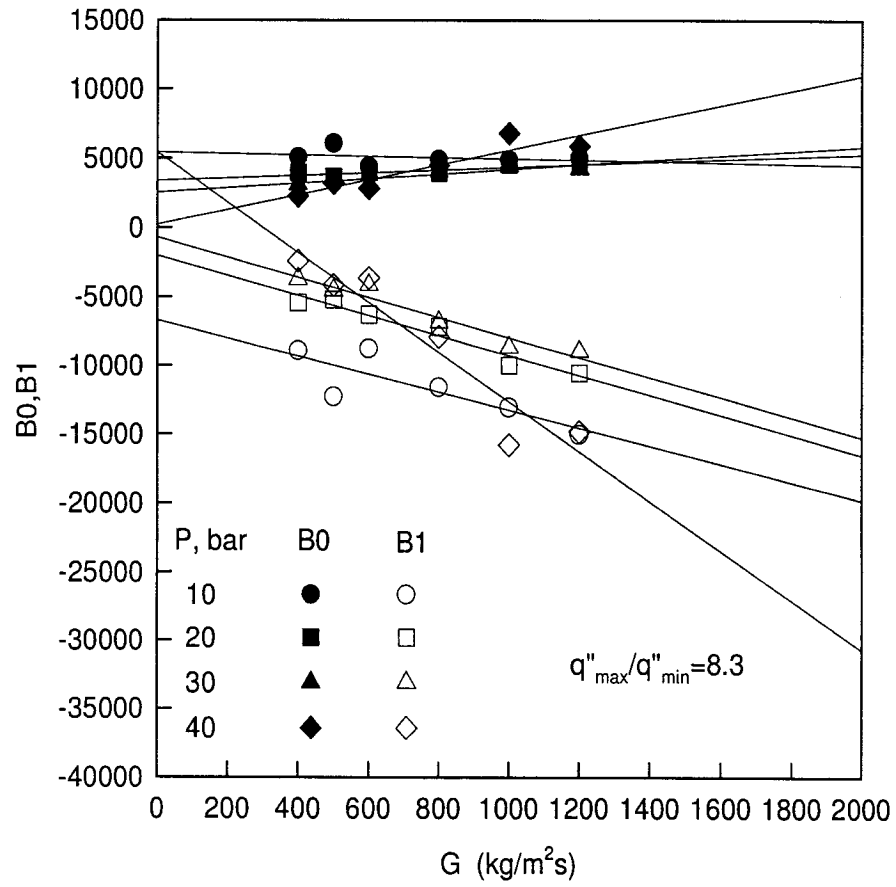
Figure 5.3: The effect of the mass flux on the regression coefficients B0 and B1 for $\frac{q''_{max}}{q''_{min}} = 8.3$.
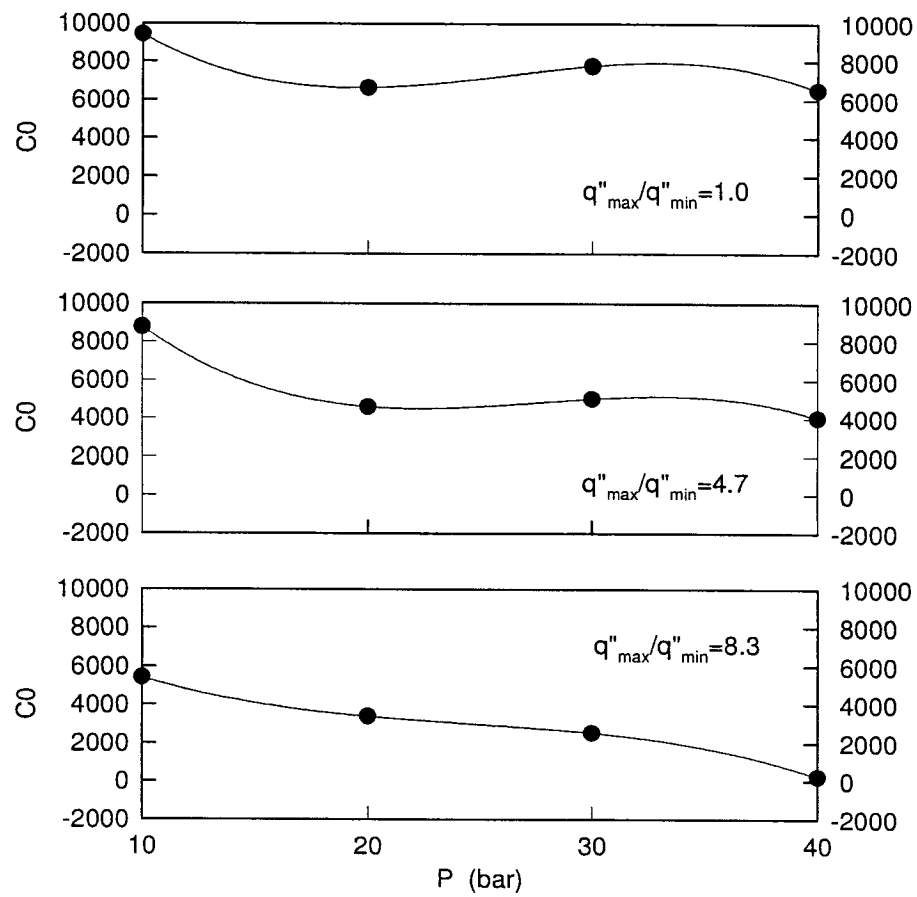
Figure 5.4: The effect of the flow pressure on the regression coefficient C0 for $\frac{q''_{max}}{q''_{min}} = 1.0; 4.7; 8.3$.
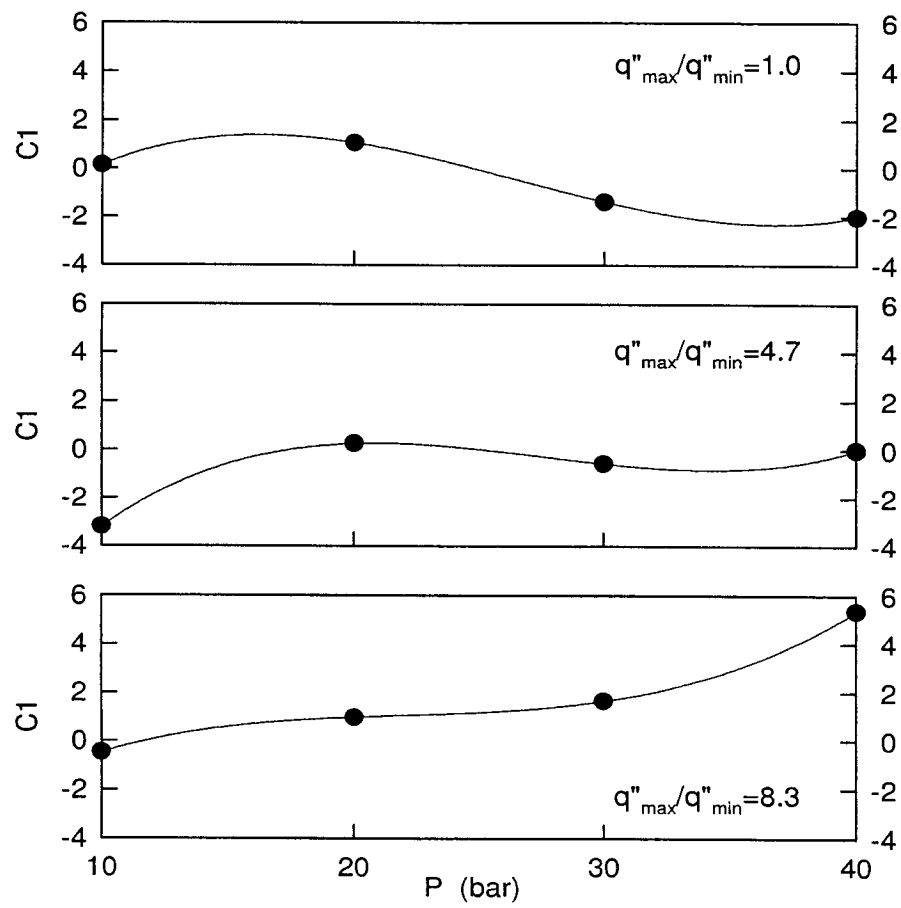
Figure 5.5: The effect of the flow pressure on the regression coefficient C1 for $\frac{q''_{max}}{q''_{min}} = 1.0; 4.7; 8.3.$
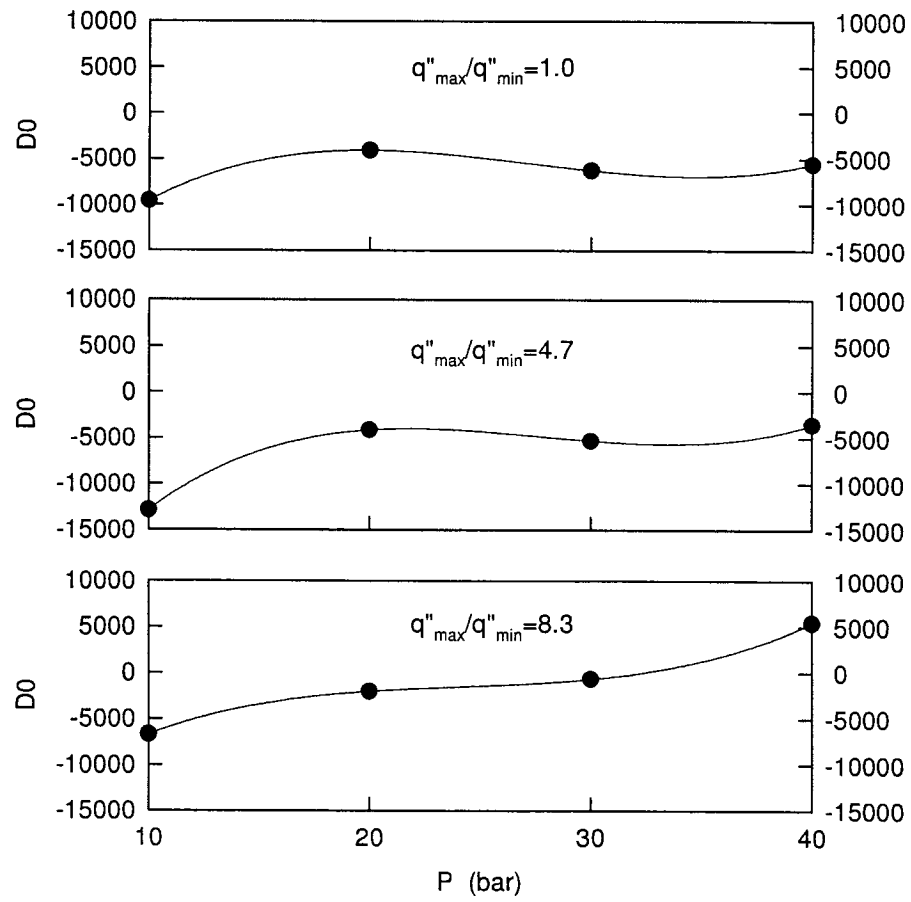
Figure 5.6: The effect of the flow pressure on the regression coefficient D0 for $\frac{q''_{max}}{q''_{min}} = 1.0; 4.7; 8.3$.
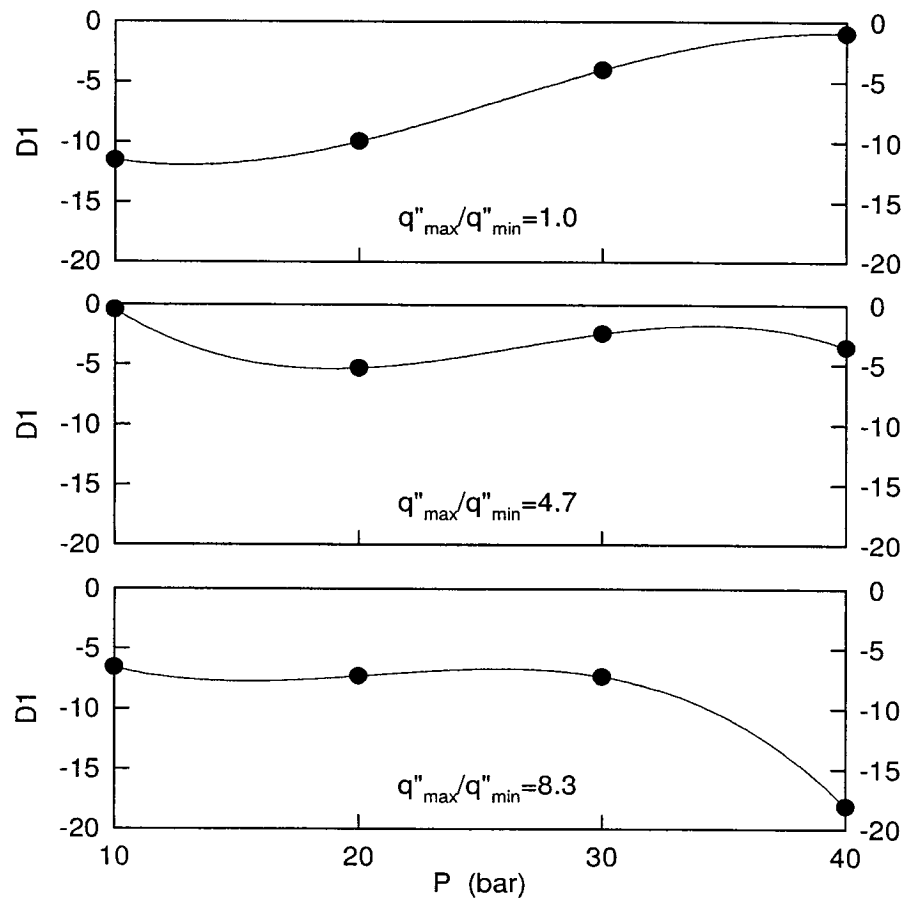
Figure 5.7: The effect of the flow pressure on the regression coefficient D1 for $\frac{q''_{max}}{q''_{min}} = 1.0; 4.7; 8.3.$

Table 5.1 Regression coefficients based on the thermodynamic
quality CHF representation.

		E(0)	E(1)	E(2)	E(3)
$\frac{q''_{max}}{q''_{min}} = 1.0$	C0	22376	-2014	82.36	-1.048
	C1	-9.302	1.545	-0.06854	8.624
	D0	-33390	3646	-144.3	1.764
	D1	-1.364	-1.841	0.09486	-1.215E-3
$\frac{q''_{max}}{q''_{min}} = 4.7$	C0	22640	-2219	83.54	-1.008
	C1	-16.53	2.016	-0.07765	9.390E-4
	D0	-44330	4712	-177.9	2.139
	D1	24.03	-3.818	0.1569	-1.966E-3
$\frac{q''_{max}}{q''_{min}} = 8.3$	C0	11340	-873.7	32.68	-0.4446
	C1	-6.483	0.9547	-0.04177	6.328E-4
	D0	-22900	2467	-98.24	1.357
	D1	6.261	-2.266	0.1176	-1.904E-3

5.1.3 Performance of the proposed CHF correlation method

based on the thermodynamic quality approach

The values given in the Table 5.1 are used to calculate the coefficients B0 and B1 used in Equation (4.4) or (4.8) that corresponds to both DSM and HBM methods respectively.

Figures 5.8 and 5.9 show the results for the CHF_{DSM} and the CHF_{HBM} for a total of 941 data points obtained for three different nonuniform heating configurations. The range of flow conditions covered by these experiments were: pressure ranging from 10 to 40 $bars$, mass flux ranging from 300 to 1600 kg/m^2s and inlet subcooling ranging from 5 to 40 ^oC.

From Figure 5.8 and Figure 5.9 we can see that the CHF_{HBM} is more accurate than the CHF_{DSM}. The relative and absolute RMS errors of the CHF_{HBM} are 4.2% and 51.922 kW/m^2 respectively, while the relative and absolute RMS errors of CHF_{DSM} are 16.8 % and 201.877 kW/m^2 respectively.

Based on the above results, we can conclude that the use of this semi-empirical
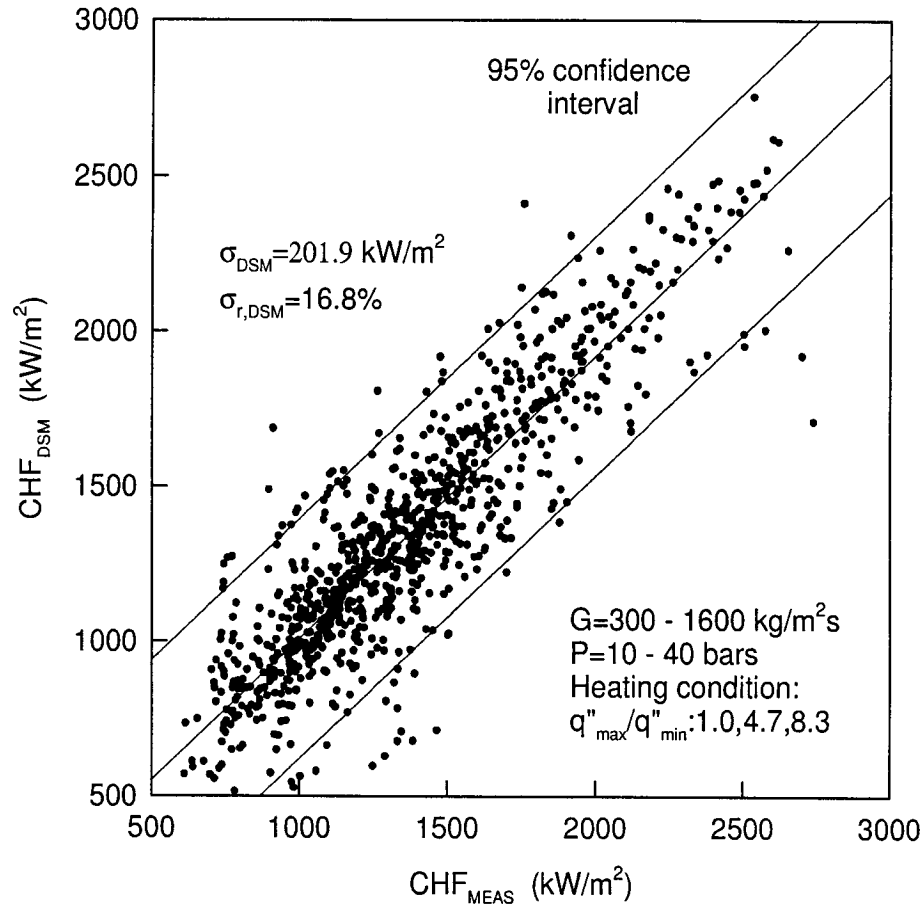
Figure 5.8: A comparison between CHF_{MEAS} and CHF_{DSM}

(CHF_{DSM} is calculated by using regression formula and equation (4-4)).

method (Equation 4.8) to predict CHF permits to obtain a better accuracy (i.e., a relative RMS error of 4.2%). The higher accuracy of this method is due to the fact that it takes into consideration both the heat flux and the quality at the same time. Note that the heat flux has been considered in an implicit manner; therefore, this method constituts an implicit approach. On the other hand, the CHF can be obtained in an explicit way by using the quality representation. As we know, the quality is affected by a number of factors, such as outlet pressure, inlet subcooling, etc.; thus, it is quite difficult to calculate the quality precisely. Due to the inlet subcooling and low mass flux, there is a large dispersion on the quality. Therefore, the explicit approach for calculating CHF (Equation 4.4) can
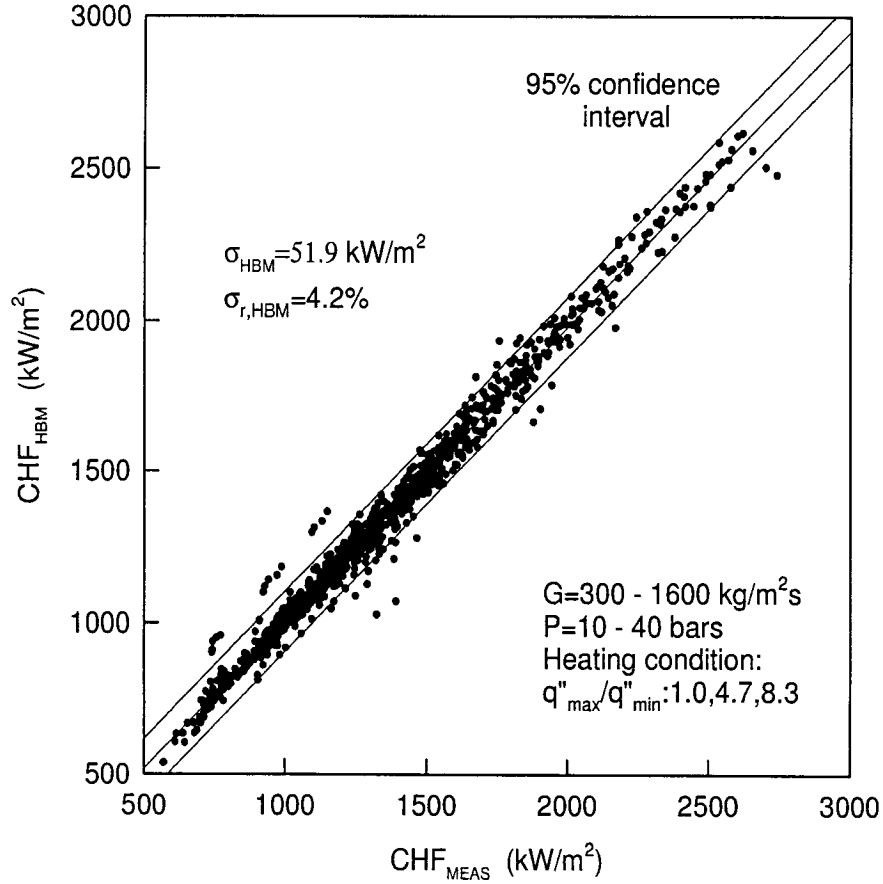
Figure 5.9: A comparison between CHF_{MEAS} and CHF_{HBM}

(CHF_{HBM} is calculated by using regression formula and equation (4-7)).

cause huge errors (i.e., a relative RMS error of 16.8%).

In Chapter 4, we have fitted the CHF by using the coefficients given in Table 4.1. The advantage of using this method is that we do not need to normalize the mass flux, the pressure and the inlet subcooling any more. This regression works well in the following flow range: pressure ranging from 10 to 40 $bars$, mass flux ranging from 300 to 1600 $kg/m^2 s$ and inlet subcooling ranging from 5 to 40 ^oC. Table 5.2 summerized the performance of the different methods used for correlating CHF with key variables, i.e., flow pressure, mass flux and nonuniformity.

Table 5.2: A comparison between the CHF correlation method based on the coefficients given in Table 4.1 and regression Equations (5.1) to (5.3).

	$\sigma_{r,DSM}$	σ_{DSM}	$\sigma_{r,HBM}$	σ_{HBM}
Prediction method based on the coefficient Table 4.1	11.2%	144.76 kW/m^2	2.3%	33.4 kW/m^2
Prediction method based on the regression Equation(5.1) to (5.3)	16.8%	201.88 kW/m^2	4.2%	51.92 kW/m^2

Another advantage of using the proposed regression formula consists of the fact that it can be used to carry out parametric trends analysis. Figure 5.10 shows the relationship that exists between CHF and key variables such as: non-uniform heating and the heated length for fixed inlet conditions. The solid lines in the figure correspond to the CHF correlation calculated with Equation (4.5), while the dashed lines are obtained with Equation (4.6) that represent the heat balance carried out over the heated length. Figure 5.10 shows that the heat balance method approach has a much higher accuracy.

From Figure 5.10, it is apparent that the proposed CHF representation permits both the effect of the heated length and the heat flux ratio on the CHF to be taken into account. We can observe that for the same geometric parameter and fixed inlet flow conditions, CHF decreases with increasing heated length and exit thermodynamic quality. On the other hand, for the same heated length and fixed inlet flow conditions the influence of nonuniform heating on CHF shows that the higher is the nonuniformity $\frac{q''_{max}}{q''_{min}}$, the lower is the mean values of CHF. However, with increasing heated length the effect of nonuniform heating on the mean CHF value decreases.

Figure 5.11 shows the effect of mass flux on CHF for fixed inlet flow conditions, the lines in this figure are based on the regression formula. It is interesting to note the excellent performance obtained by the proposed prediction method in the range of the test conditions used for the experiments.

From Figure 5.11, we can say that for fixed inlet flow conditions CHF increases with increasing the mass flux. It is also found that the heated length play an important role on the value of CHF.

Both from Figure 5.10 and Figure 5.11, it is observed that for the same heated length and at fixed inlet flow conditions passing from uniform to nonuniform heating conditions provokes a big drop in CHF. However increasing the nonuniformity $\frac{q''_{max}}{q''_{min}}$, the effect on CHF is less apparent.
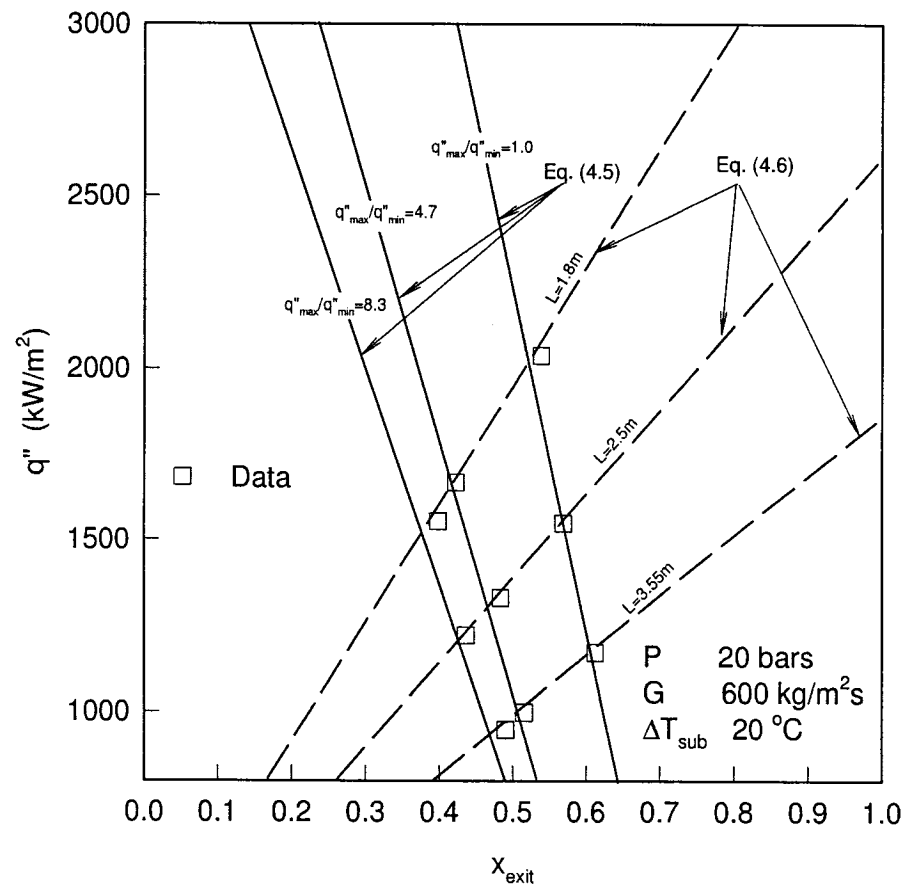
Figure 5.10: The relationship between CHF, non-uniform heating and heated length; thermodymamic quality approach.
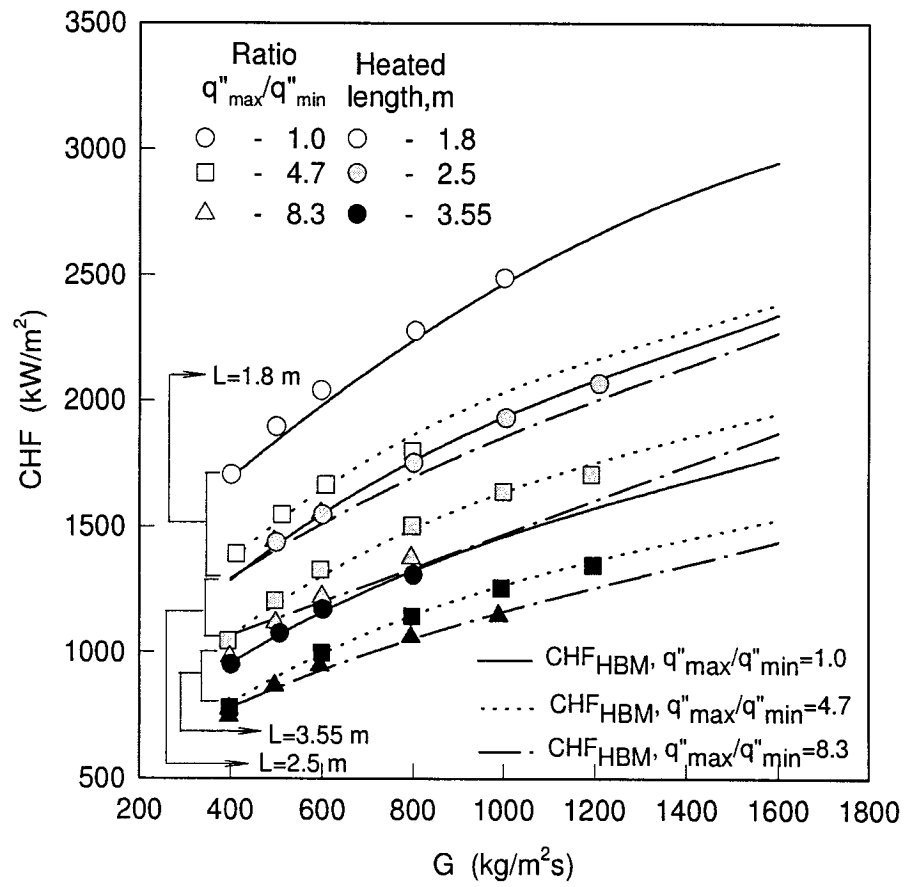
Figure 5.11: Mass flux effect for fixed inlet flow conditions
$(P(in) = 20 \; bars, \; T_{in} = 192 \; {}^0C)$.

Now let us examine the Equation (4.9) that is represented under the following form:

$$CHF_{HBM} = (B0 \cdot h_{fg} + B1 \cdot h_{in} - B1 \cdot h_f) / \left(h_{fg} - \frac{4B1 \cdot LD}{G} \right), \qquad (5.8)$$

where LD : ratio of heated length to the tube inside diameter.

Since the coefficients B0 and B1 are functions of the mass flux and the pressure, we can write:

$$B0 = f(G, P) \quad and \quad B1 = f(G, P). \qquad (5.9)$$

Note that in the Equation (5.8) h_{fg}, h_f, h_{fg} are also function of the pressure, h_{in} is the inlet subcooling. Thus, CHF can be rewritten by using the following relationship:

$$CHF = f\left(G, (\Delta T_{sub})_i, p, D, z \right). \qquad (5.10)$$

At this point we arrived to the hypothesis we made at the very beginning of Chapter 4 which is now proved to be right, i.e., CHF can be represented as a complex function of inlet flow conditions, the flow pressure, the mass flux and the geomtry.

5.2 The dispersed annular flow length approach

As we discussed before this approach is based on a new representation of CHF, i.e., $CHF = f(L_{dan})$. The length over which the dispersed annular flow exists is calculated by Equation (4.14). In the following section we will present the effect of mass flux and pressure on the regression coefficients for the dispersed annular flow length approach.

5.2.1 The effect of the mass flux on CHF

B0 and B1 coefficients given in Table 4.2 are plotted in Figures 5.12 to 5.14 as a function of the mass flux for each geometric configuration and each exit pressure. It is apparent that by regression, we can obtain a straight line for each group of these coefficients with new regression coefficients C0 and C1, D0 and D1 (see Figures 5.12 to 5.14). Then B0 and B1 can be calculated by following equations:

$$B0 = C0 + C1 \cdot G, \tag{5.11}$$

$$B1 = D0 + D1 \cdot G. \tag{5.12}$$

5.2.2 The effect of the pressure on CHF

Figures 5.15 to 5.18 represents the relationships between C0, C1, D0, D1 and the pressure. The data is then fitted by using a third order polynomial; thus, we obtain a series of coefficients that are given in the Table 5.3. These coefficients are then used to calculate C0, C1, D0, D1 by using the following given in a generalized form:

$$C_n \ or \ D_n = E(0) + E(1) \times P + E(2) \times P^2 + E(3) \times P^3, \tag{5.13}$$

with $n = 0 \ or \ 1$.

Table 5.3 Regression coefficients based on the dispersed annular flow length CHF representation.

		E(0)	E(1)	E(2)	E(3)
$\frac{q''_{max}}{q''_{min}} = 1.0$	C0	0.1002	-0.02256	-3.690E-4	2.428E-5
	C1	2.454E-4	-8.122E-5	4.247E-6	-8.590E-8
	D0	973.9	94.62	-0.6859	-0.03265
	D1	1.599	0.1454	-6.726E-3	1.230E-4
$\frac{q''_{max}}{q''_{min}} = 4.7$	C0	1.052	-0.1835	9.252E-3	-1.417E-4
	C1	-1.123	1.535E-4	-1.125E-5	1.945E-7
	D0	-1933	475.8	-20.97	0.2875
	D1	6.189	-0.5579	0.02968	-4.522E-4
$\frac{q''_{max}}{q''_{min}} = 8.3$	C0	0.9887	-0.2339	0.01071	-1.687E-4
	C1	-2.525E-3	3.806E-4	-1.957E-5	3.130E-7
	D0	-471.4	351.2	-15.57	0.2298
	D1	4.653	-0.4978	0.02741	-4.444E-4
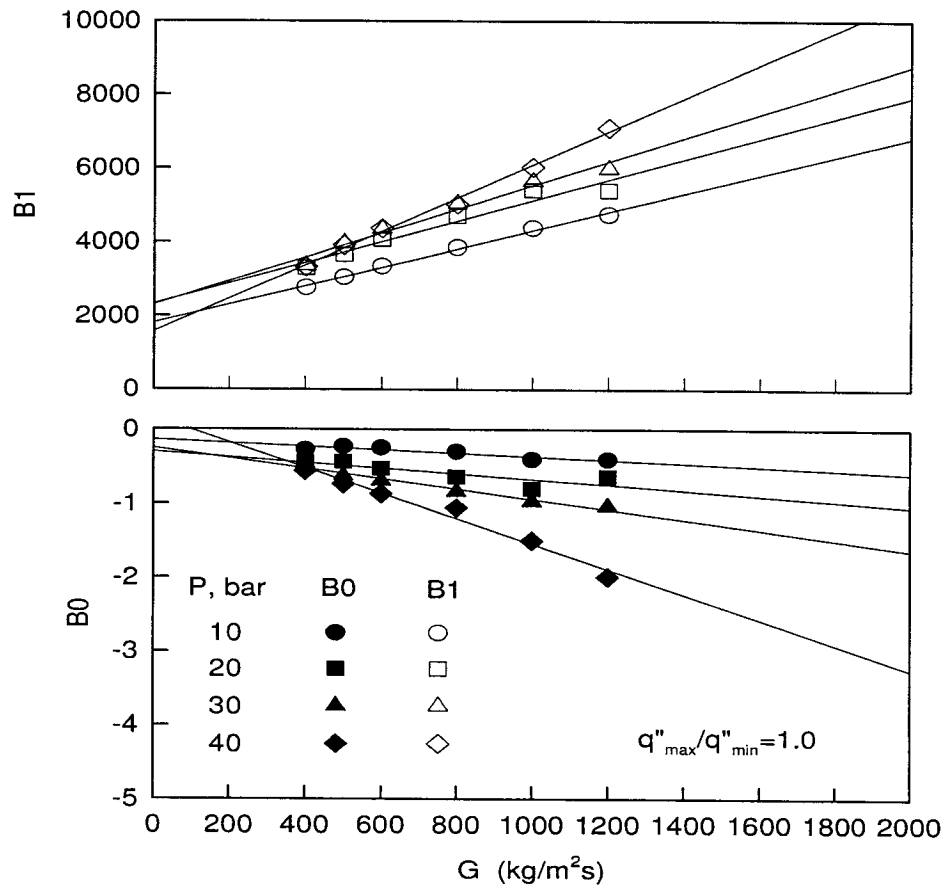
Figure 5.12: The effect of the mass flux on the regression coefficients B0 and B1 for $\frac{q"_{max}}{q"_{min}} = 1.0$.
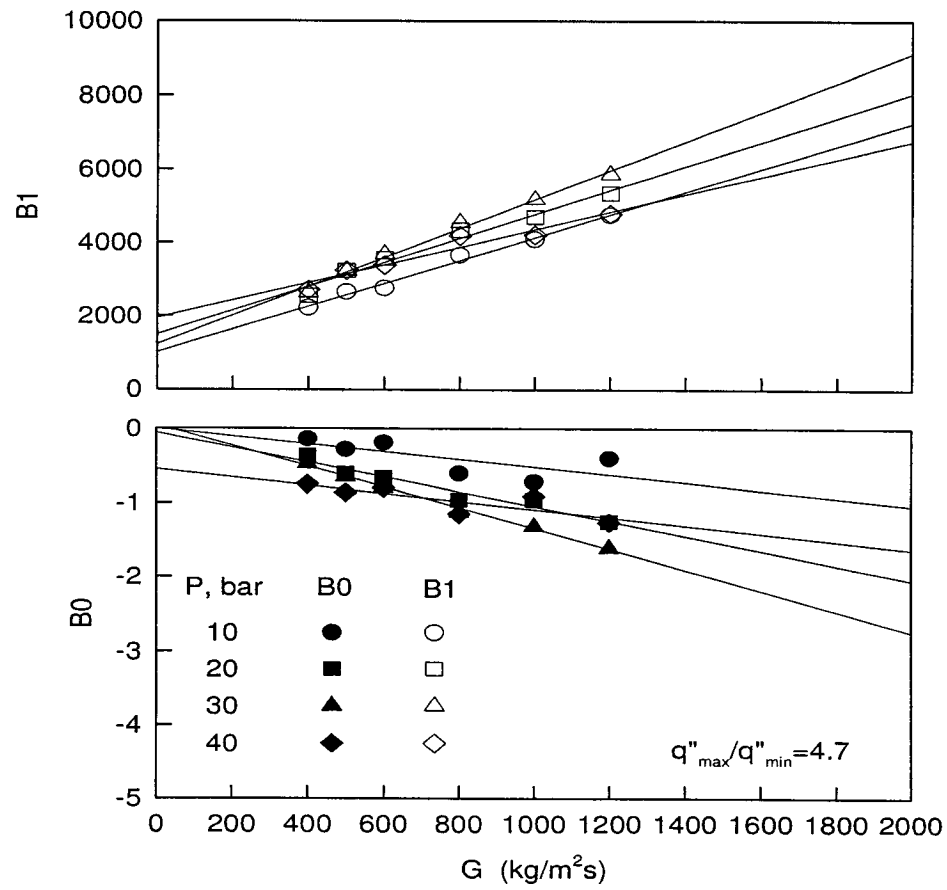
Figure 5.13: The effect of the mass flux on the regression coefficients B0 and B1 for $\frac{q''_{max}}{q''_{min}} = 4.7$.
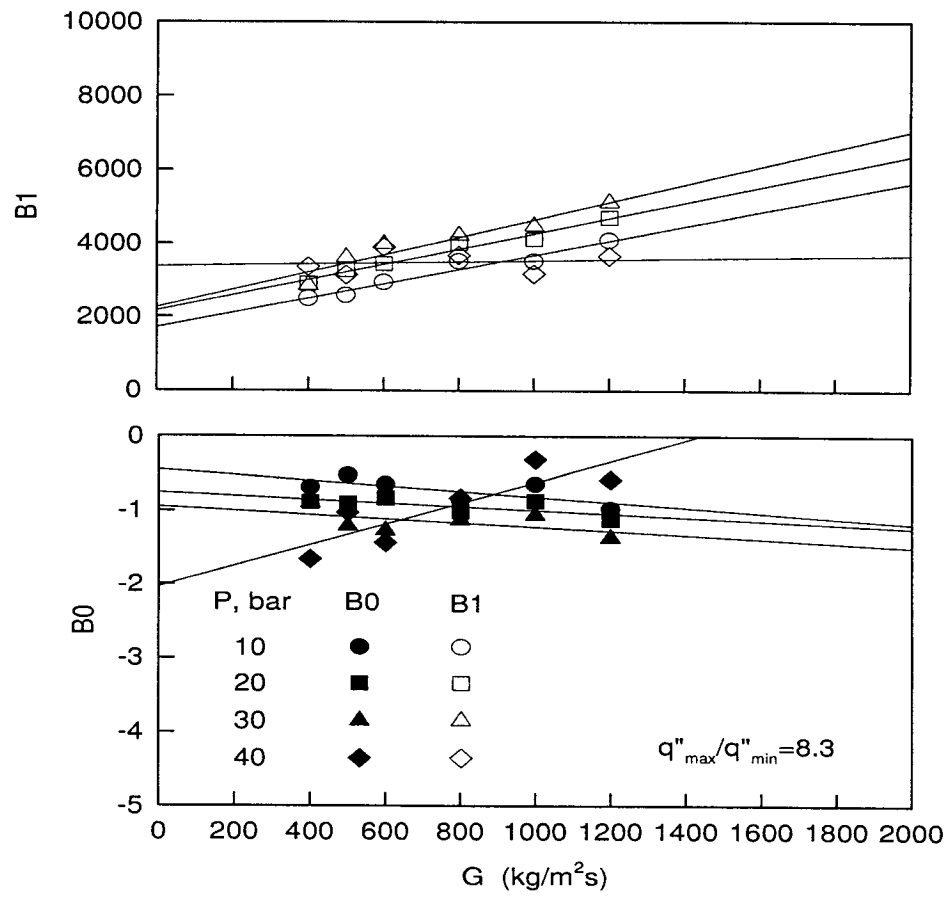
Figure 5.14: The effect of the mass flux on the regression coefficients B0 and B1 for $\frac{q''_{max}}{q''_{min}} = 8.3$.
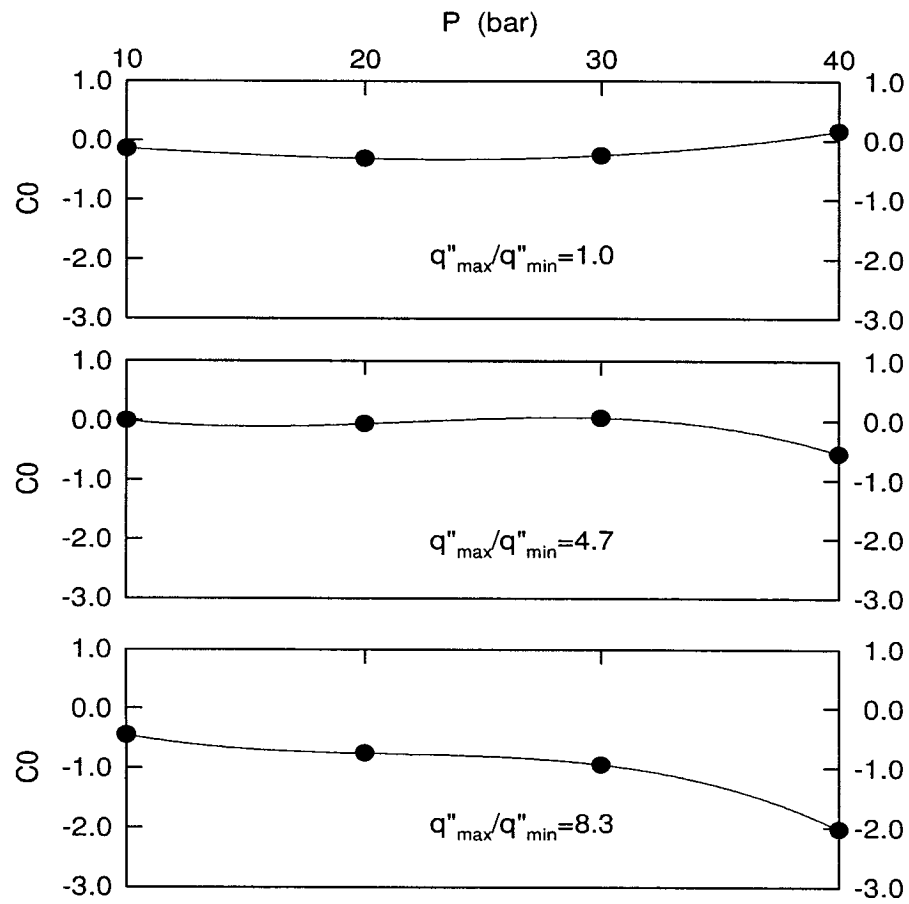
Figure 5.15: The effect of the flow pressure on the regression coefficient C0 for $\frac{q''_{max}}{q''_{min}} = 1.0; 4.7; 8.3$.
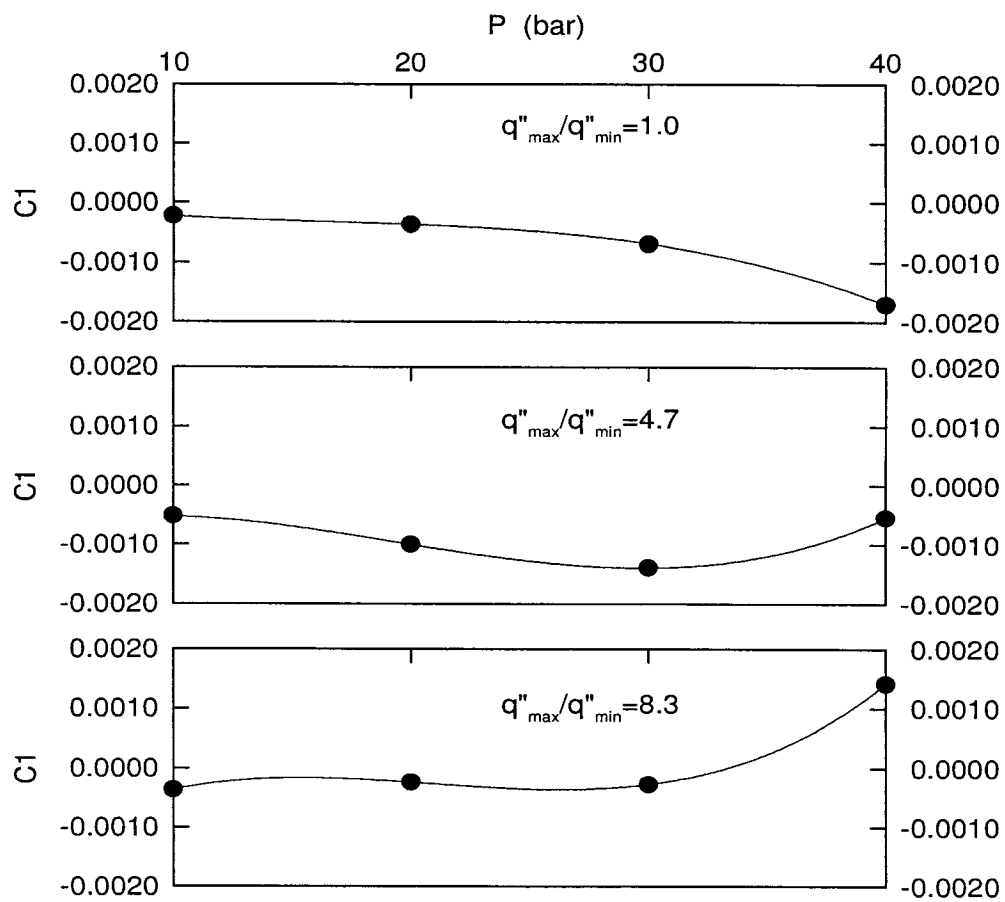
Figure 5.16: The effect of the flow pressure on the regression coefficients C1 for $\frac{q''_{max}}{q''_{min}} = 1.0; 4.7; 8.3$.
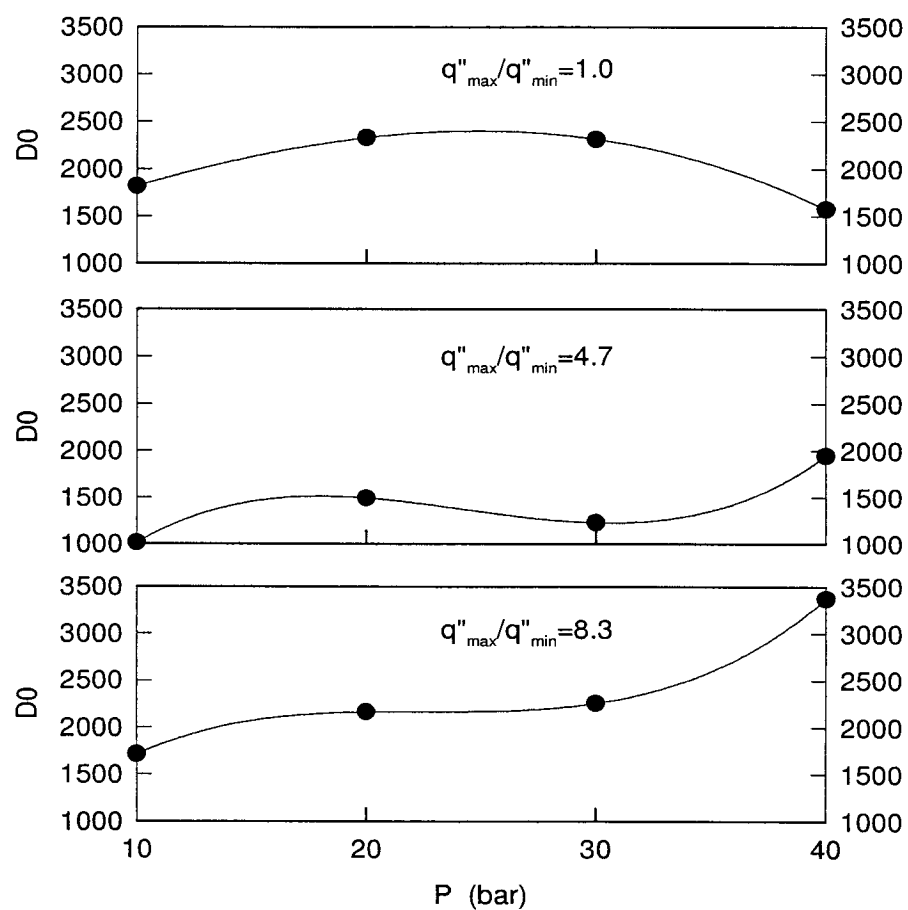
Figure 5.17: The effect of the flow pressure on the regression
coefficients D0 for $\frac{q''_{max}}{q''_{min}} = 1.0; 4.7; 8.3.$
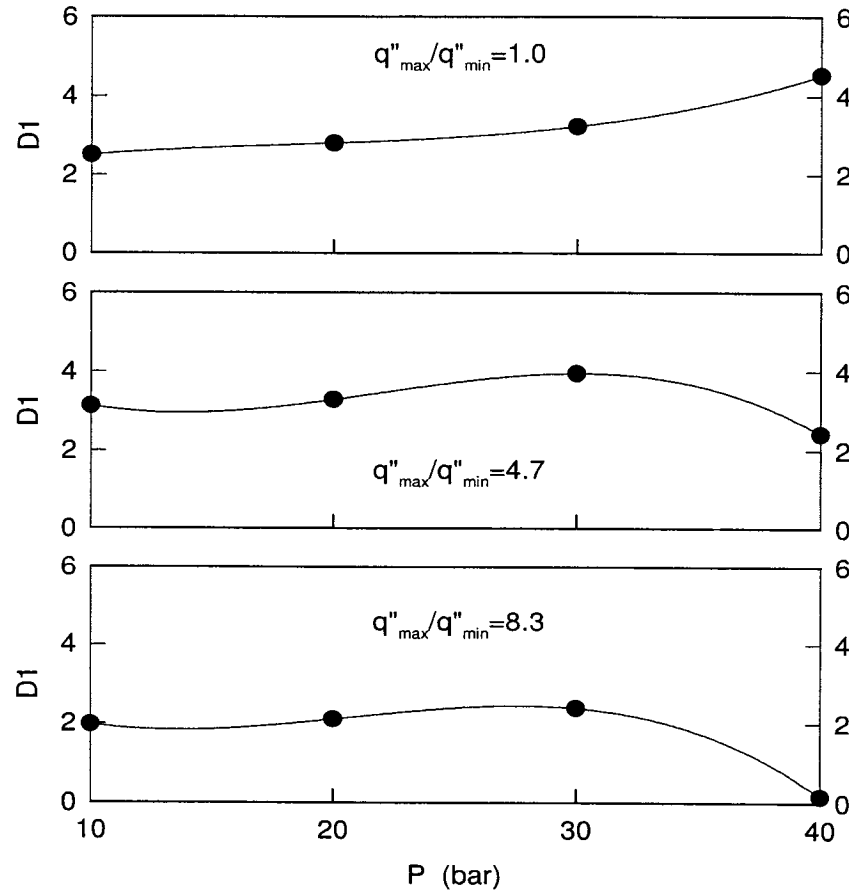
Figure 5.18: The effect of the flow pressure on the regression coefficients D1 for $\frac{q''_{max}}{q''_{min}} = 1.0; 4.7; 8.3$.

5.2.3 Performance of the proposed CHF correlation method based on the dispersed annular flow length approach

After calculating C0, C1, D0 and D1 by using equation (5.13), B0 and B1 are obtained from Equations (5.11) and (5.12). With these coefficients we can calculate CHF_{DSM} and CHF_{HBM} from Equations (4.15) and (4.17). Figure 5.19 and Figure 5.20 show the results of CHF_{DSM} and CHF_{HBM} for a total of 941 test points obtained by using three different angular heat distributions, outlet pressure ranging from 10 to 40 $bars$, mass flux ranging from 300 to 1600 kg/m^2s and inlet subcooling ranging from 5 to 40 ^oC.
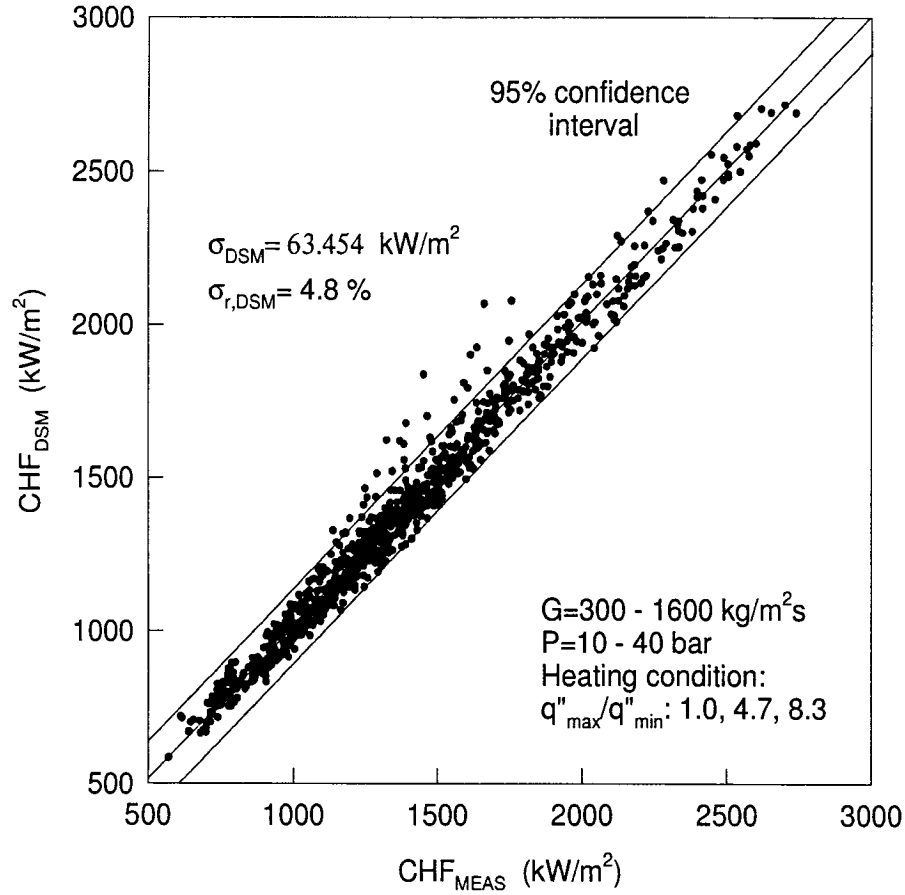
Figure 5.19: A comparison between CHF_{MEAS} and CHF_{DSM}
(CHF_{DSM} is calculated by using the Equations (5.11)
to (5.13) and the Equation (4.15)).

In Chapter 4 we have presented a CHF correlation method based on the coefficients given in the Table 4.2. The advantage of the present method is that we do not need to normalize the mass flux, the outlet pressure and the inlet subcooling, it works well in the range of flow conditions given by: flow pressure from 10 to 40 $bars$, mass flux from 300 to 1600 kg/m^2s and inlet subcooling from 5 to 40 ^{o}C. The accuracy of the present method is quite acceptable. A comparison between the method based on the coefficient of Table 4.2 and regression Equations (5.11) to (5.13) are summerized in the Table 5.4.
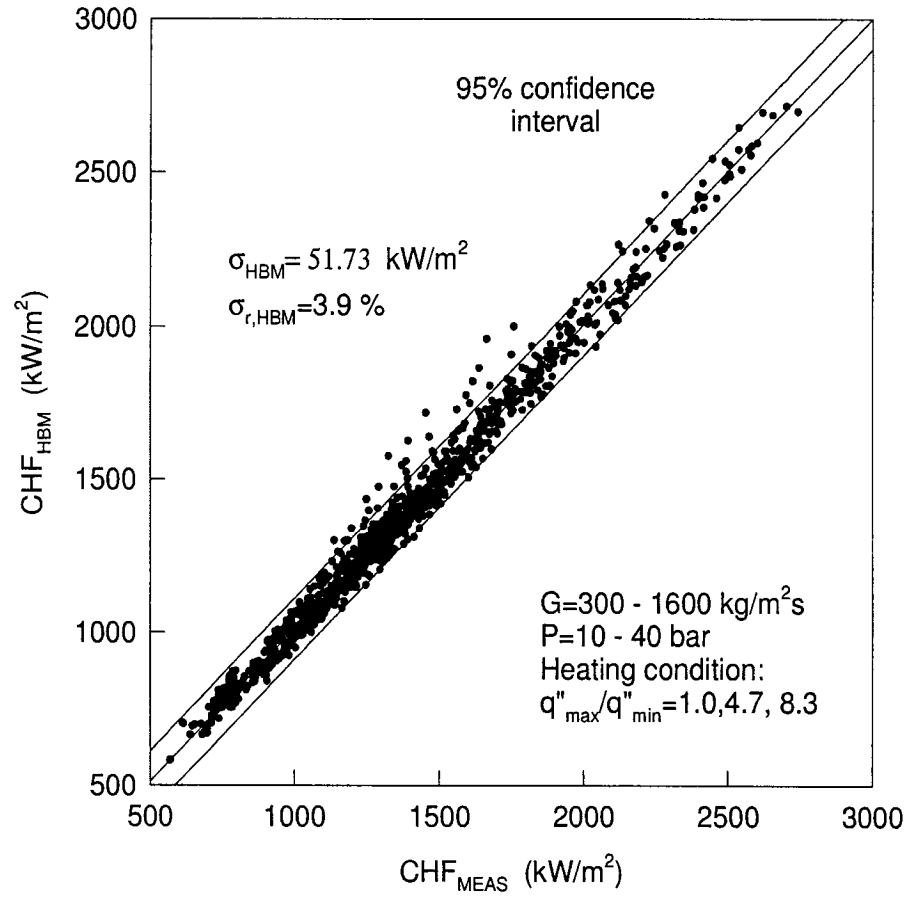
Figure 5.20: A comparison between CHF_{MEAS} and CHF_{HBM}
(CHF_{HBM} is calculated by using the Equations (5.11)
to (5.13) and the Equation (4.18)).

Table 5.4: A comparison between the CHF correlation method based on
the coefficients given in Table 4.2 and regression Equations (5.11) to (5.13).

	$\sigma_{r,DSM}$	σ_{DSM}	$\sigma_{r,HBM}$	σ_{HBM}
Prediction method based on the coefficient Table 4.2	2.6%	37.25 kW/m^2	2.2%	30.44 kW/m^2
Prediction method based on the regression Equation(5.11) to (5.13)	3.9%	51.73 kW/m^2	4.8%	63.45 kW/m^2

Another advantage of the proposed CHF correlation technique is that the use of the regression Equations (5.11) through (5.13) permits a parametric trends analysis to be carried out. Figure 5.21 shows the relationship that exits between the CHF, the nonuniform heating and heated length for fixed inlet flow conditions. The solid lines in the figure come from the Equation (4.16) where B0 and B1 are calculated by using the proposed method, while the dashed lines are obtained with Equation (4.17) that represents the heat balance carried out over the heated length. From Figure 5.21, we can conclude that the accuracy obtained by using the heat balance method approach is quite high.

It is established that for the same geometric parameter and for fixed inlet flow conditions, CHF decreases with increasing the heated length. On the other hand, for the same heated length and fixed inlet flow conditions, the effect of the nonuniform heating on CHF shows that the higher is the heat nonuniformity, $\frac{q''_{max}}{q''_{min}}$, the lower is the mean values of CHF. However, with an increase in the heated length this effect diminishes. It is apparent that for the range of flow conditions covered in this work, the method proposed for correlating CHF is quite good.
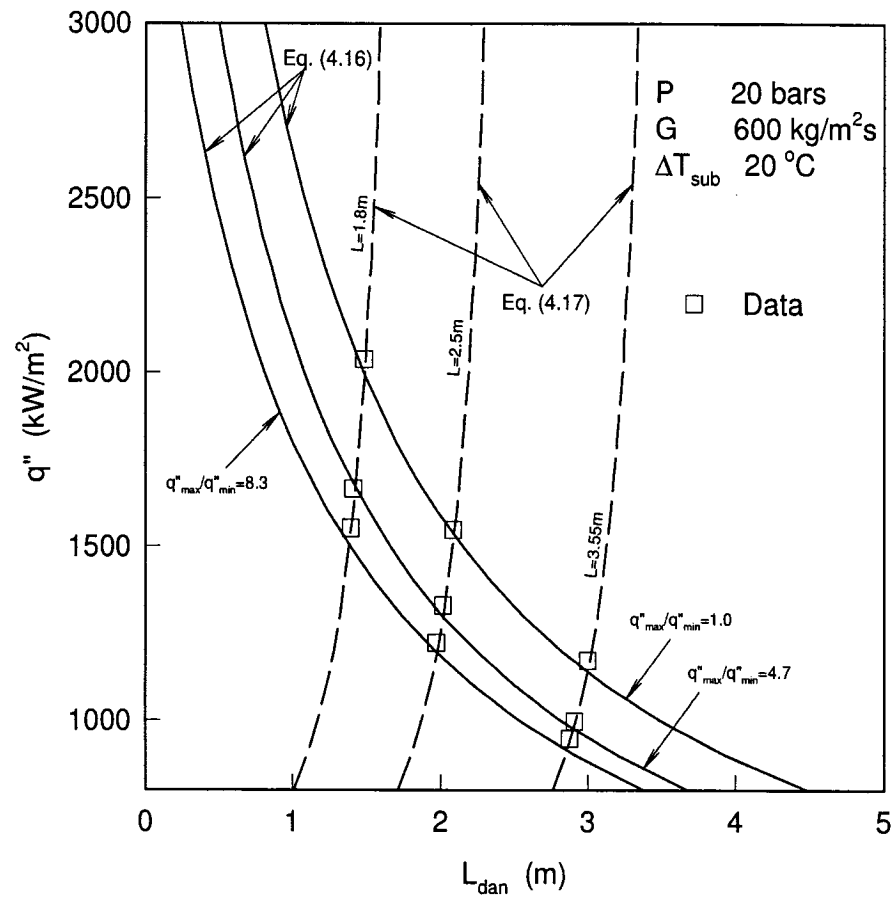
Figure 5.21: The relationship between CHF, nonuniform heating and heated length; dispersed annular flow length approach.

CHAPTER 6

CONCLUSIONS

A study of the critical heat flux (CHF) under low-pressure vertical flow conditions was carried out. More than 1000 CHF data were obtained under three different angular heat flux distributions and three different heated lengths. The experiments were carried out by using extra strong tubes having an inside diameter of 22 mm.

Two different representations for dryout type of CHF were proposed. The classical CHF representation as a function of the thermodynamic quality was discussed. A new representation of CHF as a function of the dispersed annular flow length was introduced.

For a constant exit pressure and constant inlet conditions and for different heated lengths, the CHF was represented as a function of the thermodynamic quality. By using this kind of CHF representation, CHF data were then fitted by using a simple regression based on two coefficients. Within the range of flow conditions covered by the experiments, the regression function can be used to predict the CHF. The performance of the proposed regression was determined from the absolute and relative RMS errors. These errors are respectively 144.76 kW/m^2 and 11.2%. We have observed that the use of the thermodynamic quality can introduce big uncertainties on the value of CHF. As a matter of fact, the thermodynamic quality is strongly affected by the flow pressure, the inlet flow subcooling and the heat losses from the test section.

The aforementioned CHF regression technique is based on the Direct Substitution Method (DSM). However, the accuracy of the regression can be significantly improved by using a Heat Balance Method (HBM). It is observed that CHF varies inversely with the thermodynamic quality, i.e., the higher is the thermodynamic quality the lower is the value of the CHF. On the other hand the quality increases

with increasing the heat flux. It is obvious that the two curves, i.e., $CHF = f(x)$ and $x = f(q")$, intercept in a single point. This intersection corresponds to the value of CHF determined by using the HBM.

The test results show that the regrssion of CHF by using the heat balance method has higher accuracy, the relative and absolute RMS errors of CHF_{HBM} are 2.3% and 33.4 kW/m^2 respectively. The high accuracy of this method is due to the fact that the HBM considers both the heat flux and the quality at the same time. Note that in this method the heat flux has been considered in an implicit manner. Therefore, this method is an implicit approach.

A method based on the length over which the dispersed annular flow occurs is proposed to represent the CHF. The Levitan and Borevskiy's (1989) correlation is used to determine dispersed annular flow length. We have shown that this length follows an hyperbolic relationship with the CHF. This relationship was then used to find a correlation between CHF and the dispersed annular flow length. A simple regrssion based on two coefficients is proposed. Two regression functions were determined, one based on the DSM and the other based on the HBM. The performance of the regression method was determined from the absolute and relative RMS errors. These errors are respectivly of 2.2% and 30.44 kW/m^2 for the HBM and 2.6% and 37.25 kW/m^2 for the DSM.

The average and local CHF values obtained during the present work were compared with those given in the open litterature (Butterworth, 1972; Kitto and Weiner, 1982). Due to differences on flow conditions only a qualitative agreement between the data was observed.

A study of the effects that the mass flux and the pressure have on CHF was also carried out for both the thermodynamic quality and dispersed annular flow length CHF representation. We have observed that CHF increases with increasing the mass flux. However the effect of pressure on CHF is quite complex and non-linear. The effect of mass flux and flow pressure were introduced in the regression coefficients used to fit the data. These effects were taken into account by using third order polynomials. The study of CHF under nonuniform heating conditions

has helped us to gain more information about the characteristics of boiling flows in general and CHF in particular.

This work allows us to draw the following conclusions:

- Under low pressure conditions, the heated length has a major influence on the CHF. This behaviour is quite different from that observed under medium and high pressure conditions (Groeneveld et al., 1996), in which the influence of the heated length is small or non-existent.

- The effect of the non-uniform heating on CHF decreases with increasing the heated length.

- CHF increases with increasing the mass flux at a given exit flow pressure.

- The effect of the inlet subcooling on the CHF increases with increasing the mass flux at a given exit flow pressure.

- The effect of pressure on CHF is quite complex, there exist an inversion point between 30 and 40 bars, before this point CHF increases with pressure. After this point, CHF decreases with increasing pressure.

- CHF experiments carried out under nonuniform heating conditions shows that the higher the heat flux nonuniformity $\frac{q''_{max}}{q''_{min}}$, the lower the values of CHF. However, the effect of nonuniformity on the CHF decreases with increasing pressure and mass flux.

- Under low quality conditions, i.e., $x < 0.3$ (Kitto, 1982) and high quality conditions, i.e., $x > 0.6$ the nonuniform peak critical heat flux seems to approach the uniform average critical heat flux. This observation indicates that the CHF depends on local variables for these flow conditions.

- Under medium quality conditions, i.e., $x = 0.3-0.6$, the nonuniform average critical heat flux appears to approach the uniform average critical heat flux. This observation indicates that the CHF depends on the average flow variables for these flow conditions.

- The use of the representation of the CHF as a function of dispersed annular flow length considerably reduces the data scatter.

- Using the proposed semi-analytical method, CHF can be predicted with a good accuracy for both uniform and nonuniform heating conditions.

- With the proposed method, the relative and absolute RMS errors on CHF_{HBM}, based on quality, are 4.2% and 51.922 kW/m^2 respectively. While the relative and absolute RMS errors on CHF_{HBM}, based on dispersed annular flow length, are 3.9% and 51.733 kW/m^2 respectively.

REFERENCE

ACADEMY OF SCIENCE OF USSR, "Recommendations for the calculation of the heat transfer crisis at boiling of water in round tubes, Institute of High Temperatures of the Academy of Sciences, preprint, Moscow, (1980), pp.1-57(in Russian).

ALEKSEEV, G.V.; PESKOV, O.L.; REMIZOV, O.V.; SERGEEV, N.D.; ZENKE-VICH, B.A. and SUBBOTIN, V.I., "Critical heat flux densities with forced flow of water," Teploenergetika, 12(3), (1965), pp.47-51.

BECKER, K.; STRAND, G. and OSTERDAHL, C., "Round tube burnout data for flow boiling of water at pressures between 30 and 200 bar," KTH-NEL-14, (1971).

BECKER, K.M.; ENERHOLM, A.; SARDH, L.; KÖHLER, W.; KASTNER, W. and KrÄTZER, W., "Heat transfer in an evaporator tube with circumferentially non-uniform heating," Int. J. Multiphase Flow, Vol.14, No.5, (1988), pp.575-586.

BENNETT, A.W.; HEWITT, G.F.; KEARSEY, H.A.; KEEYS, R.K.F. and PUL-LING, D.J., "Studies of burnout in boiling heat transfer to water in round tubes with non-uniform heating," UKAEA, report AERE-5076, (1966).

BUTTERWORTH, D., "A model for predicting dryout in a tube with a circumferential variation in heat flux," UKAEA report, AERE M2436, (1972).

COLLIER, J.G., "Convective boiling and condensation," McGRAW-HILL Book Company (UK) Limited, (1972).

DENG, Z.J., "Prediction of critical heat flux for flow boiling in subcooled and saturated regimes," Ph.D dissertation, Columbia University, (1998).

DOROSHCHUK, V.E., "Heat transfer crisis in an evaporating pipe," High Temperature, Vol.4, No 4, (1966), pp.522-529.

DOROSHCHUK, V.E., "Origin of burnout in tubes with flow of subcooled water

and wet steam," Thermal Eng., 27(8), (1980), pp.44-49.

FRITZ, W., "Berechnung des maximal volume von dampfblasen," Phys. Z., 36, (1935), pp.379.

GENDELEV, V.G.; BELYAKOV, I.I.; BRAZHNIKOVA, I.V. and LAVRENT'EV, V.P., "Critical heat flux in the water-wall tubes of steam boilers," Thermal Engineering, 35(9), (1988), pp.521-527.

GLUSKER, B.N., SHVARTS, A.L. and GORLANOV, G.G., "Temperature conditions of water-wall tubes of supercritical boilers when unloading at variable pressure in the entire steam-water circuit," Thermal Engineering, (November 1985).

GROENEVELD, D.C.; LEUNG, L.K.H.; KORILLOV, P.L.; BOBKOV, V.P.; SMOGALEV, I.P.; VINOGRADOV, V.N.; HUANG, X.C. and ROYER, E., "The 1995 look-up table for critical heat flux in tubes," Nuclear Engineering and design, 163, (1996), pp.1-23.

HATTON, A.P. and HALL, I.S., "Photographic study of boiling on prepared surface," paper presented at 3rd Int. Heat Transfer Conf., Chicago, (Aug. 1966).

HEWITT, G.F., "Critical heat flux in flow boiling heat transfer," Sixth international heat transfer conference, Toronto, Vol.6, (1978), pp.143-171.

HUMPHIRES, P., DENETTE, G.F. and SCRUTON, B., "Critical Heat Flux Characteristics for vertical steam - generating tubes with circumferentially nonuniform heating," First U.K. National Conference on Heat Transfer; rugby, UK:Instn. Chem. Eng. Vol.2, number x+1312, (1984), pp.817-28.

JAKOB, M., "Heat Transfer," John Wiley, New York, (1958).

KARMAN, TH., VON., "The analogy between fluid friction and heat transfer," Trans. A.S.M.E., vol.61, (1939), pp.705-710.

KATTO, Y., "A physical approach to critical heat flux of subcooled flow boiling in round tubes," Int. J. Heat Mass Transfer, Vol.33, No 4, (1990), pp.611-620.

KITTO, J.B. and WIENER, M., "Effects of non-uniform circumferential heating and inclination on critical heat flux in smooth and ribbed bore tubes," FB21, (1982), pp.297-302.

KNAPP, R.T., "Cavitation and nuclei," Trans. ASME, 80, (1958), pp.1321.

KUTATELADZE, S.S. and LEONT'EV, A.I., "Some applications of the asymptotic theory of the turbulent boundary layer," Proc. of 3rd Int. Heat transfer Conf., Chicago, vol.3, (1966)pp.1-6.

LEE, C.H. and MUDAWAR, I., "A Mechanistic critical heat flux model for subcooled flow boiling based on local bulk conditions," Int. J. Multiphase Flow, Vol.14, No 6, (1988), pp.711-728.

LEVITAN, L.L. and BOREVSKIY, L.YA., "Holography of steam-water flows," Energoatomizdat, Moscow, (1989).

LEVITAN, L.L. and ORLOVA, I.A., "Origin of burnout in tubes with flow of subcooled water and wet steam," Thermal Engng., Vol.37, No 6, (1990), pp.300-305.

MIROPOL'SKII, Z.L., "Critical Heat Fluxes with Uniform Heating of the Perimeter of Steam - generating tubes," Teploenergetika, 11, (1958).

NARIAL, H.; ISHIKAWA, A. and INASAKA, F., "Critical Heat Flux of Subcooled Flow Boiling In Tubes With and Without Internal Twisted Tape Under Non-uniform Heating Condition," proc. NURETH-6, Grenoble, France, (1993), pp.715-722.

OLEKHNOVITH, A., "Étude du flux de chaleur critique a des pressions faibles," Ph.D dissertation, École polytechnique de Montréal, (1998).

OLEKHNOVITH, A.; TEYSSEDOU, A.; TAPUCU, A.; CHAMPAGNE, P. and GROENEVELD, D.C., "Critical heat flux in a vertical tube at low and medium pressures: Part I. Experimental results," Nuclear Engineering and design, 193, (1999a), pp.73-89.

OLEKHNOVITH, A.; TEYSSEDOU, A. and TYE, P., "Critical heat flux in a vertical tube at low and medium pressures: Part II. New data representation," Nuclear Engineering and design, 193, (1999b), pp.91-103.

OLEKHNOVITH, A.; TEYSSEDOU, A. and TYE, P., "Nouvelle représentation du flux de chaleur critique de type assèchement," Int. J. Therm. Sc., 39, (2000a), pp.63-73.

OLEKHNOVITH, A.; TEYSSEDOU, A. and TYE, P., "On the round table discussion on reactor power margins published in Nuclear Engineering and design 163 (1-2) 1996," Nucl. Eng. and Design, 201, (2000b), pp. 335-346.

REMIZOV, O.V. and SAPANKEVICH, A.P., "Burnout with non-uniform distribution of heat flux over the perimeter of a round tube," Teploenergetika, 22(12), (1975), pp.70-74.

TARASOVA, N.V. and LEONT'EV, A.I., "Hydraulic resistance with a steam-water mixture flowing in a vertical heated tube," High Temperature, Vol.3, No.1, (1965), pp.102-109.

THOMPSON, B. and MACBETH R.V., "Boiling water heat transfer-Burnout in uniformly heated round tubes: A compilation of world data with accurate correlations," AEEW-R356, (1964).

TONG, L.S. and HEWITT, G.F., "Overall viewpoint of flow boiling CHF mechanism," ASME paper, 72-HT-54, (1972).

WEISMAN J. and PEI, B.S., "Prediction of critical heat flux in flow boiling of at low qualities," Int. J. Heat Mass Transfer, Vol.26, No 8, (1983), pp.1463-1477.

WHALLY, P.B., "Boiling, Condensation, and Gas-Liquid Flow," Clarendon Press, Oxford, (1987).

ZENKEVITCH, B.A.; PESKOV, O.L.; PETRISHCHEVA, G.A.; SERGEEV, N.D.; SUBBOTIN, V.I., "The analysis and the generalization of the experimental data of critical heat flux in forced boiling tubes," Atomizdat, Mosco, (1969), (in Russian).

ZUBER, N., "Nucleate boiling-the region of isolated bubbles-similarity with natural convection," Int. J. Heat Mass Transfer, 6, (1963), pp.53.

APPENDIX

Table A: CHF data of vertical up flow heating tubes *

L	$\frac{q''_{max}}{q''_{min}}$	P_{out}	G	t_{in}	P_{in}	$\Delta h_{sub}(P_{out})$	$\Delta h_{sub}(P_{in})$	x	Q	CHF
m	–	bars	$kg/(m^2 s)$	^{0}C	bars	kJ/kg	kJ/kg		kW	kW/m^2
1.80	1.0	9.92	402.9	175.3	10.41	28.4	19.3	0.594	188.0	1504.6
1.80	1.0	9.92	501.0	175.0	10.52	31.7	20.6	0.539	212.6	1700.9
1.80	1.0	9.95	602.0	174.9	10.66	34.7	21.6	0.488	232.3	1858.7
1.80	1.0	9.93	805.1	174.8	10.87	38.9	21.6	0.413	263.8	2110.7
1.80	1.0	9.95	1001.7	174.7	11.10	43.4	22.4	0.363	290.1	2321.2
1.80	1.0	9.94	1203.4	175.1	11.32	45.5	20.5	0.326	313.2	2506.4
1.80	1.0	9.84	1408.2	175.8	11.47	45.1	15.5	0.306	342.4	2739.9
1.80	1.0	9.90	403.0	170.2	10.39	50.1	40.9	0.584	188.2	1505.9
1.80	1.0	9.90	504.0	170.4	10.50	51.2	40.0	0.530	214.3	1715.0
1.80	1.0	9.89	601.3	170.2	10.60	53.9	40.7	0.486	235.2	1882.1
1.80	1.0	9.94	802.7	169.7	10.86	60.7	43.8	0.410	268.0	2144.4
1.80	1.0	9.96	1003.7	170.0	11.10	63.7	42.9	0.362	297.4	2379.7
1.80	1.0	9.95	1203.1	169.7	11.30	68.4	44.0	0.324	322.0	2576.8
1.80	1.0	9.88	401.8	160.2	10.36	92.7	83.7	0.571	190.4	1523.6
1.80	1.0	9.94	500.0	159.9	10.52	96.9	86.1	0.521	217.9	1743.8
1.80	1.0	9.91	604.9	159.7	10.61	99.4	86.4	0.472	241.1	1929.1
1.80	1.0	9.92	804.8	159.7	10.82	103.2	86.6	0.401	276.5	2212.2
1.80	1.0	9.93	1002.6	160.1	11.01	104.8	85.0	0.347	302.0	2416.6
1.80	1.0	9.88	1207.0	159.6	11.16	109.6	86.2	0.312	331.6	2653.1
1.80	1.0	9.92	401.5	150.0	10.40	137.5	128.5	0.559	193.5	1548.2
1.80	1.0	9.92	500.1	150.0	10.50	139.3	128.5	0.506	220.4	1763.6
1.80	1.0	9.92	601.7	150.4	10.60	139.4	126.7	0.461	243.7	1949.9
1.80	1.0	9.94	804.7	150.6	10.81	142.3	126.3	0.392	282.8	2262.9

* I.D.=0.0221 m for $\frac{q''_{max}}{q''_{min}} = 1.0$; I.D.=0.0222 m for $\frac{q''_{max}}{q''_{min}} = 4.7$; I.D.=0.02223 m for $\frac{q''_{max}}{q''_{min}} = 8.3$

Table A: CHF data of vertical up flow heating tubes (Cont.)

L	$\frac{q"_{max}}{q"_{min}}$	P_{out}	G	t_{in}	P_{in}	$\Delta h_{sub}(P_{out})$	$\Delta h_{sub}(P_{in})$	x	Q	CHF
m	–	bars	$kg/(m^2 s)$	^0C	bars	kJ/kg	kJ/kg		kW	kW/m^2
1.80	1.0	9.92	1004.0	149.9	10.96	148.0	128.9	0.337	311.1	2489.0
1.80	1.0	9.89	398.2	140.2	10.37	179.3	170.3	0.560	198.4	1587.8
1.80	1.0	9.86	498.9	139.8	10.44	182.3	171.5	0.503	227.0	1816.4
1.80	1.0	9.96	607.4	139.9	10.62	185.1	172.9	0.450	251.8	2014.5
1.80	1.0	9.97	797.5	139.6	10.81	189.7	174.2	0.383	289.2	2314.2
1.80	1.0	9.93	1005.5	140.0	10.91	189.9	171.9	0.322	317.0	2536.1
1.80	1.0	19.87	401.2	206.9	20.28	28.4	23.7	0.692	205.2	1642.0
1.80	1.0	19.83	498.8	207.1	20.31	27.8	22.3	0.623	230.0	1840.1
1.80	1.0	20.01	602.6	207.1	20.56	30.7	24.4	0.551	246.4	1971.6
1.80	1.0	19.97	807.0	206.8	20.64	33.0	25.3	0.452	272.6	2181.2
1.80	1.0	19.95	1000.4	206.7	20.73	34.4	25.5	0.388	291.0	2328.9
1.80	1.0	19.96	1206.9	206.5	20.86	36.8	26.5	0.343	313.0	2504.2
1.80	1.0	19.94	1404.4	206.7	20.95	36.9	25.4	0.308	327.3	2618.7
1.80	1.0	19.93	403.8	201.7	20.34	52.6	47.9	0.688	209.0	1672.3
1.80	1.0	19.91	503.6	202.2	20.39	50.9	45.4	0.609	231.3	1850.8
1.80	1.0	19.95	601.6	201.6	20.49	54.8	48.5	0.548	250.1	2001.1
1.80	1.0	19.88	803.3	202.2	20.55	52.7	45.0	0.452	277.5	2220.4
1.80	1.0	19.90	1002.8	201.7	20.68	56.5	47.5	0.384	297.9	2383.4
1.80	1.0	19.98	1201.4	202.0	20.87	57.3	47.1	0.344	321.1	2569.4
1.80	1.0	19.88	402.5	192.6	20.29	92.8	88.0	0.683	213.1	1705.1
1.80	1.0	19.88	500.4	191.9	20.35	96.5	91.1	0.604	236.8	1894.8
1.80	1.0	19.88	598.4	191.8	20.42	97.8	91.6	0.538	254.7	2038.3
1.80	1.0	19.95	805.4	192.4	20.60	97.2	89.7	0.440	284.7	2278.1
1.80	1.0	19.95	1002.7	192.5	20.72	98.1	89.2	0.380	311.0	2488.2
1.80	1.0	19.94	398.7	182.3	20.34	138.6	134.0	0.676	216.1	1729.1
1.80	1.0	19.95	496.4	182.1	20.42	140.4	134.9	0.600	241.5	1932.5
1.80	1.0	19.93	597.3	182.0	20.45	141.1	135.1	0.530	260.7	2086.4
1.80	1.0	19.95	804.8	182.3	20.59	141.4	134.1	0.428	291.5	2332.4

Table A: CHF data of vertical up flow heating tubes (Cont.)

L	$\frac{q''_{max}}{q''_{min}}$	P_{out}	G	t_{in}	P_{in}	$\Delta h_{sub}(P_{out})$	$\Delta h_{sub}(P_{in})$	x	Q	CHF
m	–	bars	$kg/(m^2 s)$	^0C	bars	kJ/kg	kJ/kg		kW	kW/m^2
1.80	1.0	19.92	1000.6	181.3	20.67	146.7	138.1	0.371	322.4	2579.6
1.80	1.0	19.87	396.2	172.2	20.27	182.2	177.6	0.660	216.8	1734.4
1.80	1.0	19.96	498.6	171.8	20.42	185.7	180.4	0.581	244.8	1958.7
1.80	1.0	19.88	603.8	171.9	20.40	185.0	179.0	0.510	264.7	2117.8
1.80	1.0	19.96	808.1	172.2	20.58	185.8	178.6	0.417	299.5	2397.0
1.80	1.0	9.92	401.5	175.1	10.41	29.3	20.1	0.595	187.8	1502.4
1.80	1.0	9.90	509.1	175.1	10.51	31.1	19.8	0.528	211.8	1694.6
1.80	1.0	9.91	597.7	175.0	10.62	33.6	20.4	0.491	231.5	1852.4
1.80	1.0	9.96	800.4	174.9	10.89	38.8	21.7	0.417	264.8	2118.6
1.80	1.0	9.97	1003.8	174.7	11.13	43.9	22.8	0.365	291.8	2334.7
1.80	1.0	9.93	1203.6	174.4	11.30	48.2	23.3	0.325	313.0	2504.4
1.80	1.0	9.97	1405.1	174.8	11.56	50.9	22.3	0.300	337.5	2700.7
1.80	1.0	30.00	399.8	229.1	30.38	25.8	22.5	0.750	209.8	1678.6
1.80	1.0	29.89	498.9	229.3	30.32	24.3	20.6	0.652	228.1	1825.4
1.80	1.0	29.95	602.5	229.2	30.43	25.7	21.6	0.575	243.6	1949.5
1.80	1.0	29.91	804.3	229.2	30.48	26.2	21.2	0.472	268.1	2145.6
1.80	1.0	29.95	1010.1	228.9	30.60	28.6	23.0	0.398	286.0	2288.5
1.80	1.0	29.89	1206.0	228.5	30.62	30.7	24.3	0.347	299.6	2397.1
1.80	1.0	29.90	1406.8	228.8	30.70	29.9	23.0	0.303	305.6	2445.4
1.80	1.0	29.95	403.0	224.4	30.34	47.4	44.0	0.742	212.7	1702.2
1.80	1.0	29.89	504.1	224.3	30.33	47.7	43.9	0.638	230.1	1840.9
1.80	1.0	29.93	604.1	224.2	30.41	48.9	44.7	0.570	247.5	1980.6
1.80	1.0	29.92	803.0	223.6	30.49	52.4	47.4	0.471	275.2	2202.1
1.80	1.0	29.93	1002.5	223.9	30.58	51.8	46.1	0.396	291.4	2331.5
1.80	1.0	29.93	1204.1	223.9	30.65	52.4	46.1	0.338	301.5	2412.2
1.80	1.0	29.86	398.8	214.1	30.25	94.2	90.8	0.739	216.9	1735.7
1.80	1.0	29.88	500.5	213.8	30.32	96.1	92.3	0.636	237.0	1896.5
1.80	1.0	29.90	599.0	213.8	30.38	96.7	92.5	0.568	255.5	2044.2

Table A: CHF data of vertical up flow heating tubes (Cont.)

L	$\frac{q"_{max}}{q"_{min}}$	P_{out}	G	t_{in}	P_{in}	$\Delta h_{sub}(P_{out})$	$\Delta h_{sub}(P_{in})$	x	Q	CHF
m	–	bars	$kg/(m^2 s)$	^{0}C	bars	kJ/kg	kJ/kg		kW	kW/m^2
1.80	1.0	29.93	804.4	214.1	30.50	96.3	91.4	0.462	284.1	2273.1
1.80	1.0	29.91	1010.2	213.7	30.56	98.7	93.0	0.390	307.4	2459.4
1.80	1.0	29.96	1202.1	213.9	30.66	98.6	92.5	0.331	316.8	2534.6
1.80	1.0	29.90	400.9	203.9	30.30	141.1	137.6	0.717	219.1	1753.3
1.80	1.0	30.03	500.2	204.3	30.47	140.7	136.9	0.632	244.0	1952.4
1.80	1.0	29.88	605.7	204.1	30.37	140.8	136.5	0.555	263.4	2107.8
1.80	1.0	29.96	807.1	203.9	30.52	143.0	138.1	0.451	293.2	2346.4
1.80	1.0	29.88	1006.8	203.8	30.52	143.4	137.8	0.382	318.1	2545.7
1.80	1.0	29.82	400.9	194.1	30.22	184.3	180.8	0.708	223.4	1787.4
1.80	1.0	29.90	502.5	194.1	30.35	185.4	181.5	0.626	251.6	2013.7
1.80	1.0	29.87	605.6	194.4	30.35	184.0	179.9	0.547	270.1	2161.4
1.80	1.0	29.85	804.6	193.7	30.41	187.7	182.8	0.443	301.9	2415.8
1.80	1.0	29.99	999.8	193.9	30.62	188.6	183.1	0.370	325.0	2600.9
1.80	1.0	39.99	401.9	245.1	40.37	28.2	25.3	0.746	200.9	1607.8
1.80	1.0	40.03	503.0	245.2	40.45	28.3	25.1	0.649	219.1	1753.1
1.80	1.0	40.05	602.3	244.9	40.51	30.1	26.7	0.575	233.5	1868.4
1.80	1.0	39.95	801.4	244.9	40.47	29.8	26.0	0.470	255.2	2042.3
1.80	1.0	40.02	1009.2	245.0	40.60	30.3	26.0	0.383	263.7	2110.1
1.80	1.0	39.87	1205.5	244.9	40.50	30.1	25.4	0.325	269.6	2157.2
1.80	1.0	39.94	1406.5	244.9	40.62	30.9	25.9	0.278	271.3	2171.1
1.80	1.0	39.91	401.9	240.0	40.30	51.9	49.0	0.742	203.4	1627.6
1.80	1.0	39.93	502.0	240.2	40.36	51.4	48.2	0.640	220.5	1764.3
1.80	1.0	39.95	600.9	239.9	40.41	53.2	49.8	0.569	236.2	1889.8
1.80	1.0	39.93	804.1	239.9	40.46	53.5	49.6	0.458	257.1	2057.1
1.80	1.0	39.97	1011.0	239.7	40.54	55.1	50.8	0.370	265.8	2126.8
1.80	1.0	39.96	1208.0	240.5	40.59	51.6	47.0	0.314	270.6	2165.6
1.80	1.0	39.81	399.0	229.8	40.20	99.2	96.3	0.726	205.3	1642.9

Table A: CHF data of vertical up flow heating tubes (Cont.)

L	$\frac{q''_{max}}{q''_{min}}$	P_{out}	G	t_{in}	P_{in}	$\Delta h_{sub}(P_{out})$	$\Delta h_{sub}(P_{in})$	x	Q	CHF
m	–	bars	$kg/(m^2 s)$	^0C	bars	kJ/kg	kJ/kg		kW	kW/m^2
1.80	1.0	39.91	501.5	229.6	40.34	101.2	97.9	0.629	226.2	1810.2
1.80	1.0	40.02	604.1	230.1	40.49	99.9	96.4	0.552	241.4	1931.7
1.80	1.0	40.03	803.1	230.2	40.54	99.8	96.0	0.442	262.6	2101.1
1.80	1.0	39.97	1005.0	229.7	40.53	102.0	97.9	0.356	273.0	2184.7
1.80	1.0	40.05	1208.2	229.8	40.66	102.5	98.0	0.292	276.8	2214.7
1.80	1.0	39.96	398.2	210.3	40.35	190.3	187.4	0.720	216.9	1736.0
1.80	1.0	39.96	497.0	210.1	40.38	191.4	188.3	0.617	237.2	1898.3
1.80	1.0	39.88	602.8	210.2	40.34	190.7	187.3	0.527	252.1	2017.2
1.80	1.0	39.91	809.7	210.2	40.41	191.2	187.5	0.403	272.5	2180.1
1.80	1.0	39.98	1009.6	210.5	40.53	190.7	186.6	0.314	280.3	2243.1
1.80	1.0	40.03	1209.0	209.7	40.60	194.8	190.6	0.248	285.1	2281.0
1.80	1.0	39.95	404.4	219.8	40.35	146.7	143.7	0.707	210.2	1681.8
1.80	1.0	39.98	500.1	219.8	40.42	147.2	143.9	0.619	230.9	1848.0
1.80	1.0	39.94	602.0	219.9	40.40	146.6	143.2	0.540	246.5	1972.5
1.80	1.0	39.93	801.4	219.7	40.44	147.8	144.1	0.420	265.7	2125.8
1.80	1.0	39.97	1005.6	219.8	40.52	147.9	143.9	0.329	272.6	2181.1
1.80	1.0	39.90	1203.5	219.8	40.49	147.7	143.4	0.268	278.3	2227.0
2.50	1.0	9.92	403.1	175.0	10.40	29.6	20.6	0.610	193.2	1113.1
2.50	1.0	9.92	503.2	175.1	10.53	31.5	20.1	0.553	219.3	1263.3
2.50	1.0	9.91	600.7	175.0	10.65	34.1	20.4	0.506	239.7	1380.8
2.50	1.0	9.90	707.1	175.0	10.77	36.3	20.2	0.461	257.9	1485.5
2.50	1.0	9.91	805.7	174.8	10.91	39.6	21.2	0.430	274.2	1579.6
2.50	1.0	9.96	1004.5	174.5	11.21	46.2	23.4	0.379	303.4	1748.0
2.50	1.0	9.88	1204.4	174.3	11.37	49.8	22.8	0.332	320.3	1845.1
2.50	1.0	9.95	1410.5	175.0	11.70	52.4	21.1	0.304	342.6	1973.8
2.50	1.0	10.01	1613.3	175.0	12.03	57.9	22.2	0.284	368.1	2120.6
2.50	1.0	9.92	403.7	170.2	10.40	50.3	41.3	0.606	195.7	1127.3

Table A: CHF data of vertical up flow heating tubes (Cont.)

L	$\frac{q''_{max}}{q''_{min}}$	P_{out}	G	t_{in}	P_{in}	$\Delta h_{sub}(P_{out})$	$\Delta h_{sub}(P_{in})$	x	Q	CHF
m	–	bars	$kg/(m^2 s)$	^0C	bars	kJ/kg	kJ/kg		kW	kW/m^2
2.50	1.0	9.89	501.1	170.0	10.50	52.9	41.6	0.546	219.8	1266.1
2.50	1.0	9.92	602.5	169.9	10.65	56.1	42.6	0.497	241.4	1390.5
2.50	1.0	9.92	802.5	169.7	10.91	61.6	43.4	0.426	278.0	1601.4
2.50	1.0	9.92	1004.7	169.7	11.16	66.0	43.4	0.373	306.1	1763.6
2.50	1.0	9.96	1204.6	170.1	11.43	68.9	42.4	0.330	327.0	1883.6
2.50	1.0	9.92	1407.0	169.9	11.65	73.6	42.5	0.302	351.1	2022.6
2.50	1.0	9.92	400.2	160.0	10.39	94.1	85.3	0.600	198.6	1144.2
2.50	1.0	9.88	503.8	160.4	10.48	94.0	82.8	0.535	224.4	1293.1
2.50	1.0	9.91	601.0	160.1	10.62	97.8	84.7	0.487	246.1	1417.7
2.50	1.0	9.92	801.6	160.0	10.88	102.9	85.3	0.417	284.4	1638.3
2.50	1.0	9.96	1006.7	159.7	11.15	109.0	87.3	0.362	315.5	1817.9
2.50	1.0	9.95	1206.6	159.4	11.36	113.9	88.4	0.321	340.6	1962.1
2.50	1.0	9.98	1405.6	160.3	11.66	115.1	85.1	0.299	370.4	2134.1
2.50	1.0	9.94	1207.5	150.6	11.34	151.6	126.2	0.321	358.3	2064.2
2.50	1.0	9.97	1001.2	149.8	11.13	151.4	130.3	0.358	326.9	1883.5
2.50	1.0	9.88	402.5	150.5	10.36	134.6	125.6	0.587	202.1	1164.4
2.50	1.0	9.91	501.0	150.3	10.50	138.0	127.0	0.528	229.0	1319.3
2.50	1.0	9.90	601.8	149.8	10.60	142.0	129.0	0.479	252.8	1456.5
2.50	1.0	9.94	804.4	149.4	10.88	148.7	131.4	0.409	294.9	1698.9
2.50	1.0	9.95	1003.8	140.5	11.07	190.6	170.1	0.344	332.3	1914.7
2.50	1.0	9.88	399.7	140.1	10.35	179.4	170.5	0.583	206.5	1189.8
2.50	1.0	9.91	502.2	140.5	10.49	180.2	169.4	0.524	236.0	1359.6
2.50	1.0	9.91	602.5	140.0	10.61	184.5	171.5	0.471	259.3	1493.9
2.50	1.0	9.92	803.5	140.0	10.84	188.7	171.7	0.399	301.1	1734.7
2.50	1.0	9.98	1006.1	139.9	11.11	193.9	173.3	0.347	336.6	1939.4
2.50	1.0	19.95	402.3	207.4	20.34	26.8	22.3	0.720	213.5	1230.0
2.50	1.0	19.85	503.4	207.3	20.32	27.1	21.6	0.646	240.2	1384.1

Table A: CHF data of vertical up flow heating tubes (Cont.)

L	$\frac{q"_{max}}{q"_{min}}$	P_{out}	G	t_{in}	P_{in}	$\Delta h_{sub}(P_{out})$	$\Delta h_{sub}(P_{in})$	x	Q	CHF
m	–	bars	$kg/(m^2 s)$	^0C	bars	kJ/kg	kJ/kg		kW	kW/m^2
2.50	1.0	19.91	601.2	207.5	20.46	27.7	21.4	0.585	260.2	1499.0
2.50	1.0	19.95	802.5	206.9	20.65	32.6	24.6	0.486	290.3	1672.6
2.50	1.0	19.89	1003.2	207.0	20.76	33.4	23.4	0.424	317.5	1828.9
2.50	1.0	19.89	1203.1	207.0	20.92	35.2	23.4	0.377	339.5	1955.9
2.50	1.0	19.82	1203.5	201.8	20.83	57.7	46.1	0.372	346.4	1995.7
2.50	1.0	19.98	1000.3	201.7	20.83	58.2	48.4	0.417	321.2	1850.7
2.50	1.0	19.76	399.6	202.2	20.15	48.2	43.6	0.730	218.5	1258.7
2.50	1.0	19.88	502.4	202.3	20.36	50.1	44.6	0.649	245.3	1413.3
2.50	1.0	19.85	607.5	202.2	20.41	51.1	44.7	0.577	265.0	1526.6
2.50	1.0	19.99	800.1	202.1	20.70	54.9	46.7	0.486	296.1	1706.1
2.50	1.0	20.04	403.7	192.0	20.43	97.0	92.5	0.721	225.3	1297.9
2.50	1.0	19.79	499.9	192.2	20.26	94.2	88.7	0.641	249.5	1437.2
2.50	1.0	19.96	601.1	192.4	20.50	96.0	89.8	0.569	268.6	1547.5
2.50	1.0	20.05	802.2	191.7	20.73	101.7	94.0	0.473	304.2	1752.6
2.50	1.0	19.92	1006.4	191.7	20.76	102.1	92.4	0.410	335.2	1931.3
2.50	1.0	19.88	1210.4	191.7	20.87	103.3	92.0	0.360	358.6	2066.1
2.50	1.0	19.98	1004.8	182.1	20.80	144.7	135.3	0.402	344.9	1987.3
2.50	1.0	19.93	801.4	181.6	20.61	144.7	136.9	0.467	313.5	1806.0
2.50	1.0	19.97	604.8	182.1	20.51	141.4	135.2	0.561	277.6	1599.3
2.50	1.0	19.94	497.5	182.7	20.41	137.6	132.2	0.635	254.3	1464.8
2.50	1.0	19.90	398.5	182.4	20.30	137.7	133.1	0.713	226.4	1304.6
2.50	1.0	19.89	401.3	172.1	20.28	182.8	178.3	0.702	231.8	1335.2
2.50	1.0	19.95	503.7	172.3	20.43	183.6	178.1	0.626	262.9	1514.8
2.50	1.0	19.87	602.7	172.1	20.41	184.3	178.0	0.554	283.3	1631.9
2.50	1.0	19.98	803.9	172.0	20.65	187.4	179.7	0.456	321.5	1852.3
2.50	1.0	19.89	1000.4	172.0	20.70	188.0	178.7	0.396	355.9	2050.3
2.50	1.0	29.99	404.1	229.2	30.35	25.1	21.9	0.771	217.8	1254.9

Table A: CHF data of vertical up flow heating tubes (Cont.)

L	$\frac{q"_{max}}{q"_{min}}$	P_{out}	G	t_{in}	P_{in}	$\Delta h_{sub}(P_{out})$	$\Delta h_{sub}(P_{in})$	x	Q	CHF
m	–	bars	$kg/(m^2 s)$	^0C	bars	kJ/kg	kJ/kg		kW	kW/m^2
2.50	1.0	29.94	501.9	229.1	30.36	25.6	22.0	0.695	244.3	1407.6
2.50	1.0	29.89	603.0	229.3	30.38	24.9	20.6	0.624	263.9	1520.1
2.50	1.0	29.80	803.3	229.1	30.40	26.0	20.7	0.515	291.2	1677.9
2.50	1.0	29.90	1007.7	229.0	30.61	28.2	22.1	0.442	315.4	1817.3
2.50	1.0	29.89	1206.6	228.9	30.71	29.6	22.5	0.388	333.2	1919.7
2.50	1.0	29.93	1409.0	228.7	30.84	31.6	23.7	0.346	348.7	2009.2
2.50	1.0	29.76	402.0	224.5	30.13	45.1	41.8	0.779	222.4	1281.3
2.50	1.0	29.96	499.8	224.3	30.39	48.3	44.5	0.686	244.7	1409.6
2.50	1.0	29.96	607.1	224.2	30.45	49.2	45.0	0.616	267.9	1543.6
2.50	1.0	29.96	803.9	224.0	30.55	51.0	45.9	0.511	297.2	1712.3
2.50	1.0	29.96	1011.8	223.8	30.67	53.0	46.8	0.435	321.3	1850.8
2.50	1.0	29.92	1203.9	223.7	30.72	53.9	47.0	0.381	337.5	1944.2
2.50	1.0	29.93	1406.4	223.6	30.83	55.3	47.5	0.339	353.6	2037.4
2.50	1.0	29.96	400.4	213.9	30.32	95.7	92.5	0.773	227.4	1310.0
2.50	1.0	29.94	502.3	214.2	30.36	94.6	91.0	0.679	252.4	1453.8
2.50	1.0	29.93	604.2	214.2	30.41	95.1	90.9	0.608	274.2	1579.8
2.50	1.0	29.95	802.7	213.9	30.53	97.5	92.5	0.500	304.6	1754.8
2.50	1.0	29.92	1003.8	213.6	30.61	99.5	93.6	0.425	329.8	1900.1
2.50	1.0	29.93	1212.8	213.8	30.71	99.5	92.7	0.368	350.6	2019.7
2.50	1.0	29.94	404.0	204.0	30.30	140.6	137.5	0.758	232.1	1337.3
2.50	1.0	29.86	497.8	204.3	30.28	139.1	135.4	0.683	260.0	1497.6
2.50	1.0	29.93	604.5	204.2	30.41	140.7	136.5	0.593	278.6	1604.8
2.50	1.0	29.90	803.8	204.2	30.48	141.3	136.2	0.487	311.5	1794.3
2.50	1.0	29.91	1006.5	204.1	30.58	142.6	136.8	0.413	339.2	1954.2
2.50	1.0	29.94	1004.4	194.0	30.60	188.0	182.2	0.404	349.5	2013.4
2.50	1.0	29.93	801.0	194.0	30.51	187.2	182.2	0.482	322.1	1855.8
2.50	1.0	29.83	603.3	193.7	30.31	186.8	182.6	0.583	284.5	1639.3

Table A: CHF data of vertical up flow heating tubes (Cont.)

L	$\frac{q"_{max}}{q"_{min}}$	P_{out}	G	t_{in}	P_{in}	$\Delta h_{sub}(P_{out})$	$\Delta h_{sub}(P_{in})$	x	Q	CHF
m	–	bars	$kg/(m^2s)$	^0C	bars	kJ/kg	kJ/kg		kW	kW/m^2
2.50	1.0	29.94	504.2	193.8	30.37	186.9	183.1	0.657	263.4	1517.7
2.50	1.0	29.99	402.6	193.8	30.37	186.9	183.6	0.746	235.2	1355.1
2.50	1.0	39.80	402.3	244.6	40.16	28.9	26.4	0.784	211.4	1218.0
2.50	1.0	39.87	504.3	245.1	40.27	27.5	24.5	0.705	238.5	1373.9
2.50	1.0	39.89	604.8	244.8	40.34	29.4	26.0	0.627	255.2	1470.3
2.50	1.0	39.83	803.3	245.1	40.37	28.2	24.2	0.516	279.8	1611.7
2.50	1.0	39.99	1005.1	245.0	40.61	30.4	25.8	0.435	297.4	1713.2
2.50	1.0	40.04	1211.6	245.1	40.73	30.7	25.7	0.381	315.1	1815.5
2.50	1.0	39.89	1408.4	245.0	40.66	30.7	25.1	0.338	326.1	1878.7
2.50	1.0	39.90	400.5	239.5	40.26	54.0	51.3	0.791	216.2	1245.4
2.50	1.0	39.90	500.3	240.3	40.31	50.6	47.5	0.702	239.9	1382.1
2.50	1.0	39.90	603.1	240.4	40.35	50.4	47.0	0.624	258.1	1487.2
2.50	1.0	39.99	810.1	239.9	40.53	54.0	50.0	0.505	284.2	1637.4
2.50	1.0	39.93	1005.7	239.4	40.54	56.5	52.0	0.431	304.5	1754.5
2.50	1.0	39.91	1211.6	240.5	40.60	51.7	46.6	0.373	318.7	1836.0
2.50	1.0	39.89	1408.2	239.9	40.64	54.8	49.3	0.328	330.6	1904.4
2.50	1.0	39.94	401.4	229.5	40.32	101.5	98.6	0.777	220.2	1268.4
2.50	1.0	39.90	505.9	229.6	40.32	101.0	97.9	0.675	243.5	1402.8
2.50	1.0	40.01	603.4	229.8	40.47	101.1	97.7	0.602	261.4	1506.0
2.50	1.0	39.89	798.1	230.0	40.43	99.9	95.9	0.493	288.0	1659.5
2.50	1.0	39.96	1003.9	230.0	40.57	100.9	96.4	0.413	309.5	1782.9
2.50	1.0	39.92	1212.0	229.8	40.59	102.0	97.1	0.351	324.9	1871.7
2.50	1.0	40.06	1407.8	229.9	40.79	102.9	97.6	0.308	337.5	1944.5
2.50	1.0	39.84	401.1	220.1	40.20	144.3	141.6	0.770	224.8	1295.3
2.50	1.0	39.95	506.4	220.2	40.36	145.0	141.9	0.666	249.1	1434.8
2.50	1.0	39.87	603.1	220.3	40.33	144.3	140.9	0.593	267.6	1541.9
2.50	1.0	39.87	800.5	220.2	40.40	145.2	141.3	0.478	295.0	1699.7

Table A: CHF data of vertical up flow heating tubes (Cont.)

L	$\frac{q''_{max}}{q''_{min}}$	P_{out}	G	t_{in}	P_{in}	$\Delta h_{sub}(P_{out})$	$\Delta h_{sub}(P_{in})$	x	Q	CHF
m	–	bars	$kg/(m^2 s)$	^0C	bars	kJ/kg	kJ/kg		kW	kW/m^2
2.50	1.0	40.02	1005.5	220.1	40.62	147.3	142.8	0.398	317.7	1830.2
2.50	1.0	39.85	1207.3	219.8	40.50	147.8	143.0	0.336	332.7	1916.7
2.50	1.0	39.86	401.6	210.1	40.23	190.4	187.6	0.757	228.8	1317.9
2.50	1.0	40.06	504.2	210.3	40.48	191.2	188.1	0.659	254.5	1466.4
2.50	1.0	39.98	603.4	210.2	40.44	191.4	188.0	0.577	272.4	1569.1
2.50	1.0	39.94	803.2	210.2	40.47	191.6	187.7	0.464	302.8	1744.6
2.50	1.0	39.94	1005.5	209.8	40.52	193.8	189.5	0.381	324.7	1870.8
2.50	1.0	40.03	1205.7	210.0	40.67	193.9	189.2	0.318	339.1	1953.8
3.55	1.0	9.94	404.3	174.5	10.39	31.5	23.1	0.619	197.2	800.1
3.55	1.0	9.90	504.5	175.2	10.50	30.5	19.3	0.560	222.2	901.4
3.55	1.0	9.89	605.1	175.0	10.61	33.4	20.0	0.511	244.0	990.1
3.55	1.0	9.92	801.6	174.7	10.94	40.6	21.8	0.444	282.1	1144.5
3.55	1.0	9.92	1002.5	174.8	11.25	45.6	21.4	0.395	314.2	1274.9
3.55	1.0	9.94	1204.7	174.7	11.58	51.7	22.2	0.359	344.8	1398.8
3.55	1.0	9.92	403.4	170.0	10.37	50.6	42.1	0.619	199.6	809.7
3.55	1.0	9.89	503.3	170.1	10.48	52.1	41.1	0.559	225.6	915.5
3.55	1.0	9.90	603.1	169.9	10.63	55.7	42.2	0.510	247.7	1005.1
3.55	1.0	9.93	809.3	169.8	10.95	61.9	43.2	0.435	285.8	1159.6
3.55	1.0	9.91	1006.5	169.9	11.23	66.4	42.3	0.393	322.6	1308.7
3.55	1.0	9.93	1212.4	169.7	11.56	72.9	43.6	0.353	351.2	1424.9
3.55	1.0	9.90	403.8	159.9	10.35	93.8	85.3	0.610	203.8	827.0
3.55	1.0	9.88	503.5	160.1	10.45	94.8	84.1	0.549	230.0	933.2
3.55	1.0	9.95	601.1	160.3	10.67	97.9	84.6	0.507	255.0	1034.6
3.55	1.0	9.92	804.7	160.2	10.92	102.8	84.4	0.433	295.4	1198.5
3.55	1.0	9.92	1007.0	159.7	11.22	110.2	86.5	0.384	332.9	1350.5
3.55	1.0	9.94	1004.3	149.9	11.20	152.2	129.3	0.377	342.6	1390.2
3.55	1.0	9.92	801.2	150.1	10.90	146.0	128.0	0.430	305.8	1240.5

Table A: CHF data of vertical up flow heating tubes (Cont.)

L	$\frac{q''_{max}}{q''_{min}}$	P_{out}	G	t_{in}	P_{in}	$\Delta h_{sub}(P_{out})$	$\Delta h_{sub}(P_{in})$	x	Q	CHF
m	–	bars	$kg/(m^2 s)$	^{0}C	bars	kJ/kg	kJ/kg		kW	kW/m^2
3.55	1.0	9.94	604.3	150.0	10.66	142.2	128.9	0.501	264.1	1071.6
3.55	1.0	9.87	504.8	150.0	10.45	138.4	127.5	0.543	236.7	960.5
3.55	1.0	9.93	403.2	150.1	10.38	136.7	128.3	0.613	211.1	856.3
3.55	1.0	9.92	399.4	139.8	10.38	181.2	172.6	0.615	216.3	877.4
3.55	1.0	9.97	501.7	139.5	10.55	185.4	174.6	0.538	242.4	983.4
3.55	1.0	9.96	600.0	139.5	10.66	187.4	174.4	0.489	266.8	1082.5
3.55	1.0	9.87	802.6	139.5	10.85	190.8	172.7	0.418	312.6	1268.4
3.55	1.0	9.92	1003.3	139.5	11.15	196.1	173.7	0.368	352.0	1428.2
3.55	1.0	19.88	402.0	207.3	20.25	26.2	22.0	0.760	224.9	912.5
3.55	1.0	19.92	501.6	207.1	20.37	28.5	23.3	0.673	249.5	1012.3
3.55	1.0	19.96	602.3	207.2	20.52	29.8	23.3	0.615	274.2	1112.5
3.55	1.0	19.91	803.1	206.8	20.66	33.2	24.6	0.521	311.2	1262.6
3.55	1.0	19.89	1007.5	206.9	20.84	34.8	23.9	0.460	345.2	1400.5
3.55	1.0	19.92	1005.1	201.6	20.86	58.9	48.2	0.453	349.0	1415.9
3.55	1.0	19.92	808.3	201.8	20.66	55.8	47.3	0.513	315.4	1279.7
3.55	1.0	19.84	603.8	202.1	20.40	51.5	45.0	0.608	276.9	1123.3
3.55	1.0	19.86	502.5	202.2	20.33	50.2	44.8	0.672	253.8	1029.8
3.55	1.0	20.07	402.0	202.3	20.44	51.0	46.8	0.760	228.6	927.5
3.55	1.0	19.91	401.4	191.7	20.28	96.6	92.4	0.757	234.6	951.7
3.55	1.0	19.86	507.5	191.9	20.33	96.3	90.9	0.671	264.7	1073.9
3.55	1.0	19.92	602.2	192.1	20.47	97.0	90.7	0.612	288.5	1170.5
3.55	1.0	19.91	801.1	191.8	20.64	100.3	91.9	0.507	322.9	1310.0
3.55	1.0	20.08	804.8	181.5	20.80	147.3	139.0	0.503	336.6	1365.6
3.55	1.0	19.91	602.4	181.9	20.46	141.7	135.3	0.594	291.0	1180.8
3.55	1.0	19.98	502.4	182.7	20.45	138.1	132.7	0.665	267.8	1086.3
3.55	1.0	19.96	404.1	182.1	20.35	139.6	135.1	0.748	240.2	974.5
3.55	1.0	19.93	401.3	172.0	20.29	183.3	179.2	0.744	244.2	990.7

Table A: CHF data of vertical up flow heating tubes (Cont.)

L	$\frac{q''_{max}}{q''_{min}}$	P_{out}	G	t_{in}	P_{in}	$\Delta h_{sub}(P_{out})$	$\Delta h_{sub}(P_{in})$	x	Q	CHF
m	–	bars	$kg/(m^2s)$	^0C	bars	kJ/kg	kJ/kg		kW	kW/m^2
3.55	1.0	19.94	503.1	172.5	20.39	182.3	177.1	0.655	273.4	1109.3
3.55	1.0	19.94	599.5	172.4	20.48	183.8	177.5	0.596	300.1	1217.8
3.55	1.0	19.95	803.7	172.1	20.66	187.1	178.9	0.500	346.4	1405.4
3.55	1.0	29.96	399.5	228.5	30.29	27.8	24.9	0.820	229.3	930.3
3.55	1.0	29.94	500.4	229.2	30.35	25.1	21.5	0.740	259.1	1051.3
3.55	1.0	29.92	609.8	229.4	30.41	24.6	20.4	0.662	282.7	1147.1
3.55	1.0	29.92	802.3	229.2	30.54	26.7	21.3	0.565	319.0	1294.3
3.55	1.0	29.94	1005.9	228.8	30.72	30.1	23.4	0.491	349.4	1417.4
3.55	1.0	29.85	402.3	224.1	30.19	47.5	44.5	0.825	235.4	955.2
3.55	1.0	29.85	502.5	224.2	30.27	47.7	44.0	0.748	267.5	1085.4
3.55	1.0	29.97	607.0	224.2	30.46	49.3	45.1	0.665	288.6	1171.1
3.55	1.0	29.89	805.1	224.0	30.52	50.8	45.3	0.560	324.5	1316.6
3.55	1.0	29.89	401.2	213.9	30.23	94.9	91.9	0.819	240.5	975.9
3.55	1.0	29.90	501.1	214.0	30.32	95.2	91.6	0.735	271.1	1100.1
3.55	1.0	30.02	602.2	214.2	30.51	95.9	91.7	0.657	293.4	1190.3
3.55	1.0	29.96	803.4	213.8	30.59	98.5	93.0	0.557	336.7	1366.2
3.55	1.0	29.92	398.7	204.5	30.25	137.9	135.0	0.814	244.2	990.8
3.55	1.0	29.91	500.7	204.4	30.32	139.0	135.4	0.725	276.2	1120.4
3.55	1.0	29.96	604.0	204.6	30.44	139.1	134.9	0.649	301.4	1222.6
3.55	1.0	29.86	803.3	203.8	30.47	143.0	137.7	0.542	342.5	1389.5
3.55	1.0	29.89	802.3	193.6	30.49	188.8	183.6	0.530	349.5	1418.1
3.55	1.0	29.96	393.8	194.1	30.29	184.9	182.0	0.812	247.7	1005.1
3.55	1.0	29.97	498.9	194.3	30.38	184.7	181.2	0.721	282.5	1146.3
3.55	1.0	29.95	600.4	194.4	30.42	184.6	180.6	0.645	308.2	1250.6
3.55	1.0	39.95	400.1	244.8	40.28	29.0	26.5	0.844	225.9	916.4
3.55	1.0	39.85	502.3	245.2	40.24	26.8	23.8	0.756	254.1	1030.9
3.55	1.0	39.94	605.8	245.1	40.39	28.3	25.0	0.679	276.1	1120.4

Table A: CHF data of vertical up flow heating tubes (Cont.)

L	$\frac{q''_{max}}{q''_{min}}$	P_{out}	G	t_{in}	P_{in}	$\Delta h_{sub}(P_{out})$	$\Delta h_{sub}(P_{in})$	x	Q	CHF
m	–	bars	$kg/(m^2 s)$	^0C	bars	kJ/kg	kJ/kg		kW	kW/m^2
3.55	1.0	40.01	807.3	245.2	40.56	29.1	25.0	0.564	306.9	1245.0
3.55	1.0	39.74	1003.8	245.0	40.39	28.8	24.0	0.486	329.9	1338.3
3.55	1.0	40.06	1209.4	244.9	40.81	32.2	26.8	0.421	346.7	1406.5
3.55	1.0	39.91	399.5	239.6	40.25	53.5	50.9	0.844	229.4	930.8
3.55	1.0	39.91	501.3	240.6	40.31	49.2	46.2	0.757	258.1	1047.3
3.55	1.0	39.99	603.0	240.4	40.44	51.0	47.7	0.676	278.8	1131.0
3.55	1.0	39.86	800.9	240.3	40.42	51.4	47.2	0.562	310.4	1259.4
3.55	1.0	40.02	1011.0	240.4	40.68	52.7	47.9	0.473	332.9	1350.6
3.55	1.0	39.85	402.3	230.0	40.18	98.0	95.6	0.825	233.0	945.2
3.55	1.0	40.08	503.2	229.8	40.47	101.1	98.2	0.740	263.5	1068.9
3.55	1.0	39.93	606.0	230.1	40.38	99.1	95.7	0.666	287.4	1166.2
3.55	1.0	40.02	808.3	230.0	40.57	100.9	96.9	0.550	322.2	1307.3
3.55	1.0	39.84	1002.4	230.1	40.48	99.8	95.1	0.468	344.9	1399.4
3.55	1.0	39.92	401.7	220.3	40.26	143.8	141.2	0.819	238.0	965.7
3.55	1.0	39.94	501.3	220.3	40.34	144.4	141.4	0.735	269.2	1092.3
3.55	1.0	39.90	604.0	220.0	40.35	145.8	142.5	0.650	291.1	1181.0
3.55	1.0	39.98	801.5	219.9	40.52	147.5	143.5	0.532	324.1	1315.0
3.55	1.0	39.96	801.2	210.0	40.50	192.7	188.7	0.516	329.8	1338.2
3.55	1.0	39.87	607.3	210.3	40.33	190.2	186.7	0.637	297.6	1207.3
3.55	1.0	39.97	500.7	209.9	40.37	192.3	189.3	0.716	271.9	1103.3
3.55	1.0	39.87	403.8	209.7	40.22	192.1	189.5	0.807	243.6	988.4
1.80	4.7	9.91	409.3	175.2	10.36	28.0	19.5	0.519	168.9	1345.5
1.80	4.7	9.92	510.0	175.0	10.44	30.3	20.6	0.459	186.9	1488.8
1.80	4.7	9.92	600.9	174.9	10.53	32.4	21.0	0.425	204.1	1626.2
1.80	4.7	9.89	579.1	175.3	10.48	29.7	18.7	0.435	201.0	1600.9
1.80	4.7	9.93	795.7	175.0	10.69	34.8	20.8	0.346	221.2	1761.9
1.80	4.7	9.93	408.4	169.9	10.36	50.8	42.8	0.504	167.4	1333.3

Table A: CHF data of vertical up flow heating tubes (Cont.)

L	$\frac{q"_{max}}{q"_{min}}$	P_{out}	G	t_{in}	P_{in}	$\Delta h_{sub}(P_{out})$	$\Delta h_{sub}(P_{in})$	x	Q	CHF
m	–	bars	$kg/(m^2 s)$	^0C	bars	kJ/kg	kJ/kg		kW	kW/m^2
1.80	4.7	9.90	514.5	170.0	10.41	51.3	41.8	0.444	186.4	1484.9
1.80	4.7	9.92	595.4	169.9	10.51	53.6	42.6	0.410	200.5	1597.2
1.80	4.7	9.91	794.8	170.1	10.65	55.2	41.5	0.332	218.8	1742.9
1.80	4.7	9.89	410.2	175.2	10.34	27.6	19.1	0.513	167.2	1332.3
1.80	4.7	9.90	525.7	174.9	10.43	30.5	20.6	0.447	187.6	1494.3
1.80	4.7	9.91	608.8	175.0	10.54	32.1	20.4	0.417	203.0	1617.0
1.80	4.7	9.92	791.4	175.2	10.68	33.8	19.7	0.343	217.6	1733.7
1.80	4.7	9.91	414.1	169.9	10.35	50.6	42.4	0.498	167.9	1337.3
1.80	4.7	9.92	519.0	169.8	10.44	52.7	43.0	0.440	186.8	1488.3
1.80	4.7	9.91	614.2	169.9	10.52	53.7	42.4	0.404	203.8	1623.6
1.80	4.7	9.92	789.9	170.2	10.65	54.8	41.3	0.335	219.3	1746.7
1.80	4.7	9.93	401.5	175.1	10.37	28.6	20.3	0.524	167.2	1332.2
1.80	4.7	9.92	520.3	174.9	10.44	30.7	21.0	0.450	186.9	1488.6
1.80	4.7	9.87	603.0	174.8	10.49	32.1	20.5	0.420	202.3	1611.4
1.80	4.7	9.95	795.8	175.0	10.71	35.2	21.1	0.344	220.0	1752.2
1.80	4.7	9.91	408.4	160.1	10.34	92.7	84.7	0.485	168.0	1338.0
1.80	4.7	9.93	516.9	159.9	10.43	95.3	85.9	0.418	185.6	1478.9
1.80	4.7	9.93	605.6	160.6	10.50	93.5	82.9	0.393	205.3	1635.5
1.80	4.7	9.92	795.4	160.1	10.61	97.7	84.9	0.312	219.5	1748.2
1.80	4.7	9.89	402.8	150.4	10.31	134.1	126.2	0.467	166.4	1325.4
1.80	4.7	9.93	509.3	150.1	10.41	137.2	128.2	0.405	186.3	1484.3
1.80	4.7	9.92	608.8	150.2	10.48	138.1	127.6	0.369	205.4	1636.4
1.80	4.7	9.95	796.5	149.9	10.61	141.7	129.5	0.291	220.6	1757.3
1.80	4.7	19.90	406.7	207.1	20.25	27.2	23.1	0.573	174.1	1386.9
1.80	4.7	19.94	532.6	207.1	20.36	28.4	23.6	0.492	196.8	1567.8
1.80	4.7	19.97	608.6	206.9	20.45	30.4	24.8	0.461	210.9	1680.2
1.80	4.7	19.98	796.4	207.2	20.55	30.1	23.6	0.379	228.1	1816.7

Table A: CHF data of vertical up flow heating tubes (Cont.)

L	$\frac{q''_{max}}{q''_{min}}$	P_{out}	G	t_{in}	P_{in}	$\Delta h_{sub}(P_{out})$	$\Delta h_{sub}(P_{in})$	x	Q	CHF
m	–	bars	$kg/(m^2s)$	^0C	bars	kJ/kg	kJ/kg		kW	kW/m^2
1.80	4.7	19.92	415.3	202.3	20.28	49.2	45.0	0.549	174.2	1387.6
1.80	4.7	19.93	509.2	202.2	20.33	50.2	45.6	0.492	192.4	1532.4
1.80	4.7	19.94	600.2	202.0	20.40	51.9	46.6	0.452	209.5	1668.9
1.80	4.7	19.92	794.3	201.9	20.47	53.2	46.8	0.363	225.7	1797.8
1.80	4.7	19.88	412.3	192.4	20.24	93.1	88.9	0.532	174.7	1391.3
1.80	4.7	19.90	511.7	191.6	20.30	97.3	92.7	0.470	194.2	1547.3
1.80	4.7	19.88	607.7	191.9	20.33	96.3	91.1	0.422	209.3	1667.0
1.80	4.7	19.94	798.5	192.4	20.47	95.7	89.6	0.339	225.9	1799.8
1.80	4.7	19.99	411.9	182.2	20.34	139.0	135.0	0.505	173.8	1384.8
1.80	4.7	19.93	523.4	181.9	20.32	140.1	135.6	0.442	196.7	1566.6
1.80	4.7	19.93	598.6	181.9	20.36	140.5	135.6	0.413	212.4	1691.7
1.80	4.7	19.92	797.2	182.2	20.43	140.0	134.2	0.320	228.4	1819.4
1.80	4.7	29.88	397.1	229.3	30.23	23.6	20.5	0.614	172.7	1375.6
1.80	4.7	30.00	506.8	229.2	30.39	25.4	22.0	0.537	193.4	1540.8
1.80	4.7	29.93	595.5	229.1	30.36	25.6	21.9	0.488	207.1	1649.7
1.80	4.7	29.92	796.5	228.7	30.42	28.0	23.7	0.392	224.3	1787.0
1.80	4.7	29.94	410.7	224.2	30.29	47.9	44.8	0.589	175.3	1396.7
1.80	4.7	29.95	503.8	223.6	30.34	51.1	47.7	0.527	193.9	1544.4
1.80	4.7	29.91	597.0	223.7	30.34	50.6	46.9	0.471	206.2	1642.6
1.80	4.7	29.96	794.2	223.8	30.45	51.1	46.8	0.379	223.6	1781.0
1.80	4.7	29.87	398.6	214.3	30.22	93.0	89.9	0.572	172.3	1372.4
1.80	4.7	29.89	497.4	213.7	30.27	96.2	92.9	0.504	192.3	1531.7
1.80	4.7	29.88	599.1	213.7	30.30	96.4	92.8	0.443	206.1	1641.9
1.80	4.7	29.97	794.9	214.2	30.46	95.5	91.3	0.361	227.3	1810.5
1.80	4.7	29.93	407.6	204.2	30.28	139.5	136.5	0.540	174.5	1390.2
1.80	4.7	29.93	510.6	203.9	30.32	141.2	137.8	0.473	194.9	1552.8
1.80	4.7	29.94	600.3	203.8	30.35	141.9	138.4	0.427	210.3	1674.9

Table A: CHF data of vertical up flow heating tubes (Cont.)

L	$\frac{q''_{max}}{q''_{min}}$	P_{out}	G	t_{in}	P_{in}	$\Delta h_{sub}(P_{out})$	$\Delta h_{sub}(P_{in})$	x	Q	CHF
m	–	bars	$kg/(m^2 s)$	^0C	bars	kJ/kg	kJ/kg		kW	kW/m^2
1.80	4.7	29.95	795.5	204.2	30.42	140.7	136.7	0.340	229.9	1831.6
1.80	4.7	39.95	398.0	245.0	40.30	28.2	25.5	0.578	156.5	1246.3
1.80	4.7	39.95	502.9	244.9	40.34	28.9	26.0	0.520	178.6	1422.6
1.80	4.7	39.94	597.5	245.0	40.36	28.6	25.4	0.465	190.3	1516.0
1.80	4.7	40.05	797.9	245.2	40.52	28.8	25.3	0.373	205.3	1635.7
1.80	4.7	39.93	397.1	240.3	40.29	50.4	47.7	0.558	154.1	1227.7
1.80	4.7	39.96	497.8	239.8	40.35	53.2	50.3	0.502	175.2	1395.8
1.80	4.7	39.91	598.0	240.0	40.33	52.2	49.0	0.447	188.7	1503.4
1.80	4.7	39.94	800.1	239.6	40.42	54.7	51.1	0.356	204.4	1628.3
1.80	4.7	39.95	395.2	230.0	40.31	99.1	96.4	0.553	159.6	1271.4
1.80	4.7	39.99	498.2	230.1	40.38	99.1	96.2	0.483	178.2	1419.3
1.80	4.7	39.98	597.9	229.9	40.40	100.2	97.0	0.422	189.8	1511.8
1.80	4.7	39.94	795.5	229.9	40.41	100.3	96.8	0.338	208.3	1659.6
1.80	4.7	40.00	397.0	219.9	40.35	146.3	143.6	0.516	157.7	1256.4
1.80	4.7	40.00	499.6	220.0	40.39	146.1	143.2	0.461	180.3	1436.2
1.80	4.7	39.88	602.9	220.2	40.30	144.5	141.4	0.402	193.6	1541.8
1.80	4.7	39.90	796.2	220.0	40.35	145.8	142.5	0.315	210.1	1673.9
1.80	4.7	19.91	407.2	202.4	20.29	48.9	44.5	0.559	173.6	1383.2
1.80	4.7	19.93	495.8	201.6	20.35	53.2	48.3	0.504	192.0	1529.7
1.80	4.7	19.92	518.2	202.0	20.35	51.4	46.4	0.489	194.7	1551.2
1.80	4.7	19.95	595.5	201.9	20.43	52.7	47.2	0.452	208.0	1656.7
1.80	4.7	19.97	792.7	201.9	20.54	54.0	47.4	0.366	226.6	1805.1
2.50	4.7	9.92	400.6	175.1	10.36	28.4	20.1	0.534	170.1	975.5
2.50	4.7	9.91	495.3	174.7	10.45	31.8	21.7	0.482	190.5	1092.7
2.50	4.7	9.89	599.7	174.9	10.55	32.7	20.4	0.442	211.5	1213.1
2.50	4.7	9.90	795.6	174.7	10.76	37.4	21.5	0.375	239.2	1371.9
2.50	4.7	9.91	992.6	174.8	10.96	40.5	21.2	0.326	260.5	1494.2

Table A: CHF data of vertical up flow heating tubes (Cont.)

L	$\frac{q''_{max}}{q''_{min}}$	P_{out}	G	t_{in}	P_{in}	$\Delta h_{sub}(P_{out})$	$\Delta h_{sub}(P_{in})$	x	Q	CHF
m	–	bars	$kg/(m^2 s)$	^0C	bars	kJ/kg	kJ/kg		kW	kW/m^2
2.50	4.7	9.93	1191.0	175.0	11.15	43.0	20.7	0.282	271.9	1559.3
2.50	4.7	9.92	397.3	169.8	10.35	51.1	43.0	0.526	169.5	972.3
2.50	4.7	9.93	496.0	170.3	10.46	50.9	41.0	0.474	191.4	1097.5
2.50	4.7	9.90	590.8	169.9	10.53	53.9	42.2	0.434	209.8	1202.9
2.50	4.7	9.93	795.3	169.9	10.77	58.2	42.7	0.371	243.5	1396.3
2.50	4.7	9.95	995.1	170.0	10.98	61.5	42.7	0.320	264.6	1517.4
2.50	4.7	9.97	1193.8	170.1	11.17	64.4	42.6	0.277	277.7	1592.5
2.50	4.7	9.88	400.3	160.0	10.31	92.6	84.5	0.511	172.8	990.8
2.50	4.7	9.91	495.8	160.1	10.43	94.4	84.7	0.462	195.0	1118.4
2.50	4.7	9.91	604.5	159.8	10.54	97.7	86.0	0.420	218.1	1250.7
2.50	4.7	9.92	795.1	160.0	10.74	100.4	85.3	0.366	253.3	1452.9
2.50	4.7	10.00	994.0	160.4	11.00	103.3	85.0	0.313	275.8	1581.6
2.50	4.7	9.92	1193.8	160.1	11.06	105.7	84.8	0.264	285.4	1637.0
2.50	4.7	9.89	398.3	149.8	10.31	136.7	128.8	0.496	174.1	998.8
2.50	4.7	9.95	494.3	150.0	10.45	138.4	129.1	0.447	197.2	1130.8
2.50	4.7	9.91	595.9	149.9	10.51	139.9	128.7	0.403	217.2	1245.5
2.50	4.7	9.97	793.4	150.1	10.76	143.6	129.0	0.355	259.1	1486.2
2.50	4.7	9.96	997.0	150.1	10.90	146.0	128.8	0.296	279.9	1605.3
2.50	4.7	10.00	1195.0	149.7	11.05	150.4	131.3	0.246	289.9	1662.6
2.50	4.7	9.94	403.0	140.3	10.34	178.3	170.8	0.466	173.2	993.5
2.50	4.7	9.93	499.9	140.4	10.42	179.3	170.2	0.434	202.3	1160.1
2.50	4.7	9.99	598.8	140.5	10.56	181.5	170.9	0.387	220.3	1263.5
2.50	4.7	9.91	796.1	139.5	10.65	187.2	173.5	0.328	257.3	1475.9
2.50	4.7	9.96	992.0	140.2	10.84	187.8	171.6	0.279	281.5	1614.8
2.50	4.7	19.88	401.6	207.2	20.23	26.5	22.4	0.597	179.1	1027.4
2.50	4.7	19.92	495.8	206.8	20.34	29.6	24.7	0.556	206.4	1183.9
2.50	4.7	19.99	598.7	207.0	20.48	30.2	24.6	0.503	226.2	1297.1

Table A: CHF data of vertical up flow heating tubes (Cont.)

L	$\frac{q"_{max}}{q"_{min}}$	P_{out}	G	t_{in}	P_{in}	$\Delta h_{sub}(P_{out})$	$\Delta h_{sub}(P_{in})$	x	Q	CHF
m	–	bars	$kg/(m^2s)$	^{o}C	bars	kJ/kg	kJ/kg		kW	kW/m^2
2.50	4.7	19.95	797.7	207.7	20.57	28.1	20.9	0.420	251.9	1444.7
2.50	4.7	19.93	1000.0	207.2	20.68	31.6	23.0	0.356	269.3	1544.5
2.50	4.7	19.97	1196.7	207.1	20.84	33.9	23.9	0.312	284.5	1631.9
2.50	4.7	19.96	397.3	202.4	20.30	49.0	45.1	0.599	181.0	1038.3
2.50	4.7	19.90	497.2	202.3	20.32	49.7	44.8	0.547	207.6	1190.5
2.50	4.7	19.96	597.0	201.8	20.45	53.4	47.8	0.496	228.0	1307.6
2.50	4.7	19.92	794.6	202.0	20.53	53.4	46.4	0.411	253.4	1453.2
2.50	4.7	20.00	996.1	202.0	20.72	55.6	47.3	0.350	273.5	1568.4
2.50	4.7	19.97	1200.8	201.8	20.81	57.5	47.9	0.303	288.0	1652.1
2.50	4.7	19.88	394.5	192.0	20.21	94.5	90.7	0.583	182.3	1045.3
2.50	4.7	19.87	496.4	192.3	20.28	94.0	89.2	0.531	210.2	1205.6
2.50	4.7	19.94	596.4	191.9	20.42	97.3	91.8	0.483	231.9	1330.2
2.50	4.7	20.01	797.5	192.0	20.60	98.9	92.2	0.401	262.3	1504.6
2.50	4.7	19.93	1000.4	192.1	20.64	99.0	90.8	0.342	285.9	1639.6
2.50	4.7	20.05	1193.1	192.2	20.86	101.0	91.7	0.293	297.8	1707.7
2.50	4.7	19.99	398.3	181.8	20.32	140.5	136.7	0.568	186.6	1070.3
2.50	4.7	19.91	497.2	182.0	20.32	139.7	134.9	0.527	217.8	1249.0
2.50	4.7	19.89	602.8	181.9	20.36	140.5	135.1	0.472	239.8	1375.3
2.50	4.7	19.96	795.9	182.0	20.54	142.2	135.5	0.392	270.3	1550.4
2.50	4.7	20.01	995.5	182.1	20.71	143.6	135.6	0.336	297.1	1703.8
2.50	4.7	19.96	396.6	172.1	20.30	183.0	179.1	0.563	191.0	1095.4
2.50	4.7	19.89	504.9	171.8	20.30	184.3	179.6	0.513	224.9	1289.7
2.50	4.7	19.87	598.5	172.0	20.33	183.8	178.5	0.463	244.3	1400.9
2.50	4.7	19.92	790.0	171.8	20.49	186.5	179.9	0.383	276.7	1587.2
2.50	4.7	29.93	398.5	229.4	30.25	23.3	20.5	0.641	180.6	1036.1
2.50	4.7	29.91	496.9	229.3	30.30	24.2	20.8	0.590	207.9	1192.1
2.50	4.7	29.93	598.4	229.2	30.36	25.1	21.4	0.531	225.6	1294.2

Table A: CHF data of vertical up flow heating tubes (Cont.)

L	$\frac{q''_{max}}{q''_{min}}$	P_{out}	G	t_{in}	P_{in}	$\Delta h_{sub}(P_{out})$	$\Delta h_{sub}(P_{in})$	x	Q	CHF
m	–	bars	$kg/(m^2s)$	^0C	bars	kJ/kg	kJ/kg		kW	kW/m^2
2.50	4.7	29.92	795.7	228.9	30.45	27.3	22.7	0.440	250.6	1437.2
2.50	4.7	29.98	1002.9	228.7	30.61	29.6	24.2	0.375	270.9	1553.7
2.50	4.7	29.99	1196.5	229.1	30.72	28.7	22.4	0.328	283.2	1624.4
2.50	4.7	29.95	398.1	224.0	30.28	48.7	45.8	0.627	180.6	1035.8
2.50	4.7	29.84	500.6	223.9	30.23	48.7	45.3	0.577	209.8	1203.2
2.50	4.7	29.92	595.1	223.9	30.35	49.8	46.0	0.528	229.1	1313.8
2.50	4.7	29.98	800.0	223.9	30.51	51.2	46.6	0.433	255.3	1464.4
2.50	4.7	29.97	998.1	224.1	30.60	51.0	45.5	0.370	274.5	1574.0
2.50	4.7	29.88	1192.2	223.9	30.59	51.8	45.7	0.322	287.6	1649.3
2.50	4.7	29.92	385.5	213.9	30.24	95.0	92.2	0.630	182.4	1046.3
2.50	4.7	29.92	495.3	214.1	30.30	94.6	91.3	0.564	211.6	1213.7
2.50	4.7	29.91	602.4	213.9	30.35	95.9	92.1	0.509	234.4	1344.6
2.50	4.7	29.90	795.0	214.0	30.42	96.1	91.6	0.423	261.8	1501.3
2.50	4.7	29.94	996.0	213.9	30.55	97.7	92.4	0.361	285.6	1637.9
2.50	4.7	29.92	1197.3	213.4	30.60	100.4	94.5	0.304	296.5	1700.6
2.50	4.7	29.87	395.5	204.4	30.19	137.8	135.1	0.593	183.8	1054.3
2.50	4.7	29.90	494.9	203.9	30.28	140.9	137.6	0.552	216.1	1239.3
2.50	4.7	29.93	597.6	204.0	30.36	141.1	137.4	0.503	240.9	1381.6
2.50	4.7	29.97	795.9	203.8	30.48	143.1	138.6	0.414	271.9	1559.2
2.50	4.7	29.92	994.7	204.2	30.52	141.6	136.4	0.348	293.2	1681.8
2.50	4.7	29.83	395.3	194.1	30.17	183.8	180.9	0.588	189.4	1086.3
2.50	4.7	29.88	498.5	194.0	30.26	185.0	181.7	0.538	221.6	1270.6
2.50	4.7	29.96	599.1	193.8	30.39	187.1	183.3	0.490	246.6	1414.4
2.50	4.7	29.87	798.7	193.8	30.38	187.0	182.5	0.400	278.3	1596.3
2.50	4.7	29.96	995.5	194.0	30.54	187.5	182.4	0.334	301.3	1727.9
2.50	4.7	39.84	397.1	244.8	40.17	28.0	25.7	0.625	168.6	967.0
2.50	4.7	39.92	500.2	244.9	40.30	28.6	25.8	0.585	198.9	1140.8

Table A: CHF data of vertical up flow heating tubes (Cont.)

L	$\frac{q''_{max}}{q''_{min}}$	P_{out}	G	t_{in}	P_{in}	$\Delta h_{sub}(P_{out})$	$\Delta h_{sub}(P_{in})$	x	Q	CHF
m	–	bars	$kg/(m^2s)$	^0C	bars	kJ/kg	kJ/kg		kW	kW/m^2
2.50	4.7	39.97	597.8	245.4	40.39	26.9	23.7	0.534	217.3	1246.2
2.50	4.7	39.98	797.1	245.1	40.47	28.9	25.3	0.440	240.0	1376.7
2.50	4.7	39.91	999.1	245.1	40.48	29.0	24.8	0.369	253.8	1455.7
2.50	4.7	39.98	1198.4	244.9	40.62	30.9	26.2	0.316	262.9	1507.5
2.50	4.7	39.82	395.7	240.0	40.15	50.7	48.4	0.621	170.3	976.8
2.50	4.7	40.05	478.7	239.8	40.42	53.7	50.9	0.590	196.7	1128.3
2.50	4.7	39.95	600.8	240.0	40.37	52.4	49.3	0.522	219.3	1257.5
2.50	4.7	39.99	797.0	239.8	40.48	54.2	50.5	0.426	240.8	1381.2
2.50	4.7	39.97	994.2	239.8	40.53	54.5	50.4	0.359	256.4	1470.2
2.50	4.7	39.96	1197.6	239.7	40.59	55.4	50.8	0.306	266.2	1526.8
2.50	4.7	39.92	399.2	230.3	40.26	97.3	94.7	0.621	178.9	1026.3
2.50	4.7	39.92	498.9	230.0	40.30	99.0	96.1	0.570	207.0	1187.3
2.50	4.7	39.91	596.9	230.2	40.33	98.3	95.1	0.519	227.4	1304.1
2.50	4.7	39.92	798.0	229.9	40.41	100.3	96.6	0.427	255.6	1466.0
2.50	4.7	39.93	996.5	229.7	40.48	101.7	97.6	0.358	274.4	1573.8
2.50	4.7	39.92	399.5	220.2	40.27	144.3	141.7	0.613	184.4	1057.5
2.50	4.7	40.03	497.3	219.9	40.41	146.7	143.8	0.559	211.8	1214.8
2.50	4.7	39.91	597.3	219.7	40.33	147.1	143.9	0.500	231.2	1326.2
2.50	4.7	40.00	801.3	219.8	40.50	147.8	144.1	0.414	264.5	1517.3
2.50	4.7	40.00	994.1	219.7	40.55	148.6	144.5	0.346	283.6	1626.6
2.50	4.7	19.93	399.7	202.1	20.27	50.0	46.1	0.596	181.4	1040.5
2.50	4.7	19.91	498.6	202.3	20.33	49.8	44.9	0.547	208.4	1195.2
2.50	4.7	19.91	595.5	202.1	20.40	51.5	45.8	0.500	228.5	1310.6
2.50	4.7	19.88	798.1	201.9	20.49	53.4	46.4	0.413	255.7	1466.3
3.55	4.7	9.96	297.7	175.1	10.24	26.2	20.9	0.596	140.9	568.9
3.55	4.7	9.95	399.0	175.2	10.35	27.8	20.3	0.543	172.2	695.6
3.55	4.7	9.95	497.7	175.3	10.46	29.4	19.9	0.485	192.2	776.4

Table A: CHF data of vertical up flow heating tubes (Cont.)

L	$\frac{q''_{max}}{q''_{min}}$	P_{out}	G	t_{in}	P_{in}	$\Delta h_{sub}(P_{out})$	$\Delta h_{sub}(P_{in})$	x	Q	CHF
m	–	bars	$kg/(m^2 s)$	^{0}C	bars	kJ/kg	kJ/kg		kW	kW/m^2
3.55	4.7	9.96	598.0	175.4	10.61	31.7	19.6	0.449	213.8	863.4
3.55	4.7	9.94	699.5	175.3	10.71	33.9	19.6	0.411	229.8	928.0
3.55	4.7	9.97	799.5	175.3	10.85	36.4	20.2	0.378	241.8	976.5
3.55	4.7	9.95	1001.3	175.1	11.08	41.3	20.7	0.336	270.5	1092.4
3.55	4.7	9.98	298.3	175.2	10.25	25.9	20.9	0.597	141.3	570.8
3.55	4.7	9.92	400.0	175.3	10.32	26.8	19.3	0.545	173.1	699.3
3.55	4.7	9.90	500.5	175.2	10.42	29.1	19.3	0.488	194.3	784.6
3.55	4.7	9.97	599.2	175.1	10.61	32.9	21.1	0.445	212.7	859.2
3.55	4.7	9.99	797.2	175.2	10.88	37.4	21.0	0.390	248.7	1004.6
3.55	4.7	9.91	993.9	175.0	11.04	41.0	20.4	0.338	270.2	1091.3
3.55	4.7	9.95	1197.3	175.8	11.32	42.5	17.6	0.302	290.1	1171.9
3.55	4.7	9.89	1395.6	176.1	11.53	44.8	15.2	0.276	309.0	1248.2
3.55	4.7	9.92	1595.8	175.6	11.80	51.5	17.9	0.254	327.7	1323.7
3.55	4.7	9.95	1600.1	170.3	11.82	74.7	41.3	0.255	344.6	1391.8
3.55	4.7	9.89	1394.1	170.6	11.50	68.0	38.9	0.274	319.4	1290.2
3.55	4.7	9.88	1198.8	169.7	11.23	67.2	42.6	0.295	296.2	1196.3
3.55	4.7	9.89	996.4	170.0	11.01	62.1	41.5	0.336	277.0	1118.6
3.55	4.7	9.89	798.8	170.3	10.79	56.9	40.3	0.387	253.4	1023.4
3.55	4.7	9.86	596.1	170.1	10.50	52.5	40.6	0.441	214.4	866.0
3.55	4.7	9.90	400.5	169.9	10.30	49.7	42.2	0.532	172.9	698.1
3.55	4.7	19.95	295.5	207.1	20.17	26.2	23.7	0.692	152.5	615.8
3.55	4.7	20.05	400.4	207.0	20.36	28.9	25.3	0.637	190.3	768.8
3.55	4.7	20.07	496.4	206.8	20.46	30.9	26.4	0.576	214.1	864.8
3.55	4.7	19.94	595.7	207.2	20.41	28.5	23.1	0.532	237.1	957.8
3.55	4.7	19.98	697.2	207.4	20.53	29.0	22.7	0.484	252.9	1021.3
3.55	4.7	20.00	799.2	207.1	20.63	31.5	24.3	0.446	268.2	1083.2
3.55	4.7	19.84	997.5	207.0	20.63	31.9	22.8	0.388	292.1	1179.8

Table A: CHF data of vertical up flow heating tubes (Cont.)

L	$\frac{q"_{max}}{q"_{min}}$	P_{out}	G	t_{in}	P_{in}	$\Delta h_{sub}(P_{out})$	$\Delta h_{sub}(P_{in})$	x	Q	CHF
m	–	bars	$kg/(m^2s)$	^{o}C	bars	kJ/kg	kJ/kg		kW	kW/m^2
3.55	4.7	19.86	1197.1	207.1	20.82	33.6	22.6	0.344	311.9	1259.7
3.55	4.7	19.90	1392.5	206.8	21.01	37.1	24.4	0.311	330.1	1333.1
3.55	4.7	20.00	1395.1	202.3	21.10	58.5	45.9	0.306	337.0	1361.1
3.55	4.7	19.97	1193.6	201.7	20.91	59.1	48.3	0.341	320.5	1294.6
3.55	4.7	19.93	995.6	202.0	20.72	55.6	46.5	0.384	297.7	1202.3
3.55	4.7	19.96	801.8	201.9	20.60	54.7	47.3	0.438	271.4	1096.3
3.55	4.7	19.85	595.8	201.9	20.33	51.6	46.0	0.525	239.4	967.1
3.55	4.7	20.01	396.4	201.8	20.32	51.9	48.3	0.631	190.4	769.0
3.55	4.7	30.06	298.8	229.4	30.27	23.4	21.6	0.758	159.7	645.0
3.55	4.7	29.95	399.1	229.3	30.23	23.6	21.1	0.687	193.6	782.1
3.55	4.7	29.92	498.2	229.2	30.25	24.2	21.3	0.603	212.9	859.7
3.55	4.7	29.97	601.4	229.2	30.38	25.3	21.8	0.562	240.0	969.3
3.55	4.7	29.93	698.0	229.1	30.40	26.0	21.9	0.517	256.7	1036.8
3.55	4.7	29.91	800.6	229.3	30.45	25.5	20.8	0.473	269.6	1089.1
3.55	4.7	29.91	1004.4	229.3	30.58	26.6	20.8	0.417	299.5	1209.5
3.55	4.7	29.92	1189.1	229.4	30.70	27.1	20.4	0.372	316.5	1278.3
3.55	4.7	29.93	1392.3	228.9	30.84	30.7	22.8	0.332	333.9	1348.7
3.55	4.7	29.96	1393.2	224.1	30.85	53.1	45.4	0.328	342.4	1382.7
3.55	4.7	29.93	1196.2	224.5	30.72	50.2	43.3	0.367	325.3	1313.7
3.55	4.7	29.92	995.3	224.1	30.58	50.8	45.1	0.413	303.2	1224.4
3.55	4.7	29.90	796.6	224.3	30.44	48.7	44.0	0.474	276.1	1115.0
3.55	4.7	29.93	602.0	224.4	30.35	47.5	43.8	0.558	243.8	984.8
3.55	4.7	29.88	398.9	224.3	30.17	46.4	43.8	0.665	191.2	772.3
3.55	4.7	9.95	790.5	175.0	10.85	37.7	21.1	0.389	246.5	995.4
3.55	4.7	9.96	1197.3	175.3	11.34	45.0	20.0	0.303	292.1	1179.7
3.55	4.7	40.03	294.5	244.3	40.27	31.3	29.4	0.758	151.4	611.4
3.55	4.7	39.93	396.9	244.8	40.22	28.6	26.3	0.679	182.8	738.4

Table A: CHF data of vertical up flow heating tubes (Cont.)

L	$\frac{q''_{max}}{q''_{min}}$	P_{out}	G	t_{in}	P_{in}	$\Delta h_{sub}(P_{out})$	$\Delta h_{sub}(P_{in})$	x	Q	CHF
m	–	bars	$kg/(m^2 s)$	$^0 C$	bars	kJ/kg	kJ/kg		kW	kW/m^2
3.55	4.7	39.97	499.2	245.0	40.32	28.3	25.7	0.600	203.5	822.1
3.55	4.7	40.03	599.6	245.1	40.43	28.6	25.6	0.554	226.2	913.5
3.55	4.7	39.89	700.3	245.3	40.33	27.0	23.7	0.505	240.9	973.1
3.55	4.7	40.03	804.6	245.0	40.52	29.7	26.1	0.463	254.9	1029.6
3.55	4.7	40.08	996.6	245.0	40.67	30.8	26.4	0.410	281.2	1135.6
3.55	4.7	40.02	1198.7	244.5	40.70	33.4	28.4	0.354	294.3	1188.8
3.55	4.7	39.91	399.6	239.8	40.20	52.2	50.0	0.667	184.4	744.9
3.55	4.7	39.89	597.6	240.2	40.28	50.9	47.9	0.540	225.0	908.7
3.55	4.7	40.01	800.5	240.3	40.50	51.9	48.3	0.456	256.9	1037.5
3.55	4.7	40.02	1008.7	240.2	40.60	53.1	48.8	0.391	280.3	1132.2
3.55	4.7	39.98	1201.1	239.6	40.64	56.2	51.4	0.339	293.7	1186.2
3.55	4.7	40.05	1196.1	235.5	40.70	76.0	71.3	0.336	299.1	1208.0
3.55	4.7	39.94	997.3	235.1	40.51	76.6	72.4	0.386	283.0	1143.2
3.55	4.7	39.95	798.9	235.3	40.43	75.1	71.5	0.444	257.5	1039.9
3.55	4.7	39.92	595.7	235.2	40.32	74.8	71.7	0.536	228.2	921.6
3.55	4.7	39.82	401.1	235.3	40.12	72.7	70.6	0.644	182.3	736.3
3.55	4.7	39.96	393.2	229.9	40.25	99.1	96.9	0.660	186.9	755.0
3.55	4.7	40.05	599.9	230.4	40.43	98.1	95.2	0.544	238.2	962.2
3.55	4.7	39.95	796.5	230.2	40.44	99.1	95.4	0.462	273.2	1103.4
3.55	4.7	39.93	998.8	229.8	40.50	101.4	97.1	0.394	298.2	1204.3
3.55	4.7	40.01	1195.3	230.3	40.67	100.2	95.4	0.341	314.1	1268.5
3.55	4.7	39.87	1195.3	220.6	40.51	144.2	139.5	0.327	323.7	1307.6
3.55	4.7	39.96	995.3	220.0	40.53	147.1	142.9	0.380	305.6	1234.3
3.55	4.7	39.82	801.0	220.2	40.31	144.6	141.0	0.441	278.2	1123.5
3.55	4.7	39.88	401.9	221.6	40.20	137.4	134.9	0.641	191.9	775.3
3.55	4.7	39.94	599.4	220.2	40.33	144.8	141.8	0.515	237.4	958.7
3.55	4.7	39.95	396.4	210.3	40.26	189.7	187.3	0.627	193.5	781.4

Table A: CHF data of vertical up flow heating tubes (Cont.)

L	$\frac{q"_{max}}{q"_{min}}$	P_{out}	G	t_{in}	P_{in}	$\Delta h_{sub}(P_{out})$	$\Delta h_{sub}(P_{in})$	x	Q	CHF
m	–	bars	$kg/(m^2 s)$	^0C	bars	kJ/kg	kJ/kg		kW	kW/m^2
3.55	4.7	39.93	596.7	210.0	40.32	191.5	188.5	0.506	243.9	985.0
3.55	4.7	40.04	802.6	209.7	40.52	194.2	190.7	0.421	283.0	1143.0
3.55	4.7	39.83	993.5	209.7	40.38	193.3	189.2	0.359	309.5	1250.2
3.55	4.7	40.05	1198.8	210.3	40.67	192.6	188.0	0.307	331.3	1338.1
3.55	4.7	9.92	797.3	175.1	10.82	36.7	20.1	0.390	248.8	1004.8
3.55	4.7	9.97	1193.5	175.1	11.34	45.8	21.0	0.304	292.8	1182.7
3.55	4.7	9.92	392.1	160.1	10.31	92.2	84.9	0.535	176.6	713.4
3.55	4.7	9.93	603.0	160.4	10.55	95.3	83.7	0.430	221.6	895.0
3.55	4.7	9.93	796.4	159.8	10.80	102.4	86.3	0.380	263.0	1062.3
3.55	4.7	9.89	991.1	159.8	10.98	105.6	85.6	0.332	290.0	1171.1
3.55	4.7	9.94	1196.8	160.0	11.28	109.9	85.6	0.299	318.6	1286.7
3.55	4.7	9.96	1390.0	159.6	11.52	115.8	87.7	0.273	342.7	1384.3
3.55	4.7	9.98	1396.1	150.0	11.50	156.9	129.6	0.269	362.7	1464.8
3.55	4.7	9.93	1196.5	149.5	11.21	154.1	130.8	0.291	332.6	1343.3
3.55	4.7	9.93	990.0	149.9	11.00	148.7	129.1	0.330	304.4	1229.3
3.55	4.7	9.93	793.9	150.1	10.76	143.6	128.2	0.368	267.7	1081.3
3.55	4.7	9.89	600.2	150.2	10.49	138.2	127.1	0.411	221.9	896.2
3.55	4.7	9.88	393.0	150.0	10.26	134.9	127.7	0.512	176.6	713.2
3.55	4.7	9.95	397.8	140.3	10.33	178.1	171.0	0.500	181.5	733.2
3.55	4.7	9.95	599.2	139.6	10.52	184.4	173.8	0.396	225.4	910.3
3.55	4.7	9.89	801.1	139.6	10.71	187.9	172.7	0.355	275.4	1112.3
3.55	4.7	9.95	998.6	139.5	10.96	192.7	174.2	0.309	308.0	1244.0
3.55	4.7	9.93	1197.7	139.4	11.14	196.3	174.3	0.276	339.1	1369.8
3.55	4.7	9.92	1395.8	139.5	11.31	198.9	173.6	0.244	359.6	1452.6
3.55	4.7	19.87	397.6	191.7	20.17	95.4	91.9	0.614	192.9	779.3
3.55	4.7	19.87	599.0	192.0	20.34	96.0	90.6	0.515	247.0	997.6
3.55	4.7	19.93	797.4	191.9	20.55	98.8	91.7	0.437	283.2	1143.7

Table A: CHF data of vertical up flow heating tubes (Cont.)

L	$\frac{q''_{max}}{q''_{min}}$	P_{out}	G	t_{in}	P_{in}	$\Delta h_{sub}(P_{out})$	$\Delta h_{sub}(P_{in})$	x	Q	CHF
m	–	bars	$kg/(m^2 s)$	^0C	bars	kJ/kg	kJ/kg		kW	kW/m^2
3.55	4.7	19.97	994.7	191.8	20.74	101.4	92.6	0.379	311.2	1256.9
3.55	4.7	19.89	1196.9	191.6	20.81	103.1	92.5	0.332	333.6	1347.5
3.55	4.7	19.93	1196.5	181.8	20.82	146.2	136.0	0.323	345.7	1396.2
3.55	4.7	19.91	996.5	182.1	20.68	143.3	134.5	0.372	323.4	1306.1
3.55	4.7	19.89	797.4	182.1	20.50	141.3	134.2	0.424	288.7	1166.2
3.55	4.7	19.93	598.0	182.2	20.41	139.8	134.3	0.510	254.3	1027.3
3.55	4.7	19.96	397.3	182.3	20.27	137.8	134.2	0.591	192.4	777.0
3.55	4.7	19.93	397.0	171.8	20.23	183.5	180.0	0.575	194.6	786.1
3.55	4.7	19.93	600.2	172.1	20.38	183.9	178.7	0.489	256.3	1035.1
3.55	4.7	19.92	795.8	171.7	20.52	187.2	180.3	0.416	298.0	1203.5
3.55	4.7	19.88	996.4	171.7	20.63	188.5	179.9	0.367	337.2	1361.9
3.55	4.7	19.90	1196.6	171.6	20.78	190.6	180.5	0.321	364.7	1473.1
3.55	4.7	29.94	398.7	214.2	30.22	93.4	91.0	0.649	193.8	782.8
3.55	4.7	29.95	600.9	214.2	30.36	94.6	91.1	0.548	250.0	1009.9
3.55	4.7	29.91	795.5	213.9	30.44	96.7	92.1	0.467	286.6	1157.7
3.55	4.7	29.94	997.7	213.9	30.59	98.0	92.4	0.404	315.9	1276.0
3.55	4.7	29.96	1198.4	213.7	30.73	100.1	93.5	0.352	336.8	1360.3
3.55	4.7	29.96	1193.9	204.0	30.70	144.0	137.6	0.344	349.2	1410.2
3.55	4.7	29.90	399.7	203.8	30.18	140.5	138.0	0.629	196.2	792.3
3.55	4.7	29.95	596.2	204.2	30.35	140.1	136.7	0.534	252.9	1021.5
3.55	4.7	29.88	794.9	204.3	30.41	140.2	135.6	0.455	293.1	1183.7
3.55	4.7	29.85	994.9	204.3	30.49	140.9	135.3	0.391	322.2	1301.5
3.55	4.7	29.68	1165.8	196.0	30.40	177.3	171.1	0.350	361.5	1460.0
3.55	4.7	29.96	996.9	194.0	30.59	187.9	182.4	0.381	334.2	1349.8
3.55	4.7	29.80	800.5	193.8	30.32	186.5	181.9	0.441	301.7	1218.7
3.55	4.7	29.98	597.7	193.4	30.39	188.8	185.3	0.519	258.5	1043.9
3.55	4.7	29.84	398.3	193.8	30.13	184.8	182.3	0.612	197.7	798.4

Table A: CHF data of vertical up flow heating tubes (Cont.)

L	$\frac{q''_{max}}{q''_{min}}$	P_{out}	G	t_{in}	P_{in}	$\Delta h_{sub}(P_{out})$	$\Delta h_{sub}(P_{in})$	x	Q	CHF
m	–	bars	$kg/(m^2s)$	$^{\circ}C$	bars	kJ/kg	kJ/kg		kW	kW/m^2
3.55	4.7	9.96	794.7	174.7	10.85	39.0	22.6	0.379	242.1	977.8
3.55	4.7	9.88	1196.3	175.0	11.24	44.5	19.8	0.292	281.4	1136.7
1.80	8.3	9.89	401.9	175.2	10.29	26.7	19.1	0.444	142.7	1135.5
1.80	8.3	9.89	397.4	174.9	10.30	28.1	20.4	0.452	143.7	1143.3
1.80	8.3	9.91	399.1	175.3	10.31	26.6	19.1	0.448	142.8	1135.6
1.80	8.3	19.84	400.7	207.3	20.18	25.4	21.5	0.510	153.2	1219.1
1.80	8.3	29.87	397.2	229.0	30.20	24.7	21.8	0.546	154.4	1228.6
1.80	8.3	39.95	401.0	245.0	40.30	28.2	25.5	0.501	137.6	1094.6
1.80	8.3	9.88	393.8	170.2	10.28	48.0	40.5	0.450	145.0	1153.4
1.80	8.3	19.85	397.9	201.6	20.19	51.3	47.4	0.512	156.8	1247.2
1.80	8.3	29.87	399.5	224.3	30.21	46.7	43.7	0.520	151.5	1204.8
1.80	8.3	39.84	397.7	239.8	40.19	51.9	49.5	0.495	138.6	1102.6
1.80	8.3	9.86	397.3	160.1	10.25	91.1	83.7	0.421	143.9	1145.1
1.80	8.3	19.88	404.2	191.9	20.23	95.2	91.1	0.491	160.1	1273.6
1.80	8.3	29.84	399.3	214.2	30.18	93.1	90.1	0.510	156.0	1241.1
1.80	8.3	39.83	401.5	229.9	40.18	98.5	96.0	0.476	142.1	1130.5
1.80	8.3	9.89	399.8	150.1	10.27	134.6	127.5	0.403	145.9	1160.3
1.80	8.3	19.81	400.3	182.2	20.16	136.9	132.9	0.480	161.8	1286.7
1.80	8.3	29.76	397.6	203.9	30.10	139.3	136.4	0.485	155.6	1237.7
1.80	8.3	39.80	397.4	219.5	40.16	146.6	144.1	0.462	144.4	1149.0
1.80	8.3	9.87	497.6	175.3	10.35	27.3	18.3	0.410	163.3	1298.9
1.80	8.3	19.89	497.8	207.4	20.29	26.3	21.6	0.463	173.4	1379.2
1.80	8.3	29.86	497.7	229.0	30.23	25.0	21.7	0.486	172.7	1373.5
1.80	8.3	39.90	500.1	244.7	40.28	29.5	26.6	0.463	159.3	1267.0
1.80	8.3	9.88	493.9	170.3	10.35	48.9	40.1	0.404	164.0	1304.9
1.80	8.3	19.85	498.1	202.0	20.24	50.1	45.6	0.451	173.8	1382.4
1.80	8.3	29.89	499.0	224.1	30.26	48.1	44.8	0.469	171.9	1367.1

Table A: CHF data of vertical up flow heating tubes (Cont.)

L	$\frac{q''_{max}}{q''_{min}}$	P_{out}	G	t_{in}	P_{in}	$\Delta h_{sub}(P_{out})$	$\Delta h_{sub}(P_{in})$	x	Q	CHF
m	–	bars	$kg/(m^2 s)$	^oC	bars	kJ/kg	kJ/kg		kW	kW/m^2
1.80	8.3	39.86	497.9	239.9	40.23	51.9	49.1	0.440	155.1	1233.4
1.80	8.3	9.88	496.0	160.2	10.34	92.3	83.7	0.390	167.4	1331.8
1.80	8.3	19.87	495.2	191.8	20.25	95.8	91.4	0.450	181.1	1440.7
1.80	8.3	29.82	498.3	214.1	30.19	93.6	90.4	0.463	178.3	1418.6
1.80	8.3	39.89	498.5	230.5	40.27	96.5	93.6	0.447	166.1	1321.7
1.80	8.3	9.88	497.3	150.1	10.33	135.7	127.3	0.364	166.3	1323.0
1.80	8.3	19.85	497.9	181.8	20.23	139.5	135.1	0.428	182.6	1452.6
1.80	8.3	29.85	497.8	204.1	30.21	139.4	136.2	0.430	175.7	1397.5
1.80	8.3	39.84	498.5	220.1	40.21	144.4	141.6	0.419	166.3	1323.1
1.80	8.3	9.88	596.5	175.1	10.43	29.7	19.4	0.371	177.6	1412.5
1.80	8.3	19.81	595.6	207.1	20.24	27.0	22.1	0.421	189.2	1505.5
1.80	8.3	29.80	595.6	229.2	30.20	23.8	20.3	0.428	182.6	1453.0
1.80	8.3	39.86	597.0	245.1	40.26	27.4	24.4	0.401	164.7	1310.5
1.80	8.3	9.87	596.2	170.2	10.42	50.6	40.3	0.366	179.9	1431.0
1.80	8.3	19.89	595.0	202.3	20.32	49.7	44.7	0.413	190.8	1518.0
1.80	8.3	29.86	595.6	224.4	30.26	46.7	43.2	0.422	185.2	1473.5
1.80	8.3	39.85	597.8	240.2	40.25	50.6	47.6	0.409	173.8	1382.2
1.80	8.3	9.87	596.3	160.1	10.39	93.7	83.9	0.341	178.6	1420.8
1.80	8.3	19.80	597.0	192.1	20.23	94.3	89.3	0.398	195.2	1553.0
1.80	8.3	29.85	596.6	214.2	30.25	93.7	90.2	0.403	188.4	1498.6
1.80	8.3	39.82	596.8	230.3	40.21	97.0	94.0	0.382	173.6	1381.2
1.80	8.3	9.89	596.2	150.3	10.39	136.0	126.6	0.326	181.2	1441.8
1.80	8.3	19.87	594.5	182.0	20.29	139.3	134.4	0.385	198.9	1582.5
1.80	8.3	29.80	598.5	204.2	30.20	138.8	135.3	0.393	195.5	1555.2
1.80	8.3	39.81	597.8	220.1	40.21	144.4	141.4	0.378	183.0	1455.8
1.80	8.3	9.86	798.0	175.4	10.52	30.0	17.7	0.294	189.0	1503.4
1.80	8.3	19.84	797.0	207.1	20.35	28.3	22.4	0.330	200.0	1591.3

Table A: CHF data of vertical up flow heating tubes (Cont.)

L	$\frac{q''_{max}}{q''_{min}}$	P_{out}	G	t_{in}	P_{in}	$\Delta h_{sub}(P_{out})$	$\Delta h_{sub}(P_{in})$	x	Q	CHF
m	–	bars	$kg/(m^2 s)$	^0C	bars	kJ/kg	kJ/kg		kW	kW/m^2
2.50	8.3	9.90	395.6	175.1	10.30	27.3	19.8	0.477	150.8	863.8
2.50	8.3	9.86	499.8	175.3	10.36	27.5	18.1	0.427	170.7	977.8
2.50	8.3	9.89	598.1	175.1	10.47	30.4	19.6	0.389	186.5	1068.0
2.50	8.3	9.88	795.6	175.0	10.62	33.6	19.8	0.324	207.8	1190.0
2.50	8.3	9.89	798.6	170.0	10.63	55.3	41.6	0.320	212.9	1219.6
2.50	8.3	9.87	598.3	170.2	10.45	51.2	40.3	0.384	189.4	1084.7
2.50	8.3	9.85	394.6	170.0	10.25	48.4	40.8	0.471	151.9	869.8
2.50	8.3	9.85	499.4	170.3	10.35	48.9	39.5	0.422	172.6	988.8
2.50	8.3	9.85	500.1	160.1	10.33	92.6	83.5	0.410	176.9	1013.5
2.50	8.3	9.90	396.9	159.8	10.31	93.5	85.8	0.464	157.3	901.0
2.50	8.3	9.87	597.9	160.3	10.43	93.5	83.0	0.376	195.3	1118.6
2.50	8.3	9.92	796.9	160.1	10.64	98.2	84.8	0.315	222.8	1275.8
2.50	8.3	9.84	792.8	150.2	10.53	139.0	126.1	0.303	227.0	1299.9
2.50	8.3	9.88	594.1	149.9	10.42	138.3	128.2	0.356	195.3	1118.3
2.50	8.3	9.88	497.0	150.1	10.35	136.1	127.3	0.395	178.0	1019.7
2.50	8.3	9.88	397.9	150.1	10.27	134.6	127.3	0.445	158.2	906.2
2.50	8.3	9.91	397.3	139.7	10.30	180.0	172.7	0.438	162.9	932.8
2.50	8.3	9.87	495.4	139.9	10.32	179.7	171.2	0.374	177.8	1018.5
2.50	8.3	9.88	598.4	139.5	10.41	182.9	172.9	0.342	200.5	1148.4
2.50	8.3	9.90	794.2	140.0	10.57	183.8	171.3	0.288	231.9	1328.2
2.50	8.3	19.91	398.6	206.8	20.24	28.4	24.6	0.549	164.4	941.8
2.50	8.3	19.83	496.5	206.9	20.23	27.8	23.2	0.503	187.7	1075.2
2.50	8.3	19.88	595.0	206.8	20.34	29.6	24.2	0.457	205.1	1174.4
2.50	8.3	19.93	797.4	206.9	20.49	30.8	24.4	0.373	225.8	1293.0
2.50	8.3	19.88	397.5	201.7	20.21	51.1	47.3	0.550	167.9	961.6
2.50	8.3	19.86	499.7	202.4	20.26	48.5	43.9	0.495	190.0	1088.2
2.50	8.3	19.85	598.1	202.2	20.31	50.0	44.7	0.450	208.2	1192.4

Table A: CHF data of vertical up flow heating tubes (Cont.)

L	$\frac{q''_{max}}{q''_{min}}$	P_{out}	G	t_{in}	P_{in}	$\Delta h_{sub}(P_{out})$	$\Delta h_{sub}(P_{in})$	x	Q	CHF
m	–	bars	$kg/(m^2 s)$	$^0 C$	bars	kJ/kg	kJ/kg		kW	kW/m^2
2.50	8.3	19.87	799.6	201.7	20.43	53.6	47.2	0.370	231.6	1326.3
2.50	8.3	19.89	398.3	191.8	20.22	95.5	91.7	0.537	171.1	980.1
2.50	8.3	19.86	497.9	192.0	20.25	95.0	90.4	0.485	194.9	1116.3
2.50	8.3	19.89	599.4	191.7	20.34	97.3	92.1	0.436	213.3	1221.7
2.50	8.3	19.90	795.6	192.0	20.45	97.2	90.9	0.364	240.5	1377.7
2.50	8.3	19.94	397.7	182.1	20.27	138.6	134.8	0.531	175.7	1006.3
2.50	8.3	19.84	496.3	182.2	20.23	137.8	133.2	0.475	198.8	1138.4
2.50	8.3	19.86	598.9	181.9	20.31	140.0	134.8	0.430	220.5	1263.0
2.50	8.3	19.88	796.7	181.9	20.42	141.2	135.0	0.355	249.6	1429.7
2.50	8.3	19.86	793.7	171.8	20.38	185.2	179.2	0.344	255.7	1464.3
2.50	8.3	19.84	594.6	171.9	20.28	183.6	178.5	0.418	223.7	1281.2
2.50	8.3	19.86	501.5	171.9	20.25	183.3	178.8	0.458	203.3	1164.2
2.50	8.3	19.88	395.5	172.1	20.21	182.0	178.2	0.518	177.8	1018.4
2.50	8.3	29.87	399.4	229.2	30.19	23.7	20.9	0.600	170.4	976.2
2.50	8.3	29.88	498.7	229.4	30.25	23.3	20.0	0.538	191.0	1093.9
2.50	8.3	29.90	596.6	229.0	30.31	25.6	22.1	0.493	210.2	1203.9
2.50	8.3	29.88	792.3	229.0	30.38	26.3	21.9	0.408	231.9	1328.1
2.50	8.3	29.85	400.2	223.9	30.16	48.1	45.4	0.583	169.6	971.6
2.50	8.3	29.92	498.0	224.1	30.28	48.2	45.1	0.532	193.4	1107.4
2.50	8.3	29.87	597.0	223.9	30.28	49.2	45.6	0.481	210.7	1206.6
2.50	8.3	29.85	798.7	224.0	30.35	49.3	45.0	0.400	236.9	1356.7
2.50	8.3	29.87	395.8	213.8	30.19	95.0	92.2	0.575	172.8	989.5
2.50	8.3	29.92	500.6	214.4	30.29	93.1	89.9	0.519	198.4	1136.5
2.50	8.3	29.91	595.8	214.0	30.32	95.2	91.7	0.472	217.1	1243.4
2.50	8.3	29.89	793.5	214.0	30.39	95.8	91.5	0.392	244.8	1402.0
2.50	8.3	29.91	398.6	204.3	30.23	138.6	135.9	0.571	179.6	1028.6
2.50	8.3	29.84	496.9	204.2	30.21	138.9	135.7	0.520	206.2	1181.1

Table A: CHF data of vertical up flow heating tubes (Cont.)

L	$\frac{q''_{max}}{q''_{min}}$	P_{out}	G	t_{in}	P_{in}	$\Delta h_{sub}(P_{out})$	$\Delta h_{sub}(P_{in})$	x	Q	CHF
m	–	bars	$kg/(m^2 s)$	^0C	bars	kJ/kg	kJ/kg		kW	kW/m^2
2.50	8.3	29.90	597.2	204.1	30.32	140.3	136.7	0.467	225.9	1293.8
2.50	8.3	29.83	797.2	204.2	30.31	139.8	135.6	0.379	252.7	1447.2
2.50	8.3	29.86	598.2	194.0	30.27	185.1	181.6	0.447	228.4	1307.9
2.50	8.3	29.86	498.8	194.3	30.23	183.5	180.2	0.494	206.8	1184.4
2.50	8.3	29.82	397.5	193.9	30.16	184.6	181.7	0.562	183.8	1052.5
2.50	8.3	39.87	399.1	245.0	40.19	27.2	24.9	0.593	161.4	924.3
2.50	8.3	39.85	503.4	245.2	40.22	26.6	23.8	0.540	185.6	1062.9
2.50	8.3	39.90	596.1	245.2	40.30	27.2	24.2	0.498	203.2	1163.6
2.50	8.3	39.95	796.0	245.3	40.42	27.6	24.1	0.413	225.9	1293.9
2.50	8.3	39.89	799.0	240.2	40.37	51.5	47.9	0.406	230.5	1320.2
2.50	8.3	39.85	596.5	240.3	40.26	50.2	47.2	0.488	204.5	1171.5
2.50	8.3	39.90	396.2	240.0	40.22	51.4	48.9	0.587	162.2	929.1
2.50	8.3	39.86	495.4	240.1	40.22	50.9	48.2	0.543	188.2	1078.1
2.50	8.3	39.81	495.7	230.0	40.18	98.0	95.4	0.533	194.0	1111.3
2.50	8.3	39.93	396.6	230.2	40.26	97.8	95.3	0.568	164.5	942.2
2.50	8.3	39.88	596.5	230.3	40.28	97.5	94.5	0.479	211.9	1213.4
2.50	8.3	39.82	798.1	230.6	40.30	96.2	92.6	0.403	242.8	1390.7
2.50	8.3	39.86	798.1	220.1	40.33	145.2	141.7	0.387	249.4	1428.3
2.50	8.3	39.88	596.8	219.8	40.29	146.3	143.2	0.463	217.1	1243.3
2.50	8.3	39.83	398.9	220.1	40.16	143.9	141.5	0.557	169.8	972.4
2.50	8.3	39.84	496.9	219.8	40.22	145.8	143.0	0.518	198.7	1138.1
2.50	8.3	39.96	398.1	209.8	40.30	192.2	189.6	0.541	172.5	987.8
2.50	8.3	39.90	497.6	210.0	40.27	191.1	188.3	0.506	203.6	1166.3
2.50	8.3	39.83	596.7	210.0	40.23	190.8	187.8	0.455	224.2	1284.0
2.50	8.3	9.86	990.8	175.2	10.78	35.6	18.6	0.286	228.9	1311.3
2.50	8.3	19.89	996.2	206.8	20.57	32.2	24.3	0.322	245.3	1404.9
2.50	8.3	29.81	995.8	228.8	30.40	27.4	22.2	0.348	250.4	1434.0

Table A: CHF data of vertical up flow heating tubes (Cont.)

L	$\frac{q''_{max}}{q''_{min}}$	P_{out}	G	t_{in}	P_{in}	$\Delta h_{sub}(P_{out})$	$\Delta h_{sub}(P_{in})$	x	Q	CHF
m	–	bars	$kg/(m^2 s)$	$^0 C$	bars	kJ/kg	kJ/kg		kW	kW/m^2
2.50	8.3	39.82	992.0	245.2	40.36	27.6	23.6	0.354	242.9	1391.5
2.50	8.3	9.87	991.1	169.9	10.76	58.1	41.6	0.277	230.6	1321.0
2.50	8.3	19.86	993.6	201.7	20.53	54.8	47.0	0.322	253.1	1449.4
2.50	8.3	29.90	998.2	224.5	30.49	48.2	43.1	0.349	259.8	1487.8
2.50	8.3	39.89	996.3	240.3	40.44	51.5	47.4	0.352	251.5	1440.3
2.50	8.3	9.89	990.5	160.3	10.74	99.1	83.4	0.269	240.6	1378.3
2.50	8.3	19.91	995.8	191.7	20.56	99.8	92.3	0.309	261.4	1497.2
2.50	8.3	29.85	988.3	214.4	30.42	94.2	89.3	0.339	268.1	1535.7
2.50	8.3	39.88	996.3	230.3	40.42	98.5	94.5	0.337	259.8	1488.0
2.50	8.3	9.86	1191.1	175.1	10.93	38.7	19.0	0.248	240.4	1377.0
2.50	8.3	9.91	1199.1	170.0	10.95	61.0	41.9	0.241	245.5	1406.3
2.50	8.3	19.89	1198.2	207.1	20.68	32.1	23.0	0.282	258.9	1482.6
2.50	8.3	29.92	1192.8	229.1	30.59	27.6	21.8	0.303	262.3	1502.4
2.50	8.3	39.92	1201.0	245.2	40.53	28.8	24.3	0.303	253.7	1453.1
2.50	8.3	9.87	1200.7	159.9	10.84	102.7	84.7	0.226	252.2	1444.6
2.50	8.3	19.87	1194.8	201.8	20.65	55.7	46.7	0.280	267.0	1529.4
2.50	8.3	39.89	1195.3	240.1	40.48	52.7	48.4	0.297	258.5	1480.4
2.50	8.3	29.94	1192.6	223.8	30.62	52.6	46.7	0.302	272.8	1562.4
3.55	8.3	9.89	400.1	175.0	10.26	27.0	20.0	0.497	158.7	640.0
3.55	8.3	19.92	394.1	207.1	20.22	26.8	23.3	0.626	184.6	744.5
3.55	8.3	29.90	402.6	229.0	30.19	24.6	22.1	0.673	192.2	775.2
3.55	8.3	39.85	396.4	244.4	40.14	29.7	27.7	0.682	183.9	741.8
3.55	8.3	39.92	397.7	240.0	40.21	51.3	49.1	0.669	184.4	743.9
3.55	8.3	9.88	398.7	170.4	10.28	47.2	39.7	0.528	170.9	689.4
3.55	8.3	9.88	401.8	175.2	10.28	26.5	19.0	0.527	168.6	679.9
3.55	8.3	9.88	397.7	159.9	10.26	92.1	85.0	0.517	174.1	702.2
3.55	8.3	9.87	394.2	150.1	10.26	134.5	127.1	0.511	177.0	713.9

Table A: CHF data of vertical up flow heating tubes (Cont.)

L	$\frac{q''_{max}}{q''_{min}}$	P_{out}	G	t_{in}	P_{in}	$\Delta h_{sub}(P_{out})$	$\Delta h_{sub}(P_{in})$	x	Q	CHF
m	–	bars	$kg/(m^2 s)$	$^{\circ}C$	bars	kJ/kg	kJ/kg		kW	kW/m^2
3.55	8.3	9.87	396.0	139.9	10.25	178.4	171.2	0.499	180.9	729.5
3.55	8.3	19.87	398.7	207.0	20.19	26.9	23.2	0.624	186.3	751.4
3.55	8.3	19.92	396.7	202.4	20.23	48.2	44.6	0.618	186.9	753.8
3.55	8.3	19.91	396.6	192.5	20.21	92.3	88.8	0.613	192.1	775.0
3.55	8.3	19.90	396.4	181.8	20.22	139.4	135.7	0.603	196.2	791.2
3.55	8.3	19.79	398.0	172.1	20.11	180.8	177.1	0.579	196.6	792.8
3.55	8.3	29.88	396.6	223.7	30.16	49.1	46.6	0.643	184.8	745.5
3.55	8.3	29.88	399.9	213.5	30.17	96.2	93.7	0.624	188.5	760.3
3.55	8.3	29.86	399.2	203.8	30.15	140.2	137.7	0.613	191.9	774.2
3.55	8.3	29.78	397.1	193.9	30.07	183.8	181.3	0.593	192.2	775.4
3.55	8.3	39.87	393.2	229.4	40.16	100.7	98.6	0.649	184.7	745.0
3.55	8.3	39.84	394.0	219.8	40.14	145.1	143.0	0.632	187.6	756.7
3.55	8.3	39.82	398.9	210.3	40.13	188.6	186.4	0.613	191.6	772.9
3.55	8.3	39.80	496.6	244.7	40.13	28.2	25.9	0.578	196.0	790.6
3.55	8.3	39.81	496.9	239.6	40.15	52.6	50.2	0.576	200.1	807.0
3.55	8.3	39.97	496.5	229.7	40.32	100.6	97.9	0.562	204.2	823.8
3.55	8.3	39.91	496.7	220.0	40.25	145.1	142.5	0.550	209.1	843.3
3.55	8.3	39.92	493.7	209.8	40.27	192.0	189.4	0.538	212.8	858.1
3.55	8.3	9.91	497.5	174.9	10.41	30.2	20.8	0.460	183.1	738.5
3.55	8.3	9.89	496.6	160.0	10.37	93.7	84.7	0.428	182.8	737.5
3.55	8.3	9.90	496.0	150.1	10.38	136.7	127.7	0.434	193.2	779.3
3.55	8.3	9.91	496.1	140.2	10.39	179.7	170.7	0.433	200.9	810.2
3.55	8.3	9.95	493.9	170.6	10.44	49.3	40.1	0.441	178.2	718.6
3.55	8.3	19.87	500.3	206.8	20.26	28.6	24.1	0.549	206.4	832.5
3.55	8.3	19.90	496.7	202.2	20.29	49.8	45.3	0.546	207.9	838.4
3.55	8.3	19.87	496.0	192.3	20.26	93.7	89.2	0.543	214.9	866.9
3.55	8.3	19.90	496.3	182.1	20.29	138.9	134.4	0.528	218.3	880.3

Table A: CHF data of vertical up flow heating tubes (Cont.)

L	$\frac{q''_{max}}{q''_{min}}$	P_{out}	G	t_{in}	P_{in}	$\Delta h_{sub}(P_{out})$	$\Delta h_{sub}(P_{in})$	x	Q	CHF
m	–	bars	$kg/(m^2s)$	^0C	bars	kJ/kg	kJ/kg		kW	kW/m^2
3.55	8.3	19.94	499.3	172.2	20.33	182.9	178.4	0.525	227.1	916.2
3.55	8.3	29.79	494.5	194.1	30.16	183.7	180.5	0.574	232.7	938.7
3.55	8.3	29.84	498.3	203.9	30.20	140.2	137.1	0.573	225.6	910.2
3.55	8.3	9.86	596.4	174.5	10.46	32.8	21.6	0.412	197.4	796.2
3.55	8.3	9.88	594.3	170.4	10.47	50.7	39.6	0.410	199.9	806.2
3.55	8.3	9.88	593.7	160.2	10.47	94.7	83.7	0.404	207.2	835.7
3.55	8.3	9.89	595.2	150.4	10.47	137.0	126.2	0.396	213.7	861.9
3.55	8.3	9.91	593.6	140.4	10.49	180.6	169.8	0.392	221.2	892.2
3.55	8.3	29.87	493.8	214.2	30.21	93.4	90.4	0.586	219.0	883.4
3.55	8.3	29.82	498.3	223.7	30.17	49.1	46.1	0.586	212.7	857.9
3.55	8.3	29.88	497.5	228.6	30.23	26.8	23.8	0.598	212.0	855.2
3.55	8.3	19.86	594.4	206.9	20.34	29.1	23.5	0.494	221.2	892.2
3.55	8.3	19.86	596.9	201.5	20.34	53.5	48.0	0.486	223.9	903.0
3.55	8.3	19.88	594.6	191.9	20.35	96.5	91.1	0.490	234.9	947.6
3.55	8.3	19.91	595.9	182.0	20.36	140.1	134.9	0.476	239.6	966.3
3.55	8.3	19.86	595.2	171.6	20.31	185.3	180.1	0.470	247.1	996.6
3.55	8.3	30.03	596.5	229.2	30.43	25.7	22.3	0.535	227.7	918.3
3.55	8.3	29.81	595.0	224.0	30.23	48.3	44.6	0.537	233.0	939.8
3.55	8.3	29.85	596.2	214.2	30.25	93.7	90.2	0.528	240.3	969.2
3.55	8.3	29.94	595.8	203.8	30.34	141.9	138.4	0.519	247.5	998.4
3.55	8.3	29.81	597.0	194.1	30.22	184.3	180.7	0.509	253.6	1022.9
3.55	8.3	39.68	596.6	245.0	40.07	26.4	23.6	0.551	224.4	905.0
3.55	8.3	39.79	595.0	239.7	40.17	52.3	49.6	0.537	224.1	903.8
3.55	8.3	39.85	598.6	230.3	40.24	97.2	94.2	0.520	228.9	923.3
3.55	8.3	39.87	597.1	220.0	40.26	145.2	142.2	0.504	233.0	939.9
3.55	8.3	39.84	594.2	210.0	40.23	190.8	187.9	0.496	239.4	965.7
3.55	8.3	39.88	798.6	210.4	40.35	189.9	186.3	0.415	278.1	1121.7

Table A: CHF data of vertical up flow heating tubes (Cont.)

L	$\frac{q''_{max}}{q''_{min}}$	P_{out}	G	t_{in}	P_{in}	$\Delta h_{sub}(P_{out})$	$\Delta h_{sub}(P_{in})$	x	Q	CHF
m	–	bars	$kg/(m^2 s)$	$^0 C$	bars	kJ/kg	kJ/kg		kW	kW/m^2
3.55	8.3	39.82	795.5	220.0	40.30	145.5	141.9	0.430	271.4	1094.8
3.55	8.3	39.81	795.6	229.9	40.29	99.4	95.8	0.440	262.3	1057.8
3.55	8.3	9.92	796.3	174.9	10.74	36.1	21.0	0.349	223.6	901.9
3.55	8.3	9.86	794.7	170.1	10.66	55.4	40.6	0.345	226.9	915.1
3.55	8.3	9.89	795.9	160.2	10.68	98.5	83.8	0.341	238.3	961.2
3.55	8.3	9.88	793.1	150.5	10.65	139.8	125.6	0.336	247.1	996.6
3.55	8.3	9.87	792.7	140.3	10.64	183.8	169.5	0.333	258.7	1043.6
3.55	8.3	19.80	792.3	172.4	20.37	182.5	175.9	0.391	281.8	1136.5
3.55	8.3	19.89	796.0	181.8	20.48	142.3	135.5	0.398	274.2	1105.9
3.55	8.3	19.92	794.8	191.6	20.52	99.8	92.9	0.402	263.4	1062.3
3.55	8.3	19.91	794.7	206.8	20.51	31.5	24.6	0.408	245.7	991.2
3.55	8.3	19.86	797.1	201.9	20.46	53.1	46.1	0.405	251.4	1014.1
3.55	8.3	29.92	786.5	228.8	30.44	27.7	23.2	0.450	253.7	1023.5
3.55	8.3	29.89	795.1	223.9	30.41	50.3	45.8	0.444	260.1	1048.9
3.55	8.3	29.85	795.9	213.8	30.37	96.6	92.0	0.437	270.9	1092.5
3.55	8.3	29.88	794.9	204.0	30.39	141.4	136.9	0.427	279.0	1125.6
3.55	8.3	29.90	802.1	194.0	30.41	186.3	181.9	0.412	286.7	1156.5
3.55	8.3	39.92	794.9	239.6	40.40	54.5	51.0	0.441	248.7	1003.2
3.55	8.3	39.94	798.3	245.0	40.43	29.1	25.4	0.444	243.4	981.5
3.55	8.3	9.88	996.0	175.0	10.90	38.6	19.8	0.298	239.7	966.8
3.55	8.3	9.91	1200.4	174.7	11.14	44.1	21.6	0.265	258.9	1044.3
3.55	8.3	9.88	992.5	170.3	10.89	58.7	40.1	0.298	247.2	997.3
3.55	8.3	9.86	1192.3	170.2	11.08	62.4	40.1	0.266	266.8	1076.0
3.55	8.3	9.89	998.9	160.4	10.88	101.2	83.0	0.291	259.7	1047.7
3.55	8.3	9.89	397.2	160.1	10.27	91.4	84.3	0.481	162.6	656.0
3.55	8.3	9.86	399.6	160.0	10.25	91.5	84.2	0.495	167.8	676.7
3.55	8.3	9.90	400.0	174.9	10.28	27.8	20.6	0.495	158.1	637.8

Table A: CHF data of vertical up flow heating tubes (Cont.)

L	$\frac{q''_{max}}{q''_{min}}$	P_{out}	G	t_{in}	P_{in}	$\Delta h_{sub}(P_{out})$	$\Delta h_{sub}(P_{in})$	x	Q	CHF
m	--	bars	$kg/(m^2 s)$	^{o}C	bars	kJ/kg	kJ/kg		kW	kW/m^2
3.55	8.3	19.94	994.7	206.9	20.69	33.1	24.5	0.351	265.8	1072.2
3.55	8.3	19.85	1193.2	207.0	20.77	33.5	23.0	0.315	286.6	1155.9
3.55	8.3	19.87	992.8	201.9	20.62	54.9	46.3	0.349	272.5	1099.0
3.55	8.3	19.86	1191.8	202.0	20.76	56.0	45.7	0.313	295.4	1191.4
3.55	8.3	19.77	988.9	192.2	20.50	96.9	88.5	0.345	284.4	1147.2
3.55	8.3	19.79	396.8	191.9	20.10	93.7	90.1	0.587	185.1	746.5
3.55	8.3	19.89	397.3	207.1	20.20	26.6	23.0	0.593	176.4	711.6
3.55	8.3	29.88	993.0	228.8	30.52	28.4	22.8	0.388	277.1	1117.5
3.55	8.3	29.92	1192.4	229.1	30.68	28.4	21.8	0.343	294.8	1188.9
3.55	8.3	29.88	994.3	223.6	30.53	52.7	47.1	0.382	282.6	1140.0
3.55	8.3	29.90	1189.7	223.8	30.65	52.8	46.3	0.340	303.3	1223.5
3.55	8.3	29.88	993.8	214.0	30.51	96.9	91.4	0.375	295.2	1190.8
3.55	8.3	29.84	396.8	213.5	30.13	95.9	93.3	0.608	182.6	736.6
3.55	8.3	29.89	399.0	229.4	30.19	22.7	20.1	0.631	178.5	719.8
3.55	8.3	39.93	1003.9	245.0	40.49	29.5	25.4	0.369	256.4	1034.1
3.55	8.3	39.87	1196.9	244.9	40.50	30.1	25.4	0.324	269.4	1086.4
3.55	8.3	39.77	993.8	240.1	40.32	51.6	47.5	0.365	259.8	1047.7
3.55	8.3	39.88	1192.8	239.9	40.51	53.9	49.3	0.316	273.3	1102.2
3.55	8.3	39.92	996.4	230.2	40.45	99.1	95.2	0.340	261.9	1056.4
3.55	8.3	19.89	399.1	207.0	20.19	26.9	23.4	0.583	174.4	703.3
3.55	8.3	19.86	495.2	207.2	20.24	26.6	22.2	0.537	199.6	804.9
3.55	8.3	19.89	597.3	207.2	20.34	27.7	22.5	0.478	215.0	867.2
3.55	8.3	19.86	792.6	207.4	20.47	28.3	21.3	0.405	242.2	977.0
3.55	8.3	19.93	992.0	207.0	20.68	32.5	23.9	0.349	263.5	1062.9
3.55	8.3	19.89	1192.7	206.9	20.79	34.2	23.9	0.312	284.3	1146.6